

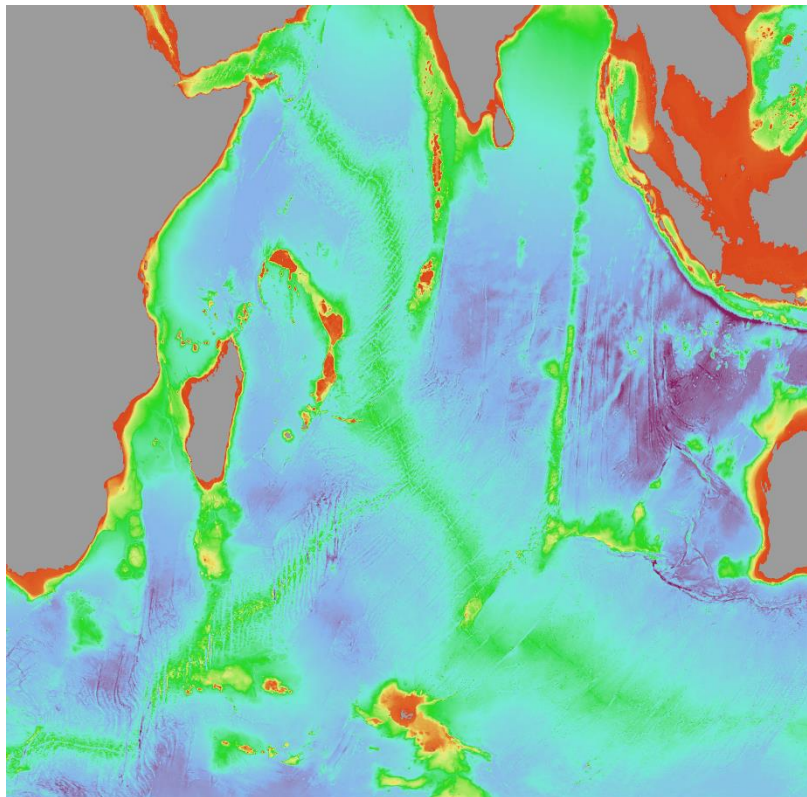
## Data Report:

Produced as a background document for the Workshop on the development of a Regional Environmental Management Plan for the Area of the Indian Ocean

Chennai, India

1-5 May 2023

Sarah DeLand, Jesse Cleary, Elisabetta Menini, Beatrice Smith, Patrick N. Halpin  
Marine Geospatial Ecology Lab, Duke University



The preparation of this report was financially supported through the commissioning of a consultancy by the ISA secretariat.

**Legal Notice:**

This document has been prepared for the International Seabed Authority, however it reflects the views only of the authors, and the Authority cannot be held responsible for any use which may be made of the information contained therein.

**Important Notice:**

Information contained in this publication comprises general statements based on scientific research. The authors advise the reader to note that such information may be incomplete or unable to be used in any specific situation. No reliance or actions must therefore be made on that information without seeking prior expert professional, scientific and technical advice. Additionally, some data sets used herein require permission from the data providers for use.

**Citation:**

DeLand, S., J. Cleary, E. Menini, B. Smith, P.N. Halpin (2023) "Data Report: Workshop on the development of a Regional Environmental Management Plan for the Area of the Indian Ocean", 165 pp.

**Maps:**

Digital versions of individual maps herein are also available online:  
<https://duke.box.com/s/27ju9golud7txc7t9zesj7zhuzgnp2pv>

# 1 Table of Contents

1.1	GEOGRAPHICAL AREA TO BE ADDRESSED IN THIS REPORT .....	9
<b>2</b>	<b>ENVIRONMENTAL DATA.....</b>	<b>10</b>
2.1	BATHYMETRY AND SLOPE (GEBCO) .....	10
2.2	GMRT BATHYMETRY.....	12
2.3	SEAFLOOR GEOMORPHIC FEATURES.....	14
2.4	SEAFLOOR CRUST AGE .....	16
2.5	INDIAN OCEAN BASINS.....	18
2.6	INTERRIDGE VENTS DATABASE .....	20
2.7	FRACTURE ZONES .....	21
2.8	GLOBAL DISTRIBUTION OF SEAMOUNTS .....	22
2.9	GLOBAL SEAMOUNT CLASSIFICATION .....	24
2.10	TOTAL SEDIMENT THICKNESS OF THE WORLD'S OCEANS & MARGINAL SEAS .....	26
2.11	SEAFLOOR SEDIMENTS .....	27
2.12	GLOBAL SEABED SEDIMENT DATABASE.....	29
2.13	MULTIBEAM BATHYMETRIC SURVEY TRACKLINES .....	31
2.14	HYBRID COORDINATE OCEAN MODEL (HYCOM) DATA.....	32
2.15	DRIFTER CLIMATOLOGY OF NEAR-SURFACE CURRENTS.....	34
2.16	SEAFLOOR POC FLUX.....	36
2.17	MODIS DATA.....	38
2.18	VERTICALLY GENERALIZED PRODUCTION MODEL (VGPM) PRIMARY PRODUCTIVITY .....	42
2.19	GLOBAL OCEAN LOW AND MID TROPIC LEVELS BIOMASS HINDCAST .....	43
2.20	ENVIRONMENTAL PREDICTORS FOR POLYMETALLIC NODULES.....	45
2.21	GEOLOGY OF LONGQI-1 HYDROTHERMAL SYSTEM ON ULTRASLOW-SPREADING SOUTHWEST INDIAN RIDGE.....	48
2.22	THE DAXI VENT FIELD.....	51
2.23	GEOMORPHOLOGY AND SEAFLOOR PROCESSES IN THE REMOTE SOUTHEAST INDIAN OCEAN.....	53
2.24	TRACING WATER MASS FRACTIONS IN THE DEEP WESTERN INDIAN OCEAN .....	56
2.25	THE INDIAN OCEAN DEEP MERIDIONAL OVERTURNING CIRCULATION IN THREE OCEAN REANALYSIS PRODUCTS.....	58
2.26	MONSOON AND CARBON FLUXES IN THE NORTHERN INDIAN OCEAN .....	60
2.27	TEMPORAL AND SPATIAL DYNAMICS OF PRIMARY PRODUCTION .....	63
2.28	A NUTRIENT LIMITATION MOSAIC .....	65
2.29	A CENTURY OF OBSERVED TEMPERATURE CHANGE IN THE INDIAN OCEAN.....	67
2.30	INTERANNUAL VARIABILITY OF SEA SURFACE CHLOROPHYLL A.....	69
2.31	PROJECTED TIMING OF CLIMATE DEPARTURE.....	70
2.32	NOAA CLIMATE CHANGE PORTAL .....	71
2.33	DYNAMIC SEASCAPE PELAGIC HABITAT CLASSIFICATION .....	72
<b>3</b>	<b>BIOLOGICAL DATA.....</b>	<b>75</b>
3.1	OCEAN BIODIVERSITY INFORMATION SYSTEM (OBIS) DATA .....	75
3.2	OBIS VULNERABLE MARINE ECOSYSTEMS (VMEs) INDICATOR TAXA.....	77
3.3	GLOBAL DISTRIBUTION OF DEEP-WATER ANTIPATHARIA HABITAT.....	80
3.4	PREDICTIONS OF HABITAT SUITABILITY FOR COLD-WATER OCTOCORALS.....	82
3.5	PREDICTIONS OF HABITAT SUITABILITY FOR FRAMEWORK-FORMING SCLERACTINIAN CORALS .....	87
3.6	INTERNATIONAL SEABED AUTHORITY DEEP DATA PORTAL.....	91
3.7	MICROBIAL DIVERSITY IN NEWLY DISCOVERED HYDROTHERMAL VENTS .....	93
3.8	STRUCTURE AND CONNECTIVITY OF HYDROTHERMAL VENT COMMUNITIES .....	95
3.9	MICRO NEKTONIC FISH SPECIES OVER THREE SEAMOUNTS IN THE SOUTHWESTERN INDIAN OCEAN.....	97
3.10	MICRONEKTON DIEL MIGRATION, COMMUNITY COMPOSITION AND TROPHIC POSITION WITHIN TWO BIOGEOCHEMICAL PROVINCES OF THE SOUTH WEST INDIAN OCEAN.....	99
3.11	NEW GENERA, SPECIES AND OCCURRENCE RECORDS OF GONIASTERIDAE.....	101
3.12	NEW EELPOUT <i>PACHYCARA ANGELOI</i> SP. NOV.....	102

3.13	TROPHIC ECOLOGY OF VAMPIRE SQUID <i>VAMPYROTEUTHIS INFERNALIS</i> .....	103
3.14	BALEEN WHALE DISTRIBUTION.....	104
3.15	PHYLOGEOGRAPHY OF HYDROTHERMAL VENT STALKED BARNACLES .....	106
3.16	BACTERIAL AND FUNGAL BIODIVERSITY IN THE INDIAN OCEAN .....	108
3.17	PREDICTED FAUNAL ASSEMBLAGE WITH 3D HIGH RESOLUTION DATA.....	110
3.18	GLOBAL PATTERNS IN BENTHIC BIOMASS.....	113
3.19	OBIS-SEAMAP DATA SUMMARIES.....	115
3.20	GLOBAL PATTERNS OF MARINE TURTLE BYCATCH.....	116
3.21	SEA TURTLE CONNECTIVITY .....	118
3.22	IMPORTANT BIRD AREAS (IBAS).....	120
3.23	IMPORTANT MARINE MAMMAL AREAS (IMMAS).....	121
3.24	MIGRATORY CONNECTIVITY IN THE OCEAN SEA TURTLE AREA USE.....	123
<b>4</b>	<b>BIOGEOGRAPHIC CLASSIFICATION.....</b>	<b>125</b>
4.1	GLOBAL OPEN OCEAN AND DEEP SEABED (GOODS) BIOGEOGRAPHIC CLASSIFICATION .....	125
4.2	GLOBAL MESOPELAGIC BIOGEOGRAPHY .....	128
4.3	PELAGIC PROVINCES OF THE WORLD .....	130
4.4	LONGHURST MARINE PROVINCES .....	132
4.5	BIOREGIONS OF THE INDIAN OCEAN.....	133
4.6	GLOBAL SEASCAPES.....	135
4.7	BIOGEOGRAPHY OF HYDROTHERMAL VENTS IN THE INDIAN OCEAN .....	137
4.8	BIOGEOGRAPHY AND POPULATION DIVERGENCE OF MICROEUKARYOTES.....	139
4.9	BIOGEOGRAPHY OF ALVINIVONCHA SNAIL IN INDIAN OCEAN HYDROTHERMAL VENTS.....	141
4.10	GLOBAL HYDROTHERMAL VENTS BIOGEOGRAPHY .....	144
<b>5</b>	<b>HUMAN USES.....</b>	<b>146</b>
5.1	DEMERSAL DESTRUCTIVE FISHING.....	146
5.2	FISHING EFFORT BY GEAR TYPE, GLOBAL FISHING WATCH .....	147
5.3	COMMERCIAL SHIPPING.....	151
5.4	ISA CONTRACT AREAS FOR THE EXPLORATION OF MINERAL RESOURCES.....	153
5.5	UNDERSEA TELECOMMUNICATIONS CABLES.....	154
5.6	CUMULATIVE HUMAN IMPACTS ON THE WORLD'S OCEAN.....	155
<b>6</b>	<b>AREAS DEFINED FOR MANAGEMENT AND/OR CONSERVATION OBJECTIVES .....</b>	<b>157</b>
6.1	REGIONAL FISHERIES MANAGEMENT ORGANIZATIONS (RFMO).....	157
6.2	VME CLOSED AREAS TO BOTTOM FISHING ACTIVITIES .....	158
6.3	MARINE PROTECTED AREAS.....	159
6.4	CONVENTION ON BIOLOGICAL DIVERSITY ECOLOGICALLY OR BIOLOGICALLY SIGNIFICANT AREAS (EBSAs).....	160
6.5	ASSESSMENT FOR SITES IN NEED OF PROTECTION IN THE INDIAN OCEAN .....	161
6.6	WESTERN INDIAN OCEAN SYMPHONY TOOL .....	163
<b>7</b>	<b>ACKNOWLEDGMENTS.....</b>	<b>165</b>

## Figures

Figure 1.1-1 Scope for data collection and existing limits .....	9
Figure 2.1-1 Bathymetry .....	10
Figure 2.1-2 Seafloor slope .....	11
Figure 2.1-3 Seafloor slope acceleration .....	11
Figure 2.2-1 GMRT bathymetry .....	13
Figure 2.3-1 Seafloor geomorphic features .....	15
Figure 2.4-1 Seafloor crust age .....	17
Figure 2.5-1 Basins of the Indian Ocean .....	19
Figure 2.6-1 Hydrothermal vents along the Indian Ocean ridges.....	20
Figure 2.7-1 Fracture zones .....	21
Figure 2.8-1 Seamount locations .....	23
Figure 2.9-1 Global seamount classification.....	25
Figure 2.10-1 Sediment thickness.....	26
Figure 2.11-1 Seafloor sediments .....	28
Figure 2.12-1 Global seabed sediment maps .....	30
Figure 2.13-1 Multibeam bathymetry survey tracklines .....	31
Figure 2.14-1 Current velocity, Surface, January average from 2017-2021.....	32
Figure 2.14-2 Current velocity, Bottom, 2022 .....	33
Figure 2.14-3 Sea surface elevation, January average from 2017-2021 .....	33
Figure 2.15-1 Drifter-derived climatology of near-surface currents .....	35
Figure 2.16-1 Seafloor POC flux .....	37
Figure 2.17-1 Mean Chlorophyll a concentration from 2012-2021.....	39
Figure 2.17-2 Sea surface temperature, January 2017-2021 .....	39
Figure 2.17-3 Particulate organic carbon flux, January 2017-2022.....	40
Figure 2.17-3 Net primary productivity climatology from 2017-2022 .....	40
Figure 2.18-1 Vertically generalized production model - primary productivity climatology from 2015-2019 .....	42
Figure 2.19-1 Zooplankton biomass, June 2016 .....	43
Figure 2.19-2 Epipelagic micronekton biomass, June 2018.....	44
Figure 2.19-3 Epipelagic layer depth, June 2018.....	44
Figure 2.20-1 Global distribution of polymetallic nodules .....	46
Figure 2.20-2 Predicted distribution of polymetallic nodules .....	46
Figure 2.21-1 Bathymetry and benthic features along the Longqi-1 hydrothermal vent system	49
Figure 2.22-1 Hydrothermal vents in the Daxi Vent Field .....	52
Figure 2.22-2 Location of active hydrothermal vents in the Daxi Vent Field .....	52
Figure 2.23-1 Location of data collection in the Indian Ocean.....	54
Figure 2.24-1 Water masses in the Indian Ocean.....	56
Figure 2.25-1 Results and trends from three ocean reanalysis products.....	59
Figure 2.26-1 Sea surface temperature, ocean circulation, and minimum oxygen concentration in the Indian Ocean.....	61
Figure 2.27-1 Chl a climatology during two monsoon seasons .....	64
Figure 2.28-1 Nutrient concentrations in the Indian Ocean.....	66

Figure 2.29-1 Temperature sampling sites in the Indian Ocean.....	67
Figure 2.29-2 Temperature change by latitude and depth in the Indian Ocean.....	68
Figure 2.30-1 Interannual variation of chl a concentration in the Indian Ocean.....	69
Figure 2.31-1 The projected timing of climate departure.....	70
Figure 2.32-1 Climate change variables from CMIP5 data.....	71
Figure 2.33-1 Most commonly occurring seascape class in January, from 2012-2021.....	73
Figure 2.33-2 Most commonly occurring seascape class in June, from 2012-2021.....	74
Figure 3.1-1 All OBIS records below 500 m.....	76
Figure 3.2-1 OBIS records for all VME taxa.....	78
Figure 3.2-2 OBIS records of Octocorals.....	78
Figure 3.2-3 OBIS records of Scleractinia.....	79
Figure 3.2-4 OBIS records of Sponges.....	79
Figure 3.3-1 Deep-Water Antipatharia Habitat Suitability.....	81
Figure 3.4-1 Deep-Sea Octocoral habitat suitability across seven species.....	82
Figure 3.4-2 Deep-Sea Octocoral habitat suitability - Alcyoniina.....	83
Figure 3.4-3 Deep-Sea Octocoral habitat suitability - Holaxonia.....	83
Figure 3.4-4 Deep-Sea Octocoral habitat suitability - Calcaxonia.....	84
Figure 3.4-5 Deep-Sea Octocoral habitat suitability - Scleraxonia.....	84
Figure 3.4-6 Deep-Sea Octocoral habitat suitability - Sessiliflorae.....	85
Figure 3.4-7 Deep-Sea Octocoral habitat suitability - Stolonifera.....	85
Figure 3.4-8 Deep-Sea Octocoral habitat suitability - Subselliflorae.....	86
Figure 3.5-1 Deep-Sea Scleractinia habitat suitability – all five framework forming species.....	88
Figure 3.5-2 Deep-Sea Scleractinia habitat suitability – <i>Lophelia pertusa</i> .....	88
Figure 3.5-3 Deep-Sea Scleractinia habitat suitability – <i>Madrepora oculata</i> .....	89
Figure 3.5-4 Deep-Sea Scleractinia habitat suitability – <i>Solenosmilia variabilis</i> .....	89
Figure 3.5-5 Deep-Sea Scleractinia habitat suitability – <i>Goniocorella dumosa</i> .....	90
Figure 3.5-6 Deep-Sea Scleractinia habitat suitability – <i>Enallopsammia rostrata</i> .....	90
Figure 3.6-1 Chart of data types in Deep Data.....	91
Figure 3.6-2 ISA Deep Data portal.....	92
Figure 3.7-1 Hydrothermal vent fields along the Indian Ocean ridges and sampling locations ..	94
Figure 3.8-1 Biologically active hydrothermal vents along the Indian Ocean ridges.....	96
Figure 3.9-1 Study seamounts in the Indian Ocean.....	97
Figure 3.10-1 Two biogeochemical provinces in the Indian Ocean and their properties.....	100
Figure 3.13-1 Study sample locations.....	103
Figure 3.14-1 Acoustic array in the Indian Ocean.....	105
Figure 3.15-1 Locations of study hydrothermal vents in the Indian Ocean.....	107
Figure 3.16-1 Locations of study sites in the Indian Ocean.....	109
Figure 3.17-1 Figure 4 from Gerdes et al. (2019).....	111
Figure 3.17-2 Figure 7 from Gerdes et al. (2019).....	112
Figure 3.18-1 Mean annual field of total modelled seafloor biomass.....	114
Figure 3.19-1 Turtle observations.....	115
Figure 3.19-2 Marine mammal observations.....	115
Figure 3.20-1 Overview of sea turtle bycatch data.....	117
Figure 3.21-1 Sea turtle tracking data distribution.....	119

Figure 3.22-1 Important Bird Areas (BirdLife) .....	120
Figure 3.23-1 Important Marine Mammal Areas.....	122
Figure 3.24-1 Loggerhead turtle area use.....	124
Figure 4.1-1 GOODS abyssal provinces.....	126
Figure 4.1-2 GOODS bathyal provinces.....	126
Figure 4.1-3 GOODS pelagic provinces .....	127
Figure 4.2-1 Mesopelagic provinces .....	129
Figure 4.3-1 Pelagic provinces .....	131
Figure 4.4-1 Longhurst marine provinces .....	132
Figure 4.5-1 Benthic bioregions .....	133
Figure 4.5-2 Epipelagic bioregions.....	134
Figure 4.6-1 Global seascapes.....	136
Figure 4.7-1 Biogeographic patterns of vent fauna along Indian Ocean ridges .....	138
Figure 4.8-1 Microeukaryote species richness along Indian Ocean hydrothermal vents .....	140
Figure 4.9-1 Biogeographic patterns of Alviniconcha snails along Indian Ocean ridges .....	142
Figure 4.10-1 Results of geographically constrained clustering using multivariate regression trees. Figure 6 from Rogers et al. (2012) .....	145
Figure 5.1-1 Demersal destructive bottom fishing.....	146
Figure 5.2-1 Total fishing effort for all gears from 2019-2020 .....	148
Figure 5.2-2 Longline fishing effort from 2019-2020.....	149
Figure 5.2-3 Trawler fishing effort from 2019-2020.....	150
Figure 5.3-1 Commercial shipping .....	152
Figure 5.4-1 ISA exploration areas for polymetallic sulphides and polymetallic nodules in the Indian Ocean .....	153
Figure 5.5-1 Undersea telecommunications cables .....	154
Figure 5.6-1 Cumulative human impact, 2013 .....	155
Figure 5.6-2 Change in cumulative human impact, 2008 to 2013.....	156
Figure 6.1-1 RFMOs in the North Atlantic Ocean .....	157
Figure 6.2-1 VME closed areas.....	158
Figure 6.3-1 Marine protected areas.....	159
Figure 6.4-1 Convention on Biological Diversity's Ecologically or Biologically Significant Areas (EBSAs) .....	160
Figure 6.5-1 Confirmed active hydrothermal vents along the Indian Ocean ridges .....	162
Figure 6.6-1 An example of the WIO Symphony tool .....	164

# 1 Context

The Marine Geospatial Ecology Lab at Duke University was contracted to provide data discovery and mapping support for experts attending the “Workshop on the development of a Regional Environmental Management Plan for the Area of the Indian Ocean” (from 1-5 May 2023 in Chennai, India). This workshop is convened by the International Seabed Authority in collaboration with the Ministry of Earth Sciences of the Government of India and the National Institute of Ocean Technology of India. The preparation of this report was financially supported through the commissioning of a consultancy by the ISA secretariat.

As part of this support, a large number of datasets and analyses pertaining to the region of ISA interest in the Area of the Indian Ocean have been collected and mapped. These datasets and supporting references have been compiled into this data report, an annotated catalog of available spatial data and selected publications to brief workshop participants and aid with data discovery.

This data report accompanies a Regional Environmental Assessment that provides an aggregation and synthesis of existing information relating to the Area of the Indian Ocean, including geomorphology, physical and chemical characteristics and biological communities.

The datasets described herein will be available on-site at the Chennai workshop supported by live GIS and mapping capabilities. Workshop participants will be able to request simple map overlays and analyses be performed at the workshop that will aid in their discussions. The results of the mapping work performed at the workshop will be included in the subsequent ISA Workshop Report.

## 1.1 Geographical area to be addressed in this report

For the purposes of this report on the Indian Ocean, data were collected or generated for areas between 30°N and 70°S and 20°E and 120°E. The area to be included in the draft REMP will be discussed in the ISA meetings and will not necessarily coincide with the area covered by this data report.

The following datasets will be included in many of the subsequent maps without repeated inclusion in the map legends:

EEZ Data Source - VLIZ v11, <http://www.marineregions.org/eez.php>

ECS Data Source - <https://www.marineregions.org/sources.php#marbound>

Plate Boundary Data Source - <https://ig.utexas.edu/marine-and-tectonics/plates-project/>

Bathymetry Data Source -

[https://www.gebco.net/data\\_and\\_products/gridded\\_bathymetry\\_data/gebco\\_2022/](https://www.gebco.net/data_and_products/gridded_bathymetry_data/gebco_2022/)

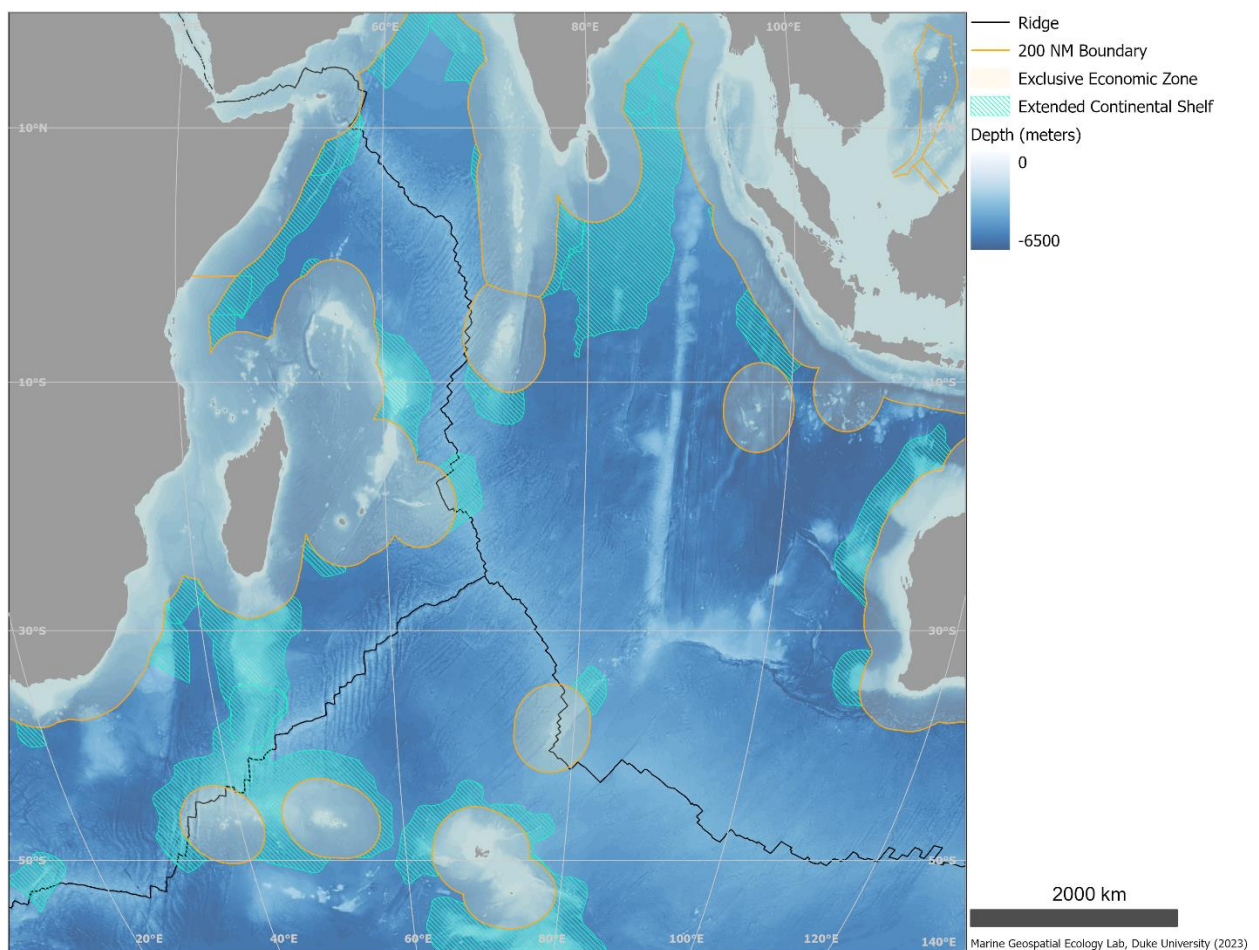


Figure 1.1-1 Scope for data collection and existing limits

## 2 Environmental Data

### 2.1 Bathymetry and Slope (GEBCO)

GEBCO's gridded bathymetric data set, the GEBCO\_2022 grid, is a global terrain model for ocean and land at 15 arc-second intervals. The GEBCO\_2022 Grid is the latest global bathymetric product released by the General Bathymetric Chart of the Oceans (GEBCO) and has been developed through the Nippon Foundation-GEBCO Seabed 2030 Project.

The complete GEBCO\_2022 data set provides global coverage, spanning 89° 59' 52.5"N, 179° 59' 52.5"W to 89° 59' 52.5"S, 179° 59' 52.5"E on a 15 arc-second geographic latitude and longitude grid. It consists of 43200 rows x 86400 columns, giving 3,732,480,000 data points. The data values are pixel-centre registered i.e. they refer to elevations, in meters, at the centre of grid cells.

Slope and slope acceleration were derived from GEBCO bathymetry with ArcPro 2.8.8.

Source:

[https://www.gebco.net/data\\_and\\_products/gridded\\_bathymetry\\_data/gebco\\_2022/](https://www.gebco.net/data_and_products/gridded_bathymetry_data/gebco_2022/)

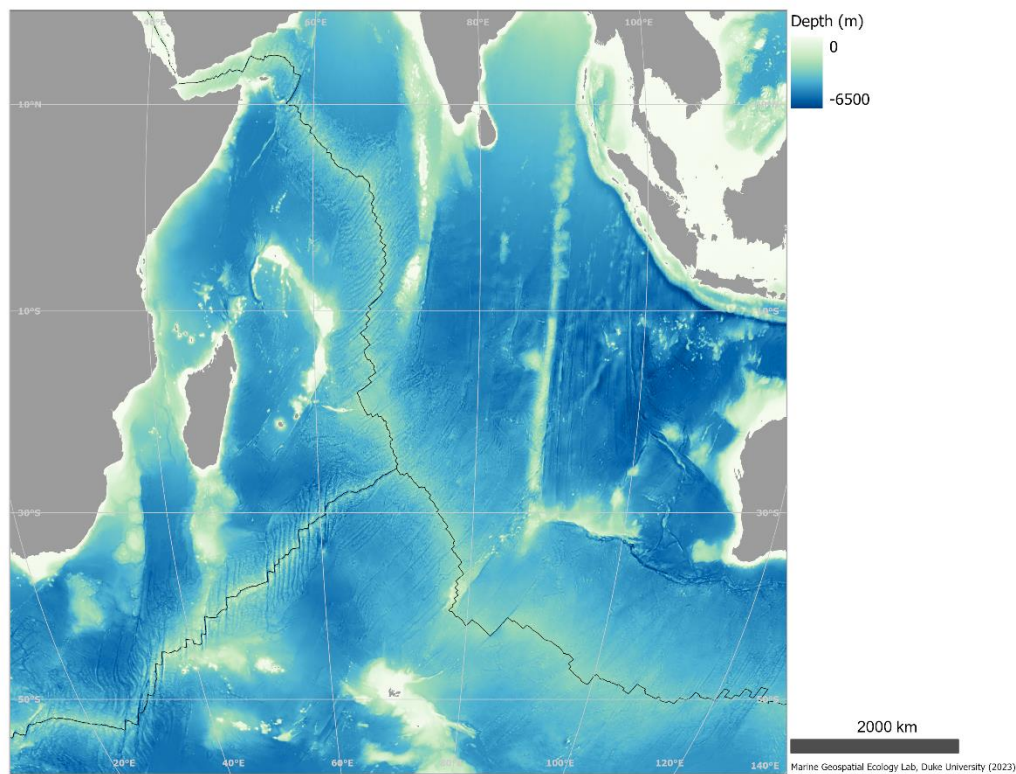


Figure 2.1-1 Bathymetry

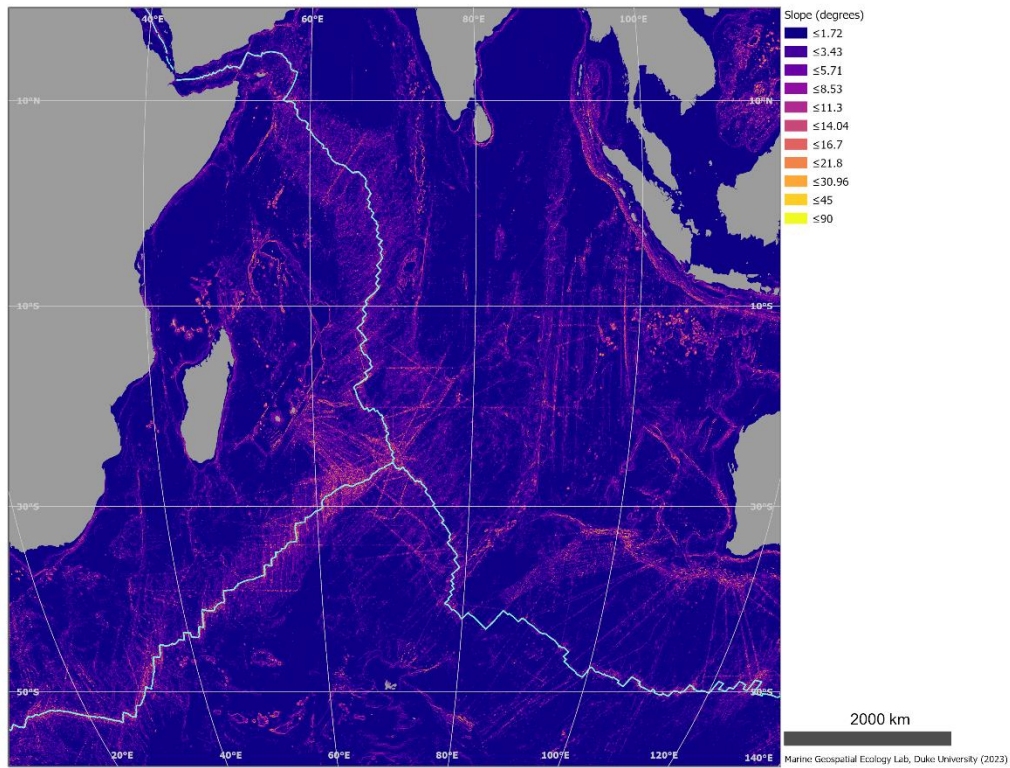


Figure 2.1-2 Seafloor slope

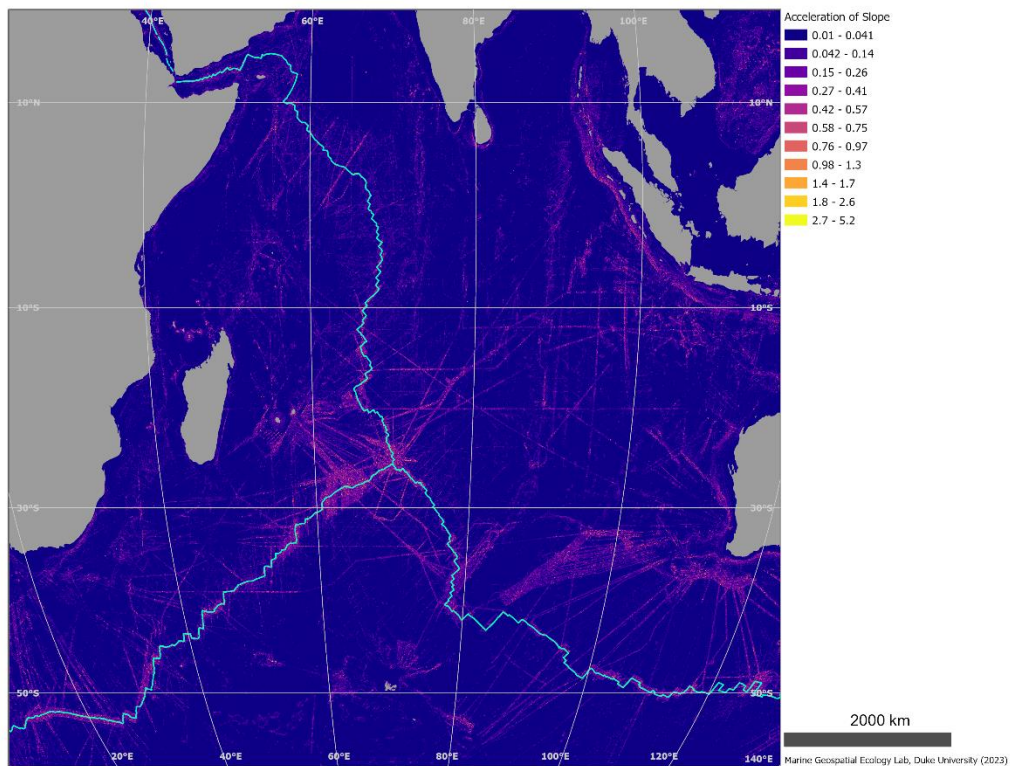


Figure 2.1-3 Seafloor slope acceleration

## 2.2 GMRT Bathymetry

The Global Multi-Resolution Topography (GMRT) Synthesis is a multi-resolution Digital Elevation Model (DEM) maintained in three projections and managed with a scalable global architecture that offers infrastructure for accessing the DEM as grids, images, points and profiles. A mask layer is available that highlights the location of high-resolution data. Most curatorial effort for GMRT is focused on cleaning and processing ship-based multibeam sonar data acquired by the US Academic Research Fleet (ARF) so they can be gridded at their full spatial resolution (~100m in the deep sea). These data are seamlessly overlain on lower resolution observed and predicted bathymetry data and are integrated with terrestrial elevation data to deliver to users the best resolution data that have been curated for a particular area of interest.

Multibeam bathymetry data are unique among the marine geophysical data types in their relevance for a broad range of scientific investigations and non-academic uses, providing fundamental characterization of the physical environment and serving as primary base maps for multidisciplinary programs. While specialist expertise is needed to access, quality control and process multibeam bathymetry data files to generate high-quality bathymetric maps, the GMRT Synthesis provides free open access to bathymetric images and gridded bathymetric data for specialist and non-specialist users alike. Details about the tiling method and procedures used for creating and serving the GMRT synthesis is available in Ryan et al., 2009.

### Reference:

Ryan, W.B.F., S.M. Carbotte, J.O. Coplan, S. O'Hara, A. Melkonian, R. Arko, R.A. Weissel, V. Ferrini, A. Goodwillie, F. Nitsche, J. Bonczkowski, and R. Zemsky (2009), Global Multi-Resolution Topography synthesis, *Geochem. Geophys. Geosyst.*, 10, Q03014, doi: 10.1029/2008GC002332

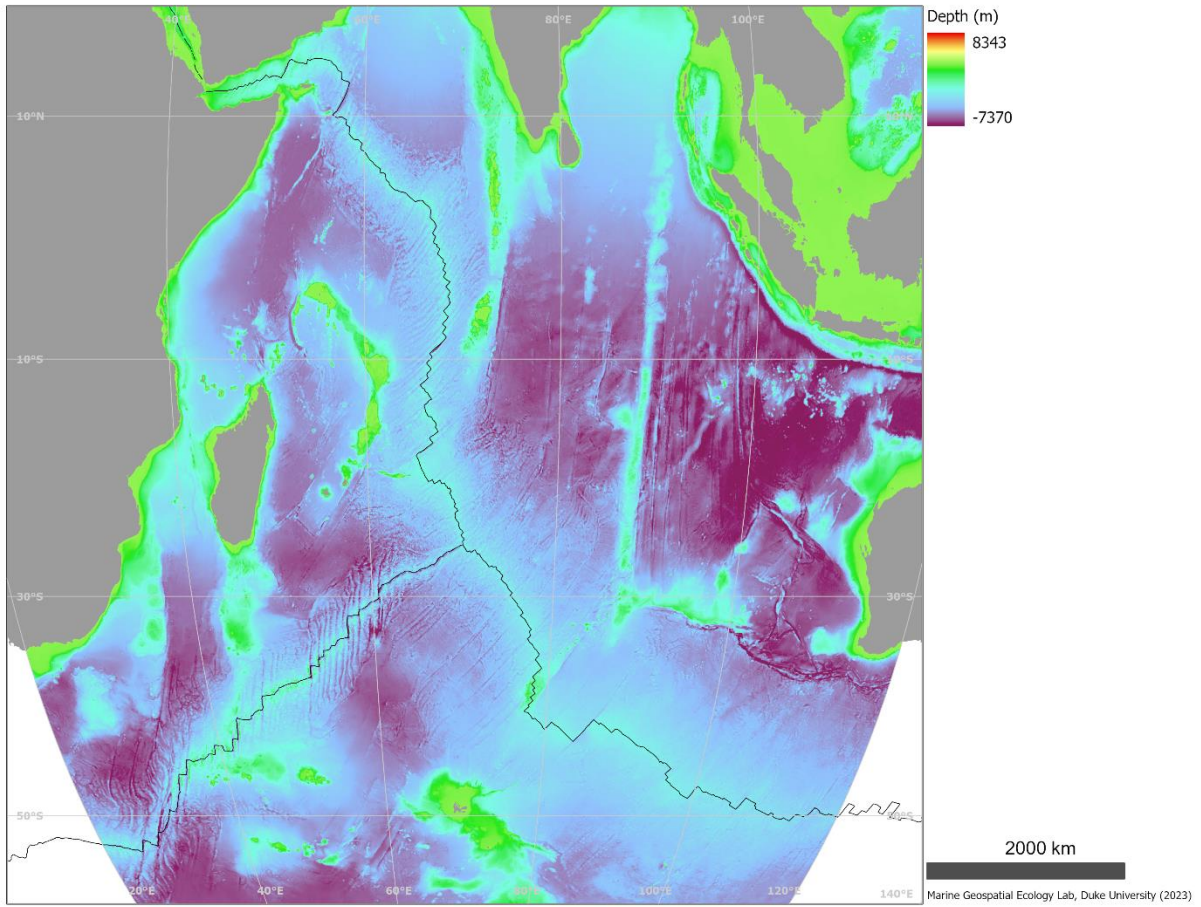


Figure 2.2-1 GMRT bathymetry

## 2.3 Seafloor Geomorphic Features

Abstract (Harris et al. 2014):

“We present the first digital seafloor geomorphic features map (GSFM) of the global ocean. The GSFM includes 131,192 separate polygons in 29 geomorphic feature categories, used here to assess differences between passive and active continental margins as well as between 8 major ocean regions (the Arctic, Indian, North Atlantic, North Pacific, South Atlantic, South Pacific and the Southern Oceans and the Mediterranean and Black Seas). The GSFM provides quantitative assessments of differences between passive and active margins: continental shelf width of passive margins (88 km) is nearly three times that of active margins (31 km); the average width of active slopes (36 km) is less than the average width of passive margin slopes (46 km); active margin slopes contain an area of 3.4 million km<sup>2</sup> where the gradient exceeds 5°, compared with 1.3 million km<sup>2</sup> on passive margin slopes; the continental rise covers 27 million km<sup>2</sup> adjacent to passive margins and less than 2.3 million km<sup>2</sup> adjacent to active margins. Examples of specific applications of the GSFM are presented to show that: 1) larger rift valley segments are generally associated with slow-spreading rates and smaller rift valley segments are associated with fast spreading; 2) polar submarine canyons are twice the average size of non-polar canyons and abyssal polar regions exhibit lower seafloor roughness than non-polar regions, expressed as spatially extensive fan, rise and abyssal plain sediment deposits — all of which are attributed here to the effects of continental glaciations; and 3) recognition of seamounts as a separate category of feature from ridges results in a lower estimate of seamount number compared with estimates of previous workers.”

Reference:

Harris PT, Macmillan-Lawler M, Rupp J, Baker EK (2014), Geomorphology of the oceans. *Marine Geology*. doi: 10.1016/j.margeo.2014.01.011

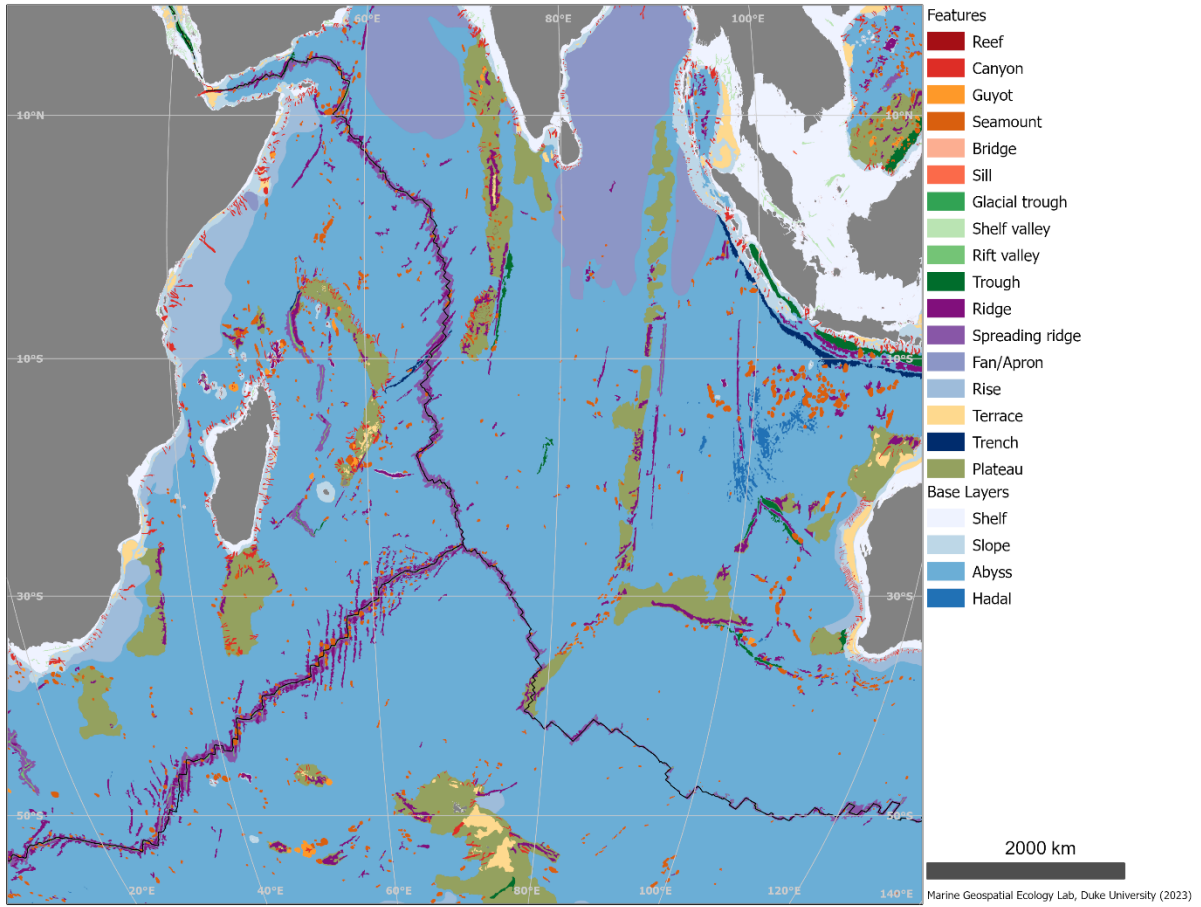


Figure 2.3-1 Seafloor geomorphic features

## 2.4 Seafloor Crust Age

Abstract (Seton et al. 2020):

“We present an updated oceanic crustal age grid and a set of complementary grids including spreading rate, asymmetry, direction and obliquity. Our dataset is based on a selected set of magnetic anomaly identifications and the plate tectonic model of Müller et al. (2019). We find the mean age of oceanic crust is 64.2 Myrs, slightly older than previous estimates, mainly due to the inclusion of pockets of Mesozoic aged crust in the Atlantic and Mediterranean and improvements to the Jurassic Pacific triangle. This older crust is partly compensated by additional Cenozoic-aged back-arc basin crust not included in previous models. The distribution of spreading modes based on area of preserved crust is relatively equal between slow (20–55 mm/yr) and fast (75–180 mm/yr) spreading systems at 33 and 39%, respectively. Crust transitional between fast and slow, or intermediate systems (55–75 mm/yr), cover 20% of the preserved ocean floor with much smaller proportions of crust formed at ultra-slow (5%) and super-fast (3%) spreading systems. Slow and intermediate spreading systems exhibit the most stable behavior in terms of spreading asymmetry and obliquity, with the widest distribution of obliquities occurring at ultra-slow spreading systems, consistent with present-day observations. Our confidence grid provides a complementary resource for non-experts to identify those parts of the age grid that are least well constrained. Our grids in 6, 2 and 1 arc-minute resolution as well as our python workflow, isoplate, used to compute our datasets are freely available in online repositories and on the GPlates data portal.”

Reference:

Seton, M., Müller, R. D., Zahirovic, S., Williams, S., Wright, N., Cannon, J., Whittaker, J., Matthews, K., McGirr, R., (2020), A global dataset of present-day oceanic crustal age and seafloor spreading parameters, *Geochemistry, Geophysics, Geosystems*, doi: 10.1029/2020GC009214

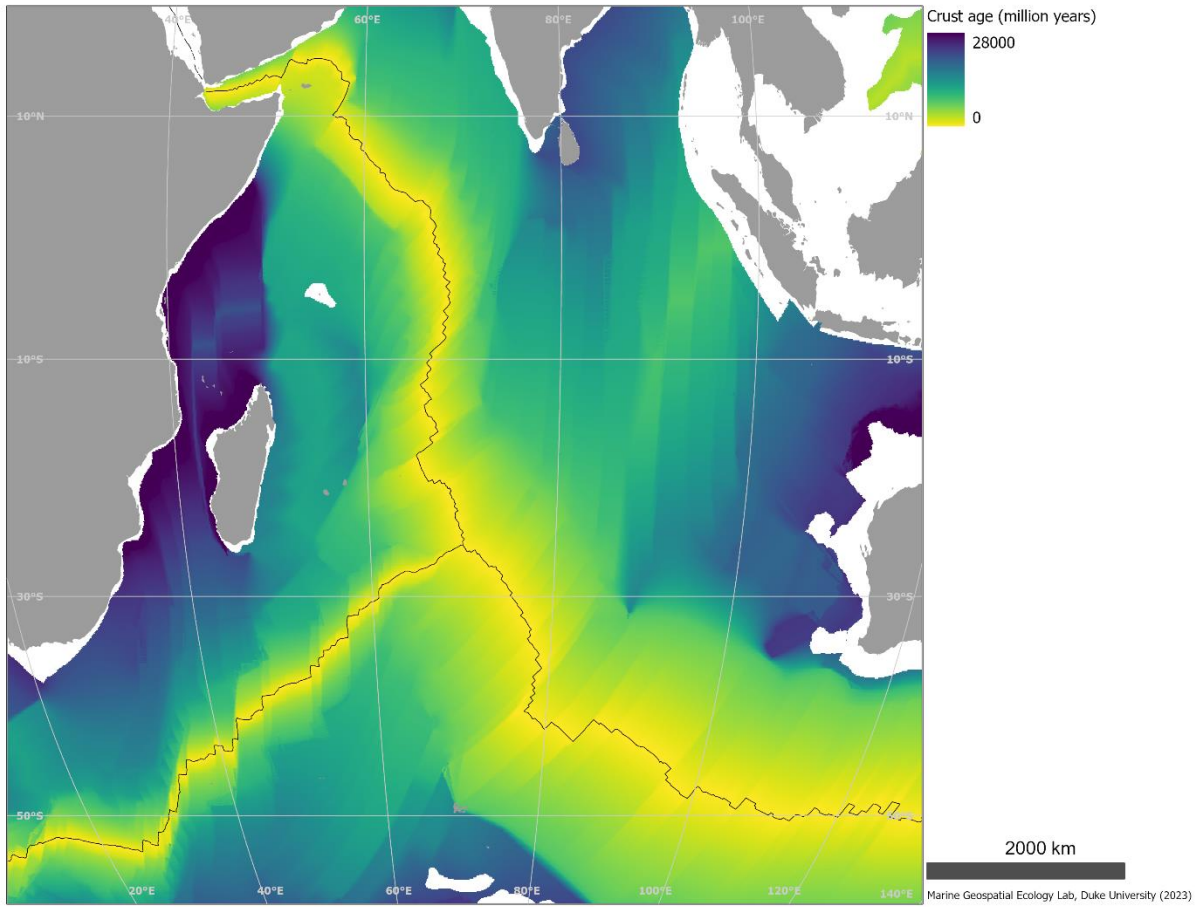


Figure 2.4-1 Seafloor crust age

## 2.5 Indian Ocean Basins

“A shapefile of 311 undersea features from all major oceans and seas has been created as an aid for retrieving georeferenced information resources. Version 1.1 of the data set also includes a linked data representation of 299 of these features and their spatial extents. The geographic extent of the data set is 0 degrees E to 0 degrees W longitude and 75 degrees S to 90 degrees N latitude. Many of the undersea features (UF) in the shapefile were selected from a list assembled by Weatherall and Cramer (2008) in a report from the British Oceanographic Data Centre (BODC) to the General Bathymetric Chart of the Oceans (GEBCO) Sub-Committee on Undersea Feature Names (SCUFN). Annex II of the Weatherall and Cramer report (p. 20-22) lists 183 undersea features that "may need additional points to define their shape" and includes online links to additional BODC documents providing coordinate pairs sufficient to define detailed linestrings for these features. For the first phase of the U.S. Geological Survey (USGS) project, Wingfield created polygons for 87 of the undersea features on the BODC list, using the linestrings as guides; the selected features were primarily ridges, rises, trenches, fracture zones, basins, and seamount chains. In the second phase of the USGS project, Wingfield and Hartwell created polygons for an additional 224 undersea features, mostly basins, abyssal plains, and fracture zones. Because USGS is a Federal agency, the attribute tables follow the conventions of the National Geospatial-Intelligence Agency (NGA) GEOnet Names Server (<http://geonames.nga.mil/gns/html/>).”

### Reference:

Hartwell, S.R., Wingfield, D.K., Allwardt, A.O., Lightsom, F.L., and Wong, F.L., 2018, Polygons of global undersea features for geographic searches (ver. 1.1, June 2018): U.S. Geological Survey Open-File Report 2014–1040, <https://doi.org/10.3133/ofr20141040>.

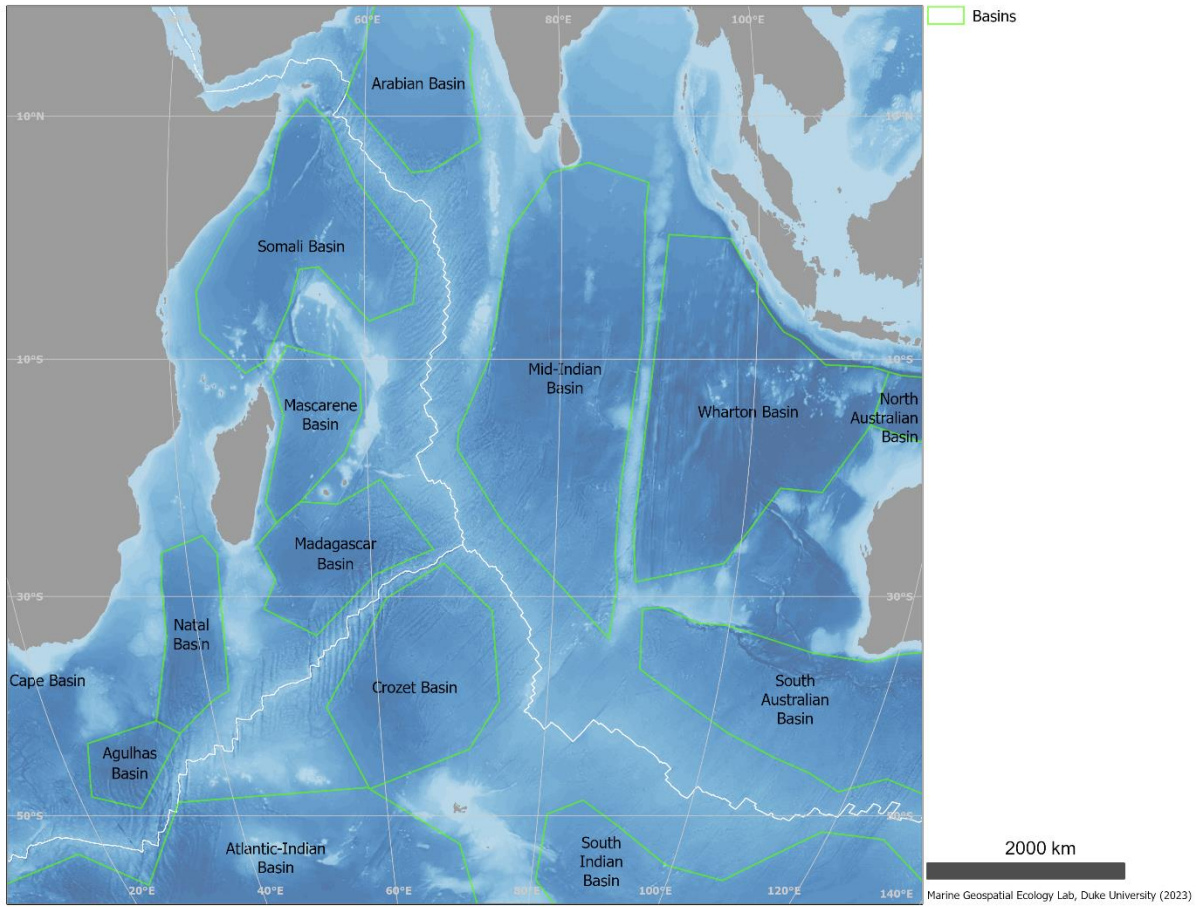


**Figure 2.5-1 Basins of the Indian Ocean**

## 2.6 InterRidge Vents Database

“The InterRidge Global Database of Active Submarine Hydrothermal Vent Fields, hereafter referred to as the InterRidge Vents Database, is available online as the authoritative source for locations of hydrothermal vent fields worldwide (linked to InterRidge homepage: <http://www.interridge.org>). The InterRidge Vents Database was developed to provide a comprehensive list of active submarine hydrothermal vent fields for use in academic research and education.”

Source: <http://vents-data.interridge.org/>, database version 3.4

Reference:

Beaulieu, S. E., E. T. Baker, C. R. German, and A. Maffei (2013), An authoritative global database for active submarine hydrothermal vent fields, *Geochem. Geophys. Geosys.*, 14, 4892–4905, doi:10.1002/2013GC004998.

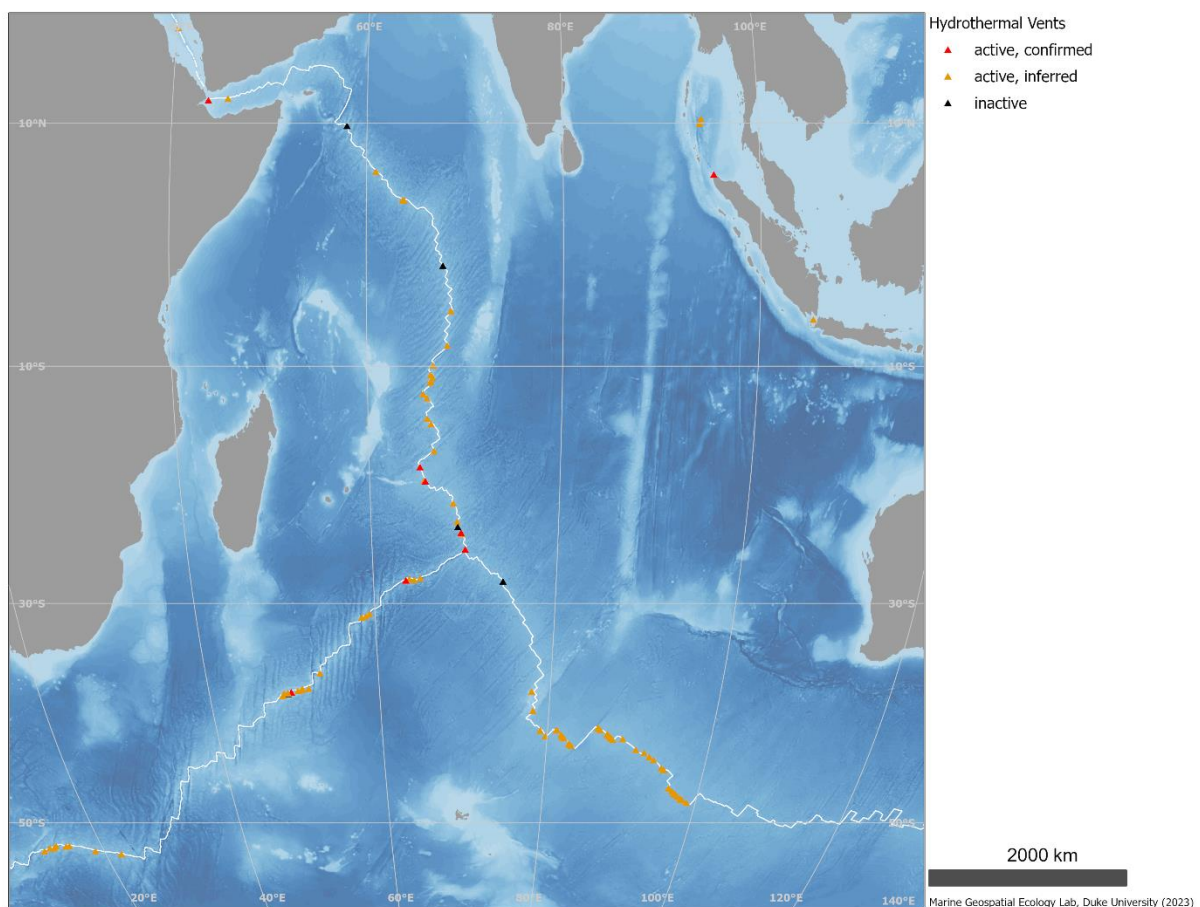


Figure 2.6-1 Hydrothermal vents along the Indian Ocean ridges

## 2.7 Fracture Zones

Included in this archive are shapefiles of Undersea Feature Names and their geometries for geospatial applications. These data were generated by the General Bathymetric Chart of the Oceans (GEBCO) Gazetteer of Undersea Feature Names. For this region, we extracted the fracture zone features.

Source: [https://www.gebco.net/data\\_and\\_products/undersea\\_feature\\_names/](https://www.gebco.net/data_and_products/undersea_feature_names/)

Reference: IHO-IOC GEBCO Gazetteer of Undersea Feature Names, [www.gebco.net](http://www.gebco.net)

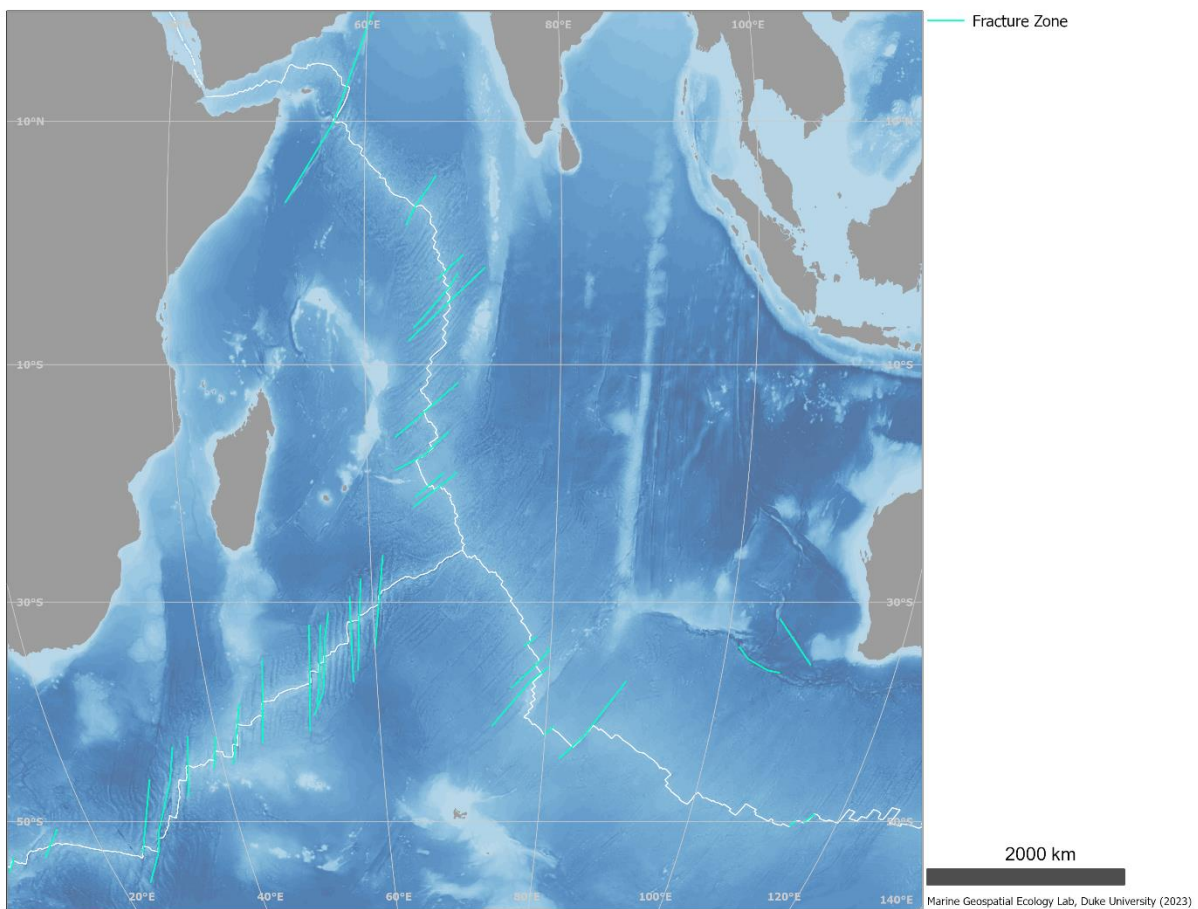


Figure 2.7-1 Fracture zones

## 2.8 Global Distribution of Seamounts

Abstract (Yesson et al. 2011):

“Seamounts and knolls are ‘undersea mountains’, the former rising more than 1000 m from the seafloor. These features provide important habitats for aquatic predators, demersal deep-sea fish and benthic invertebrates. However most seamounts have not been surveyed and their numbers and locations are not well known. Previous efforts to locate and quantify seamounts have used relatively coarse bathymetry grids. Here we use global bathymetric data at 30 arc-second resolution to identify seamounts and knolls. We identify 33,452 seamounts and 138,412 knolls, representing the largest global set of identified seamounts and knolls to date. We compare estimated seamount numbers, locations, and depths with validation sets of seamount data from New Zealand and Azores. This comparison indicates the method we apply finds 94% of seamounts, but may overestimate seamount numbers along ridges and in areas where faulting and seafloor spreading creates highly complex topography. The seamounts and knolls identified herein are significantly geographically biased towards areas surveyed with ship-based soundings. As only 6.5% of the ocean floor has been surveyed with soundings it is likely that new seamounts will be uncovered as surveying improves. Seamount habitats constitute approximately 4.7% of the ocean floor, whilst knolls cover 16.3%. Regional distribution of these features is examined, and we find a disproportionate number of productive knolls, with a summit depth of  $\approx 1.5$  km, located in the Southern Ocean. Less than 2% of seamounts are within marine protected areas and the majority of these are located within exclusive economic zones with few on the High Seas. The database of seamounts and knolls resulting from this study will be a useful resource for researchers and conservation planners.”

Reference:

Yesson, C., Clark, M. R., Taylor, M. L., & Rogers, A. D. (2011). The global distribution of seamounts based on 30 arc seconds bathymetry data. *Deep Sea Research Part I: Oceanographic Research Papers*, 58(4), 442-453. doi: 10.1016/j.dsr.2011.02.004

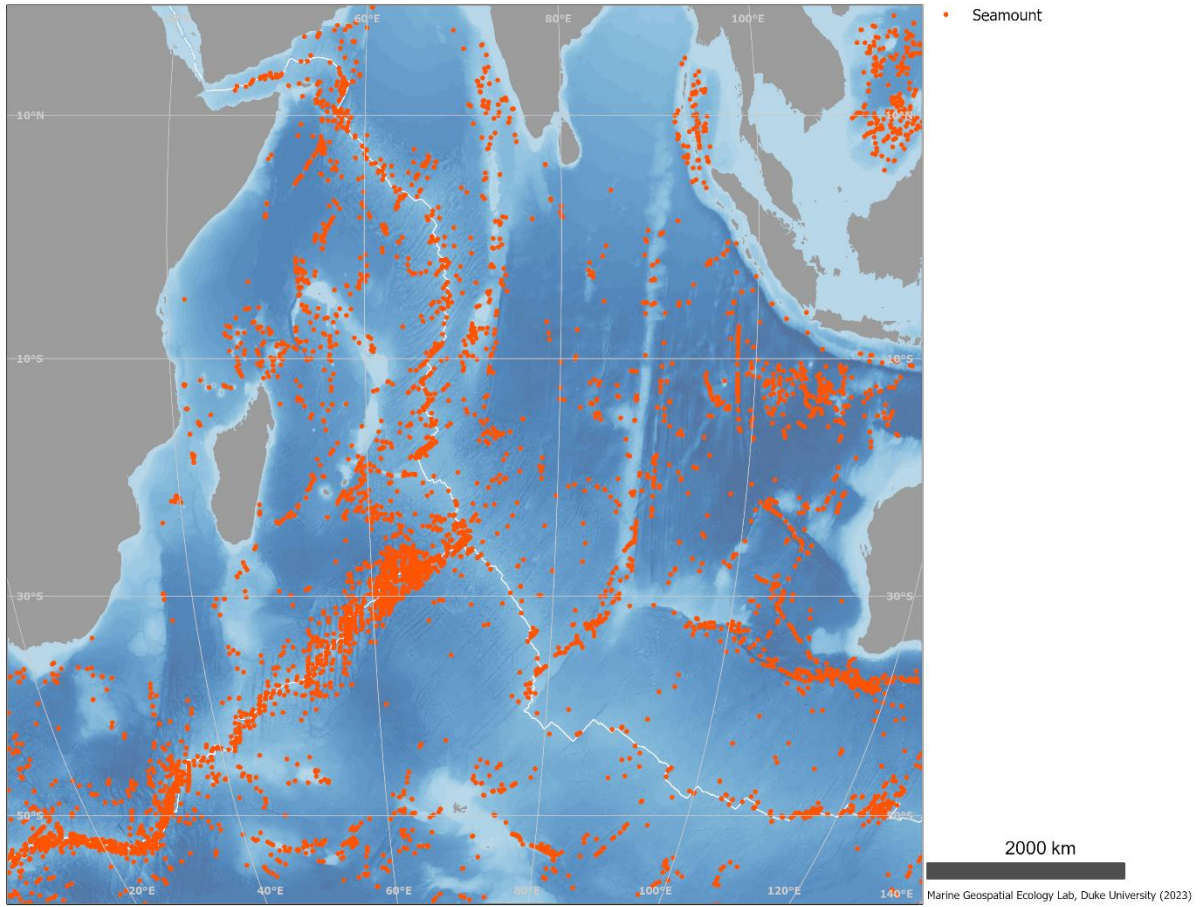


Figure 2.8-1 Seamount locations

## 2.9 Global Seamount Classification

Abstract (Clark et al. 2011):

“Seamounts are prominent features of the world’s seafloor, and are the target of deep-sea commercial fisheries, and of interest for minerals exploitation. They can host vulnerable benthic communities, which can be rapidly and severely impacted by human activities. There have been recent calls to establish networks of marine protected areas on the High Seas, including seamounts. However, there is little biological information on the benthic communities on seamounts, and this has limited the ability of scientists to inform managers about seamounts that should be protected as part of a network. In this paper we present a seamount classification based on “biologically meaningful” physical variables for which global-scale data are available. The approach involves the use of a general biogeographic classification for the bathyal depth zone (near-surface to 3500 m), and then uses four key environmental variables (overlying export production, summit depth, oxygen levels, and seamount proximity) to group seamounts with similar characteristics. This procedure is done in a simple hierarchical manner, which results in 194 seamount classes throughout the world’s oceans. The method was compared against a multivariate approach, and ground-truthed against octocoral data for the North Atlantic. We believe it gives biologically realistic groupings, in a transparent process that can be used to either directly select, or aid selection of, seamounts to be protected.”

Reference:

Clark, Malcolm R., Les Watling, Ashley A. Rowden, John M. Guinotte, and Craig R. Smith. "A global seamount classification to aid the scientific design of marine protected area networks." *Ocean & Coastal Management* 54, no. 1 (2011): 19-36. doi: 10.1016/j.ocecoaman.2010.10.006

Source: <http://seamounts.sdsc.edu/>

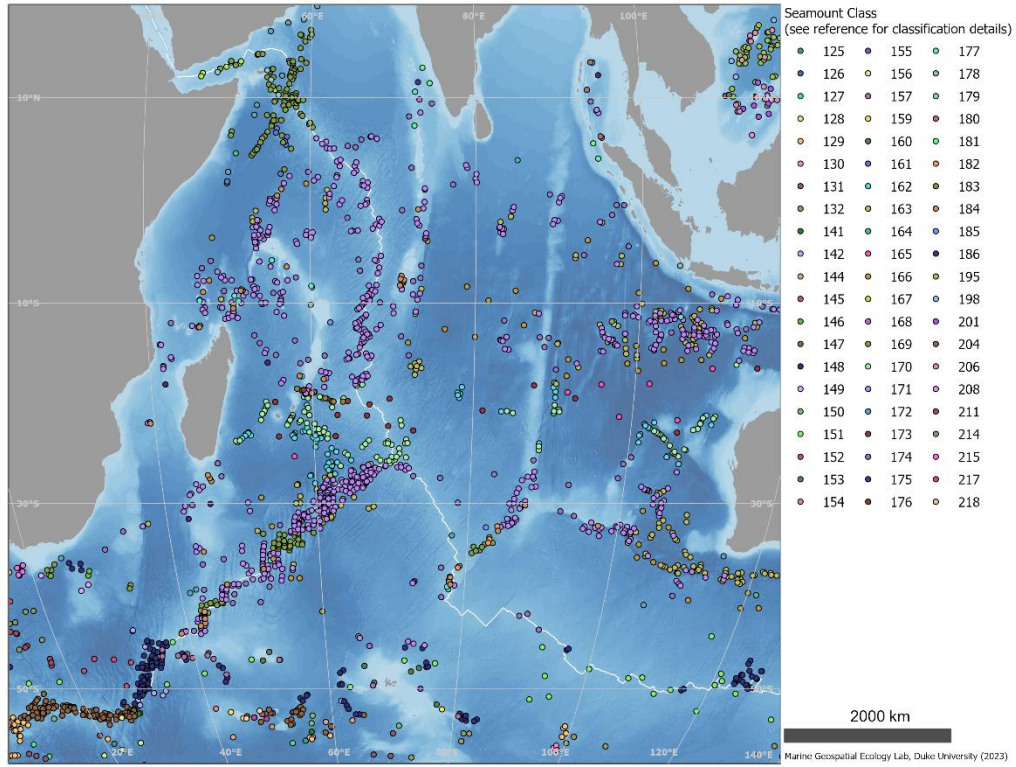


Figure 2.9-1 Global seamount classification

## 2.10 Total Sediment Thickness of the World's Oceans & Marginal Seas

“NCEI's global ocean sediment thickness grid of Divins (2003) updated by Whittaker et al. (2013) has been updated again for the NE Atlantic, Arctic, Southern Ocean, and Mediterranean regions. The new global 5-arc-minute total sediment thickness grid, GlobSed, incorporates new data and several regional oceanic sediment thickness maps, which have been compiled and published for the, (1) NE Atlantic (Funck et al., 2017; Hopper et al., 2014), (2) Mediterranean (Molinari & Morelli, 2011), (3) Arctic (Petrov et al., 2016), (4) Weddell Sea (Huang et al., 2014), and (5) the Ross Sea, Amundsen Sea, and Bellingshausen Sea sectors off West Antarctica (Lindeque et al., 2016; Wobbe et al., 2014). This version also includes updates in the White Sea region based on the VSEGEI map of Orlov and Fedorov (2001). GlobSed covers a larger area than NCEI's previous global grids (Divins, 2003; Whittaker et al. 2013), and the new updates results in a 29.7% increase in estimated total oceanic sediment volume.”

Source: <https://www.ngdc.noaa.gov/mgg/sedthick/>

Reference:

Straume, E.O., Gaina, C., Medvedev, S., Hochmuth, K., Gohl, K., Whittaker, J. M., et al. (2019). GlobSed: Updated total sediment thickness in the world's oceans. *Geochemistry, Geophysics, Geosystems*, 20. DOI: 10.1029/2018GC008115

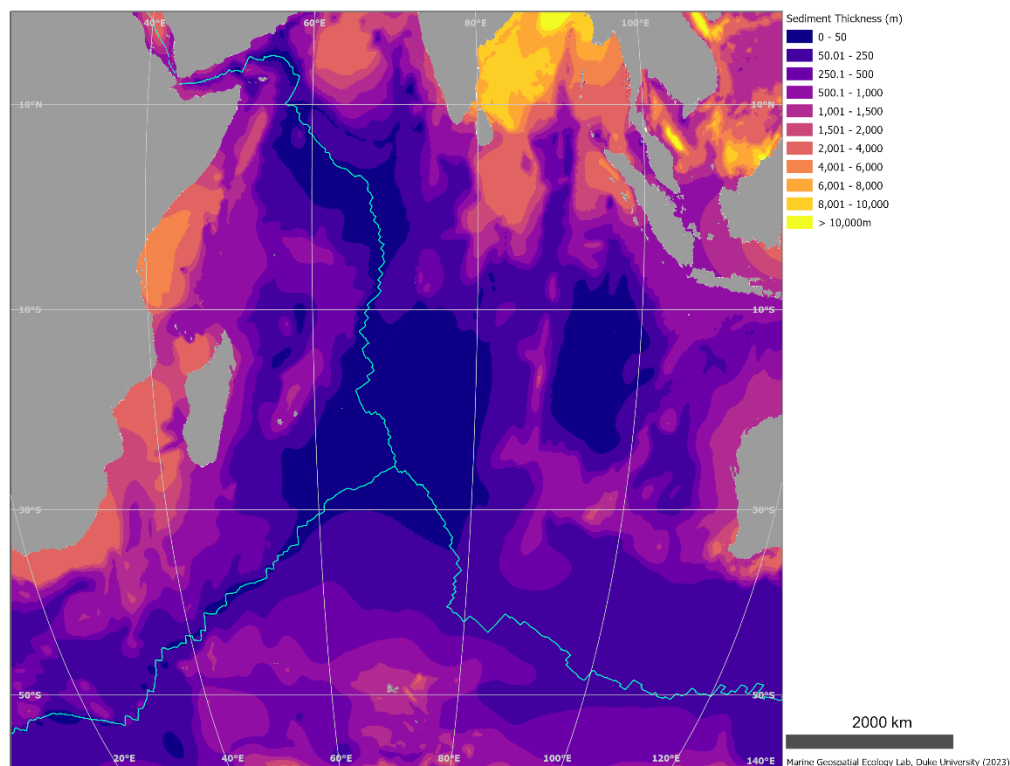


Figure 2.10-1 Sediment thickness

## 2.11 Seafloor Sediments

Abstract (Dutkiewicz et al. 2015)

“Knowing the patterns of distribution of sediments in the global ocean is critical for understanding biogeochemical cycles and how deep-sea deposits respond to environmental change at the sea surface. We present the first digital map of seafloor lithologies based on descriptions of nearly 14,500 samples from original cruise reports, interpolated using a support vector machine algorithm. We show that sediment distribution is more complex, with significant deviations from earlier hand-drawn maps, and that major lithologies occur in drastically different proportions globally. By coupling our digital map to oceanographic data sets, we find that the global occurrence of biogenic oozes is strongly linked to specific ranges in sea-surface parameters. In particular, by using recent computations of diatom distributions from pigment-calibrated chlorophyll-*a* satellite data, we show that, contrary to a widely held view, diatom oozes are not a reliable proxy for surface productivity. Their global accumulation is instead strongly dependent on low surface temperature (0.9–5.7 °C) and salinity (33.8–34.0 PSS, Practical Salinity Scale 1978) and high concentrations of nutrients. Under these conditions, diatom oozes will accumulate on the seafloor regardless of surface productivity as long as there is limited competition from biogenous and detrital components, and diatom frustules are not significantly dissolved prior to preservation. Quantifying the link between the seafloor and the sea surface through the use of large digital data sets will ultimately lead to more robust reconstructions and predictions of climate change and its impact on the ocean environment.”

Reference:

Dutkiewicz, A., R. Müller, S. O’Callaghan, and H. Jónasson. 2015. “Census of Seafloor Sediments in the World’s Ocean.” *Geology* 43 (9): 795–98. <https://doi.org/10.1130/G36883.1>.

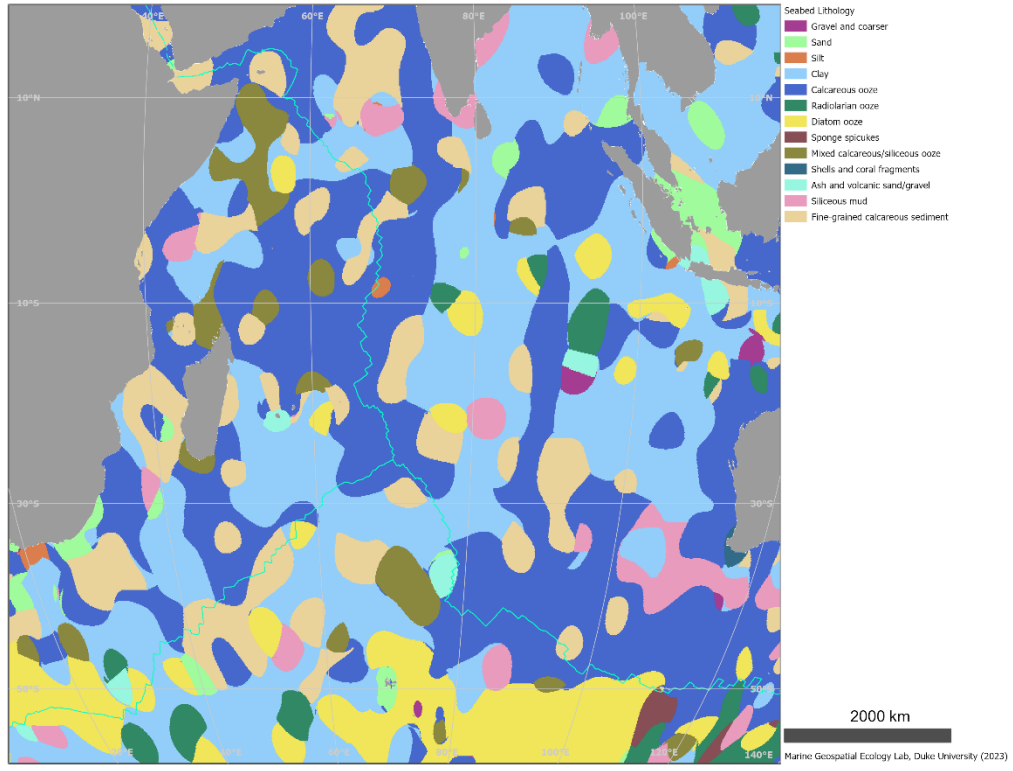


Figure 2.11-1 Seafloor sediments

## 2.12 Global Seabed Sediment Database

Abstract (Garlan et al. 2018):

“Production of a global sedimentological seabed map has been initiated in 1995 to provide the necessary tool for searches of aircraft and boats lost at sea, to give sedimentary information for nautical charts, and to provide input data for acoustic propagation modelling. This original approach had already been initiated one century ago when the French hydrographic service and the University of Nancy had produced maps of the distribution of marine sediments of the French coasts and then sediment maps of the continental shelves of Europe and North America. The current map of the sediment of oceans presented was initiated with a UNESCO's general map of the deep ocean floor. This map was adapted using a unique sediment classification to present all types of sediments: from beaches to the deep seabed and from glacial deposits to tropical sediments. In order to allow good visualization and to be adapted to the different applications, only the granularity of sediments is represented. The published seabed maps are studied, if they present an interest, the nature of the seabed is extracted from them, the sediment classification is transcribed and the resulted map is integrated in the world map. Data come also from interpretations of Multibeam Echo Sounder (MES) imagery of large hydrographic surveys of deep-ocean. These allow a very high-quality mapping of areas that until then were represented as homogeneous. The third and principal source of data comes from the integration of regional maps produced specifically for this project. These regional maps are carried out using all the bathymetric and sedimentary data of a region. This step makes it possible to produce a regional synthesis map, with the realization of generalizations in the case of over-precise data. 86 regional maps of the Atlantic Ocean, the Mediterranean Sea, and the Indian Ocean have been produced and integrated into the world sedimentary map.”

Reference:

Garlan, T., Gabelotaud, I., Lucas, S., & Marchès, E. (2018, June). A World Map of Seabed Sediment Based on 50 Years of Knowledge. In Proceedings of the 20th International Research Conference, New York, NY, USA (pp. 3-4).

Source: <https://data.shom.fr/>

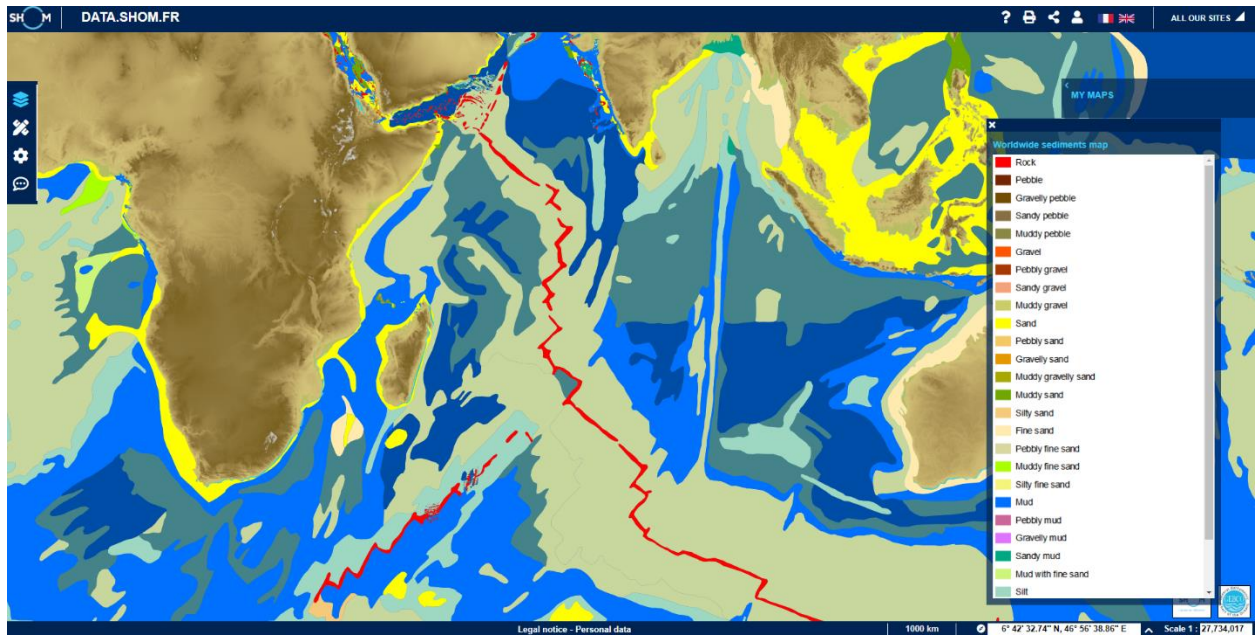


Figure 2.12-1 Global seabed sediment maps

## 2.13 Multibeam Bathymetric Survey Tracklines

“The Multibeam Bathymetry Database (MBBDB) at NCEI collects and archives multibeam data from the earliest commercial installations (circa 1980) through today's modern high-resolution collections. Data are acquired from both U.S. and international government and academic sources (see individual cruise metadata records for source information) and consist of the raw (as collected) sonar data files. Datasets may also include processed or edited versions of the sonar data, ancillary data (i.e., sound velocity data), derived products (i.e., grids), and/or metadata for the data collection. The MBBDB provides data that span the globe and are discoverable and accessible via map interface or text-only search options. This map service shows ship tracks for multibeam bathymetric surveys archived at NCEI.”

Source: <https://www.ngdc.noaa.gov/mgg/bathymetry/multibeam.html>

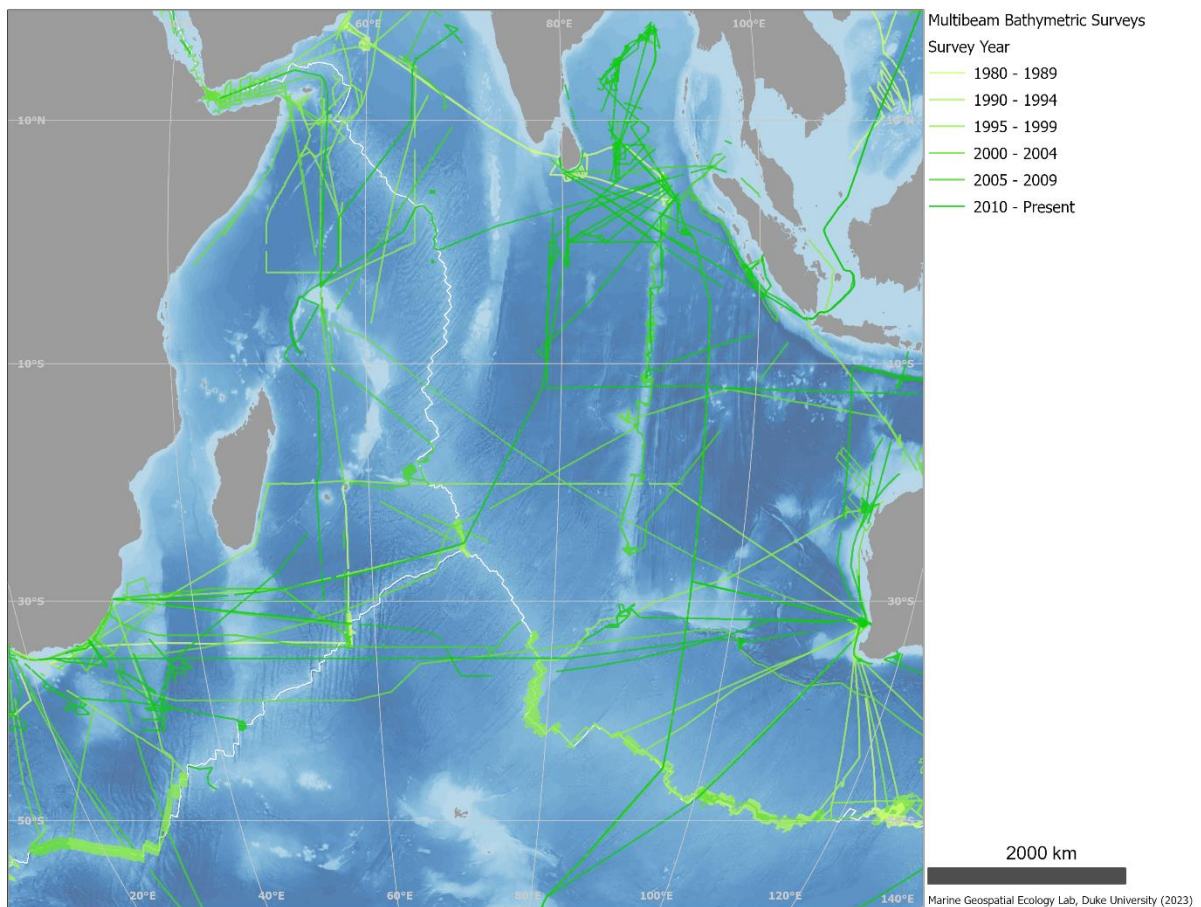


Figure 2.13-1 Multibeam bathymetry survey tracklines

## 2.14 Hybrid Coordinate Ocean Model (HYCOM) Data

The HYCOM consortium (<https://hycom.org/about>) is a multi-institutional effort sponsored by the National Ocean Partnership Program (NOPP), as part of the U.S. Global Ocean Data Assimilation Experiment (GODAE), to develop and evaluate a data-assimilative hybrid isopycnal-sigma-pressure (generalized) coordinate ocean model (called HYbrid Coordinate Ocean Model or HYCOM).

Data were summarized on Google Earth Engine as monthly averages from 2017-2022 for surface current velocity and sea surface elevation, and annually for 2022 for bottom current velocity. The maps below show examples of the monthly climatologies, but all the data layers will be available at the workshop and data can also be summarized into other climatologies as needed.

### References:

Chassignet, E. et al. 2009. US GODAE: Global Ocean Prediction with the HYbrid Coordinate Ocean Model (HYCOM). - *Oceanog.* 22: 64–75.

J. A. Cummings and O. M. Smedstad. 2013: Variational Data Assimilation for the Global Ocean. *Data Assimilation for Atmospheric, Oceanic and Hydrologic Applications vol II*, chapter 13, 303-343.

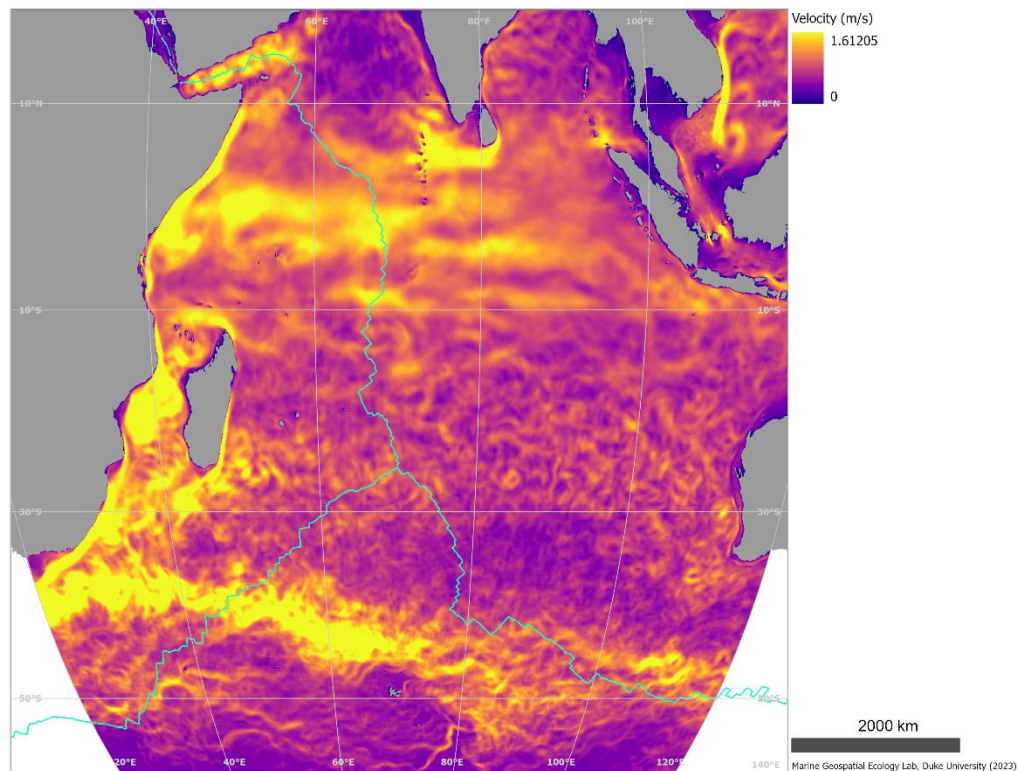


Figure 2.14-1 Current velocity, Surface, January average from 2017-2021

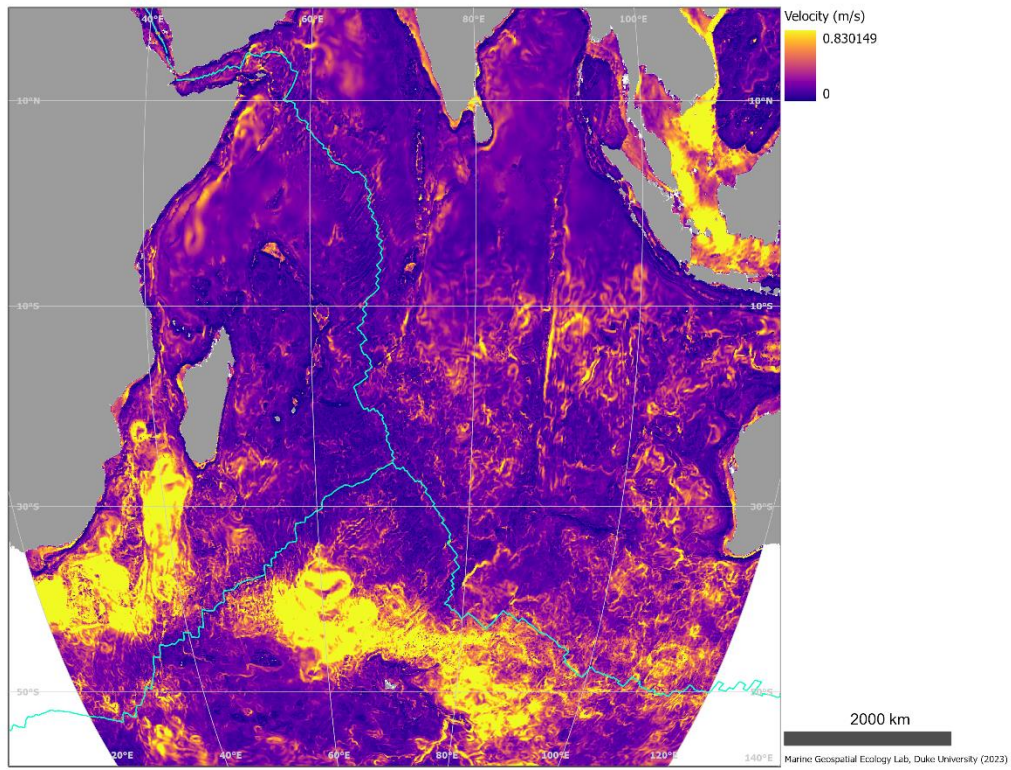


Figure 2.14-2 Current velocity, Bottom, 2022

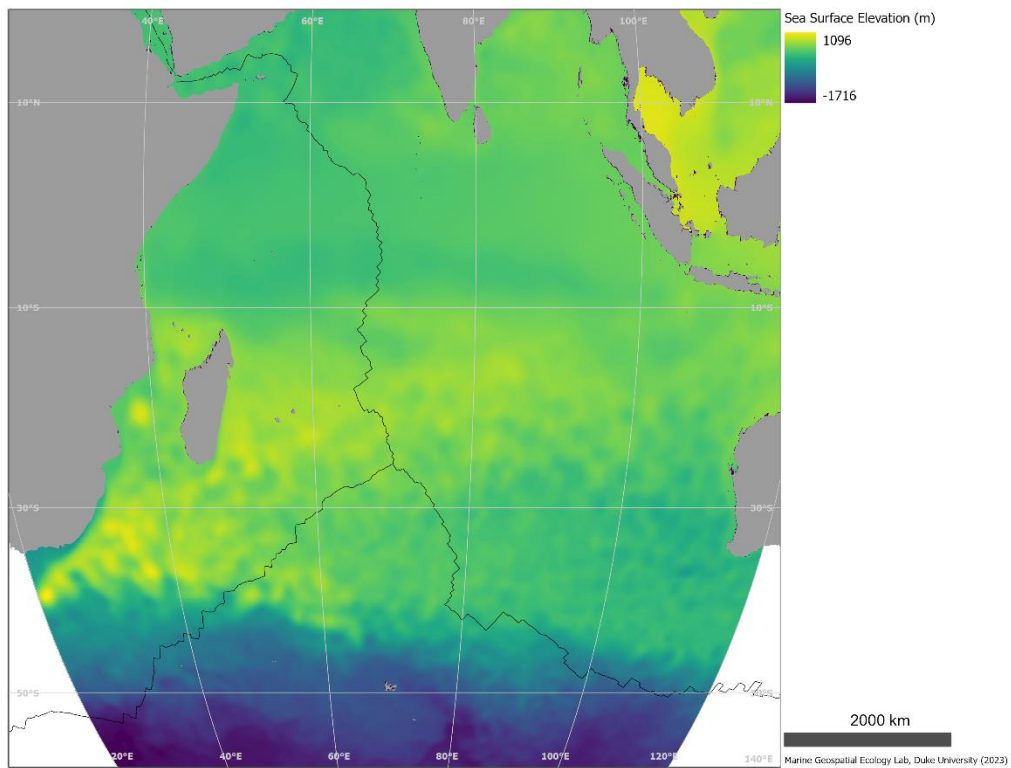


Figure 2.14-3 Sea surface elevation, January average from 2017-2021

## 2.15 Drifter Climatology of Near-Surface Currents

### Description:

“Satellite-tracked SVP drifting buoys (Sybrandy and Niiler, 1991; Niiler, 2001) provide observations of near-surface circulation at unprecedented resolution. In September 2005, the Global Drifter Array became the first fully realized component of the Global Ocean Observing System when it reached an array size of 1250 drifters. A drifter is composed of a surface float which includes a transmitter to relay data, a thermometer that reads temperature a few centimeters below the air/sea interface, and a submergence sensor used to detect when/if the drogue is lost. The surface float is tethered to a holey sock drogue, centered at 15 m depth. The drifter follows the flow integrated over the drogue depth, although some slip with respect to this motion is associated with direct wind forcing (Niiler and Paduan, 1995). This slip is greatly enhanced in drifters that have lost their drogues (Pazan and Niiler, 2000). Drifter velocities are derived from finite differences of their position fixes. These velocities, and the concurrent SST measurements, are archived at AOML's Drifting Buoy Data Assembly Center, where the data are quality controlled and interpolated to 1/4-day intervals (Hansen and Herman, 1989; Hansen and Poulain, 1996).”

Source: [https://www.aoml.noaa.gov/phod/gdp/mean\\_velocity.php](https://www.aoml.noaa.gov/phod/gdp/mean_velocity.php)

### Reference:

Laurindo, L. C., Mariano, A. J., & Lumpkin, R. (2017). An improved near-surface velocity climatology for the global ocean from drifter observations. *Deep Sea Research Part I: Oceanographic Research Papers*, 124, 73-92. doi: 10.1016/j.dsr.2017.04.009

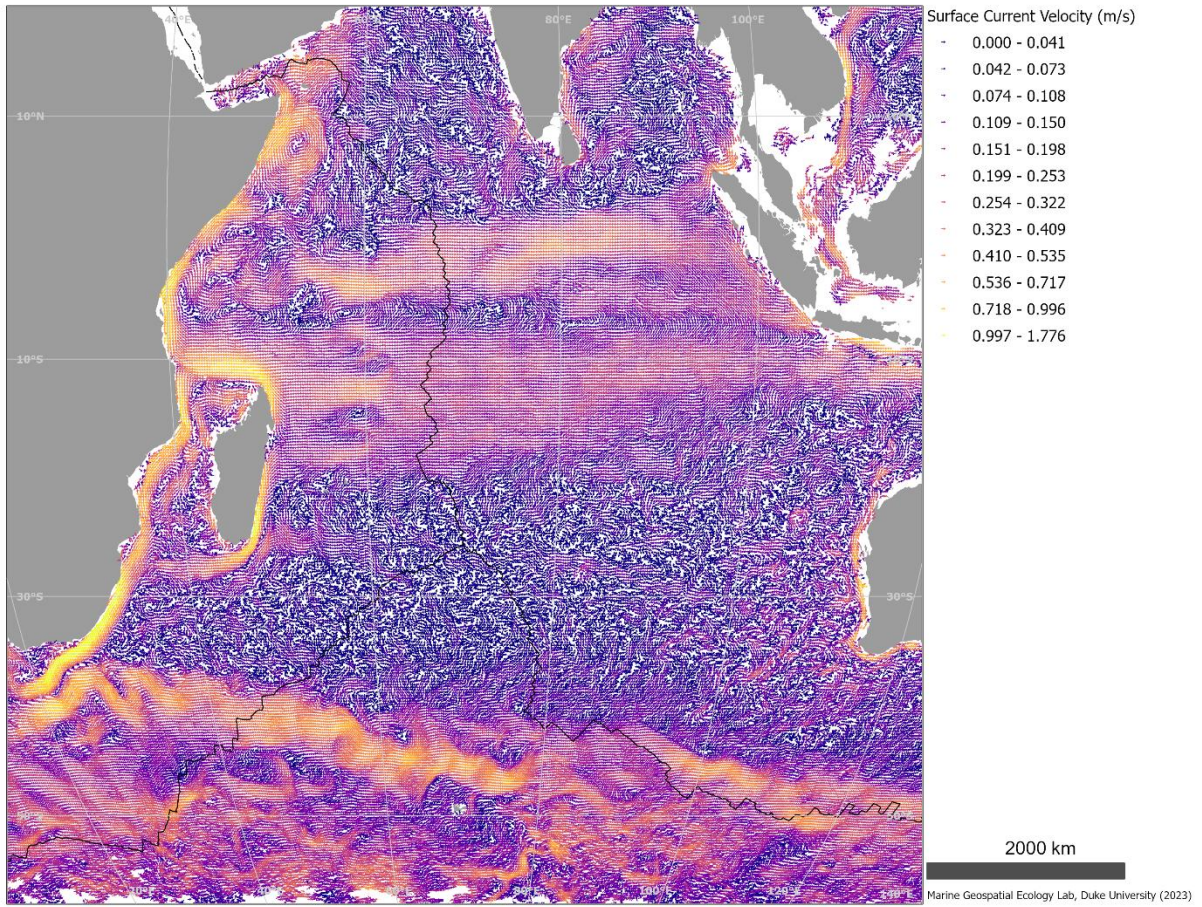


Figure 2.15-1 Drifter-derived climatology of near-surface currents

## 2.16 Seafloor POC Flux

Abstract (Sweetman et al. 2017):

The deep sea encompasses the largest ecosystems on Earth. Although poorly known, deep seafloor ecosystems provide services that are vitally important to the entire ocean and biosphere. Rising atmospheric greenhouse gases are bringing about significant changes in the environmental properties of the ocean realm in terms of water column oxygenation, temperature, pH and food supply, with concomitant impacts on deep-sea ecosystems. Projections suggest that abyssal (3000–6000 m) ocean temperatures could increase by 1°C over the next 84 years, while abyssal seafloor habitats under areas of deep-water formation may experience reductions in water column oxygen concentrations by as much as 0.03 mL L<sup>-1</sup> by 2100. Bathyal depths (200–3000 m) worldwide will undergo the most significant reductions in pH in all oceans by the year 2100 (0.29 to 0.37 pH units). O<sub>2</sub> concentrations will also decline in the bathyal NE Pacific and Southern Oceans, with losses up to 3.7% or more, especially at intermediate depths. Another important environmental parameter, the flux of particulate organic matter to the seafloor, is likely to decline significantly in most oceans, most notably in the abyssal and bathyal Indian Ocean where it is predicted to decrease by 40–55% by the end of the century. Unfortunately, how these major changes will affect deep-seafloor ecosystems is, in some cases, very poorly understood. In this paper, we provide a detailed overview of the impacts of these changing environmental parameters on deep-seafloor ecosystems that will most likely be seen by 2100 in continental margin, abyssal and polar settings. We also consider how these changes may combine with other anthropogenic stressors (e.g., fishing, mineral mining, oil and gas extraction) to further impact deep-seafloor ecosystems and discuss the possible societal implications.

Reference:

Sweetman, AK et al 2017 Major impacts of climate change on deep-sea benthic ecosystems. *Elem Sci Anth*, 5: 4, DOI: <https://doi.org/10.1525/elementa.203>

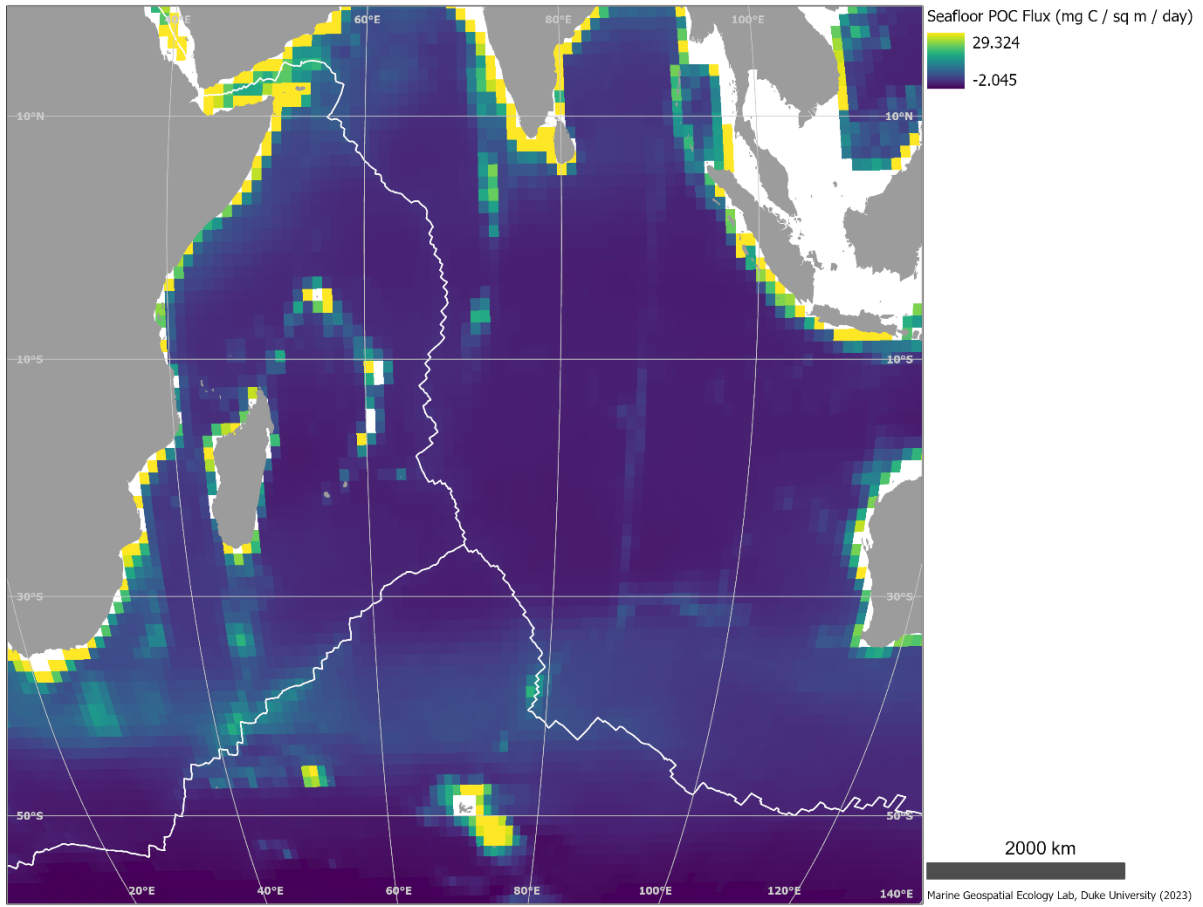


Figure 2.16-1 Seafloor POC flux

## 2.17 MODIS Data

“MODIS (or Moderate Resolution Imaging Spectroradiometer) is a key instrument aboard the Terra (EOS AM) and Aqua (EOS PM) satellites. Terra's orbit around the Earth is timed so that it passes from north to south across the equator in the morning, while Aqua passes south to north over the equator in the afternoon. Terra MODIS and Aqua MODIS view the entire Earth's surface every 2 days, acquiring data in 36 spectral bands (see MODIS Technical Specifications). These data improve our understanding of global dynamics and processes occurring on the land, in the oceans, and in the lower atmosphere. MODIS plays a vital role in the development of validated, global, interactive Earth system models able to predict global change accurately enough to assist policy makers in making sound decisions concerning the protection of our environment.”

MODIS sea surface temperature, chlorophyll a, and particulate organic carbon (POC) flux were summarized into 5 year (2017-2021) monthly climatologies using Google Earth Engine. Additionally, the chlorophyll a mean concentration from 2012-2021 was derived from Google Earth Engine. The net primary productivity (NPP) was summarized as a mean concentration from 2017-2021. The maps below show examples of the generated climatologies, but all the data layers will be available at the workshop and data can also be summarized at other time scales as needed.

Citation:

NASA Goddard Space Flight Center, Ocean Ecology Laboratory, Ocean Biology Processing Group. Moderate-resolution Imaging Spectroradiometer (MODIS) Aqua Ocean Color Data; NASA OB.DAAC, Greenbelt, MD, USA.

NPP Data Source:

<https://coastwatch.pfeg.noaa.gov/erddap/griddap/erdMH1ppmday.html>

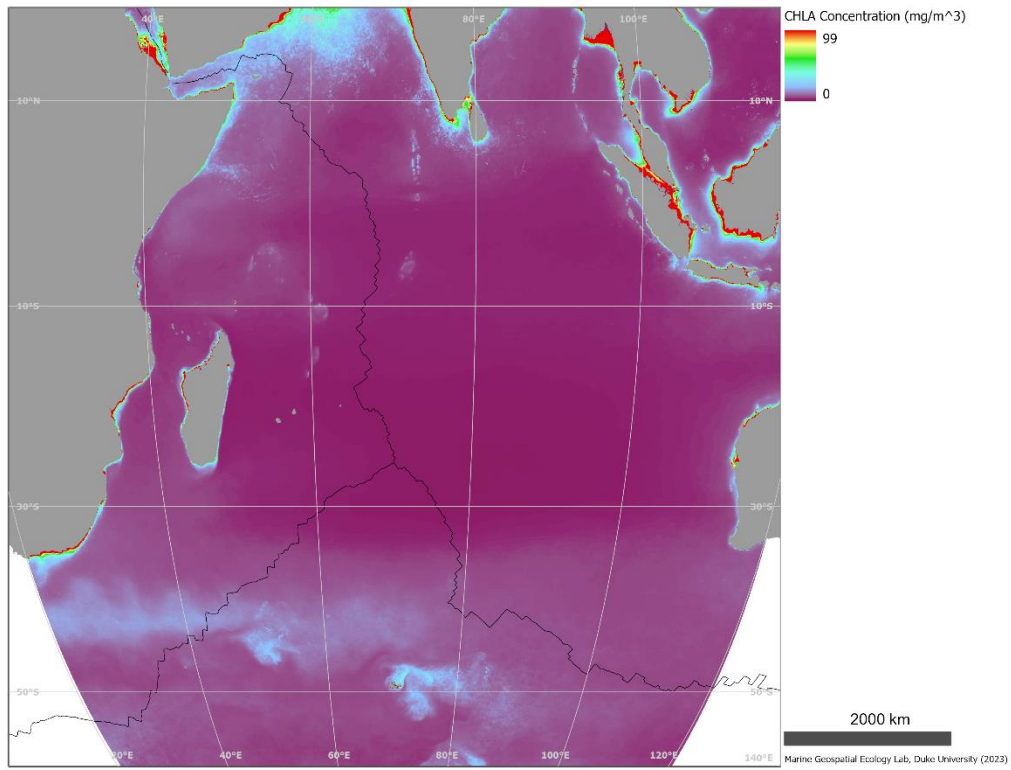


**Figure 2.17-1 Mean Chlorophyll a concentration from 2012-2021**

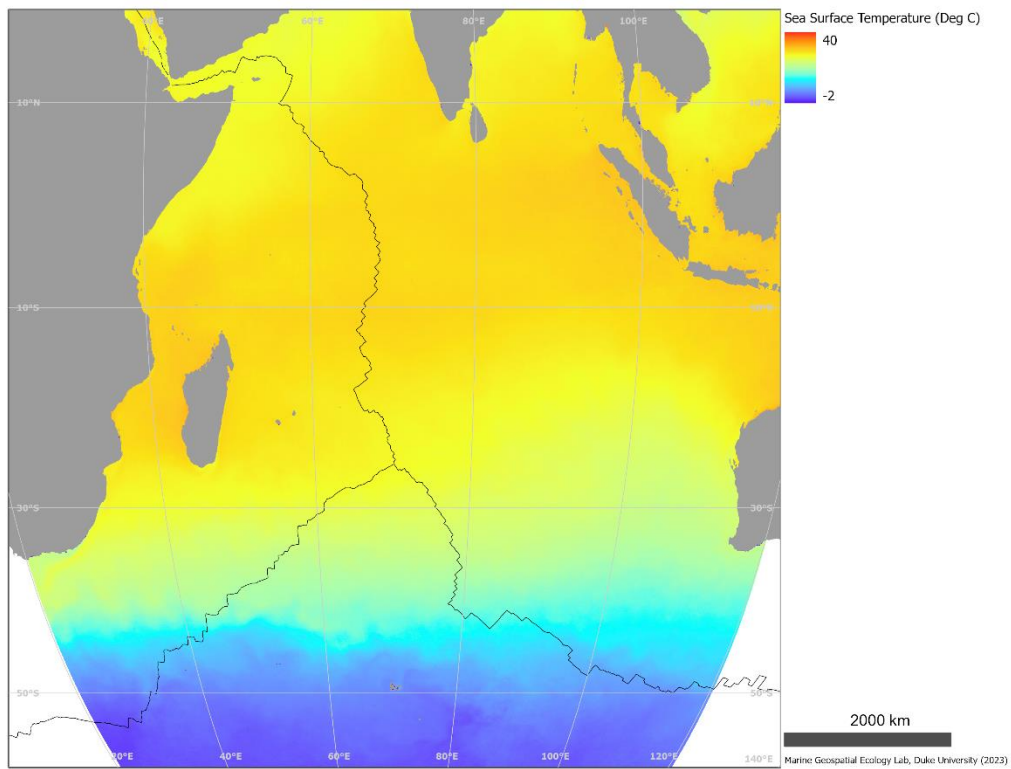


**Figure 2.17-2 Sea surface temperature, January 2017-2021**

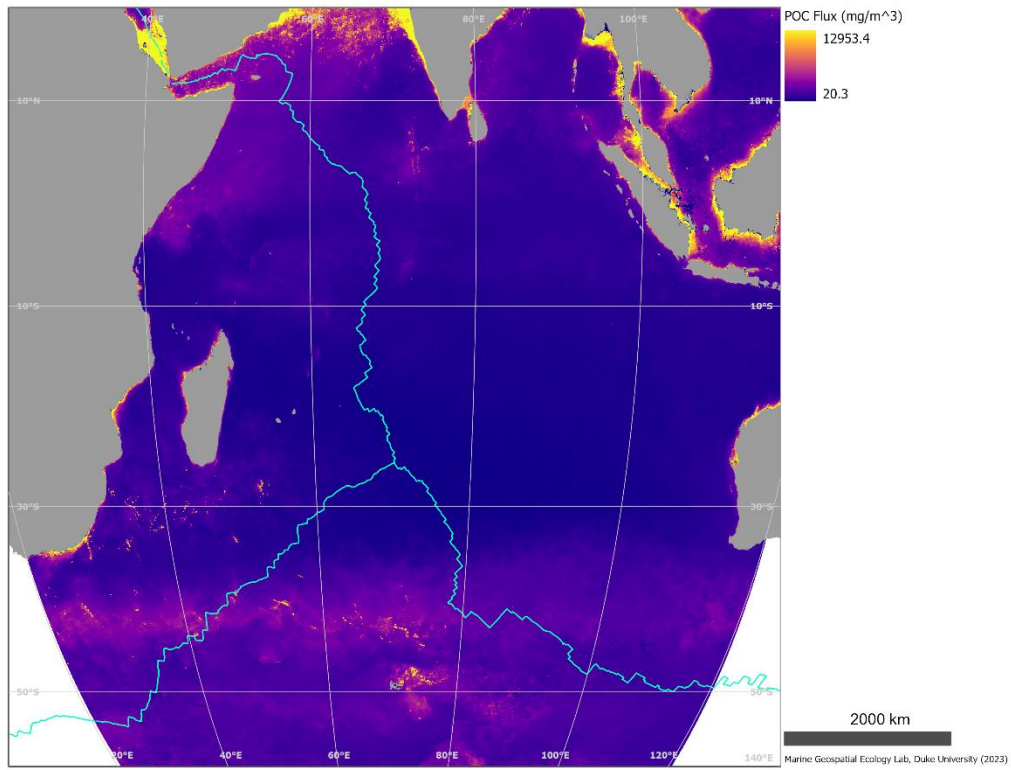


Figure 2.17-3 Particulate organic carbon flux, January 2017-2022

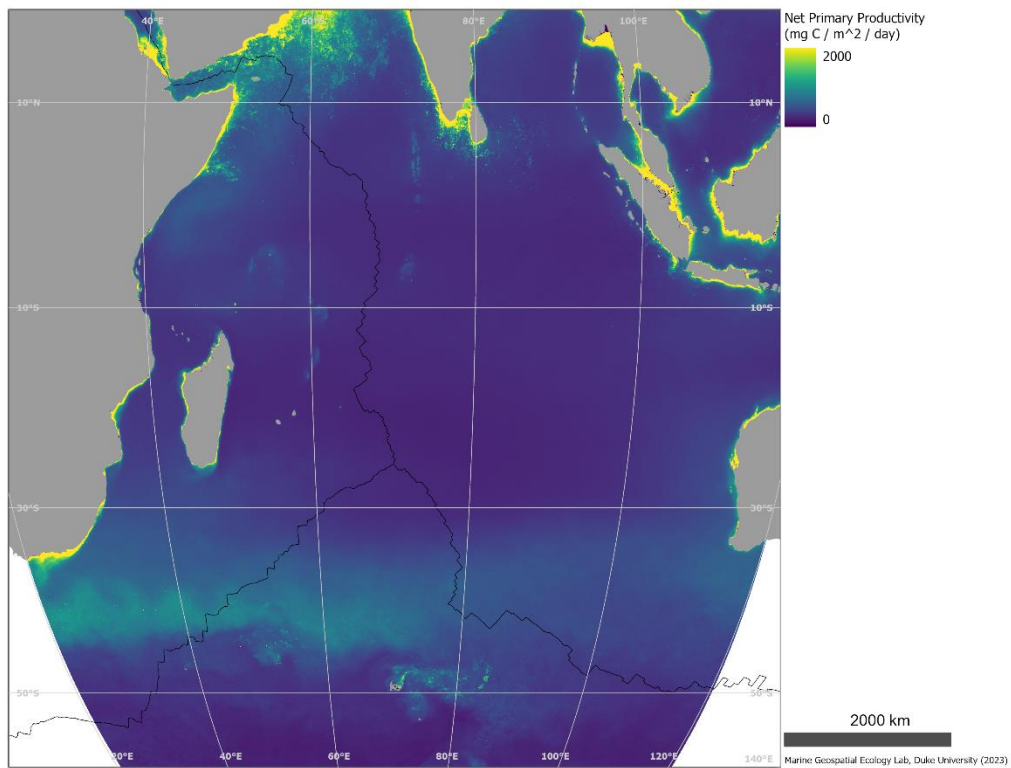


Figure 2.17-4 Net primary productivity climatology from 2017-2022



## 2.18 Vertically Generalized Production Model (VGPM) Primary Productivity

### Description:

“Standard Ocean Productivity Products are based on the original description of the Vertically Generalized Production Model (VGPM) (Behrenfeld & Falkowski 1997), MODIS surface chlorophyll concentrations (Chl<sub>sat</sub>), MODIS 11-micron daytime sea surface temperature data (SST), and MODIS cloud-corrected incident daily photosynthetically active radiation (PAR). Euphotic depths are calculated from Chl<sub>sat</sub> following Morel and Berthon (1989).”

For this effort, a cumulative climatology was created from Standard VGPM data derived from MODIS data from 2015-2019 (inclusive).

### Reference:

Behrenfeld MJ, Falkowski PG (1997) Photosynthetic rates derived from satellite-based chlorophyll concentration. *Limnology And Oceanography* 42:1–20.

### Source:

<http://sites.science.oregonstate.edu/ocean.productivity/standard.product.php>

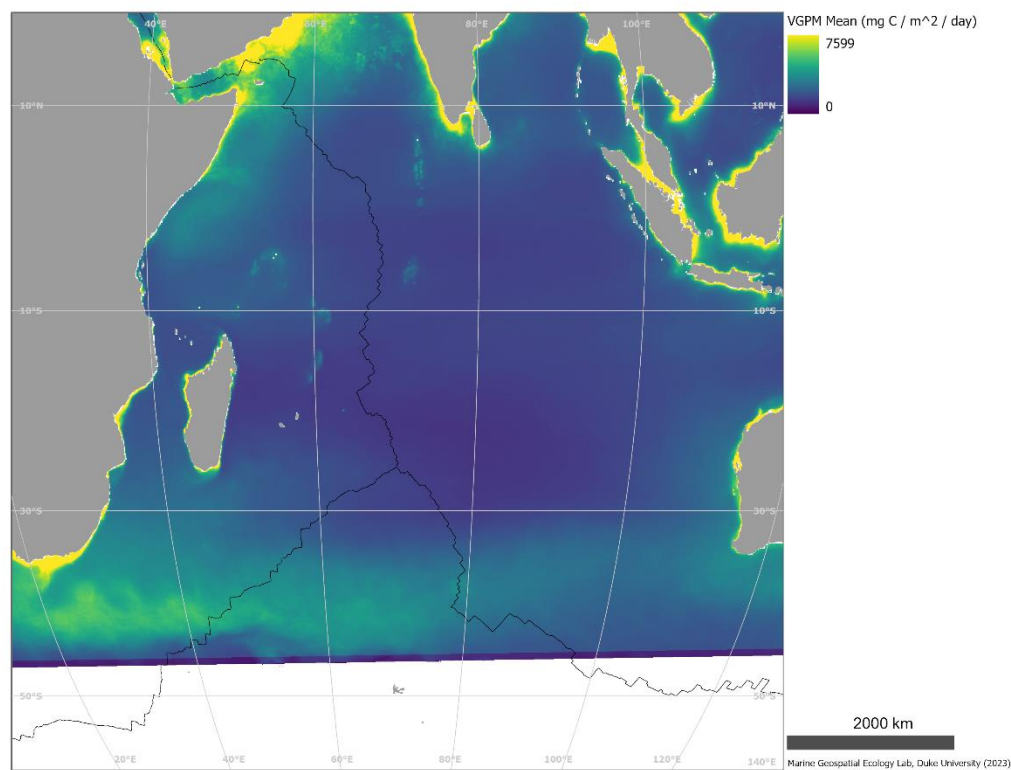


Figure 2.18-1 Vertically generalized production model - primary productivity climatology from 2015-2019

## 2.19 Global Ocean Low and Mid Trophic Levels Biomass Hindcast

### Description:

“The low and mid-trophic levels (LMTL) reanalysis for global ocean is produced at (<https://www.cls.fr>) (Toulouse, France). It provides 2D fields of zooplankton biomass and six groups of micronekton biomass for the time period 1998-2016 at 1/4 degree and weekly time resolution. It uses the LMTL component of dynamical population model (<http://www.seapodym.eu/>). No data assimilation in this product.

- Latest SEAPODYM LMTL version (2.1.03) <http://www.seapodym.eu/>

### Forcings:

- Ocean currents and ocean temperature from FREEGLORYS2V4 ocean physics produced at Mercator-Ocean
- Net Primary Production (NPP) computed from chlorophyll, Sea Surface Temperature (SST) and Photosynthetically Active Radiation (PAR) satellite observation and model
- daily SST from NOAA NCEI AVHRR-only (Reynolds (<https://www.ncdc.noaa.gov/oisst>)) and PAR from <https://apps.ecmwf.int/datasets/data/interim-full-daily/levtype=sfc>”

Source: [http://marine.copernicus.eu/services-portfolio/access-to-products/?option=com\\_csw&view=details&product\\_id=GLOBAL\\_REANALYSIS\\_BIO\\_001\\_033](http://marine.copernicus.eu/services-portfolio/access-to-products/?option=com_csw&view=details&product_id=GLOBAL_REANALYSIS_BIO_001_033)

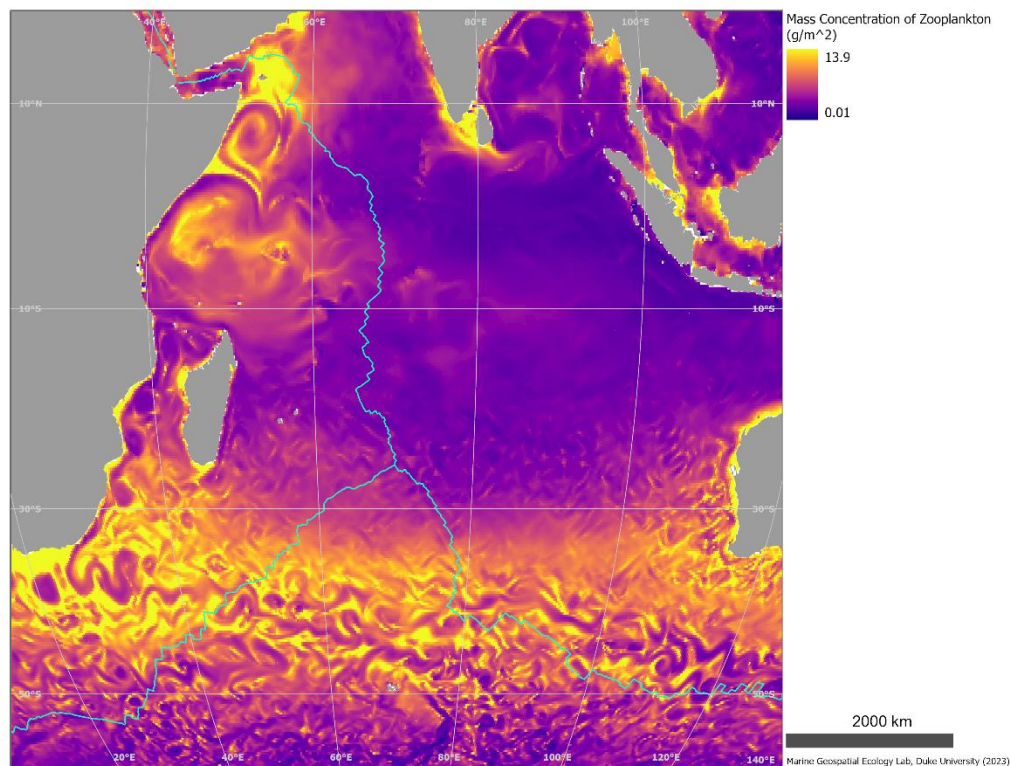


Figure 2.19-1 Zooplankton biomass, June 2016

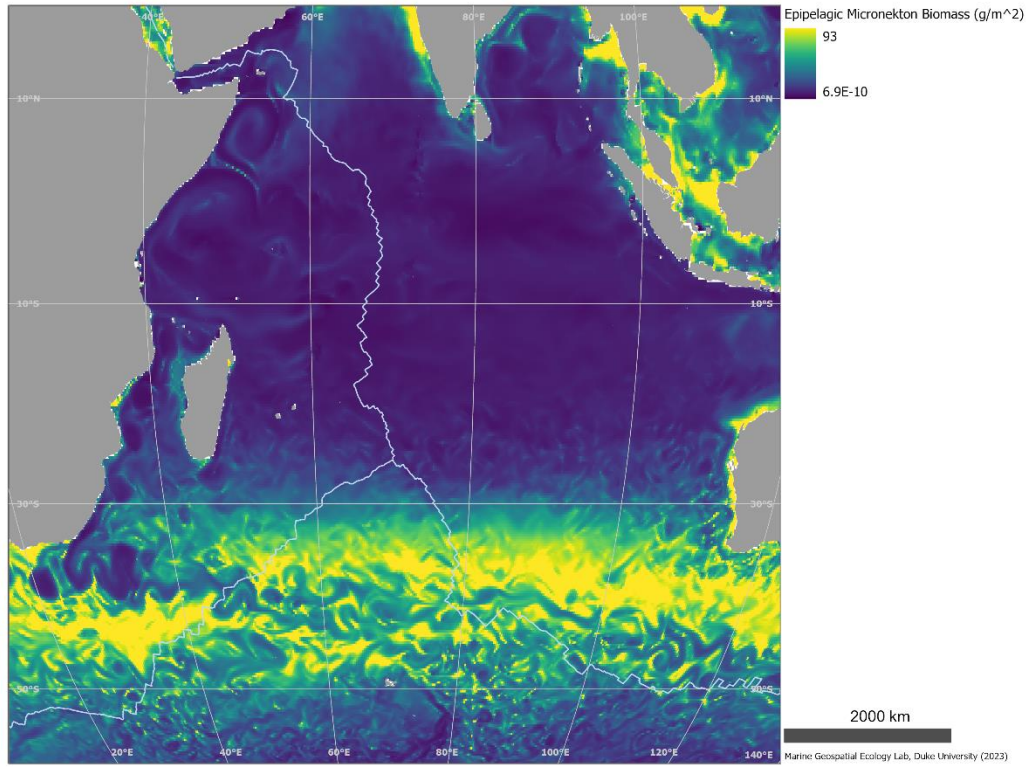


Figure 2.19-2 Epipelagic micronekton biomass, June 2018

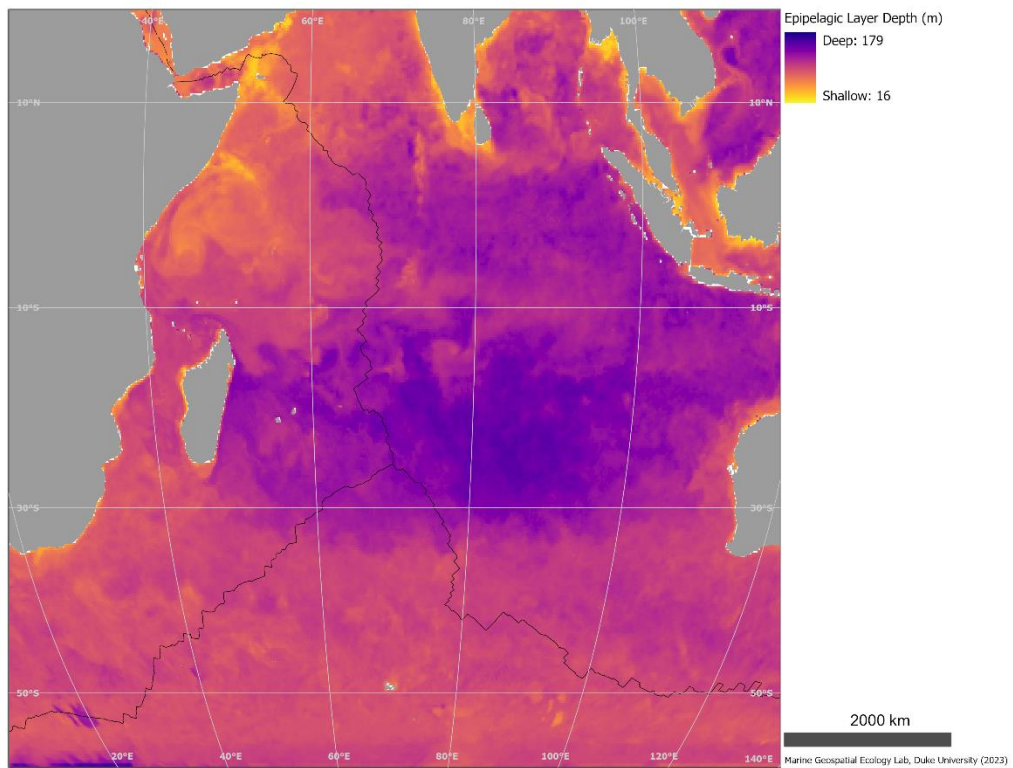


Figure 2.19-3 Epipelagic layer depth, June 2018

## 2.20 Environmental Predictors for Polymetallic Nodules

Abstract (Dutkiewicz et al. 2020):

“Polymetallic nodules found on the abyssal plains of the oceans represent one of the slowest known geological processes, and are a source of critical and rare metals for frontier technologies. A quantitative assessment of their occurrence worldwide has been hampered by a research focus on the northeastern Pacific Ocean and the lack of a global open-access data set of nodules. We have compiled a global data set of >10,000 seabed nodule and control samples, and combine it with digital grids of key environmental parameters to generate a predictive machine-learning model of nodule occurrence. In order of decreasing parameter ranking, we find that nodules are associated with very low sedimentation rates (< 0.5 cm/k.y.), moderately high oxygen values (150 and 210 mmol/m<sup>3</sup>), lithologies of clay followed by calcareous ooze, low summer surface productivity (<300 mgC/m<sup>2</sup>/day), low benthic biomass concentration (<1 log mgC/m<sup>2</sup>), water depths >4500 m, and low total organic carbon content (0.3–0.5 wt%). Competing hypotheses for nodule sustention and thus continued growth on the seafloor are the removal of sediment by bottom-water currents and biological activity. Using a high-resolution eddy-resolving ocean circulation model, we find that the bottom-current speeds over nodule fields are too low (<5 cm/s) to remove sediment, implicating the activity of epibenthic megafauna as the most likely mechanism. Our global nodule probability map combined with the assessment of a range of environmental drivers provides an improved basis for decision and policy making in the controversial area of deep-sea exploration.”

Reference:

Dutkiewicz, Adriana, Alexander Judge, and R. Dietmar Müller. "Environmental predictors of deep-sea polymetallic nodule occurrence in the global ocean." *Geology* 48, no. 3 (2020): 293-297. <https://doi.org/10.1130/G46836.1>

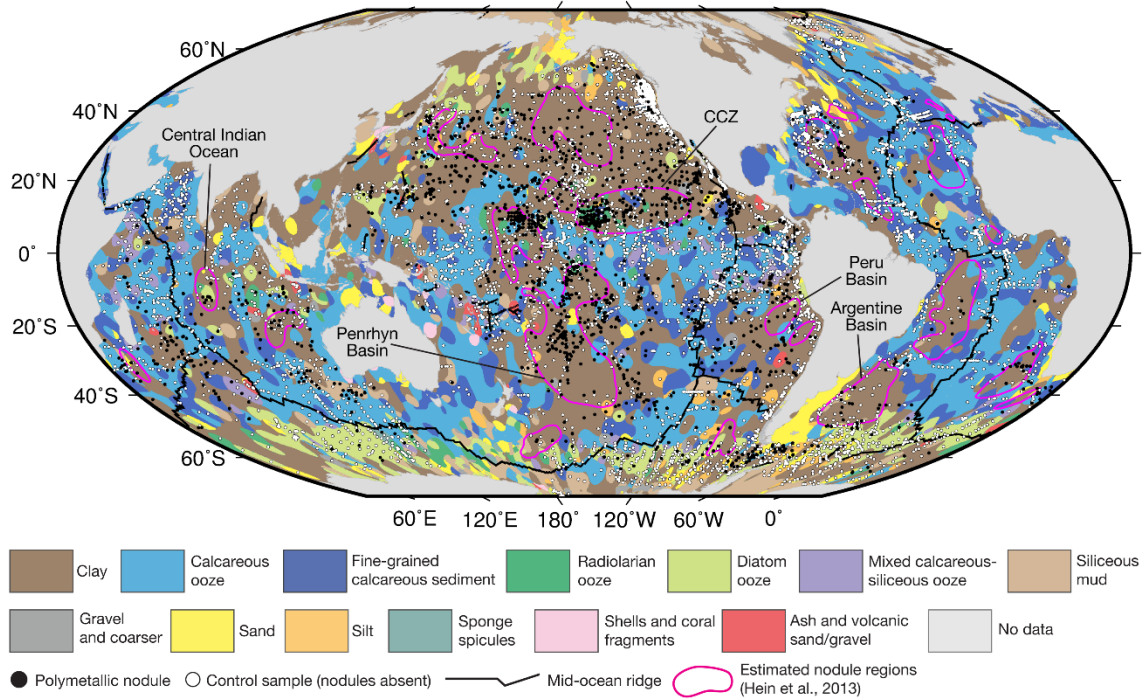


**Figure 2.20-1 Global distribution of polymetallic nodules**

*Original Caption: Figure 1. Polymetallic nodule occurrences in the global ocean. Nodules (black dots) and control samples lacking nodules (white dots) are shown in relation to seafloor lithology (Dutkiewicz et al., 2015). Mollweide projection. CCZ—Clarion-Clipperton Zone.*

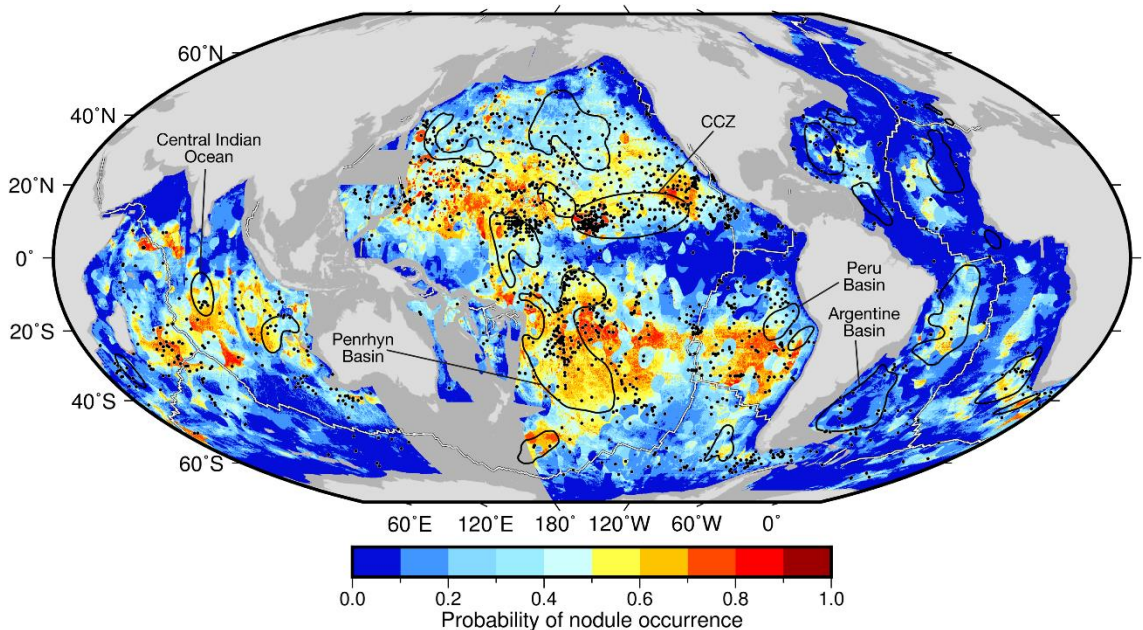


**Figure 2.20-2 Predicted distribution of polymetallic nodules**

*Original Caption: Figure 3. Prediction of probability of polymetallic nodule occurrence. Dark gray denotes regions with missing data in at least one of the environmental data sets (Figs. DR1–DR7 [see footnote 1]). Nodules are shown as black dots. Black outline indicates known nodule fields*

*and poorly explored areas that are deemed to be permissive for economic development (Hein et al., 2013). Uncertainty of nodule occurrence probability is represented by lower and upper bounds of 90% credible interval for probability estimate, based on joint uncertainty in all model parameters (Figs. DR8 and DR9 [see footnote 1]). Our predictions exclude nodule density. CCZ—Clarion-Clipperton Zone. Mollweide projection.*

## 2.21 Geology of Longqi-1 Hydrothermal System on Ultraslow-Spreading Southwest Indian Ridge

Abstract (Liang et al. 2023):

“The distribution of hydrothermal vents and the biogeography of associated faunal communities in the Indian Ocean are still not well studied, particularly the ultraslow-spreading Southwest Indian Ridge (SWIR). Herein, we present the geological and morphological data for the first reported active hydrothermal field on the ultraslow-spreading center. In this context, we created a detailed seafloor map based on visual data obtained from human-occupied vehicle (HOV) dives. Longqi-1 vent field (LVF) is an off-axis, mafic-hosted but detachment fault-controlled, high-temperature hydrothermal area with at least 28 hydrothermal structures, and their contacting host rocks were identified and mapped. The morphologies of hydrothermal structures in the LVF exhibit unique characteristics, with Zone M characterized by chimneys grown on the relatively flat-lying sulfide mound and Zone S characterized by large sulfide mounds and steep-sided structures hosting large flanges, and isolated beehive structures occurred more often at the boundary between hydrothermal deposits and basalts outcrops in both M and S zone. Microscopic examination showed that anhydrite is the dominant sulfate phase and chalcopyrite, pyrite, pyrrhotite, and sphalerite are the dominant sulfide minerals. Subseafloor hydrothermal circulation controlled by the detachment fault and local fracture zone may have directly determined the morphology of the sulfide structure in the LVF. Our results provide a picture of the LVF as well as complement and expand on previous studies on metal resource evaluation along the SWIR and Indian Ocean ridges, a detailed scenario for studying the surface distribution characteristics of hydrothermal circulation and its relationship with the distribution of hydrothermal fauna, and further enhance our understanding of the formation of modern seafloor hydrothermal systems.”

Reference:

Liang, J., Tao, C., Zheng, Y., Zhang, G., Su, C., Yang, W., Liao, S. and Wang, N., 2023. Geology context, vent morphology, and sulfide paragenesis of the Longqi-1 modern seafloor hydrothermal system on the ultraslow-spreading Southwest Indian ridge. *Deep Sea Research Part I: Oceanographic Research Papers*, p.103962. <https://doi.org/10.1016/j.dsr.2023.103962>

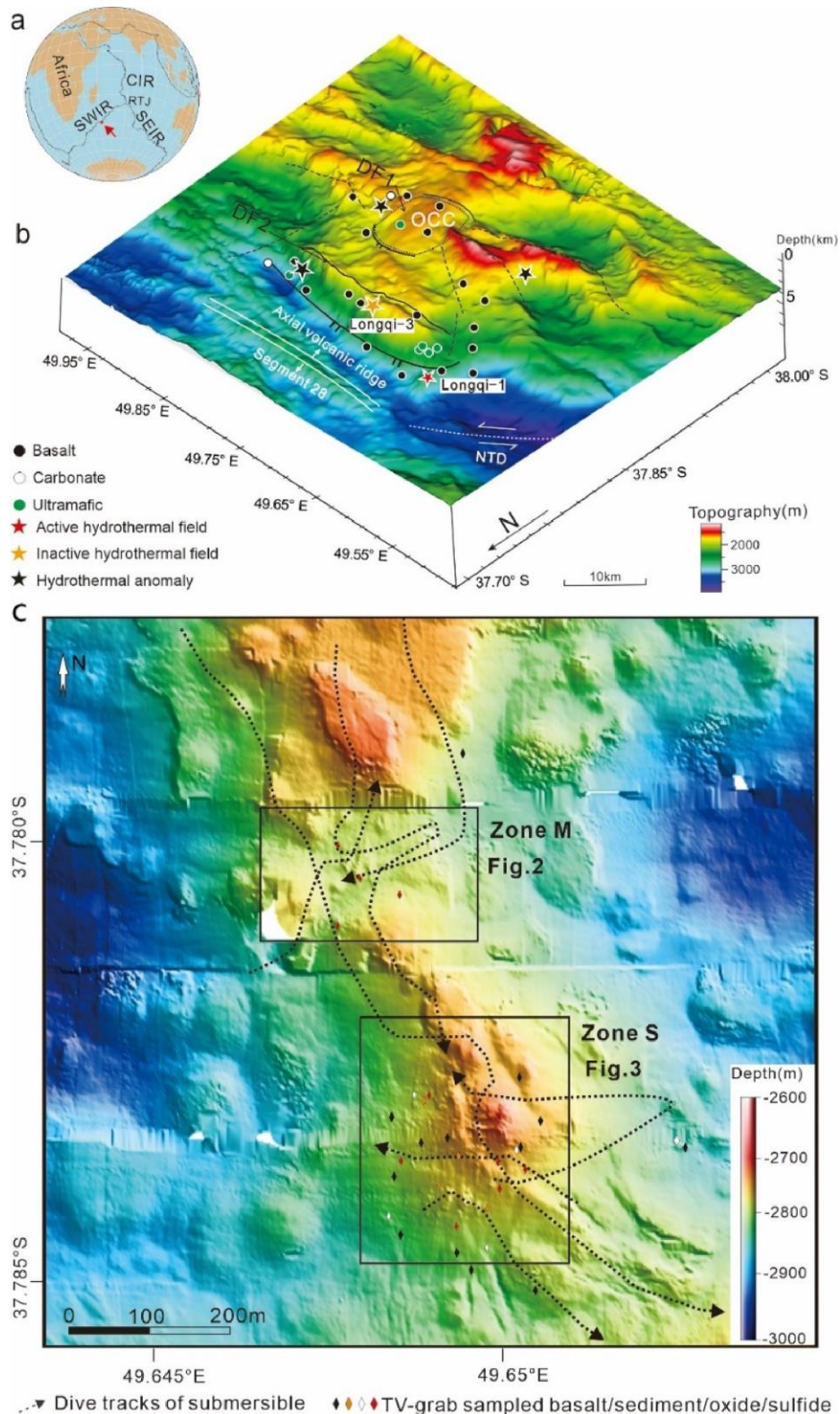


**Figure 2.21-1 Bathymetry and benthic features along the Longqi-1 hydrothermal vent system**

*Original Caption: Figure 1. a. location of the study area on the SWIR. b. Bathymetry with tectonic and hydrothermal features showing the location of the LVF on the hanging wall of the initiated detachment fault, modified from Tao et al. (2020). c. bathymetry map of LVF showing*

*the Zones S and M, and some tracks of the submersible dives. Bathymetric data were collected using multibeam surveys of Chinese Dayang cruises. BTJ- Rodriguez triple junction; RTJ- Bouvet triple junction; IFZ-Indomed fault zone; GFZ-Gallieni fault zone; NTD-Nontransform discontinuities; OCC-Oceanic core complex.*

## 2.22 The Daxi Vent Field

Abstract (Wang et al. 2021):

“The distribution of hydrothermal vents and the biogeography of associated faunal communities in the Indian Ocean are still not well studied. This is especially true for Carlsberg Ridge, the northernmost part of the Indian Ocean spreading system. Here we report geological, morphological, biological, and hydrochemical data for the newly discovered Daxi Vent Field (DVF) on the slow-spreading Carlsberg Ridge at 6°48'N. The DVF is a basalt-hosted hydrothermal field situated atop a rifted volcanic ridge, located in a non-transform offset between two second-order ridge segments. There are three hydrothermal sites, i.e. Central mound, NE mound, and South mound. Eight vigorously venting black smokers were observed in the central hydrothermal mound. The largest sulfide chimney “Baochu Pagoda” is ~24 m tall. Another inactive chimney, which is silica-rich is observed in the NE mound. The sulfide chimneys are dominated by sphalerite and pyrrhotite containing high Sn, Co and Ag. The silica-rich chimney contains high SiO<sub>2</sub> and Ba contents. Seven species of megafauna were identified, including alvinellid worms, which were collected in the Indian Ocean for the first time. *Rimicaris kairei* and actinostolid anemones dominate the community in the central areas and on the periphery of the vent field, respectively. The occurrence of DVF is quite unique as it is located on a non-transform offset and it is mafic-hosted. So far only nine hydrothermal fields with the similar geological setting have ever been reported among nearly 700 hydrothermal sites in the World’s Ocean.”

Reference:

Wang, Y., Han, X., Zhou, Y., Qiu, Z., Yu, X., Petersen, S., Li, H., Yang, M., Chen, Y., Liu, J. and Wu, X., 2021. The Daxi Vent Field: an active mafic-hosted hydrothermal system at a non-transform offset on the slow-spreading Carlsberg Ridge, 6° 48' N. *Ore Geology Reviews*, 129, p.103888.

<https://doi.org/10.1016/j.oregeorev.2020.103888>

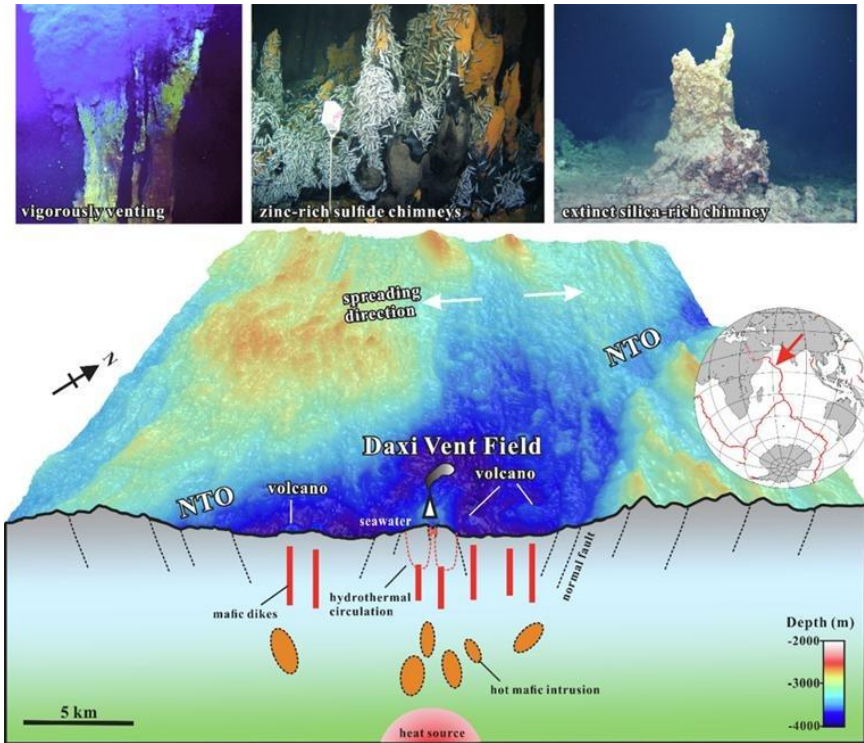


Figure 2.22-1 Hydrothermal vents in the Daxi Vent Field

Original Caption: Graphical abstract

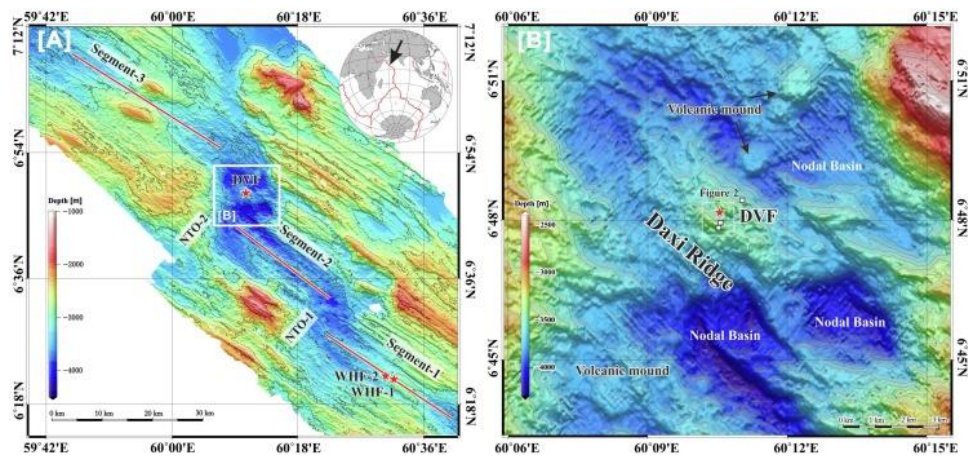


Figure 2.22-2 Location of active hydrothermal vents in the Daxi Vent Field

Original Caption: Figure 1. Map of the location of the active vent field.

## 2.23 Geomorphology and Seafloor Processes in the Remote Southeast Indian Ocean

Abstract (Picard et al. 2018):

“A high-resolution multibeam echosounder (MBES) dataset covering over 279,000 km<sup>2</sup> was acquired in the southeastern Indian Ocean to assist the search for Malaysia Airlines Flight 370 (MH370) that disappeared on 8 March 2014. The data provided an essential geospatial framework for the search and is the first large-scale coverage of MBES data in this region. Here we report on geomorphic analyses of the new MBES data, including a comparison with the Global Seafloor Geomorphic Features Map (GSFM) that is based on coarser resolution satellite altimetry data, and the insights the new data provide into geological processes that have formed and are currently shaping this remote deepsea area. Our comparison between the new MBES bathymetric model and the latest global topographic/bathymetric model (SRTM15\_plus) reveals that 62% of the satellite-derived data points for the study area are comparable with MBES measurements within the estimated vertical uncertainty of the SRTM15\_plus model ( $\pm 100$  m). However, > 38% of the SRTM15\_plus depth estimates disagree with the MBES data by > 100 m, in places by up to 1900 m. The new MBES data show that abyssal plains and basins in the study area are significantly more rugged than their representation in the GSFM, with a 20% increase in the extent of hills and mountains. The new model also reveals four times more seamounts than presented in the GSFM, suggesting more of these features than previously estimated for the broader region. This is important considering the ecological significance of high-relief structures on the seabed, such as hosting high levels of biodiversity. Analyses of the new data also enabled sea knolls, fans, valleys, canyons, troughs, and holes to be identified, doubling the number of discrete features mapped.

Importantly, mapping the study area using MBES data improves our understanding of the geological evolution of the region and reveals a range of modern sedimentary processes. For example, a large series of ridges extending over approximately 20% of the mapped area, in places capped by sea knolls, highlight the preserved seafloor spreading fabric and provide valuable insights into Southeast Indian Ridge seafloor spreading processes, especially volcanism. Rifting is also recorded along the Broken Ridge – Diamantina Escarpment, with rift blocks and well-bedded sedimentary bedrock outcrops discernible down to 2400 m water depth. Modern ocean floor sedimentary processes are documented by sediment mass transport features, especially along the northern margin of Broken Ridge, and in pockmarks (the finest-scale features mapped), which are numerous south of Diamantina Trench and appear to record gas and/or fluid discharge from underlying marine sediments. The new MBES data highlight the complexity of the search area and serve to demonstrate how little we know about the vast areas of the ocean that have not been mapped with MBES. The availability of high-resolution and accurate maps of the ocean floor can clearly provide new insights into the Earth's geological evolution, modern ocean floor processes, and the location of sites that are likely to have relatively high biodiversity.”

Reference:

Picard, K., Brooke, B.P., Harris, P.T., Siwabessy, P.J., Coffin, M.F., Tran, M., Spinoccia, M., Weales, J., Macmillan-Lawler, M. and Sullivan, J., 2018. Malaysia Airlines flight MH370 search data reveal geomorphology and seafloor processes in the remote southeast Indian Ocean. *Marine Geology*, 395, pp.301-19. <https://doi.org/10.1016/j.margeo.2017.10.014>

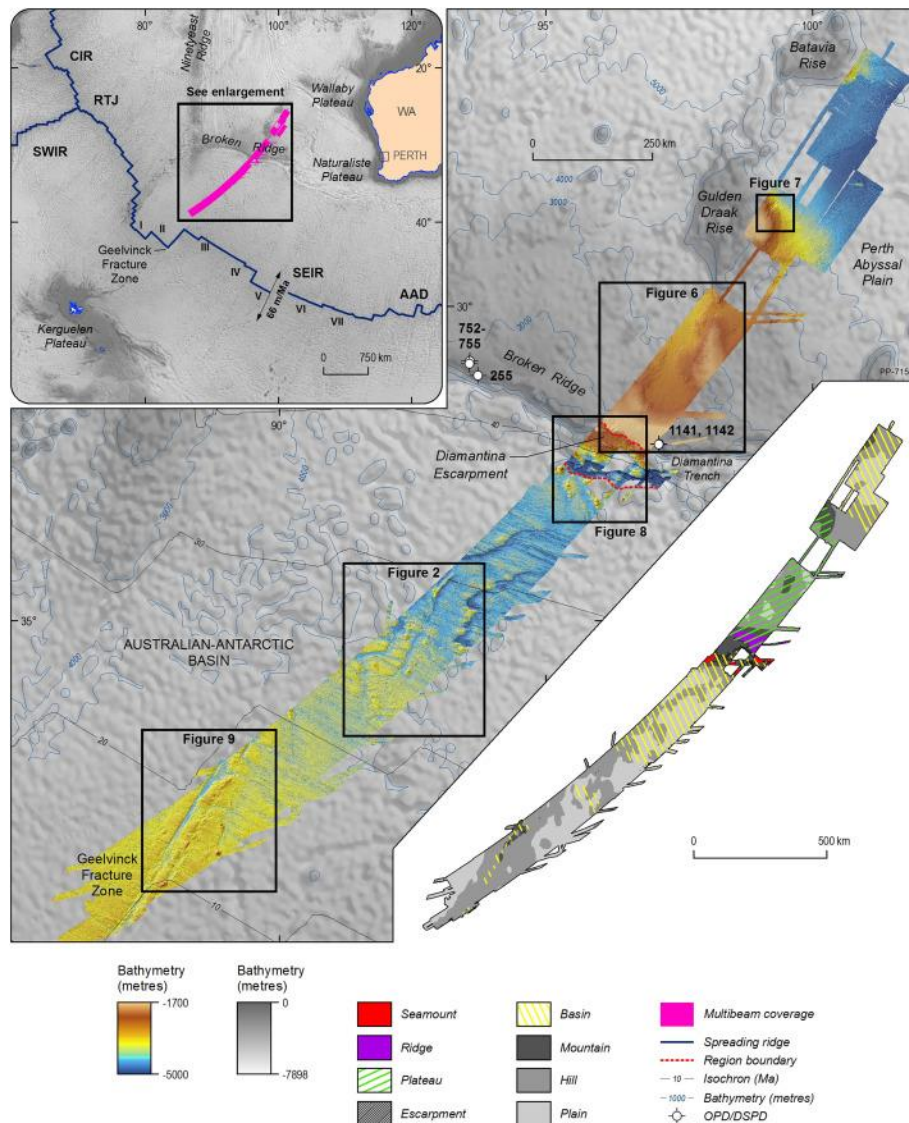


Figure 2.23-1 Location of data collection in the Indian Ocean

Original Caption: Figure 1. Location map showing the multibeam bathymetry data combined with sun-illuminated relief collected in the search for MH370. The locations of Fig. 2, Fig. 6, Fig. 7, Fig. 8, Fig. 9 are displayed as well as the locations of DSDP and ODP drill sites 255 (Leg 26), 752–755 (Leg 121), and 1141/1142 (Leg 183). Upper left inset shows a map of the multibeam bathymetric coverage (pink) overlaid on the SRTM15\_plus model (Olson et al., 2016). The map highlights the Southeast Indian Ridge (SEIR), estimated spreading rates of the SEIR (Argus et al., 2011), the magnetic isochrons (Müller et al., 2008), and interpreted SEIR segments (Small et al., 1999). SWIR: Southwest Indian Ridge; CIR: Central Indian Ridge; RTJ: Rodriguez Triple Junction;

*AAD: Australian-Antarctic Discordance; WA: Western Australia. Lower right inset is an excerpt of the Global Seafloor Geomorphic Feature Map (GSFM; Harris et al., 2014) corresponding to the search area. PP-715-1 is Geoscience Australia internal production number for this figure. (For interpretation of the references to colour in this figure legend, the reader is referred to the web version of this article.)*

## 2.24 Tracing Water Mass Fractions in the Deep Western Indian Ocean

Abstract (Kim et al. 2020):

“The meridional distributions of fluorescent dissolved organic matter (FDOM) and various hydrologic properties were investigated along 67°E in the western Indian Ocean. Our results showed that the highest fluorescence of the humic FDOM (FDOMH) was discovered in the Indian Deep Water (IDW), and relatively lower values were observed in the intruding water masses from the upper layer (e.g., Circumpolar Deep Water (CDW), Antarctic Intermediate Water (AAIW), and South Indian Central Water (SICW)). The deep FDOMH was robustly correlated with apparent oxygen utilisation (AOU), as suggested by previous studies. In particular, the slopes of the regression line AOU on FDOMH varied for different water masses and the two humic components. In this study, to identify the factor inducing the variations of the slope, we estimated the relative water mass fraction of different water masses using a three-end-member mixing model with a salinity-FDOMH diagram. The distribution of water mass fractions was in good agreement with water mass distribution from the conventional method from temperature and salinity distribution and previous studies. The FDOMH components were positively correlated with the aged water mass fraction (i.e., IDW;  $r = 0.93$ ) and negatively correlated with fresher ones originating from the upper water ( $r = -0.93, -0.51,$  and  $-0.95$  for CDW, AAIW, and SICW, respectively). The fluorescence ratio between the two FDOMH components was also observed to be linked to the water mass fractions. The results indicate that the distribution of FDOMH is attributed to the mixing of various deep-water masses during the global ocean circulation.”

Reference:

Kim, J., Kim, Y., Kang, H.W., Kim, S.H., Rho, T. and Kang, D.J., 2020. Tracing water mass fractions in the deep western Indian Ocean using fluorescent dissolved organic matter. *Marine Chemistry*, 218, p.103720. <https://doi.org/10.1016/j.marchem.2019.103720>

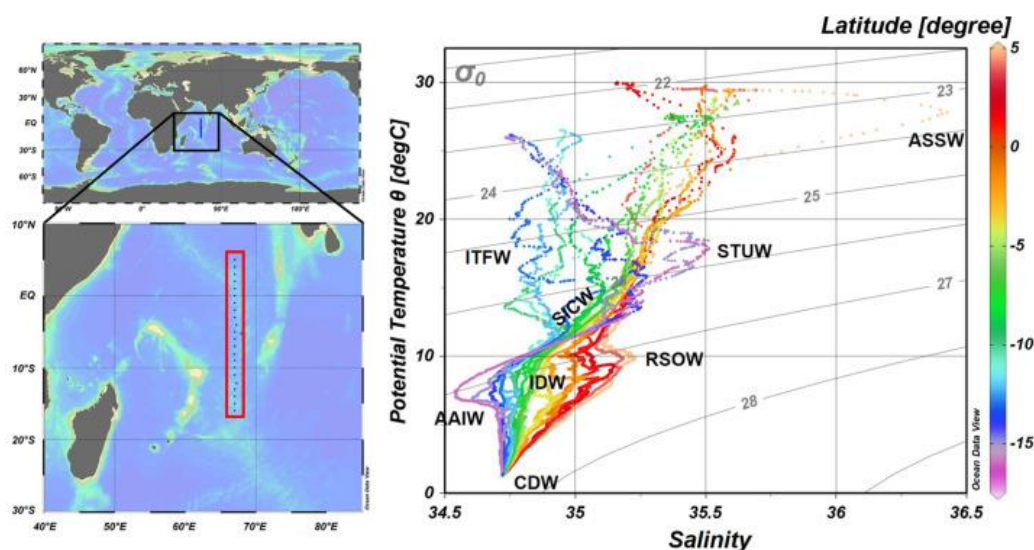


Figure 2.24-1 Water masses in the Indian Ocean

*Original Caption: Figure 1. (a) Maps of the study area and sampling stations in the Indian Ocean constructed during July 2017. (b) T-S diagram showing the distinct water masses in the western Indian Ocean: Arabian Sea Surface Water (ASSW), Indonesian Throughflow Water (ITFW), South Indian Subtropical Underwater (STUW), Red Sea Overflow Water (RSOW), South Indian Central Water (SICW), Antarctic Intermediate Water (AAIW), Circumpolar Deep Water (CDW), and Indian Deep Water (IDW).*

## 2.25 The Indian Ocean Deep Meridional Overturning Circulation in Three Ocean Reanalysis Products

Abstract (Jayasankar et al. 2019):

“The time mean Indian Ocean (IO) deep meridional overturning circulation (MOC) is compared across three ocean reanalysis products (ORAS4, GECCO2, and GFDL). The MOC stream functions obtained by vertically integrating the mass flux across a latitude-depth section in three products are found to be significantly different from each other. Detailed analysis suggests that ORAS4 delivers the best depiction of IO MOC. The inferred IO deep MOC consists of two deep and strong counterclockwise cells located south of 30°S and around 10°S, respectively. The geostrophic component along with the barotropic or external mode dominates the former, and a combination of Ekman and geostrophic components dominates the latter. GECCO2 depicts a steady decline in the northward meridional transport in the bottom layer and a consequent reduction in the MOC strength. The tropical thermocline in GECCO2 responds to this MOC variability leading to rapid and monotonic warming of the tropical IO.”

Reference:

Jayasankar, T., Murtugudde, R. and Eldho, T.I., 2019. The Indian Ocean deep meridional overturning circulation in three ocean reanalysis products. *Geophysical Research Letters*, 46(21), pp.12146-12155. <https://doi.org/10.1029/2019GL084244>

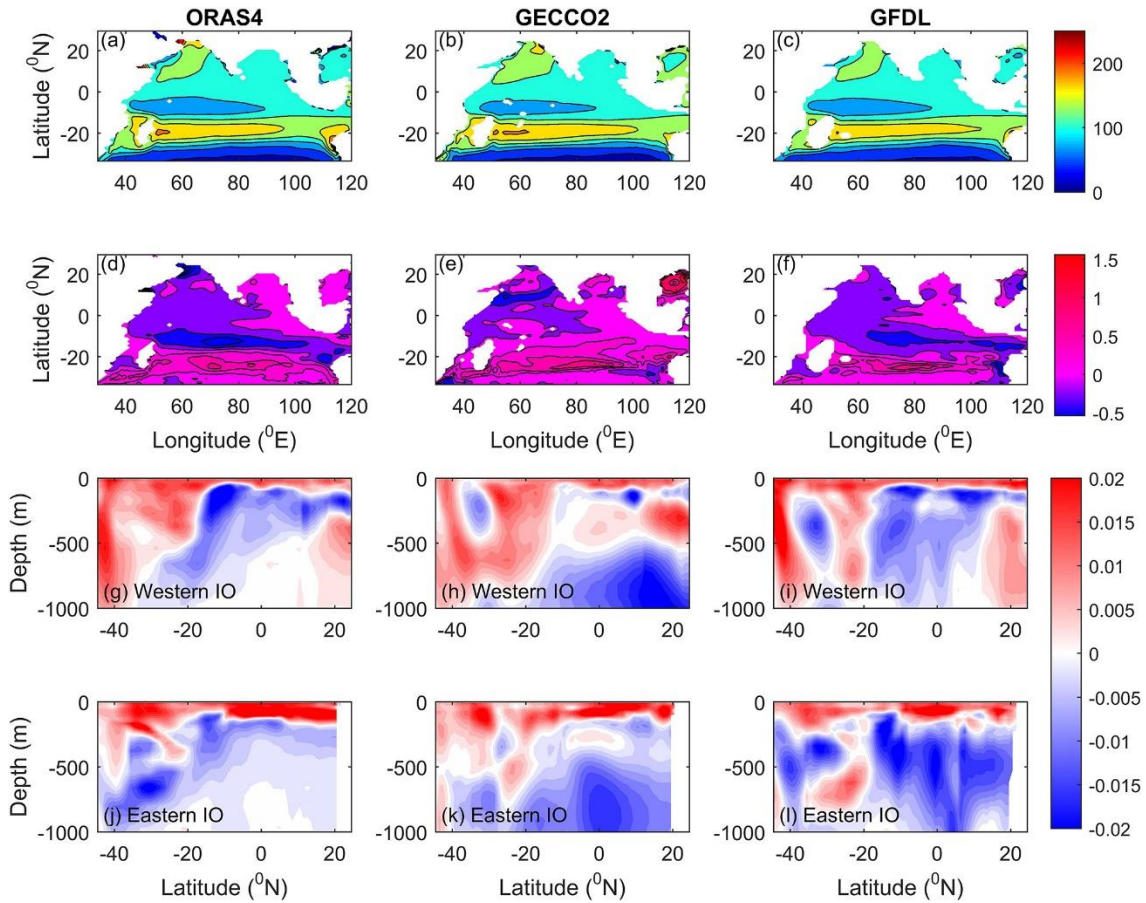


**Figure 2.25-1 Results and trends from three ocean reanalysis products**

*Original Caption: Figure 2. Mean thermocline depth (20°C isotherm) in the Indian Ocean (a, b, and c) and their respective trends in m/year (d, e, and f). Latitude-depth section of temperature trends in western (g, h, and i) and eastern (j, k, and l) Indian Ocean in degrees Celsius per year. ORAS4 = Ocean Reanalysis System 4; GECCO2 = German contribution to the consortium for Estimating the Circulation and Climate of the Ocean 2; GFDL = Ensemble Coupled Data Assimilation system by Geophysical Fluid Dynamics Laboratory; IO = Indian Ocean.*

## 2.26 Monsoon and carbon fluxes in the northern Indian Ocean

Abstract (Rixen et al. 2019):

“Time series sediment trap experiments were carried out at fifteen sites in the northern Indian Ocean between 1986 and 2007. The data on particle flux rates and composition are analyzed in combination with satellite-derived estimates of primary production and results of surface ocean studies during the Joint Global Ocean Flux Study in the Arabian Sea (JGOFS-Indik). The data highlight the influence of the monsoon on the transport of organic carbon into the deep sea and the associated functioning of the organic carbon pump.

The results illustrate the well-known concept of export production, which is driven by inputs of nutrients from the aphotic zone and external reservoirs (the atmosphere and the land) into the euphotic zone. The monsoon drives the organic carbon export through its impact on the physical nutrient supply mechanisms, such as upwelling, vertical mixing, and river discharges. Eolian dust and especially riverine supply of lithogenic matter increase organic carbon fluxes by accelerating the transport of organic matter into the deep sea. Nevertheless, it is preferentially respired in the sub-thermocline and the resulting trapping of remineralized nutrients at this water-depth enforces the influence of upwelling and vertical mixing on the organic carbon fluxes which in the northern Indian Ocean are among the highest worldwide.

Model experiments and measured organic carbon burial rates indicate that a weakening of the summer monsoon strength hardly affected the long-term annual average organic carbon export flux into the deep sea during the last approximately 7000 years. In addition to the summer and winter monsoon strength, which are assumed to be inversely related to each other, monsoon-driven physical impacts on the nutrient trapping efficiency seem to have kept organic carbon fluxes at a high level. A feedback mechanism caused by negative impacts of oxygen concentrations on the respiration and thus nutrient trapping efficiency apparently prevents the development of anoxia to the point where sulfate reduction occurs and sets an upper limit to organic carbon fluxes. Whether changes in the phytoplankton community structure observed in recent decades indicate that this self-regulating system is becoming unstable is open to question.”

Reference:

Rixen, T., Gaye, B. and Emeis, K.C., 2019. The monsoon, carbon fluxes, and the organic carbon pump in the northern Indian Ocean. *Progress in oceanography*, 175, pp.24-39.

<https://doi.org/10.1016/j.pocean.2019.03.001>

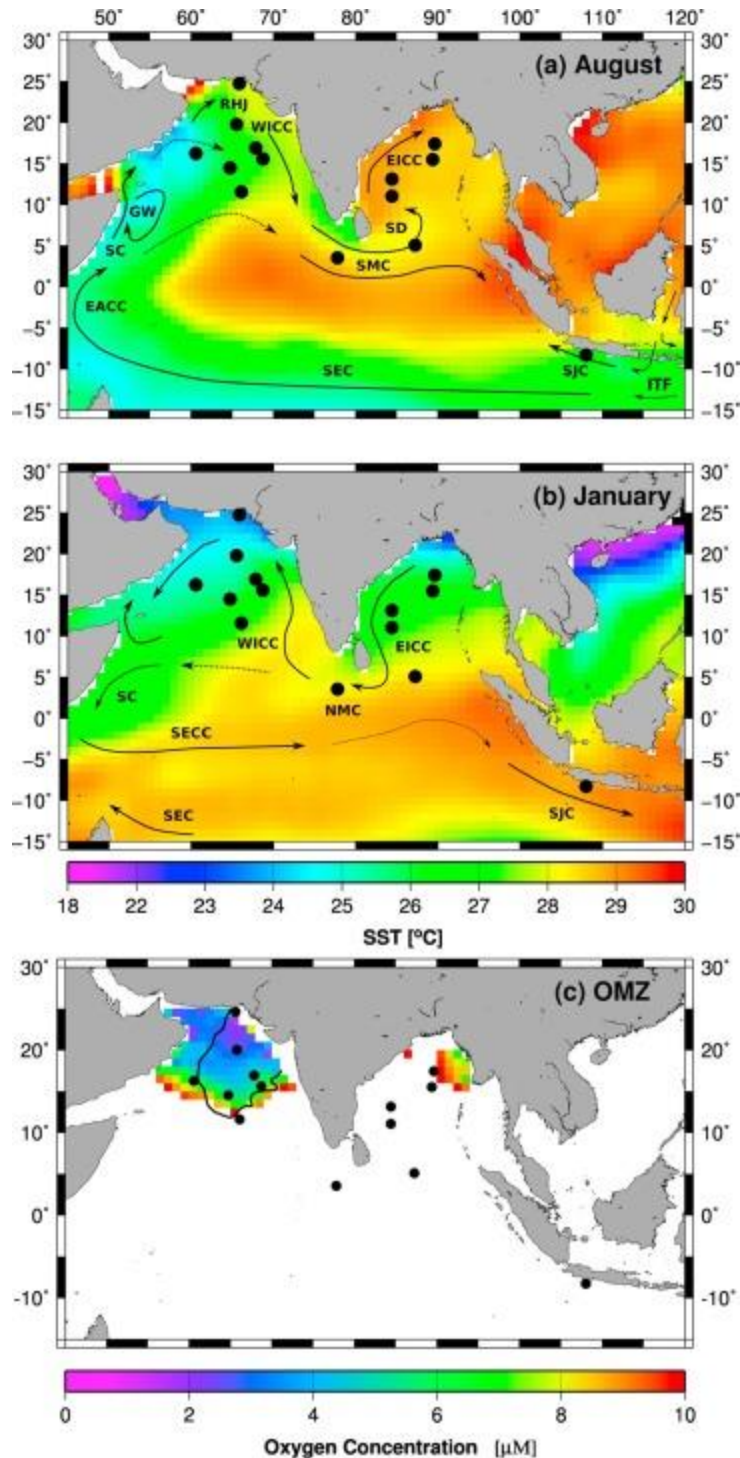


**Figure 2.26-1** Sea surface temperature, ocean circulation, and minimum oxygen concentration in the Indian Ocean  
*Original Caption: Figure 4. (a,b) Monthly mean sea surface temperature in the Indian Ocean (Smith et al., 2008) and the surface ocean circulation simplified and redrawn from Schott and McCreary (2001). The arrows indicate the South Equatorial Current (SEC), South Monsoon Current (SMC), Sri Lanka Dome (SD), East Indian Coastal Current (EICC), South Java Current (SJC), Indonesian Through Flow (ITF), Somali Current (SC), Great Whirl (GW), Ras al Had Jet (RHJ), West Indian Coastal Current (WICC), North Monsoon Current (NMC). The black circles show the*

*sediment trap sites (Fig. 2, Table 1). (c) Minimum oxygen concentration in the water column of the Indian Ocean. Oxygen concentrations > 10  $\mu\text{M}$  are indicated by white color. The data was obtained from the World Ocean Atlas 2013 (Boyer et al., 2013). The black line indicates the extent of the secondary nitrate maximum (SNM) in 1997 (Rixen et al., 2014).*

## 2.27 Temporal and Spatial Dynamics of Primary Production

Abstract (Dalpadado et al. 2021):

“The Indian Ocean, the third largest among the world’s oceans, is experiencing unprecedented changes in sea surface temperature (SST). We present temporal and spatial dynamics of phytoplankton and their response to warming in the Indian Ocean (~25°N to 30°S) during 1998–2019 using remote sensing data. Our study revealed that the area of the Indian Ocean Warm Pool (IOWP), defined as waters with SST values >28 °C, is significantly expanding in most regions, particularly in the most recent decade. The increase in IOWP area was greatest (~74%) in the south-central basin. Furthermore, SST increased significantly in most areas of the Indian Ocean (10 out of 11 regions explored) over the 22-year study period with the highest increase of 0.7 °C observed in the south-central regions. Most other regions showed an average increase in temperature of 0.4–0.5 °C. At the same time, net primary production (NPP) showed large interannual variability in northern and central regions of the Indian Ocean, with slightly decreasing trends in a few northern regions. Overall, years of the first decade (1998–2008) showed more often cooler temperatures and higher productivity, except for a few years, whereas years of the last decade (2009–2019) showed more often warmer temperature and lower productivity, except in very recent years (2017–2019) when productivity was high. Mean Chl a concentrations increased in the last decade during the northeast monsoon period in the northwestern regions, suggesting increased NPP in December to March period as a future scenario in this highly productive area of the Indian Ocean. We also observed increasing SST in several major upwelling areas during the study period, whereas Chl a showed high interannual variability with no marked significant trends in most areas. Results from this study corroborate the importance of the southwest monsoon as a key driver of seasonal patterns in Chl a in major upwelling areas of the Indian Ocean.”

Reference:

Dalpadado, P., Arrigo, K.R., van Dijken, G.L., Gunasekara, S.S., Ostrowski, M., Bianchi, G. and Sperfeld, E., 2021. Warming of the Indian Ocean and its impact on temporal and spatial dynamics of primary production. *Progress in Oceanography*, 198, p.102688.

<https://doi.org/10.1016/j.pocean.2021.102688>

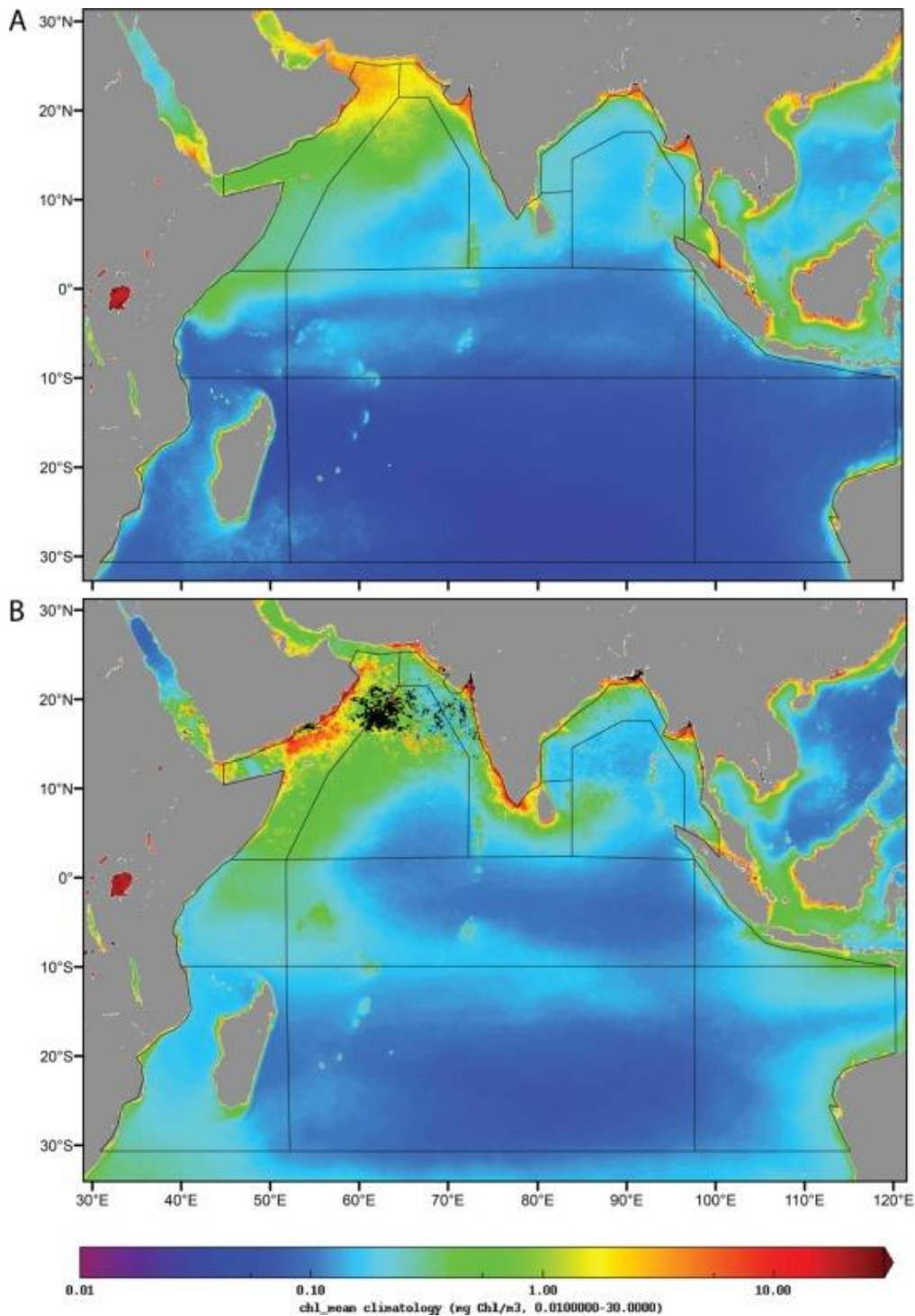


Figure 2.27-1 Chl a climatology during two monsoon seasons

Original Caption: Figure 4. Satellite derived Chl a climatology (mean 1998–2019) for the A) peak northeast monsoon (January to February) and B) peak southwest monsoon (July to August) of the Indian Ocean. See Fig. 1 for labels of the regions. The black areas in Fig. 4B indicate missing values due to persistent cloud cover in the Arabian Sea in the June-July period (Dey et al., 2015).

## 2.28 A Nutrient Limitation Mosaic

Abstract (Twining et al. 2019):

“The Indian Ocean accounts for about one fifth of global ocean net primary production but remains undersampled relative to other major ocean basins. The eastern tropical Indian Ocean is characterized by extremely low concentrations of both macronutrients and the micronutrient iron. We measured concentrations of dissolved and particulate trace metals (Fe, Mn, Zn, Pb) in the upper ocean along the GO-SHIP IO9N transect (28°S to 17°N, mostly along the 95°E meridian) during a cruise in April 2016. Cellular quotas (metal/C) of Fe, Mn, Co, Ni, Cu, and Zn were measured in small eukaryotic flagellates (2–7 μm). Deckboard bottle incubation experiments were conducted at one station in each of three putative biogeochemical regions: southern Indian Ocean gyre (SIO, 28-10°S); equatorial Indian Ocean (EqIO, 10°S - 5°N); Bay of Bengal (BoB, 5-17°N). Nitrate and phosphate were below detection limits in surface waters across the transect. Dissolved and particulate Fe were <0.2 nM south of 10°N and lowest in the EqIO. Cellular Fe/C quotas were approximately 6 μmol/mol and did not vary along the transect, nor did cellular Mn/C or Co/C quotas. Cellular Ni/C and Zn/C quotas were significantly higher at the southern terminus. Nutrient addition experiments indicated that N was the primary limiting nutrient for autotrophs using chlorophyll a as a proxy, but biomass measurements of specific phytoplankton groups pointed to a more complex nutrient limitation mosaic. *Prochlorococcus* was limited by N in the EqIO but by multiple nutrients (N, P, and/or Fe) in the BoB. *Synechococcus* was limited by N in the EqIO and BoB, while small (<20 μm) eukaryotic phytoplankton were limited by N in the EqIO and by multiple nutrients in the BoB. Stoichiometric comparisons of cells and underlying source waters indicate a gradient of N and Fe stress along the transect. These data demonstrate that autotroph communities are poised near multiple nutrient limitation horizons in extremely oligotrophic waters far from micronutrient sources.”

Reference:

Twining, B.S., Rauschenberg, S., Baer, S.E., Lomas, M.W., Martiny, A.C. and Antipova, O., 2019. A nutrient limitation mosaic in the eastern tropical Indian Ocean. *Deep Sea Research Part II: Topical Studies in Oceanography*, 166, pp.125-140. <https://doi.org/10.1016/j.dsr2.2019.05.001>

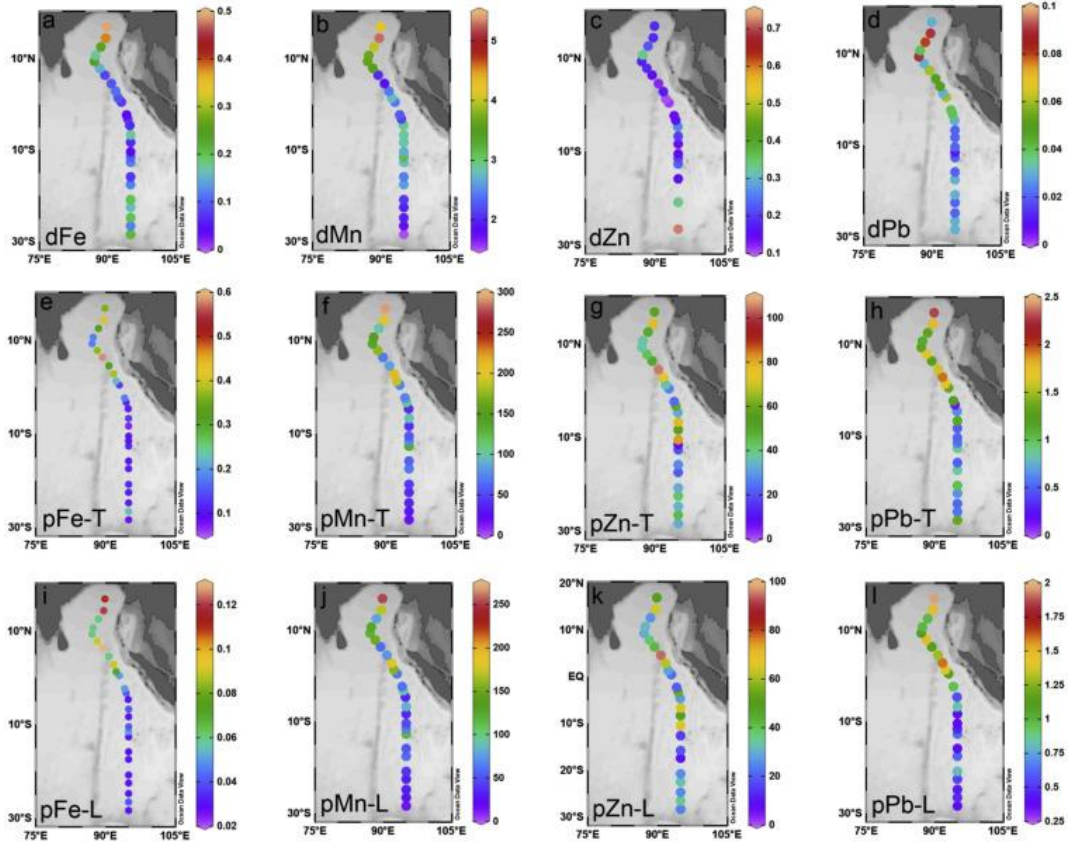


Figure 2.28-1 Nutrient concentrations in the Indian Ocean

Original Caption: Figure 2. Dissolved (a-d), total particulate (e-h), and labile particulate (i-l) Fe, Mn, Zn, and Pb concentrations from 20 m along the IO9N cruise transect. Dissolved metals are in units of nmol/L. Particulate Fe is shown as nmol/L. The other particulate metals are shown as pmol/L.

## 2.29 A Century of Observed Temperature Change in the Indian Ocean

Abstract (Wenegrat et al. 2022):

“The Indian Ocean is warming rapidly, with widespread effects on regional weather and global climate. Sea-surface temperature records indicate this warming trend extends back to the beginning of the 20th century, however the lack of a similarly long instrumental record of interior ocean temperatures leaves uncertainty around the subsurface trends. Here we utilize unique temperature observations from three historical German oceanographic expeditions of the late 19th and early 20th centuries: SMS Gazelle (1874–1876), Valdivia (1898–1899), and SMS Planet (1906–1907). These observations reveal a mean 20th century ocean warming that extends over the upper 750 m, and a spatial pattern of subsurface warming and cooling consistent with a 1°–2° southward shift of the southern subtropical gyre. These interior changes occurred largely over the last half of the 20th century, providing observational evidence for the acceleration of a multidecadal trend in subsurface Indian Ocean temperature.”

Reference:

Wenegrat, J.O., Bonanno, E., Rack, U. and Gebbie, G., 2022. A century of observed temperature change in the Indian Ocean. *Geophysical Research Letters*, 49(13), p.e2022GL098217.

<https://doi.org/10.1029/2022GL098217>

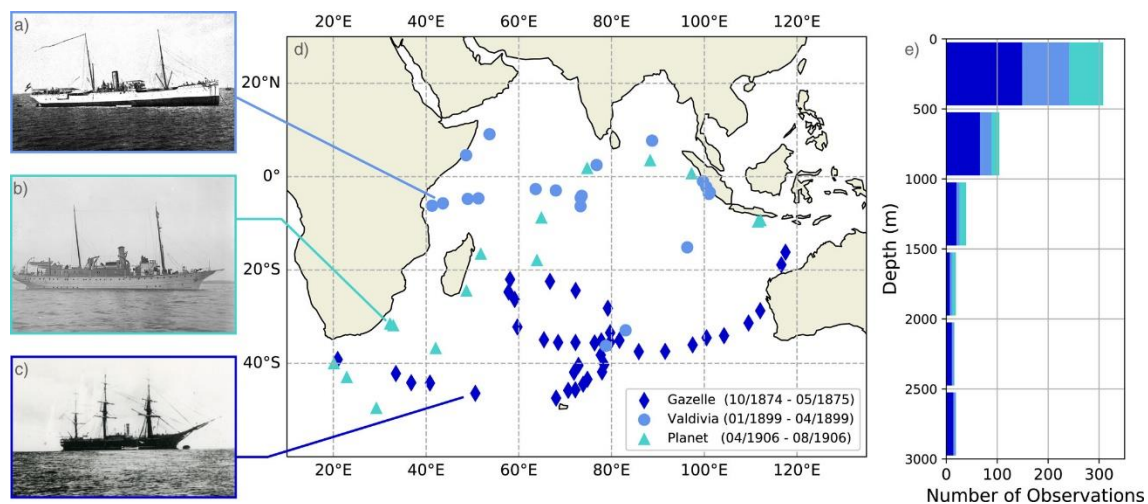


**Figure 2.29-1 Temperature sampling sites in the Indian Ocean**

*Original Caption: Figure 1. Overview of the Indian Ocean portion of the Valdivia (panel a, Chun, 1903), Planet (panel b, photo: SLUB/Deutsche Fotothek, F. Stoedtner), and Gazelle (panel c, photo: Deutsches Schifffahrtsmuseum Fotoarchiv 94-2) cruises. Stations used in this analysis are shown in panel (d). A histogram of temperature observations as a function of depth is shown in panel (e) with color indicating the originating cruise following the color convention shown in the legend of panel (d).*

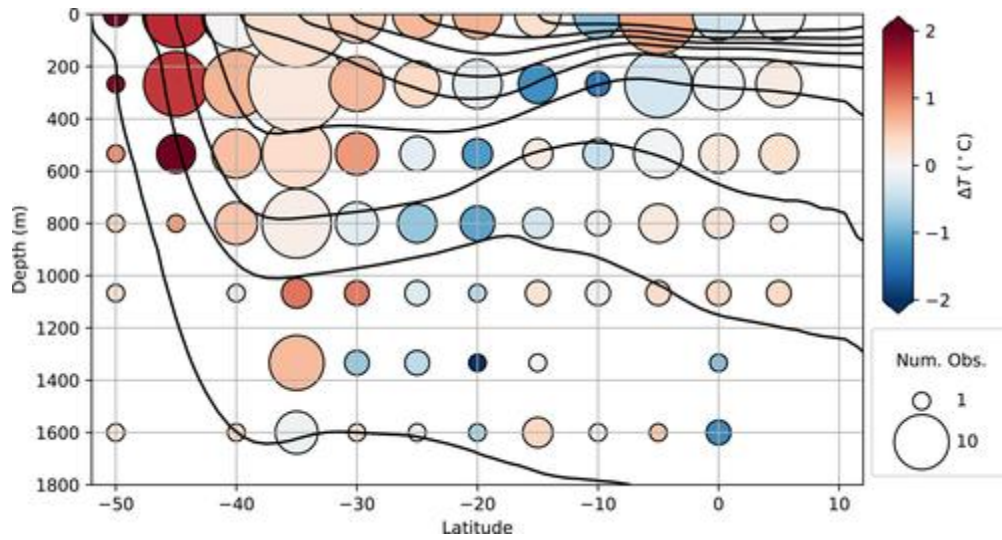


Figure 2.29-2 Temperature change by latitude and depth in the Indian Ocean

Original Caption: Figure 3. A latitude-depth slice indicates heterogeneous temperature change (colorscale) in the interior. Observations are binned into latitude-depth bins and averaged, with the number of observations in each bin indicated by the marker size (legend). Zonally averaged temperature contours from the 2005–2017 climatology are shown in black.

## 2.30 Interannual Variability of Sea Surface Chlorophyll a

Abstract (Ma et al. 2022):

“Phytoplankton are crucial to marine ecosystems and the global carbon cycle. This study investigates the characteristics and causes of the interannual variation of the surface chlorophyll a (chl a) in the southern tropical Indian Ocean (STIO). We find that in addition to the Seychelles-Chagos thermocline ridge (SCTR) upwelling zone in the southwestern basin, large interannual variability also shows up in the southeastern tropical Indian Ocean (SETIO; 6°–18°S, 70°–92°E). The chl a in the SCTR shows two dominant periods of four years and two years, whereas it shows a dominant period of six years and a weaker period of three years in the SETIO. Surface wind forcing anomalies within the STIO, but not the Indonesian throughflow, cause the interannual chl a anomaly. In the SETIO region, the thermocline dynamics control the chl a variation via a combination of equal contributions from local Ekman pumping and remote Rossby waves generated by the wind stress curl from the east. In the SCTR region, the thermocline dynamics explain only about 67% of the chl a variation, with a larger contribution from the remotely generated Rossby waves than local Ekman pumping. The circulation in the western basin also contributes to the chl a variation by transporting western equatorial chl a to this region during the boreal summer-fall. Both the Indian Ocean Dipole and the El Niño–Southern Oscillation act to modulate the chl a variation in the STIO. They make comparable contributions in the SETIO, while the Indian Ocean Dipole plays a more important role in the SCTR.”

Reference:

Ma, X., Chen, G., Li, Y. and Zeng, L., 2022. Interannual variability of sea surface chlorophyll a in the southern tropical Indian Ocean: Local versus remote forcing. *Deep Sea Research Part I: Oceanographic Research Papers*, 190, p.103914. <https://doi.org/10.1016/j.dsr.2022.103914>

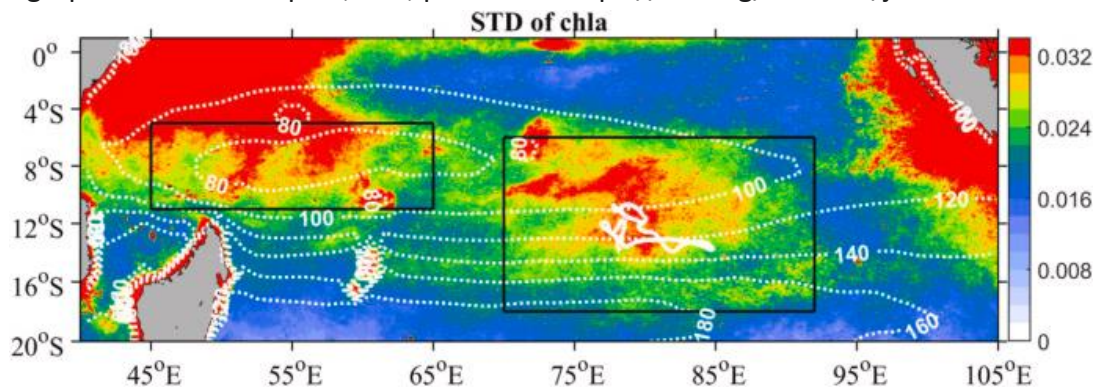


Figure 2.30-1 Interannual variation of chl a concentration in the Indian Ocean

*Original Caption: Figure 1. The STD of interannual chl a concentration (color shading; unit: mg m<sup>-3</sup>) and climatological D20 (dashed white contours; unit: m). The study regions of the SCTR (5°–11°S, 45°–65°E) and the SETIO (6°–18°S, 70°–92°E) are indicated by the black boxes, both of which show pronounced interannual variation. The white solid line represents the trajectory of BGC-Argo float 1902332.*

## 2.31 Projected Timing of Climate Departure

Abstract (Camilo et al. 2013):

“Ecological and societal disruptions by modern climate change are critically determined by the time frame over which climates shift beyond historical analogues. Here we present a new index of the year when the projected mean climate of a given location moves to a state continuously outside the bounds of historical variability under alternative greenhouse gas emissions scenarios. Using 1860 to 2005 as the historical period, this index has a global mean of 2069 ( $\pm 18$  years s.d.) for near-surface air temperature under an emissions stabilization scenario and 2047 ( $\pm 14$  years s.d.) under a ‘business-as-usual’ scenario. Unprecedented climates will occur earliest in the tropics and among low-income countries, highlighting the vulnerability of global biodiversity and the limited governmental capacity to respond to the impacts of climate change. Our findings shed light on the urgency of mitigating greenhouse gas emissions if climates potentially harmful to biodiversity and society are to be prevented.”

Reference:

Mora, Camilo, Abby G. Frazier, Ryan J. Longman, Rachel S. Dacks, Maya M. Walton, Eric J. Tong, Joseph J. Sanchez et al. "The projected timing of climate departure from recent variability." *Nature* 502, no. 7470 (2013): 183. Doi: 10.1038/nature12540

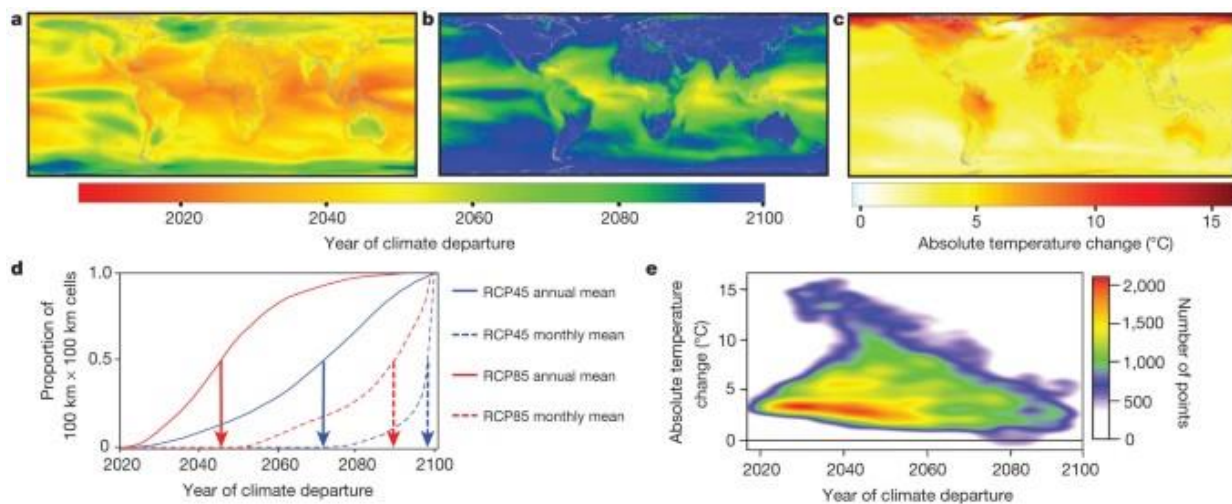


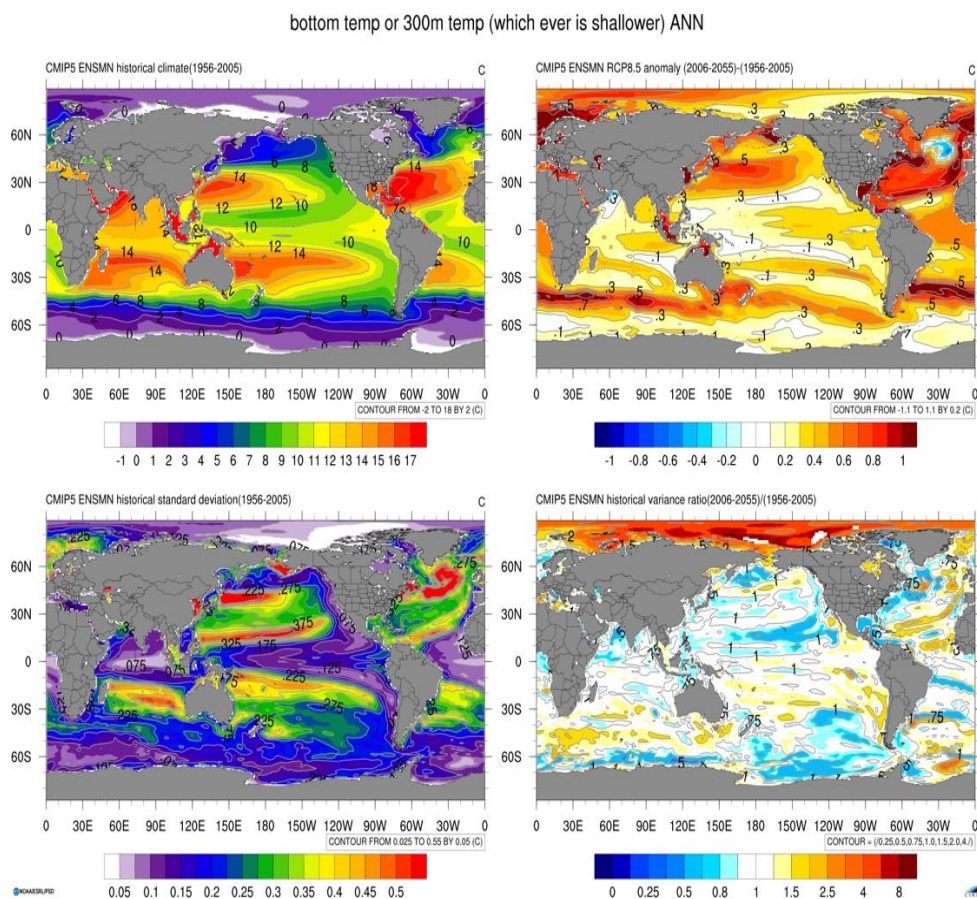
Figure 2.31-1 The projected timing of climate departure

*Original Caption: Figure 2. a, b, Projected year when annual (a) or monthly (b) air temperature means move to a state continuously outside annual or monthly historical bounds, respectively. c, Absolute change in mean annual air temperature. (Results in a–c are based on RCP85.) d, Cumulative frequency of 100-km grid cells according to the projected timing of climate departure from recent variability for air temperature under two emissions scenarios (vertical lines indicate the median year). e, Scatter plot relating the grid cells from the map of absolute change (c) to the same grid cells from the map of projected timing of climate departure (a).*

## 2.32 NOAA Climate Change Portal

“A key approach for examining climate, especially how it will change in the future, uses complex computer models of the climate system that includes atmosphere, ocean, sea ice and land components. Some models also include additional aspects of the earth system, including chemistry and biology. The Climate Change Portal is a web interface developed by the NOAA ESRL Physical Sciences Division to access and display the immense volumes of climate and earth system model output that informed the Intergovernmental Panel on Climate Change (IPCC) Fifth Assessment Report (AR5). The webtool makes climate change information more accessible to natural resource managers, decision makers and educators.”

Link: <https://www.esrl.noaa.gov/psd/ipcc/ocn/>



## 2.33 Dynamic Seascape Pelagic Habitat Classification

“The CoastWatch Seascape Pelagic Habitat Classification product (CW Seascapes) identifies spatially explicit water masses with particular biogeochemical features using a model and satellite-derived measurements. The seascape product is generated as monthly and 8-day composites at 5 km spatial resolution.

US and global Marine Biodiversity Observation Network (MBON) partnered with US Integrated Ocean Observation System (IOOS), NOAA/OAR/AOML and NOAA/NESDIS/STAR to develop and routinely generate “seascapes” products and to make them available on CoastWatch. Derived from dynamic fields of satellite and modelled data, seascapes are classified and used as a biogeographical framework to describe dynamic, changing ocean habitats for MBON and other applications. CW Seascapes provide information about the quality and extent of different oceanographic habitats or features and can be used to assess and predict the different planktonic and fisheries communities that reside within seascapes. Current CW Seascapes products include monthly and 8-day time steps at 5 km resolution. High resolution (1 km) case studies are planned on a case by case basis as through cooperation with US and global MBON partners.”

Data are available at 8-day and monthly timesteps back to January 2003:

<https://coastwatch.noaa.gov/cwn/products/seascape-pelagic-habitat-classification.html>

Reference:

Kavanaugh, Maria T., Matthew J. Oliver, Francisco P. Chavez, Ricardo M. Letelier, Frank E. Muller-Karger, and Scott C. Doney. 2016. “Seascapes as a New Vernacular for Pelagic Ocean Monitoring, Management and Conservation.” *ICES Journal of Marine Science* 73 (7): 1839–50. <https://doi.org/10.1093/icesjms/fsw086>.

Seascape Classes:

- 1 NORTH ATLANTIC SPRING, ACC TRANSITION
- 2 SUBPOLAR TRANSITION
- 3 TROPICAL SUBTROPICAL TRANSITION
- 4 WESTERN WARM POOL SUBTROPICAL
- 5 SUBTROPICAL GYRE TRANSITION
- 6 ACC, NUTRIENT STRESS
- 7 TEMPERATE TRANSITION
- 8 INDOPACIFIC SUBTROPICAL GYRE
- 9 EQUATORIAL TRANSITION
- 10 HIGHLY OLIGOTROPHIC SUBTROPICAL GYRE
- 11 TROPICAL/SUBTROPICAL UPWELLING
- 12 SUBPOLAR
- 13 SUBTROPICAL GYRE MESOSCALE INFLUENCED
- 14 TEMPERATE BLOOMS UPWELLING
- 15 TROPICAL SEAS

- 16 MEDITERRANEAN RED SEA
- 17 SUBTROPICAL TRANSITION LOW NUTRIENT STRESS
- 18 MEDITERRANEAN RED SEA
- 19 ARTIC/ SUBPOLAR SHELVES
- 20 SUBTROPICAL, FRESH INFLUENCED COASTAL
- 21 WARM, BLOOMS, HIGH NUTS
- 22 ARCTIC LATE SUMMER
- 23 FRESHWATER INFLUENCED POLAR/SUBPOLAR SHELVES
- 24 ANTARCTIC SHELVES
- 25 ICE PACK/LARGE POLYNAS
- 26 ANTARCTIC ICE EDGE
- 27 HYPERSALINE EUTROPHIC, PERSIAN GULF, RED SEA
- 28 ARCTIC ICE EDGE
- 29 ANTARCTIC
- 30 ICE EDGE BLOOM
- 31 1-30% ICE PRESENT
- 32 30-80% MARGINAL ICE
- 33 PACK ICE

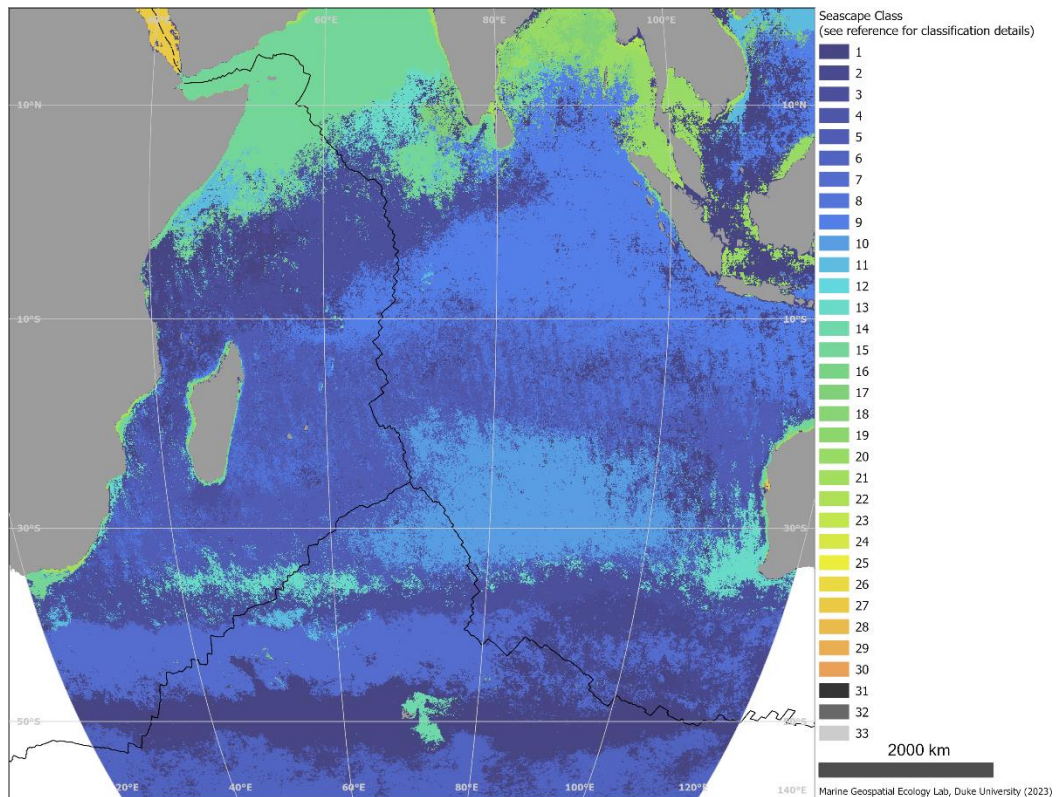


Figure 2.33-1 Most commonly occurring seascape class in January, from 2012-2021

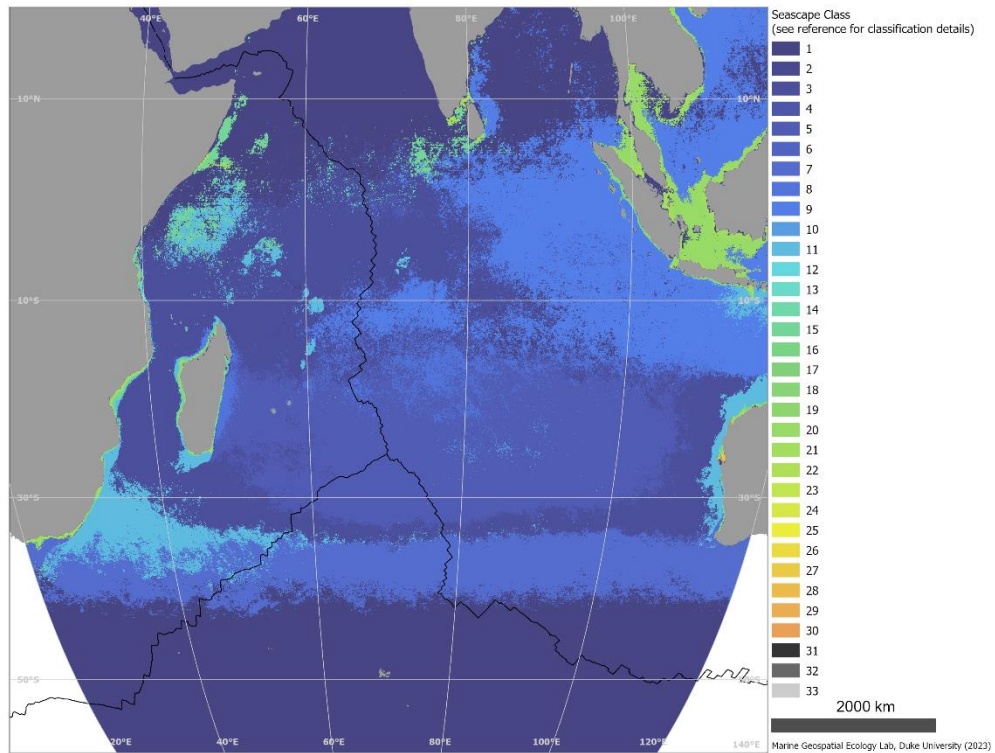


Figure 2.33-2 Most commonly occurring seascape class in June, from 2012-2021

## 3 Biological Data

### 3.1 Ocean Biodiversity Information System (OBIS) Data

“The Ocean Biodiversity Information System (OBIS) seeks to absorb, integrate, and assess isolated datasets into a larger, more comprehensive picture of life in our oceans. The system hopes to stimulate research about our oceans to generate new hypotheses concerning evolutionary processes, species distributions, and roles of organisms in marine systems on a global scale. OBIS generate maps that contribute to the ‘big picture’ of our oceans: a comprehensive, collaborative, worldwide view of our oceans.

OBIS provides a portal or gateway to many datasets containing information on where and when marine species have been recorded. The datasets are integrated so you can search them all seamlessly by species name, higher taxonomic level, geographic area, depth, and time; and then map and find environmental data related to the locations.”

The data provided here are summaries of available OBIS data for the Indian Ocean. Observation counts, Species Richness, Hurlbert’s Index (ES[50]), and Shannon Diversity data summaries are provided for all species. Observation locations are provided for VME taxa. Data gaps do exist in OBIS and thus these summaries are not exhaustive.

Source:

<https://obis.org/about/>

Reference:

Intergovernmental Oceanographic Commission (IOC) of UNESCO. The Ocean Biodiversity Information System. Web. <http://www.iobis.org>.

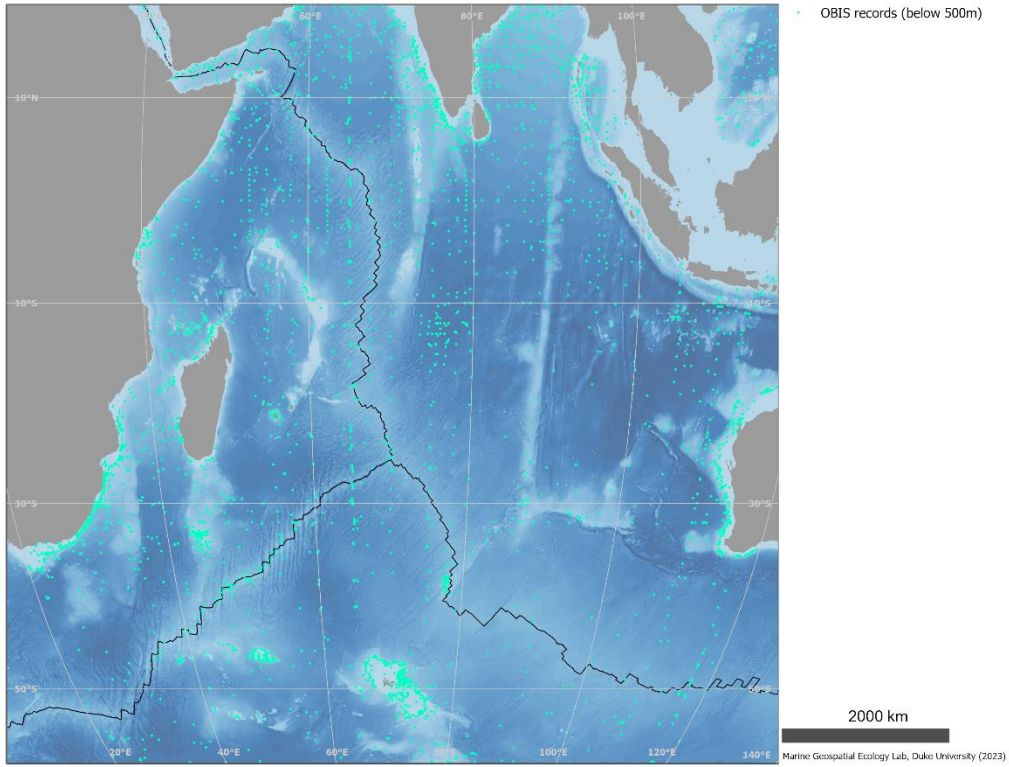


Figure 3.1-1 All OBIS records below 500 m

### 3.2 OBIS Vulnerable Marine Ecosystems (VMEs) Indicator Taxa

The Food and Agriculture Organization (FAO) of the United Nations International Guidelines for the Management of Deep-sea Fisheries in the High Seas (FAO, 2009) provide general tools and considerations for the identification of vulnerable marine ecosystems (VMEs). They include a set of criteria that should be used, individually or in combination, for the identification process. Specifically: Uniqueness or rareness, Functional significance of the habitat, Fragility, Life-history of species make recovery difficult, and Structural complexity.

#### VME Indicator taxa

---

Common name	Scientific name	Taxonomical level
Stony coral	Scleractinia	Order
Sponge	Porifera	Phylum
Black coral	Antipatharia	Order
Lace coral	Stylasteridae	Family
Gorgonian	Alcyonacea	Order
Sea-pen	Pennatulacea	Order
Blue coral	Helioporacea	Order

---

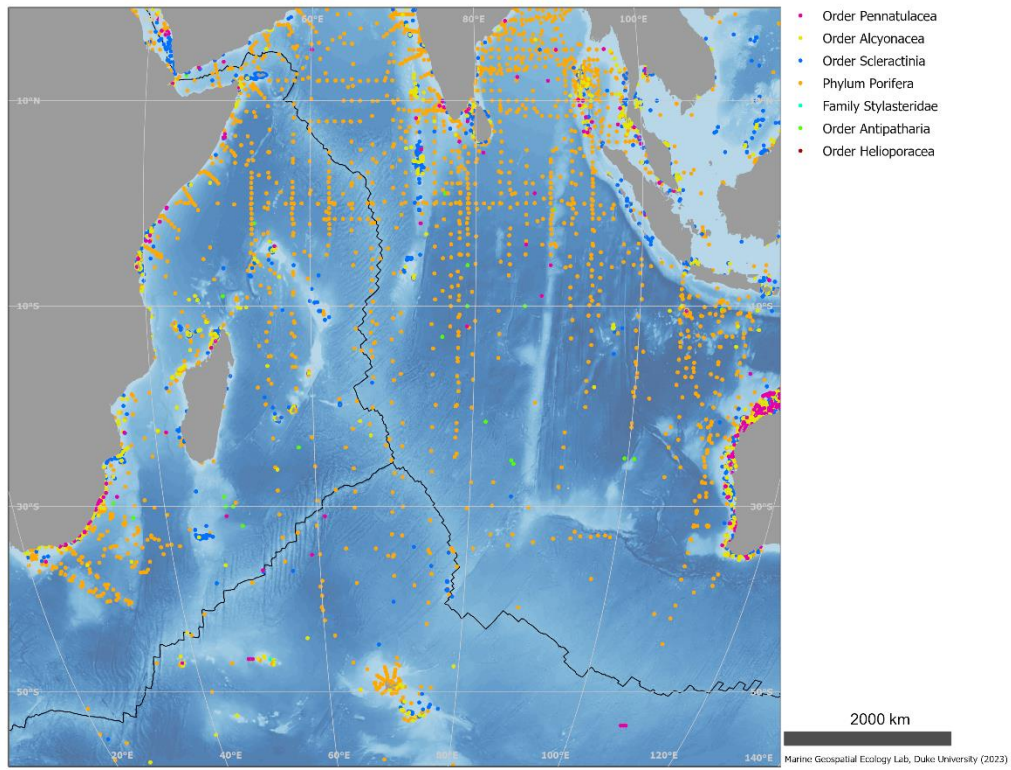


Figure 3.2-1 OBIS records for all VME taxa

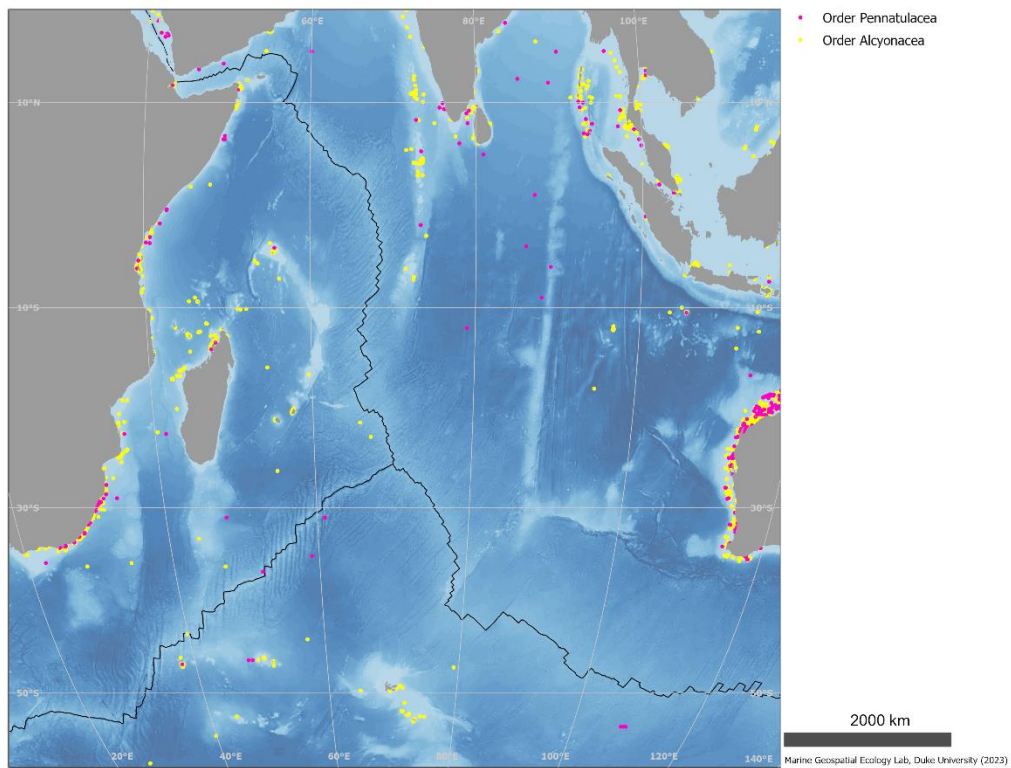


Figure 3.2-2 OBIS records of Octocorals

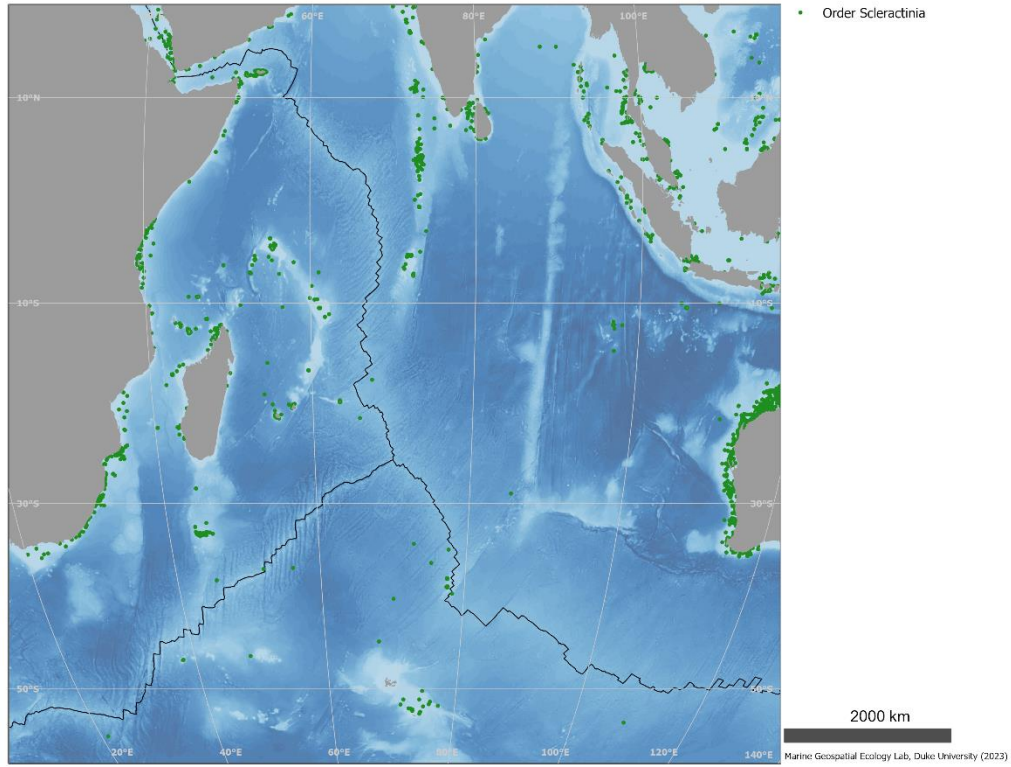


Figure 3.2-3 OBIS records of Scleractinia

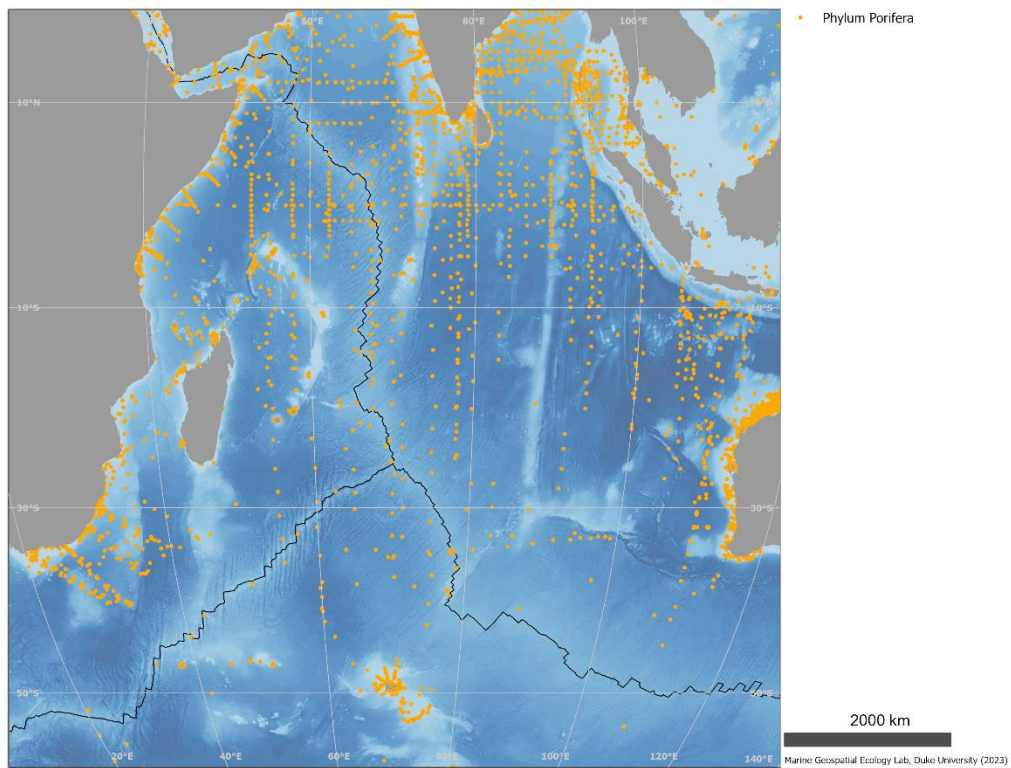


Figure 3.2-4 OBIS records of Sponges

### 3.3 Global Distribution of Deep-Water Antipatharia Habitat

Abstract (Yesson et al. 2017)

“Antipatharia are a diverse group of corals with many species found in deep water. Many Antipatharia are habitat for associates, have extreme longevity and some species can occur beyond 8500 m depth. As they are major constituents of ‘coral gardens’, which are Vulnerable Marine Ecosystems (VMEs), knowledge of their distribution and environmental requirements is an important pre-requisite for informed conservation planning particularly where the expense and difficulty of deep-sea sampling prohibits comprehensive surveys.

This study uses a global database of Antipatharia distribution data to perform habitat suitability modelling using the Maxent methodology to estimate the global extent of black coral habitat suitability. The model of habitat suitability is driven by temperature but there is notable influence from other variables of topography, surface productivity and oxygen levels.

This model can be used to predict areas of suitable habitat, which can be useful for conservation planning. The global distribution of Antipatharia habitat suitability shows a marked contrast with the distribution of specimen observations, indicating that many potentially suitable areas have not been sampled, and that sampling effort has been disproportionate to shallow, accessible areas inside marine protected areas (MPAs). Although 25% of Antipatharia observations are located in MPAs, only 7-8% of predicted suitable habitat is protected, which is short of the Convention on Biological Diversity target to protect 10% of ocean habitats by 2020.”

Reference:

Yesson, C., F. Bedford, A. Rogers, and M. Taylor. 2017. “The Global Distribution of Deep-Water Antipatharia Habitat.” *Deep Sea Research Part II: Topical Studies in Oceanography*, Towards ecosystem based management and monitoring of the deep Mediterranean, North-East Atlantic and Beyond, 145 (November): 79–86. <https://doi.org/10.1016/j.dsr2.2015.12.004>.

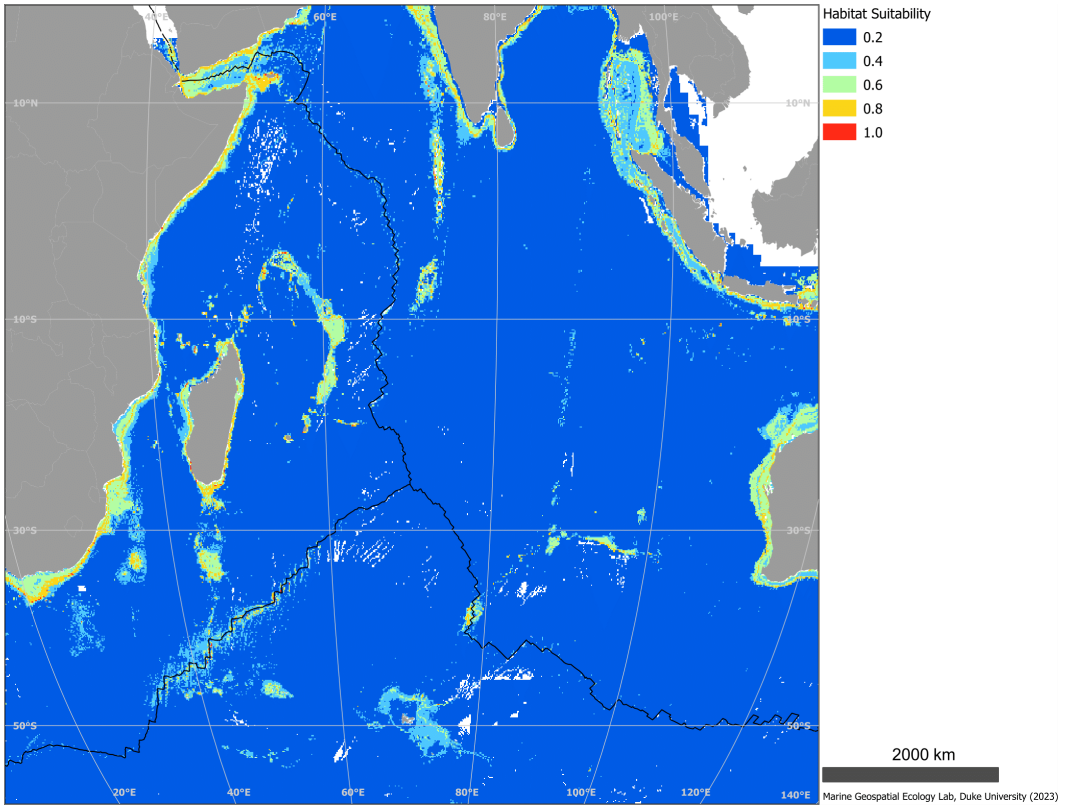


Figure 3.3-1 Deep-Water Antipatharia Habitat Suitability

### 3.4 Predictions of Habitat Suitability for Cold-Water Octocorals

Abstract (Yesson et al. 2012):

“Three-quarters of Octocorallia species are found in deep waters. These cold-water octocoral colonies can form a major constituent of structurally complex habitats. The global distribution and the habitat requirements of deep-sea octocorals are poorly understood given the expense and difficulties of sampling at depth. Habitat suitability models are useful tools to extrapolate distributions and provide an understanding of ecological requirements. Here, we present global habitat suitability models and distribution maps for seven suborders of Octocorallia: Alcyoniina, Calcaxonina, Holaxonia, Scleraxonia, Sessiliflorae, Stolonifera and Subselliflorae.”

Reference:

Yesson C, Taylor ML, Tittensor DP, Davies AJ, Guinotte J, Baco A, Black J, Hall-Spencer JM, Rogers AD (2012) Global habitat suitability of cold-water octocorals. *Journal of Biogeography* 39:1278–1292. Doi: 10.1111/j.1365-2699.2011.02681.x

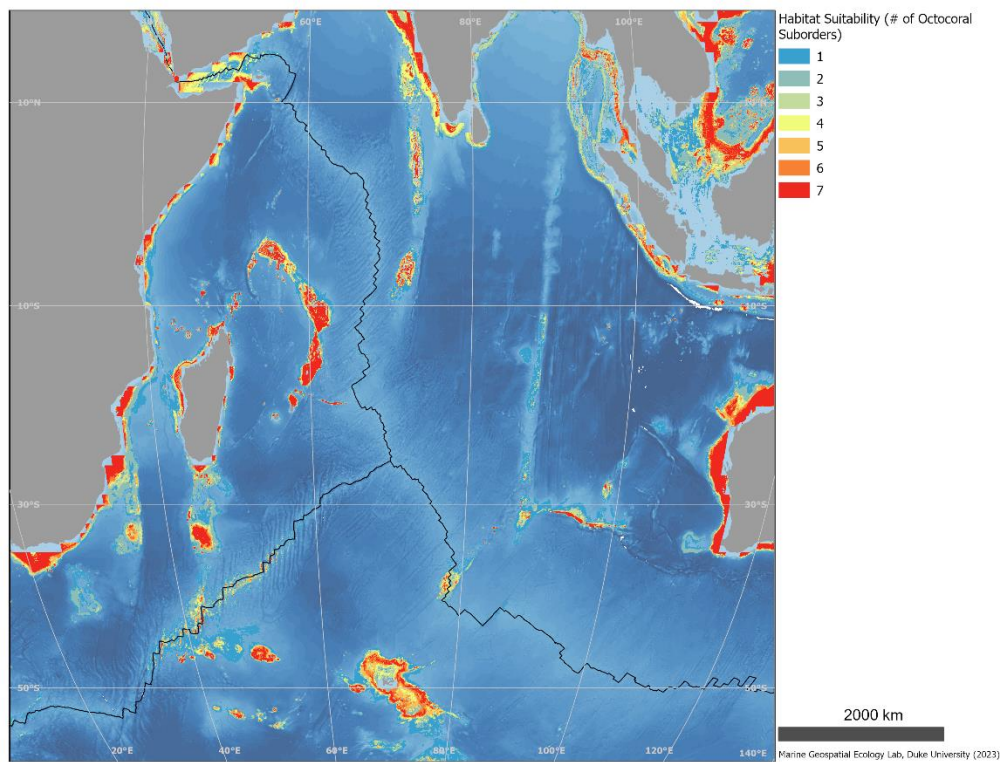


Figure 3.4-1 Deep-Sea Octocoral habitat suitability across seven species

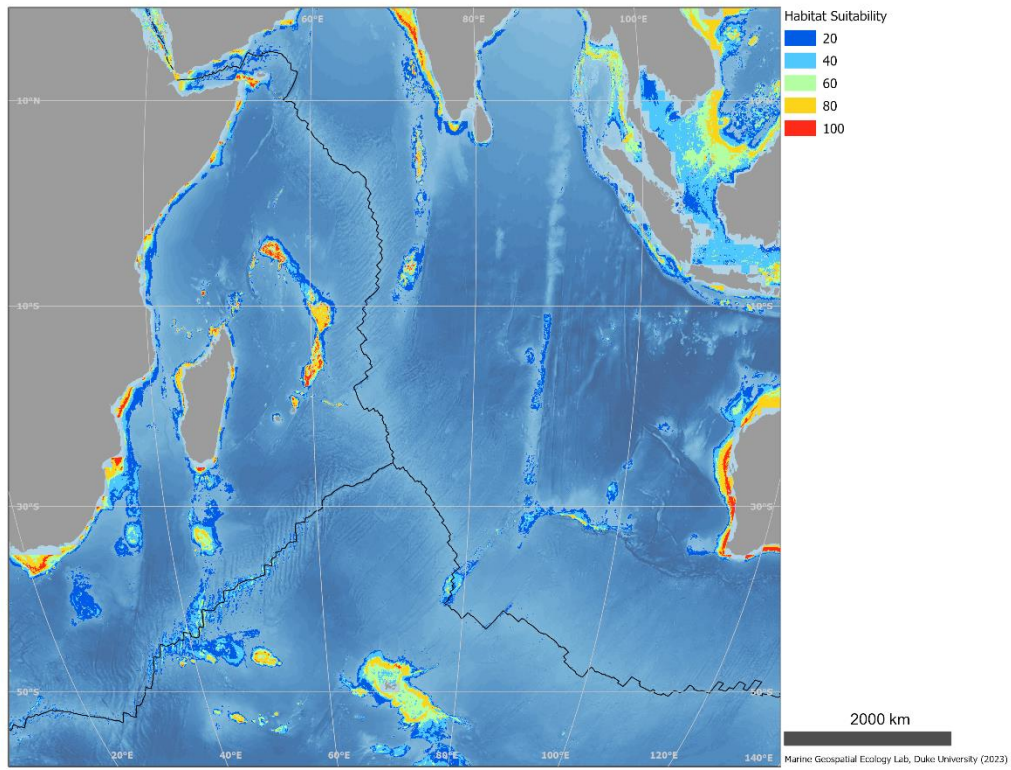


Figure 3.4-2 Deep-Sea Octocoral habitat suitability - Alcyoniina

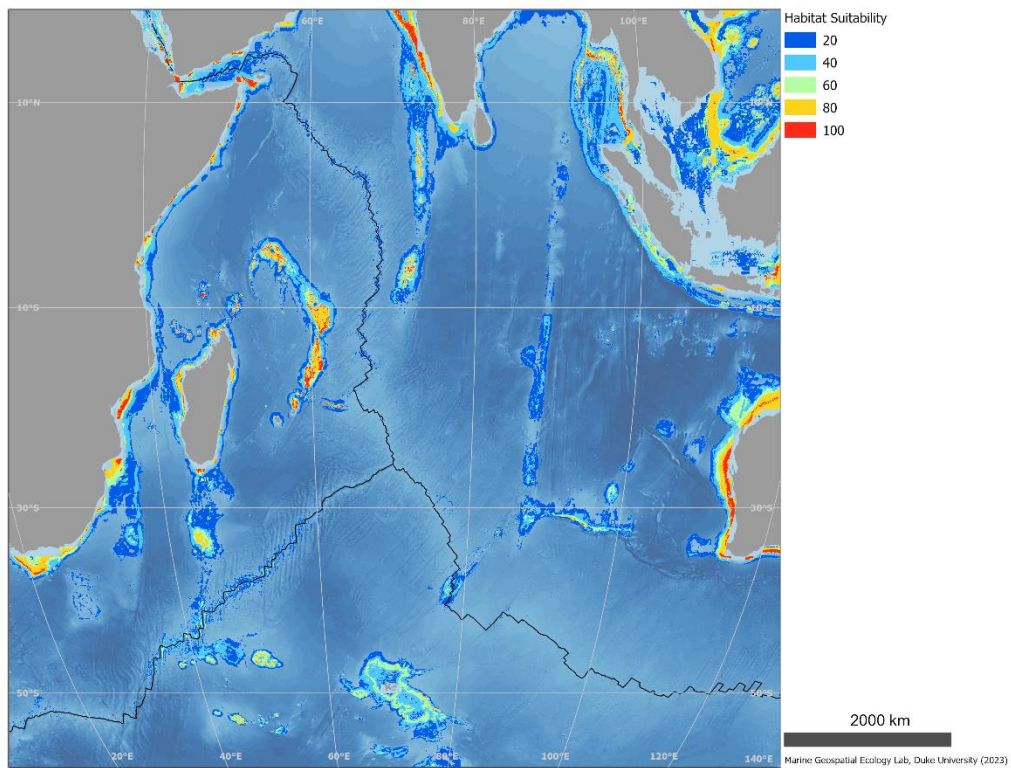


Figure 3.4-3 Deep-Sea Octocoral habitat suitability - Holaxonia

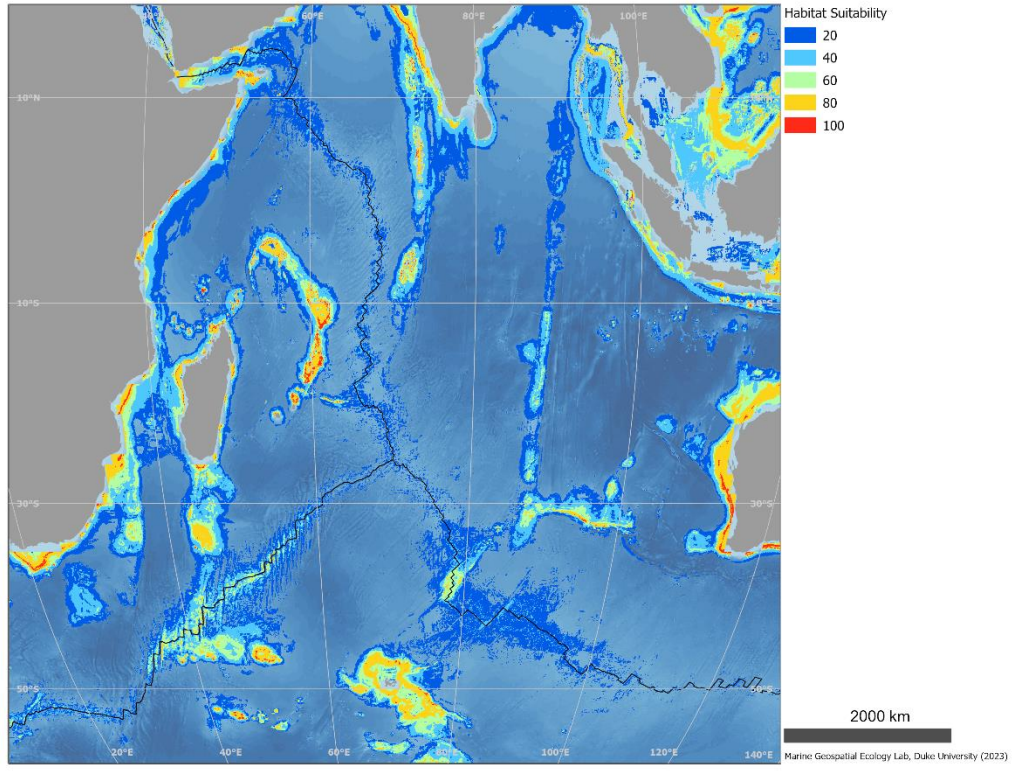


Figure 3.4-4 Deep-Sea Octocoral habitat suitability - Calcaxonina

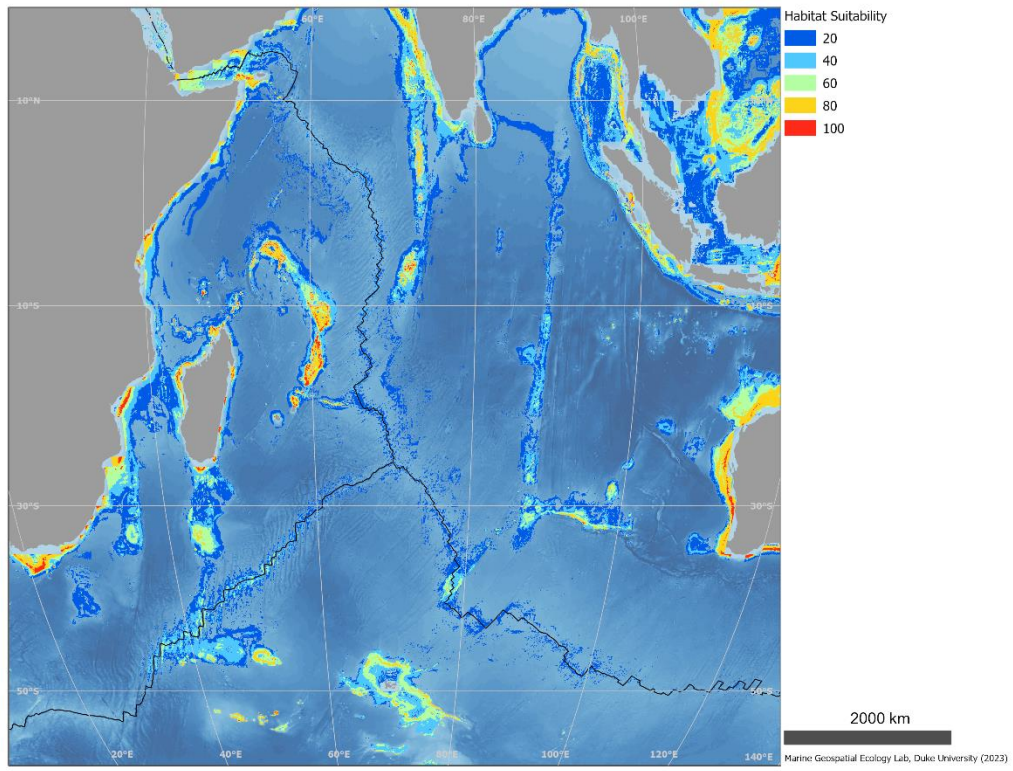


Figure 3.4-5 Deep-Sea Octocoral habitat suitability - Scleraxonia

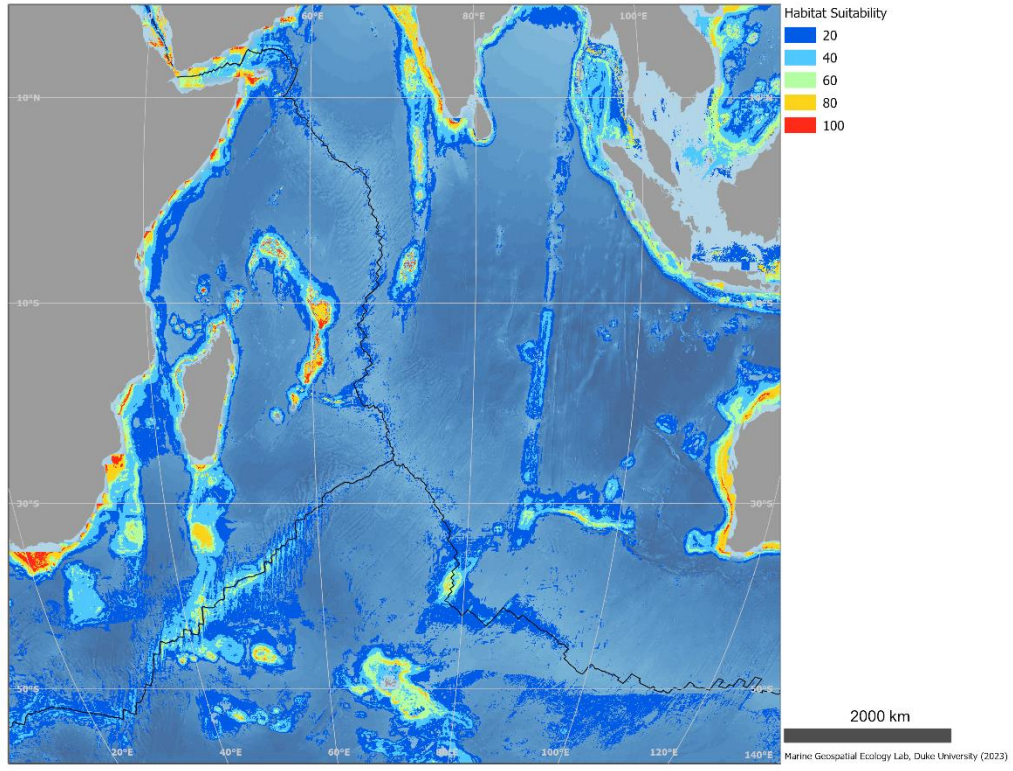


Figure 3.4-6 Deep-Sea Octocoral habitat suitability - Sessiliflorae

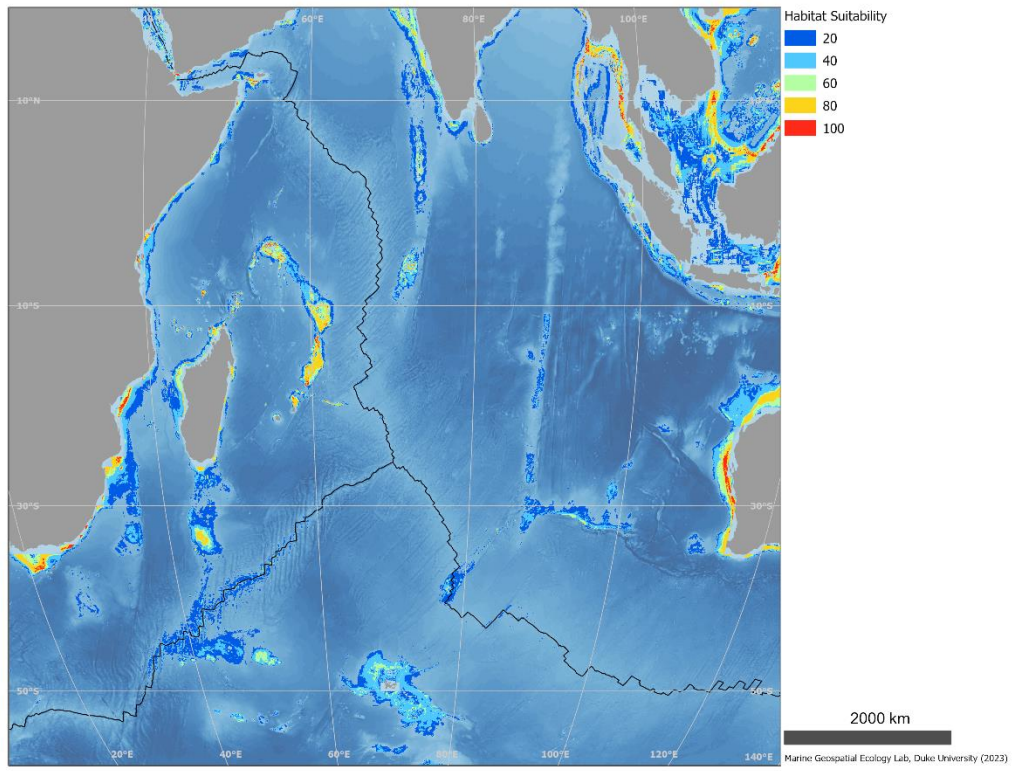


Figure 3.4-7 Deep-Sea Octocoral habitat suitability - Stolonifera

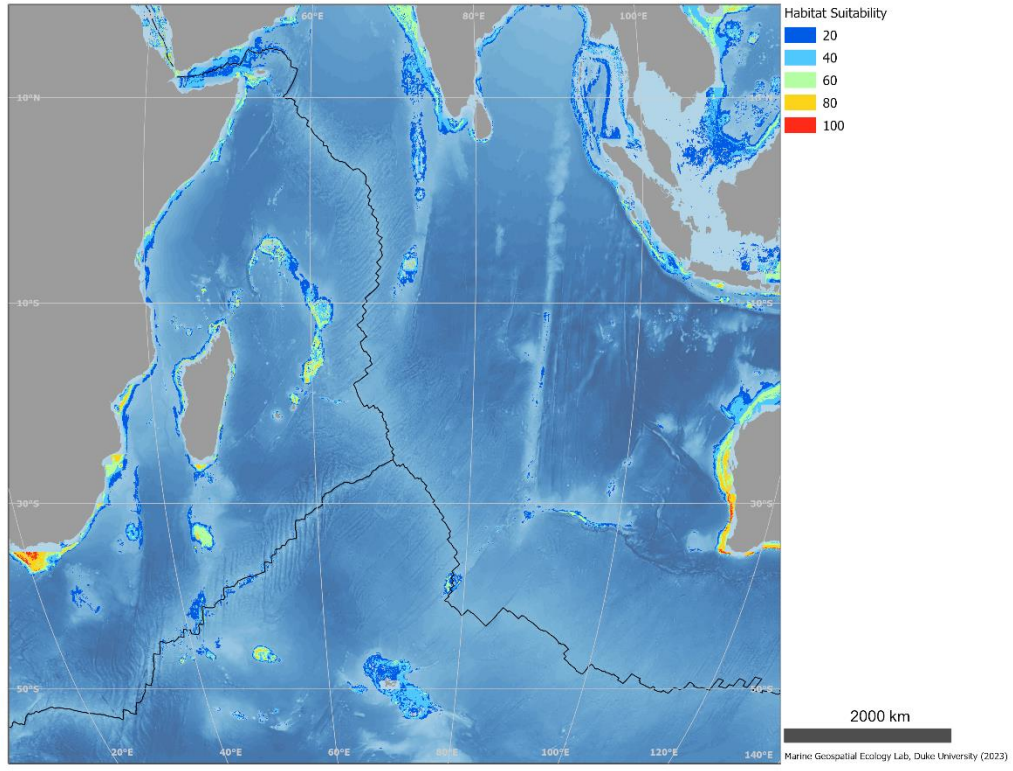


Figure 3.4-8 Deep-Sea Octocoral habitat suitability - Subselliiflorae

### 3.5 Predictions of Habitat Suitability for Framework-Forming Scleractinian Corals

Abstract (Davies & Guinotte 2011):

“Predictive habitat models are increasingly being used by conservationists, researchers and governmental bodies to identify vulnerable ecosystems and species’ distributions in areas that have not been sampled. However, in the deep sea, several limitations have restricted the widespread utilisation of this approach. These range from issues with the accuracy of species presences, the lack of reliable absence data and the limited spatial resolution of environmental factors known or thought to control deep-sea species’ distributions. To address these problems, global habitat suitability models have been generated for five species of framework-forming scleractinian corals by taking the best available data and using a novel approach to generate high resolution maps of seafloor conditions. High-resolution global bathymetry was used to resample gridded data from sources such as World Ocean Atlas to produce continuous 30-arc second (1 km<sup>2</sup>) global grids for environmental, chemical and physical data of the world’s oceans. The increased area and resolution of the environmental variables resulted in a greater number of coral presence records being incorporated into habitat models and higher accuracy of model predictions. The most important factors in determining cold-water coral habitat suitability were depth, temperature, aragonite saturation state and salinity. Model outputs indicated the majority of suitable coral habitat is likely to occur on the continental shelves and slopes of the Atlantic, South Pacific and Indian Oceans. The North Pacific has very little suitable scleractinian coral habitat. Numerous small scale features (i.e., seamounts), which have not been sampled or identified as having a high probability of supporting cold-water coral habitat were identified in all ocean basins. Field validation of newly identified areas is needed to determine the accuracy of model results, assess the utility of modeling efforts to identify vulnerable marine ecosystems for inclusion in future marine protected areas and reduce coral bycatch by commercial fisheries.”

Reference:

Davies AJ, Guinotte JM (2011) Global Habitat Suitability for Framework-Forming Cold-Water Corals. PLoS ONE 6(4): e18483. doi:10.1371/journal.pone.0018483

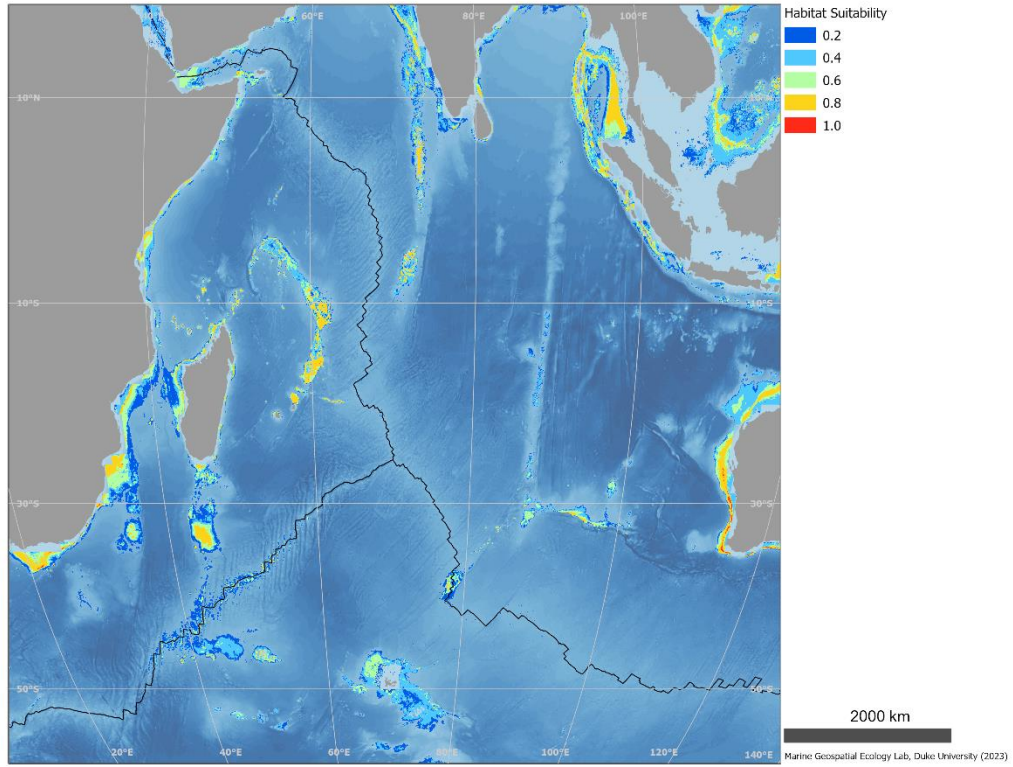


Figure 3.5-1 Deep-Sea Scleractinia habitat suitability – all five framework forming species

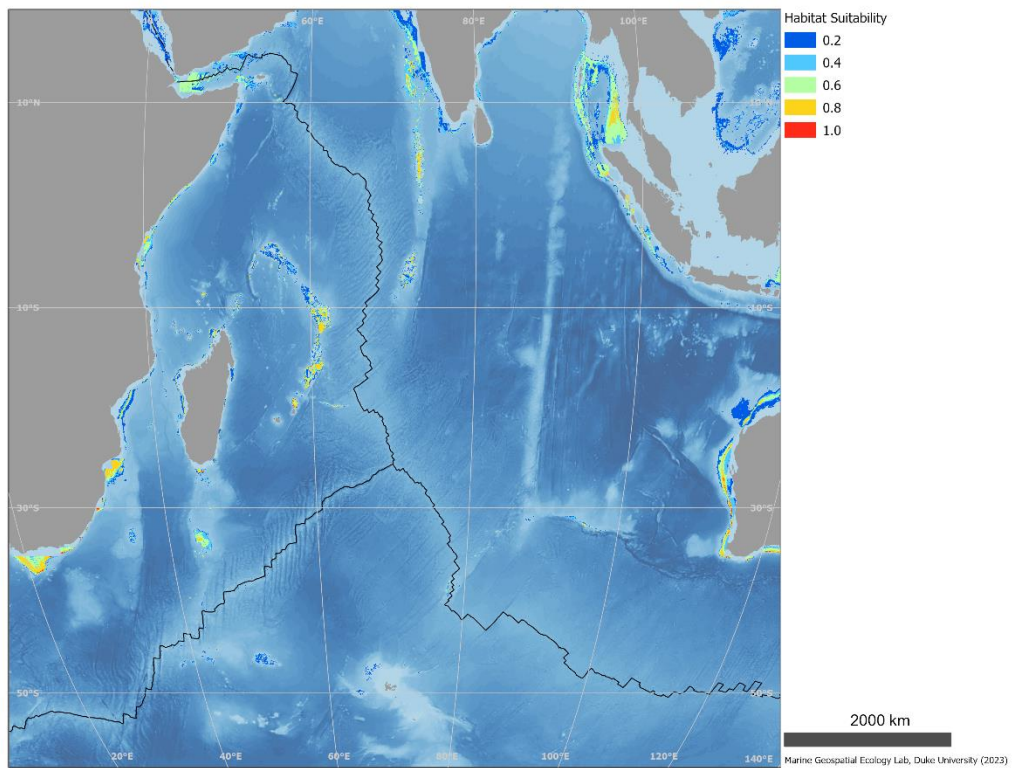


Figure 3.5-2 Deep-Sea Scleractinia habitat suitability – *Lophelia pertusa*

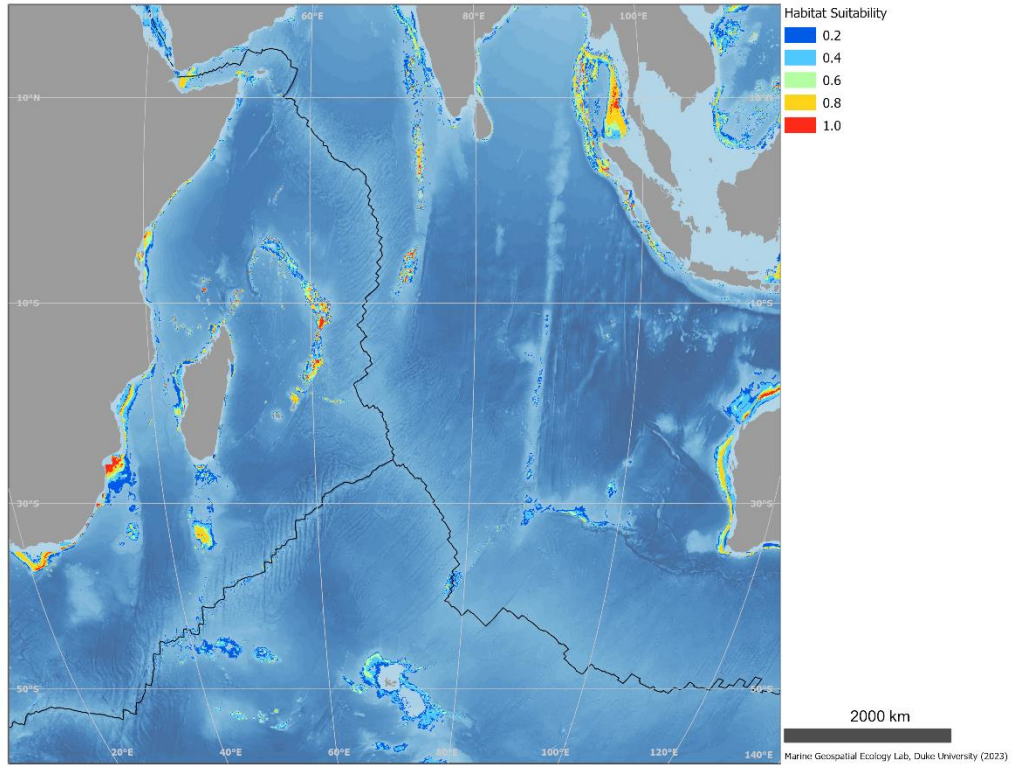


Figure 3.5-3 Deep-Sea Scleractinia habitat suitability – *Madrepora oculata*

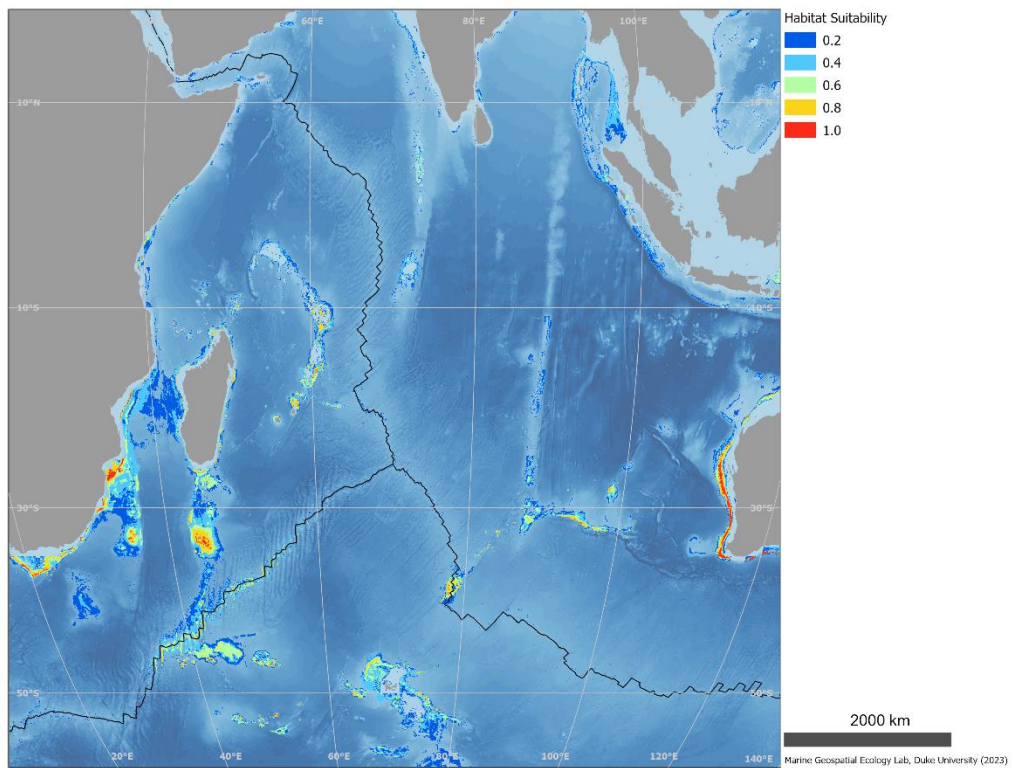


Figure 3.5-4 Deep-Sea Scleractinia habitat suitability – *Solenosmilia variabilis*

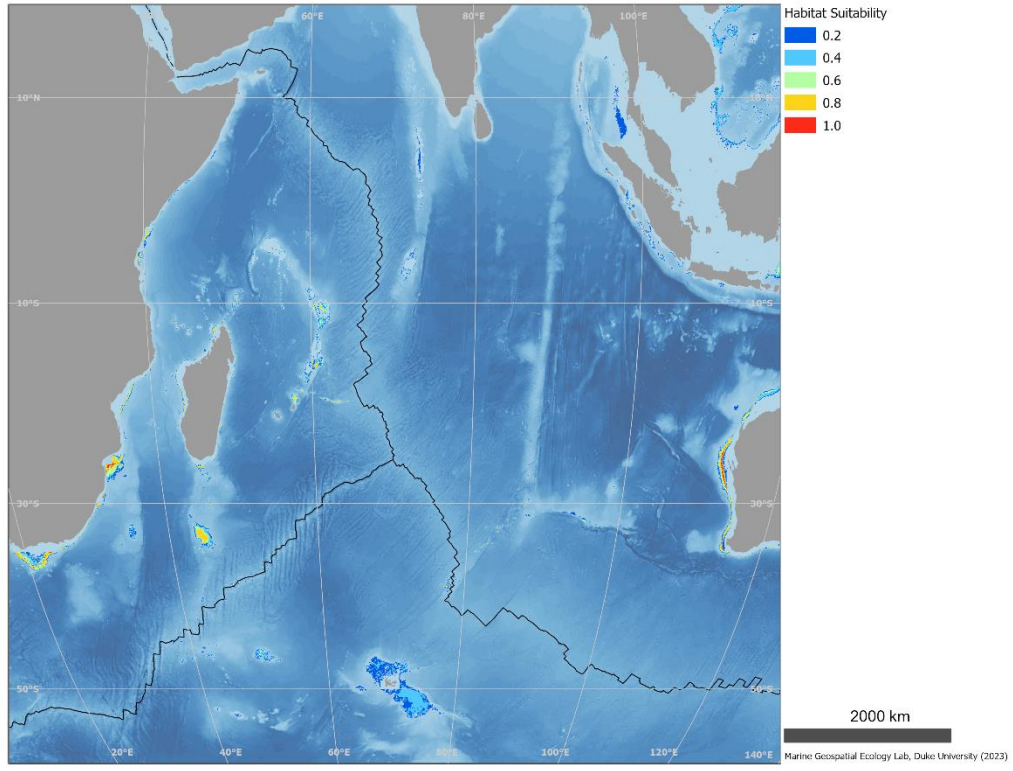


Figure 3.5-5 Deep-Sea Scleractinia habitat suitability – *Goniocorella dumosa*

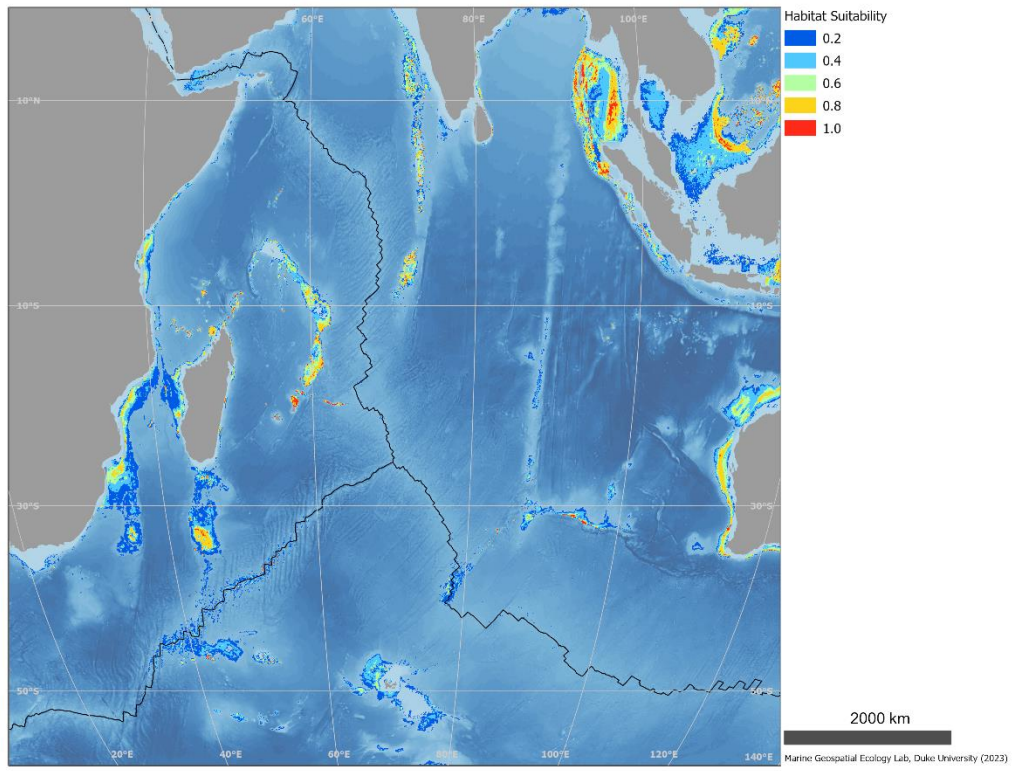


Figure 3.5-6 Deep-Sea Scleractinia habitat suitability – *Enallopsammia rostrata*

### 3.6 International Seabed Authority Deep Data Portal

“The newly developed “ISA Deep Seabed and Ocean Database” (*DeepData*) was launched in July 2019 at the Authority's 25th Session. This database has been designed to serve as a spatial, internet-based data management system. Its main function is to host all deep-seabed activities related data and in particular, data collected by the contractors on their exploration activities as well as any other relevant environmental and resources related data for the Area.

*DeepData* contains information on mineral resource assessment (geological data) and environmental baseline/assessment data. However, only the environmental data are accessible to the public. This include biological, physical and geochemical parameters of the marine ecosystems from the seafloor to the ocean surface.

The Geographical Information System (GIS) is part of *DeepData* functionalities. As such, it allows visualization of contract areas, reserved areas and designated areas of particular environmental interest (APEIs). GIS information accessible through *DeepData* also include sampling locations containing biological, physical and/or geochemical parameters of the seabed sediments and water column.”

Deep Data Portal: <https://data.isa.org.jm/isa/map/>

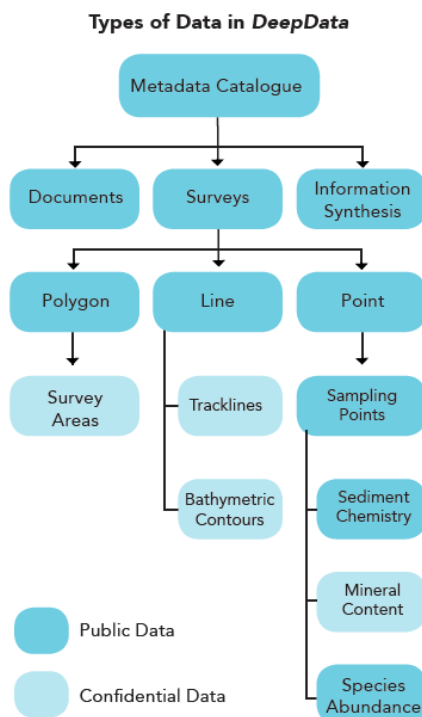


Figure 3.6-1 Chart of data types in Deep Data

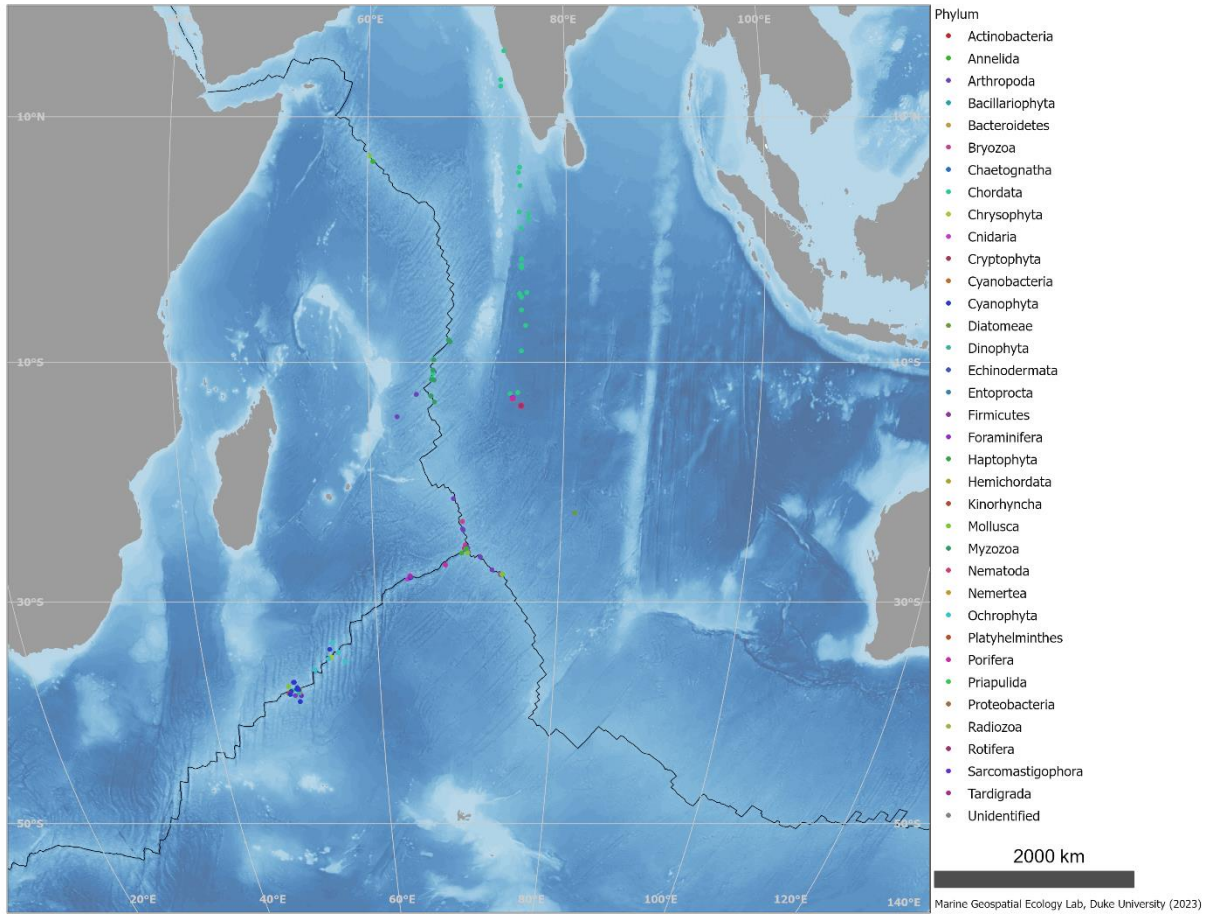


Figure 3.6-2 ISA Deep Data portal

### 3.7 Microbial diversity in newly discovered hydrothermal vents

Abstract (Namirimu et al. 2023):

“Since the discovery of hydrothermal vents in the late 1970s, deep-sea hydrothermal vent fields have attracted great attention as biological hotspots. However, compared with other ocean ridges, the structure and function of microbial communities inhabiting vent fields in the Central Indian ridge (CIR) remain understudied. Here, we provide for the first time 16S rRNA gene-based comparative metagenomic analysis of the sediment-associated microbial communities from three newly discovered vent fields in the CIR. Sediment samples collected in the Invent B, Invent E and Onnuri vent fields varied in geochemical properties, elemental concentrations and associated microbial communities. Proteobacteria (Gammaproteobacteria) was the dominant phylum in Invent B and Onnuri vent fields. In contrast, Invent E mainly consisted of Chloroflexi and Euryarchaeota. Predicted functional profiling revealed that the microbial communities in the three vents are dominated by chemoheterotrophic functions. In addition, microbial communities capable of respiration of sulfur compounds, nitrification, nitrite oxidation, methylotrophy, and methanotrophy were found to be the main chemolithoautotrophs. Compared to other vent fields, Invent E showed a predominance of archaeal methanogens suggesting it exhibits slightly different geochemistry. Multivariate analysis indicated that the biogeochemical and trace metal differences are reflected in the sediment microbial compositions of the three vent fields. This study expands our current understanding of the microbial community structure and potential ecological functions of the newly discovered hydrothermal vent fields in the CIR.”

Reference:

Namirimu, T., Park, M.J., Kim, Y.J. et al. Microbial Diversity of Deep-sea Sediments from Three Newly Discovered Hydrothermal Vent Fields in the Central Indian Ridge. *Ocean Sci. J.* 58, 11 (2023). <https://doi-org.proxy.lib.duke.edu/10.1007/s12601-023-00106-1>

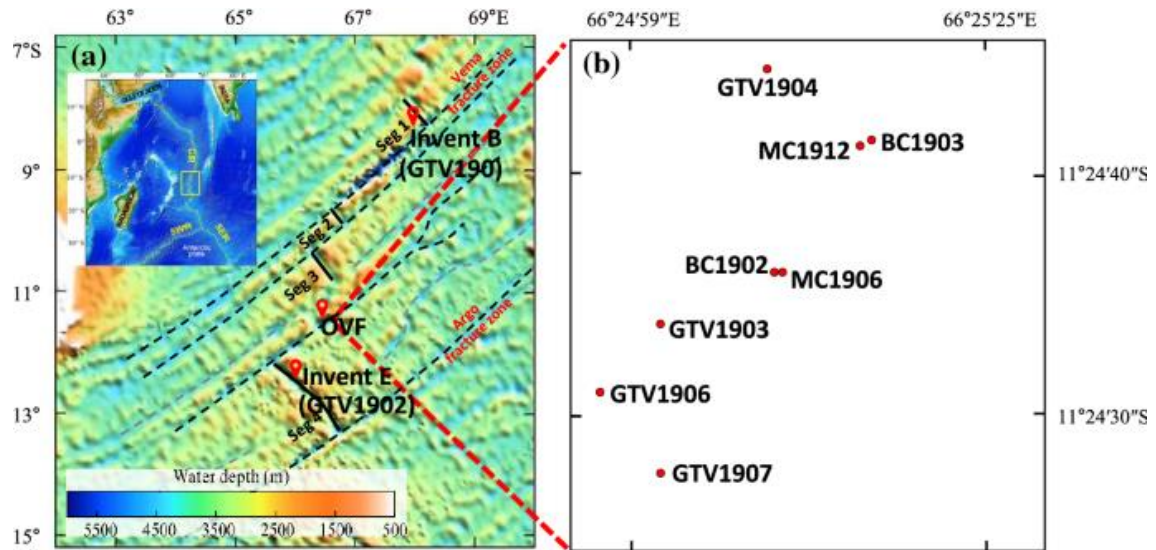


Figure 3.7-1 Hydrothermal vent fields along the Indian Ocean ridges and sampling locations

Original Caption: Figure 1. Map showing a the Indian Ocean ridges (inset) and location of the three hydrothermal vent fields (Invent B, Invent E and Onnuri vent field (OVF)) studied, b sampling sites at OVF. Map was modified from Kim et al. (2022). CIR, Central Indian ridge, SWIR and SEIR, Southwestern and Southeastern Indian ridge.

### 3.8 Structure and connectivity of hydrothermal vent communities

Abstract (Perez et al. 2021):

“To date, 13 biologically active hydrothermal vent (HTV) fields have been described on the West Indian Ocean ridges. Knowledge of benthic communities of these vent ecosystems serves as scientific bases for assessing the resilience of these ecosystems under the global effort to strike an elegant balance between future deep-sea mining and biodiversity conservation. This review aims to summarize our up-to-date knowledge of the benthic community structure and connectivity of these Indian vents and to identify knowledge gaps and key research questions to be prioritized in order to assess the resilience of these communities. The HTVs in the West Indian Ocean are home to many unique invertebrate species such as the remarkable scaly-foot snail. While distinct in composition, the macrofaunal communities of the Indian HTVs share many characteristics with those of other HTVs, including high endemism, strong zonation at the local scale, and a simple food web structure. Furthermore, Indian vent benthic communities are mosaic compositions of Atlantic, Pacific, and Antarctic HTV fauna possibly owing to multiple waves of past colonization. Phylogeographic studies have shed new light into these migratory routes. Current animal connectivity across vent fields appears to be highly influenced by distance and topological barriers. However, contrasting differences in gene flow have been documented across species. Thus, a better understanding of the reproductive biology of the Indian vent animals and the structure of their population at the local scale is crucial for conservation purposes. In addition, increased effort should be given to characterizing the vents’ missing diversity (at both the meio and micro-scale) and elucidating the functional ecology of these vents.”

Reference:

Perez, M., Sun, J., Xu, Q. and Qian, P.Y., 2021. Structure and connectivity of hydrothermal vent communities along the mid-ocean ridges in the west Indian Ocean: a review. *Frontiers in Marine Science*, 8, p.744874. <https://doi.org/10.3389/fmars.2021.744874>

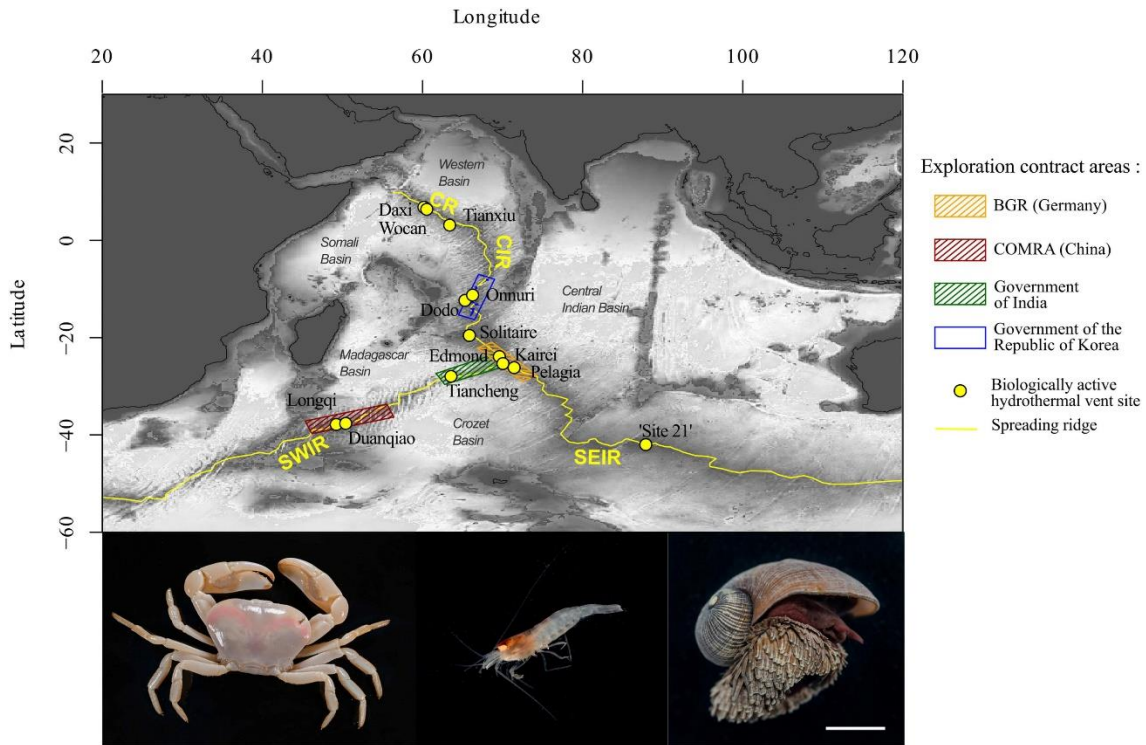


**Figure 3.8-1 Biologically active hydrothermal vents along the Indian Ocean ridges**

*Original Caption: Figure 1. Biologically active hydrothermal vents of the Indian mid-ocean ridges. The Indian Ocean counts eight topological ridges, including four that are active plate boundary rift zones. In recent years, exploration campaigns by the Federal Institute for Geosciences and Natural Resources of Germany (BGR), COMRA (China), the Government of India, and the Government of the Republic of Korea (6 areas within the blue rectangle), who were awarded exploration permits by the ISA between 2011 and 2016 (Minerals: Polymetallic Sulfides | International Seabed Authority), resulted in the discovery of additional vent fields on the CIR, CR, SWIR, and SEIR. At the time of writing this review, 13 active hydrothermal vent fields with associated macrofaunal communities have been described in the Indian mid-ocean ridge. Some of the endemic taxa of the Indian ridges are shown. Bottom-left: *Austinograea rodriguezensis*, bottom-middle: *Mirocaris indica*, bottom-right: *Chrysomallon squamiferum*. Scale bar = 2 cm. Bathymetric data from NOAA, exploration contract areas from <https://www.isa.org.jm/exploration-contracts/polymetallic-sulfides>. Photos courtesy of Dr. Jin Sun.*

### 3.9 Micro nektonic fish species over three seamounts in the southwestern Indian Ocean

Abstract (Cherel et al. 2020):

“Taxonomic composition, abundance and biological features of micronektonic fish were investigated using pelagic trawls conducted near and over the summits of three seamounts located in the western Indian Ocean (La Pérouse, MAD-Ridge and Walters Shoal). Mesopelagic fish from three families accounted for 80% by number of the total catch (5714 specimens, 121 taxa), namely myctophids (59%), gonostomatids (12%) and sternoptychids (9%). Whereas the gonostomatid *Sigmops elongatus* was the most abundant species around La Pérouse seamount, myctophids were the most diverse and dominant group by number in all three studied areas. Most myctophids were high-oceanic species, which included the numerically dominant *Benthoosema suborbitale*, *Ceratoscopelus warmingii*, *Diaphus perspicillatus*, *Hygophum hygomii*, and *Lobianchia dofleini*. The few remaining myctophids (*Diaphus suborbitalis* being the most abundant) were pseudoceanic fish, highlighting the association with landmasses. The study adds one myctophid species new to the Indian Ocean (*Diaphus bertelseni*), and a second record in the literature of the recently described sternoptychid *Argyripnus hulleyi*.”

Reference:

Cherel, Y., Romanov, E.V., Annasawmy, P., Thibault, D. and Ménard, F., 2020. Micronektonic fish species over three seamounts in the southwestern Indian Ocean. Deep Sea Research Part II: Topical Studies in Oceanography, 176, p.104777. <https://doi.org/10.1016/j.dsr2.2020.104777>

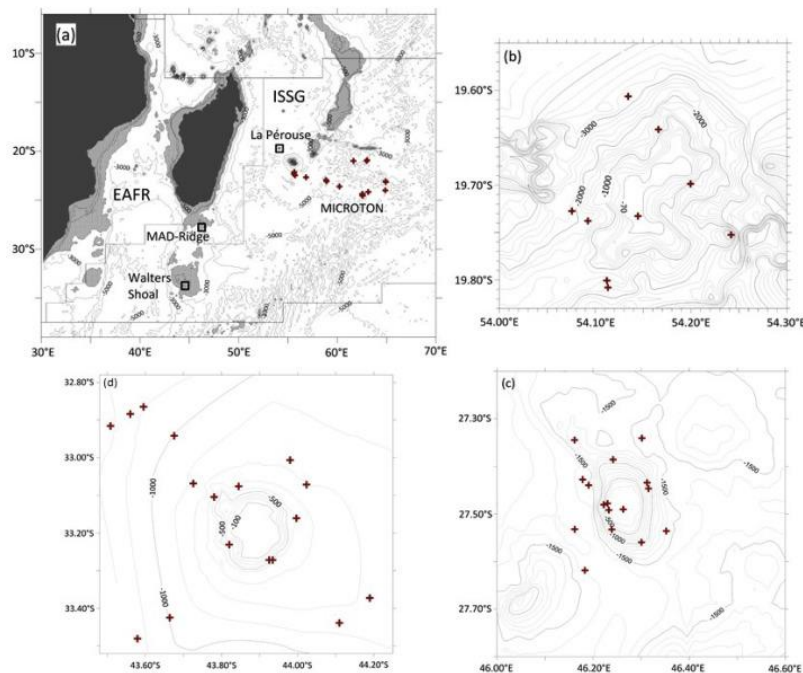


Figure 3.9-1 Study seamounts in the Indian Ocean

*Original Caption: Figure 1. (a) Map of the western Indian Ocean showing the locations of cruises and pelagic trawls (red crosses) over three seamounts: (b) La Pérouse, (c) MAD-Ridge and (d) Walters Shoal, and of the single open ocean investigation (MICROTON). EAFR (East African Coastal Province) and ISSG (Indian South Subtropical Gyre) refer to Longhurst (2007). (For interpretation of the references to colour in this figure legend, the reader is referred to the Web version of this article.)*

### 3.10 Micronekton diel migration, community composition and trophic position within two biogeochemical provinces of the South West Indian Ocean

Abstract (Annasawmy et al. 2018):

“Spatial distribution, community composition and trophic roles of micronekton (crustaceans, fishes and squids) were investigated in the Indian South Subtropical Gyre (ISSG) province and the East African Coastal province (EAFR), by combining acoustic surveys, mid-water trawls and stable isotope analyses from scientific cruises conducted in 2009 and 2010. Mesopelagic micronekton performed diel vertical migrations in both provinces, from deep (400–740 m) to surface (0–200 m) layers at dusk and in the opposite direction at dawn, with some species migrating below 740 m. The EAFR province was more dynamic than the oligotrophic ISSG province, with enhanced eddy activity and enhanced yearly productivity. The active enrichment mechanisms in the EAFR, in terms of available primary production, led to high micronekton acoustic density (as a proxy of micronekton abundance) and large micronekton weight and abundance estimates from trawl data. Particulate organic matter in the EAFR exhibited greater enrichment in  $^{13}\text{C}$  and  $^{15}\text{N}$  compared to the ISSG and, consequently, tissues of selected micronekton organisms in the EAFR were more enriched in  $^{15}\text{N}$  (higher  $\delta^{15}\text{N}$  values). In both provinces, micronekton encompassed a wide range of isotopic niches, with large overlaps between species. Micronekton and swordfish in the EAFR had an overlapping range of  $\delta^{15}\text{N}$  values, contrasting with the ISSG province where swordfish were two trophic levels higher than the sampled micronekton. Our results provide some evidence that the combined action of riverine input and the dynamics of eddies might influence productivity in the EAFR, and hence the abundance of micronekton and the enrichment of tissues in  $^{15}\text{N}$ , compared to the oligotrophic ISSG province.

Reference:

Annasawmy, P., Ternon, J.F., Marsac, F., Cherel, Y., Béhagle, N., Roudaut, G., Lebourges-Dhaussy, A., Demarcq, H., Moloney, C.L., Jaquemet, S. and Ménard, F., 2018. Micronekton diel migration, community composition and trophic position within two biogeochemical provinces of the South West Indian Ocean: Insight from acoustics and stable isotopes. *Deep Sea Research Part I: Oceanographic Research Papers*, 138, pp.85-97. <https://doi.org/10.1016/j.dsr.2018.07.002>

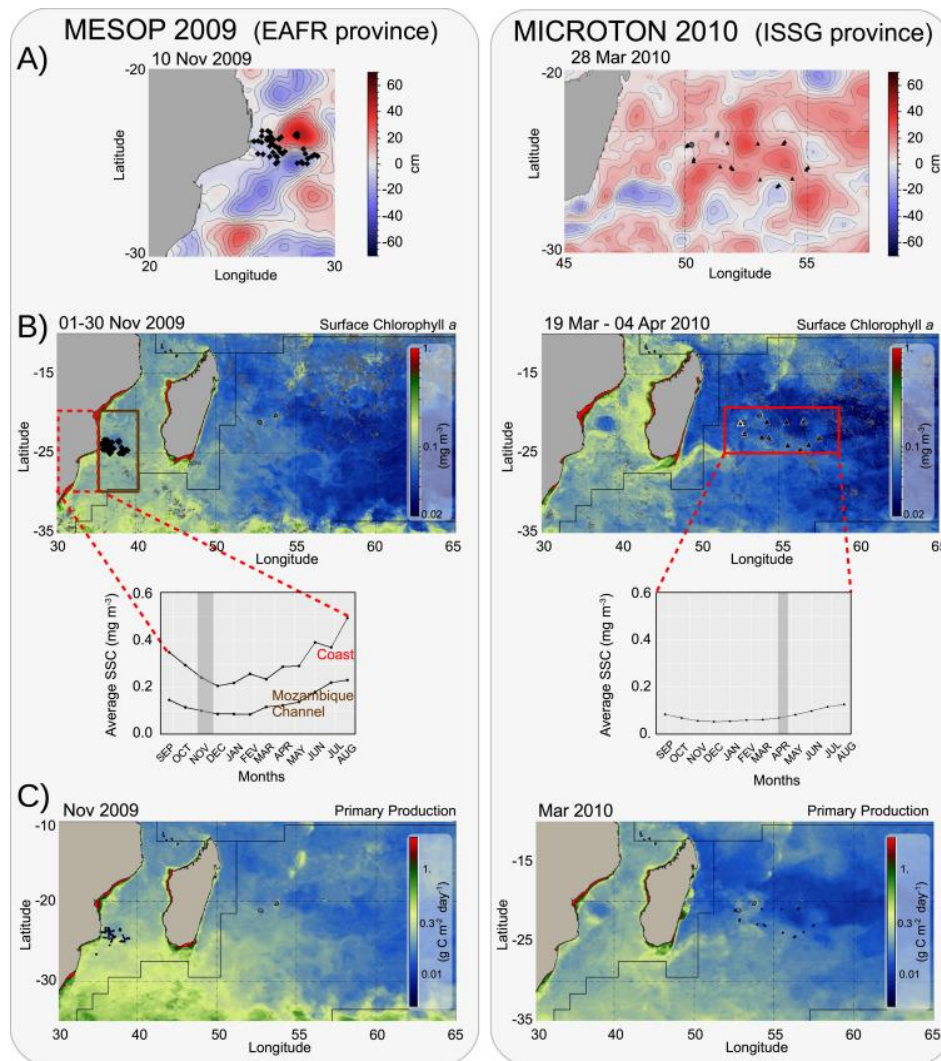


**Figure 3.10-1 Two biogeochemical provinces in the Indian Ocean and their properties**

*Original Caption: Figure 2. (A) Sea level anomaly (SLA) maps, dated 28 March 2010 for the MICROTON cruise (left) in the ISSG, and dated 10 November 2009 for the MESOP 2009 cruise (right) in the EAFR, with positive SLA (red) and negative SLA (blue). Color bar indicates the SLA in cm. (B) Averaged satellite image of chlorophyll a distribution from 19 March to 4 April 2010 in the ISSG and from 1 to 30 November 2009 in the EAFR with monthly mean chlorophyll a values depicted from September 2009 to August 2010 in the region defined in the red squares. The dates of the MICROTON and MESOP cruises are marked by grey bars on the monthly means. Color bar indicates the chlorophyll a concentration in  $\text{mg m}^{-3}$ . (C) Averaged net primary production from 1 to 31 March 2010 for the MICROTON cruise (left) in the ISSG, and from 1 to 30 November 2009 for the MESOP 2009 cruise (right) in the EAFR. Color bar indicates the net primary production in  $\text{g C m}^{-2} \text{ day}^{-1}$ . Black symbols represent the position of CTD stations for MICROTON and MESOP 2009.*

### 3.11 New genera, species and occurrence records of Goniasteridae

Abstract (Mah et al. 2018):

“Modern goniasterids are the most numerous of living asteroids in terms of described genera and species and they have important ecological roles from shallow to deep-water marine habitats. Recent MNHN expeditions and historical collections in the USNM have resulted in the discovery of 18 new species, three new genera and multiple new occurrence records from the western Indian Ocean region including Madagascar, Glorioso and Mayotte islands, Walters Shoal, South Africa, and Somalia. This report provides the first significant contribution to knowledge of deep-sea Asteroidea from the Indian Ocean since the late 20th Century. Several deep-sea species, previously known from the North Pacific are now reported from the western Indian Ocean. Gut contents from *Stellaster* and *Ogmaster* indicate deposit feeding. Feeding modes of this and other deep-sea species are discussed. Comments are made on fossil members of included taxa. A checklist of Indian Ocean Goniasteridae is also included.”

Reference:

Mah, C.L., 2018. New genera, species and occurrence records of Goniasteridae (Asteroidea; Echinodermata) from the Indian Ocean. *Zootaxa*, 4539(1), pp.1-116. DOI: 10.11646/ZOOTAXA.4539.1.1

### 3.12 New Eelpout *Pachycara angeloi* sp. Nov

Abstract (Thiel et al. 2021):

“A new species of eelpout genus *Pachycara* Zugmayer, 1911 is described based on five specimens caught at a depth of 24193275 m along the Central and Southeast Indian Ridges in the Indian Ocean. The specimens were collected during the INDEX cruises in 2016, 2018 and 2019, respectively. The new species is distinguished from its congeners by the following combination of characters: scales and pelvic fins absent; lateral line configuration mediolateral; dorsal fin origin associated with vertebrae 79 with no free predorsal pterygiophores; vertebrae 2728 + 5759 = 8587; dorsal-fin rays 7880, anal-fin rays 5862; pectoral fin rays 1315. DNA sequences of a mitochondrial COI gene fragment showed low intra-specific variation ranging from 0.3 % sequence divergence and do not reflect different vent sites. This is the 29th species of *Pachycara*, which is the fifth to be described from specimens collected only from chemosynthetic environments and the sixth known from the Indian Ocean.”

Reference:

Thiel, R., Knebelsberger, T., Kihara, T. and Gerdes, K., 2021. Description of a new eelpout *Pachycara angeloi* sp. nov. (Perciformes: Zoarcidae) from deep-sea hydrothermal vent fields in the Indian Ocean. *Zootaxa*, 4980(1), p.99112. DOI: 10.11646/zootaxa.4980.1.6

### 3.13 Trophic ecology of Vampire Squid *Vampyroteuthis infernalis*

Abstract (Golikov et al. 2019):

“*Vampyroteuthis infernalis* Chun, 1903, is a widely distributed deepwater cephalopod with unique morphology and phylogenetic position. We assessed its habitat and trophic ecology on a global scale via stable isotope analyses of a unique collection of beaks from 104 specimens from the Atlantic, Pacific and Indian Oceans. Cephalopods typically are active predators occupying a high trophic level (TL) and exhibit an ontogenetic increase in  $\delta^{15}\text{N}$  and TL. Our results, presenting the first global comparison for a deep-sea invertebrate, demonstrate that *V. infernalis* has an ontogenetic decrease in  $\delta^{15}\text{N}$  and TL, coupled with niche broadening. Juveniles are mobile zooplanktivores, while larger *Vampyroteuthis* are slow-swimming opportunistic consumers and ingest particulate organic matter. *Vampyroteuthis infernalis* occupies the same TL (3.0–4.3) over its global range and has a unique niche in deep-sea ecosystems. These traits have enabled the success and abundance of this relict species inhabiting the largest ecological realm on the planet.

Reference:

Golikov, A.V., Ceia, F.R., Sabirov, R.M. et al. The first global deep-sea stable isotope assessment reveals the unique trophic ecology of Vampire Squid *Vampyroteuthis infernalis* (Cephalopoda). *Sci Rep* 9, 19099 (2019). <https://doi.org/10.1038/s41598-019-55719-1>

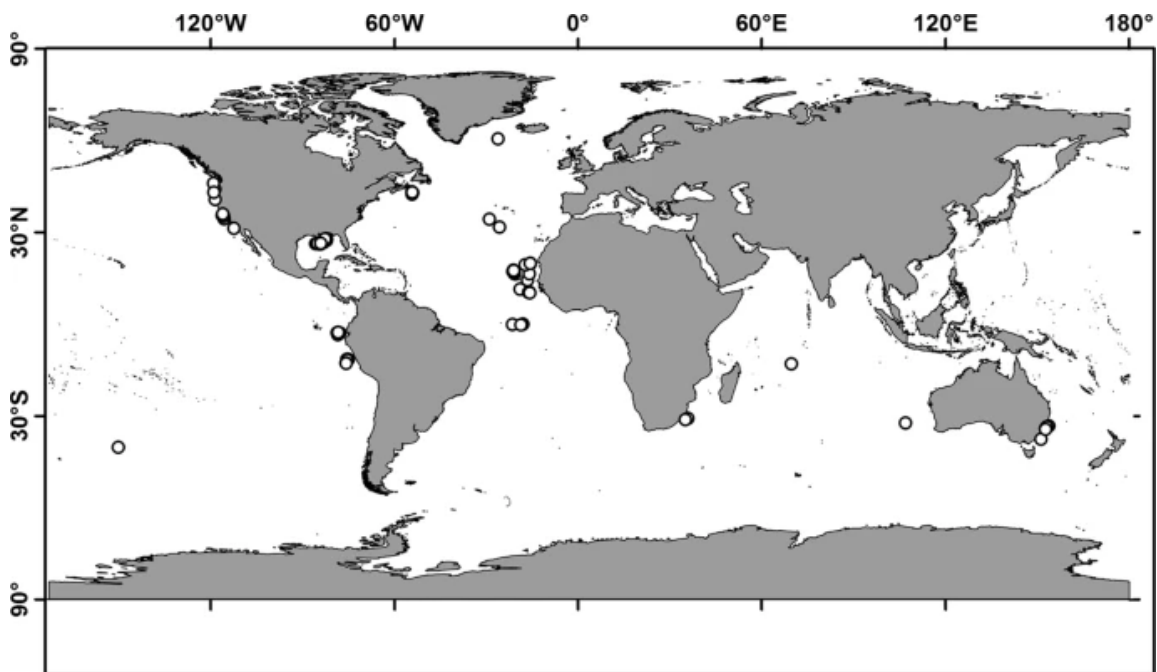


Figure 3.13-1 Study sample locations

Original Caption: Figure 1. *Vampyroteuthis infernalis* sample locations. Map created by A.V.G. in QGIS 3.8.0 (QGIS Development Team, 2009. QGIS Geographic Information System. Open Source Geospatial Foundation. <http://qgis.org>).

### 3.14 Baleen whale distribution

Abstract (Dréo et al. 2019):

“From the acoustic data acquired by the RHUM-RUM (Réunion Hotspot and Upper Mantle Réunions Unterer Mantel) Ocean Bottom Seismometer (OBS) network between October 2012 and November 2013, this study revealed baleen whale occurrence in the western Indian Ocean (IO). Low-frequency songs from three species (Antarctic Blue Whales, Pygmy Blue Whales and Fin Whales) as well as P-calls (or Spot-calls) from an unknown species were recorded on the dataset. The wide arrangement of the OBS network (2000 km × 2000 km) provided valuable information to draw seasonal patterns of occurrence and distribution all over the area. These species occurred sympatrically in the western IO, at least during austral autumn months emphasizing the importance of this region for these populations. This data set helped to refine the knowledge on their spatio-temporal distribution and complete the picture built by previous studies. A tighter sub-network of 8 OBSs deployed on the South West Indian Ridge provided ideal inter-sensor spacing for whale tracking. We demonstrated the capability of such array of detecting and tracking the three different whale species up to 50 km and for several hours. As a result and to understand the effect of acoustic wave propagation, songs from the tracking were described at a close and remote distance of the sensor. This work could also help to understand the local behavior of these species during austral autumn months in this area of the western Indian Ocean.”

Reference:

Dréo, R., Bouffaut, L., Leroy, E., Barruol, G. and Samaran, F., 2019. Baleen whale distribution and seasonal occurrence revealed by an ocean bottom seismometer network in the Western Indian Ocean. *Deep Sea Research Part II: Topical Studies in Oceanography*, 161, pp.132-144. <https://doi.org/10.1016/j.dsr2.2018.04.005>

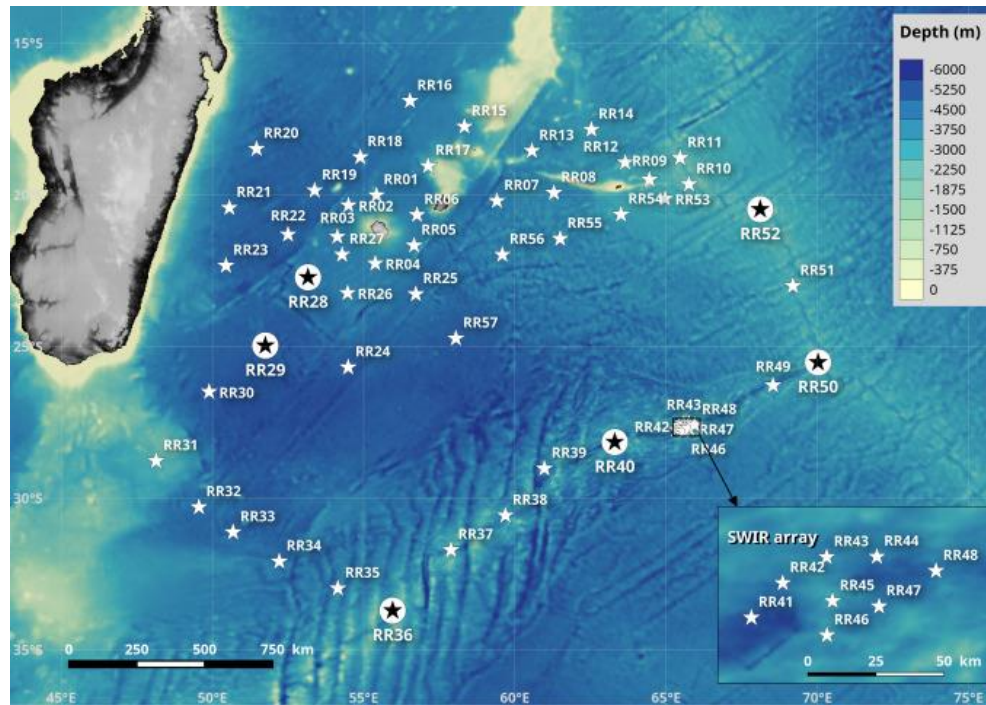


Figure 3.14-1 Acoustic array in the Indian Ocean

Original Caption: Figure 1. RHUM-RUM network and the SWIR array Stähler et al., 2016, RHUM-RUM,. Black stars indicate the OBSs used for the whales seasonal pattern description and the SWIR array shown in the zoomed inset indicate OBSs used for local whales tracking.

### 3.15 Phylogeography of hydrothermal vent stalked barnacles

Abstract (Watanabe et al. 2018):

“Phylogeography of animals provides clues to processes governing their evolution and diversification. The Indian Ocean has been hypothesized as a ‘dispersal corridor’ connecting hydrothermal vent fauna of Atlantic and Pacific oceans. Stalked barnacles of the family Eolepadidae are common associates of deep-sea vents in Southern, Pacific and Indian oceans, and the family is an ideal group for testing this hypothesis. Here, we describe *Neolepas marisindica* sp. nov. from the Indian Ocean, distinguished from *N. zevinae* and *N. rapanuii* by having a tridentoid mandible in which the second tooth lacks small elongated teeth. Morphological variations suggest that environmental differences result in phenotypic plasticity in the capitulum and scales on the peduncle in eolepadids. We suggest that diagnostic characters in Eolepadidae should be based mainly on more reliable arthropodal characters and DNA barcoding, while the plate arrangement should be used carefully with their intraspecific variation in mind. We show morphologically that *Neolepas* specimens collected from the South West Indian Ridge, the South East Indian Ridge and the Central Indian Ridge belong to the new species. Molecular phylogeny and fossil evidence indicated that *Neolepas* migrated from the southern Pacific to the Indian Ocean through the Southern Ocean, providing key evidence against the ‘dispersal corridor’ hypothesis. Exploration of the South East Indian Ridge is urgently required to understand vent biogeography in the Indian Ocean.”

Reference:

Watanabe, H.K., Chen, C., Marie, D.P., Takai, K., Fujikura, K. and Chan, B.K., 2018. Phylogeography of hydrothermal vent stalked barnacles: a new species fills a gap in the Indian Ocean ‘dispersal corridor’ hypothesis. *Royal Society Open Science*, 5(4), p.172408. <https://doi.org/10.1098/rsos.172408>

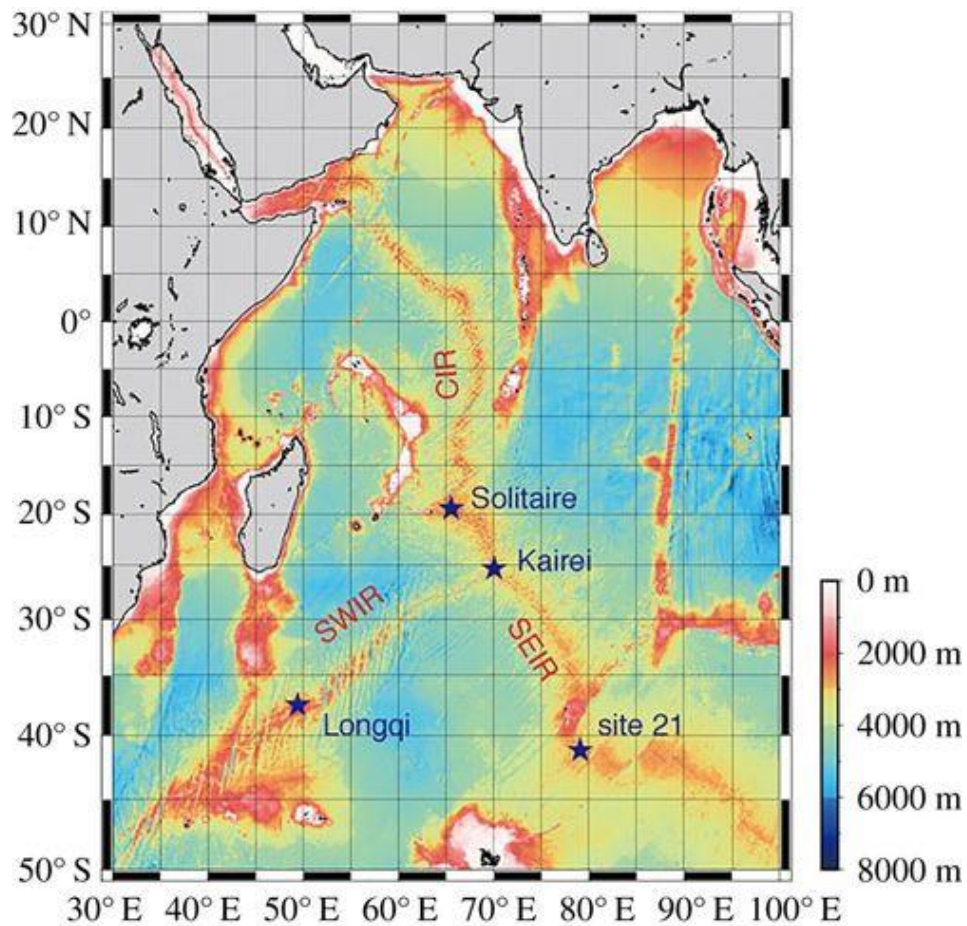


Figure 3.15-1 Locations of study hydrothermal vents in the Indian Ocean

*Original Caption: Figure 1. Map of Indian Ocean Ridges, showing the locations of the four hydrothermal vent fields; Kairei and Solitaire fields on the Central Indian Ridge, Longqi field on the South West Indian Ridge, and site 21 near Amsterdam--St Paul Plateau on the South East Indian Ridge.*

### 3.16 Bacterial and fungal biodiversity in the Indian Ocean

Abstract (Barnes et al. 2021):

“The deep sea is the largest environment on Earth, comprising important resources of commercial interest. It is composed of a wide variety of ecosystems, which is home to often unique organisms that are yet to be described. The deep-sea is one of the least studied environments, where research is strongly linked to technological access and advances. With the recent advances in the next-generation sequencing and bioinformatics tools, there is an enhanced understanding of microbial diversity and ecological functions in deep sea. Multidisciplinary programs are being undertaken to investigate into microbial communities in diverse marine environments. As compared to other Oceans, the deeper parts of Indian Ocean are still poorly sampled and studied for bacterial, and more so fungal diversity. The studies reporting usage of modern sequencing tools to describe uncultured microbial diversity have seen a rise in numbers in the last decade. In this review, we summarize the important findings of research works carried on bacterial and fungal diversity from the abyssal regions of the Indian Ocean and provide our views on possible future paths.”

Reference:

Barnes, N.M., Damare, S.R. and Shenoy, B.D., 2021. Bacterial and fungal diversity in sediment and water column from the abyssal regions of the Indian Ocean. *Frontiers in Marine Science*, 8, p.687860.<https://doi.org/10.3389/fmars.2021.687860>

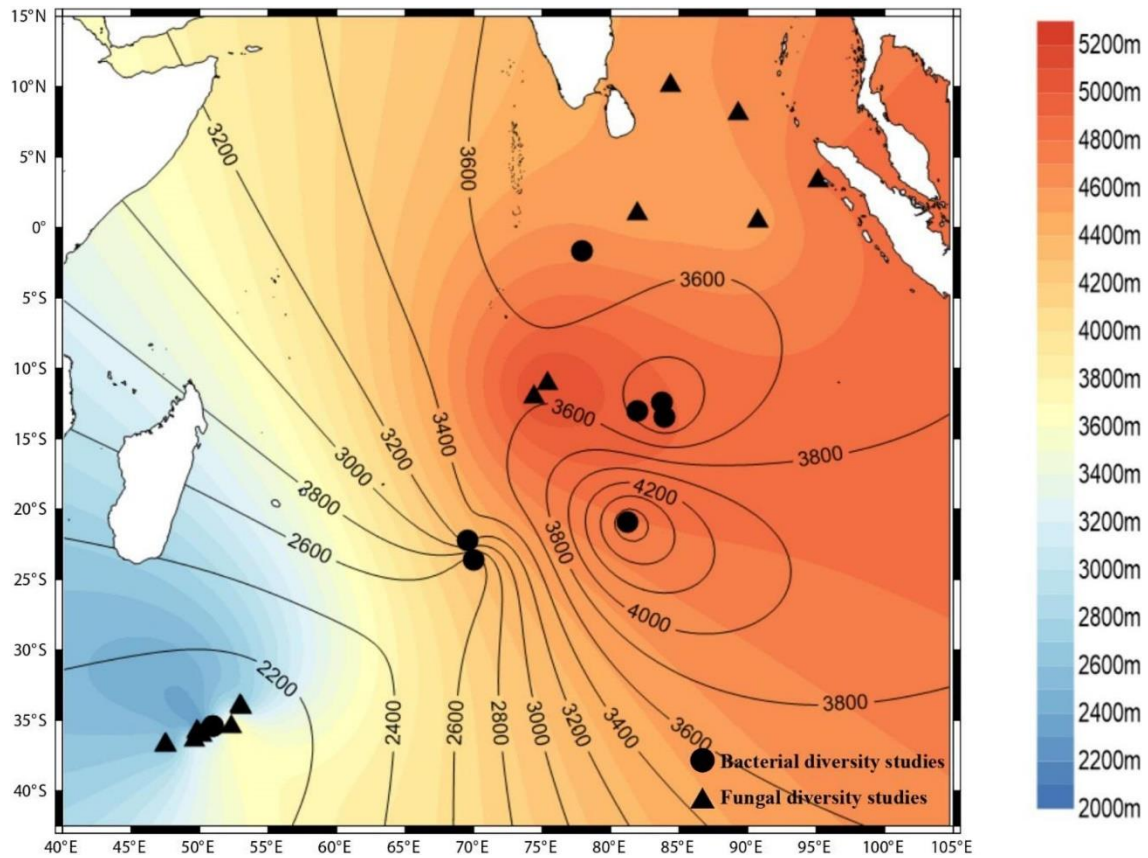


Figure 3.16-1 Locations of study sites in the Indian Ocean

Original Caption: Figure 1. Culture-independent studies carried out at various locations in the Indian Ocean. The circles depict the bacterial diversity studies; the triangles depict the fungal diversity studies. (Surfer, Golden software LLC).

### 3.17 Predicted faunal assemblage with 3D high resolution data

Abstract (Gerdes et al. 2019):

“Active hydrothermal vent fields are complex, small-scale habitats hosting endemic fauna that changes at scales of centimeters, influenced by topographical variables. In previous studies, it has been shown that the distance to hydrothermal fluids is also a major structuring factor. Imagery analysis based on two dimensional photo stitching revealed insights to the vent field zonation around fluid exits and a basic knowledge of faunal assemblages within hydrothermal vent fields. However, complex three dimensional surfaces could not be adequately replicated in those studies, and the assemblage structure, as well as their relation to abiotic terrain variables, is often only descriptive. In this study we use ROV video imagery of a hydrothermal vent field on the southeastern Indian Ridge in the Indian Ocean. Structure from Motion photogrammetry was applied to build a high resolution 3D reconstruction model of one side of a newly discovered active hydrothermal chimney complex, allowing for the quantification of abundances. Likewise, the reconstruction was used to infer terrain variables at a scale important for megabenthic specimens, which were related to the abundances of the faunal assemblages. Based on the terrain variables, applied random forest model predicted the faunal assemblage distribution with an accuracy of 84.97 %. The most important structuring variables were the distances to diffuse- and black fluid exits, as well as the height of the chimney complex. This novel approach enabled us to classify quantified abundances of megabenthic taxa to distinct faunal assemblages and relate terrain variables to their distribution. The successful prediction of faunal assemblage occurrences further supports the importance of abiotic terrain variables as key structuring factors in hydrothermal systems and offers the possibility to detect suitable areas for Marine Protected areas on larger spatial scales. This technique works for any kind of video imagery, regardless of its initial purpose and can be implemented in marine monitoring and management.”

Reference:

Gerdes, K., Martinez Arbizu, P., Schwarz-Schampera, U., Schwentner, M., & Kihara, T. C. (2019). Detailed Mapping of Hydrothermal Vent Fauna: A 3D Reconstruction Approach Based on Video Imagery. *Frontiers in Marine Science*, 6, 96.doi: 10.3389/fmars.2019.00096

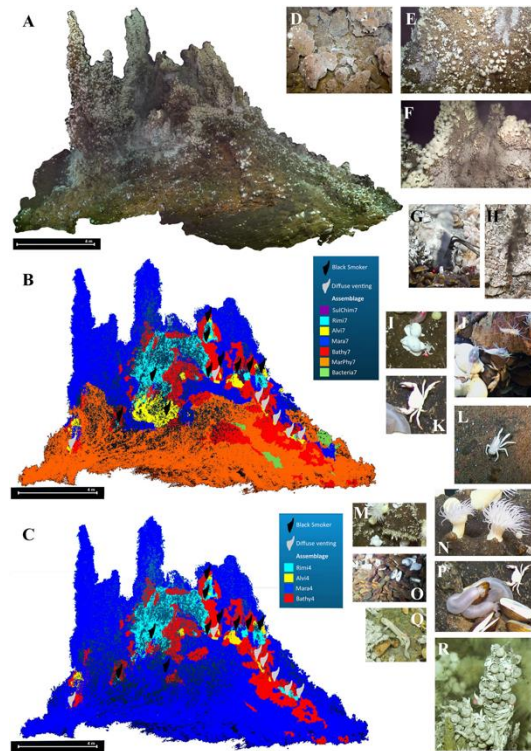


Figure 3.17-1 Figure 4 from Gerdes et al. (2019)

Original Caption: FIGURE 4 | South side structure from motion textured mesh of the 3D chimney reconstruction, detail of the textured surface and manually assigned faunal assemblages. (A) Textured reconstructed chimney. (B) Faunal assemblage distribution assigned by dominant taxa. (C) Faunal assemblage distribution based on *k*-medoid clustering. (D) Sulfide blocks of the chimney complex. (E) Overview of mussel and shrimp aggregations. (F) Overview of shrimp and anemone aggregations. (G) Diffuse fluid exit. (H) Black fluid exit. (I) *Phymorhynchus* spp.. (J) *Rimicaris kairei*. (K) *Austinograea rodriguezensis*. (L) *Munidopsis pallida*. (M) *Neolepas marisindica*. (N) *Maractis* sp.. (O) *Bathymodiolus septemdierum*. (P) *Chiridota* sp.. (Q) *Zoarcidae* gen. sp.. (R) *Alviniconcha marisindica*.

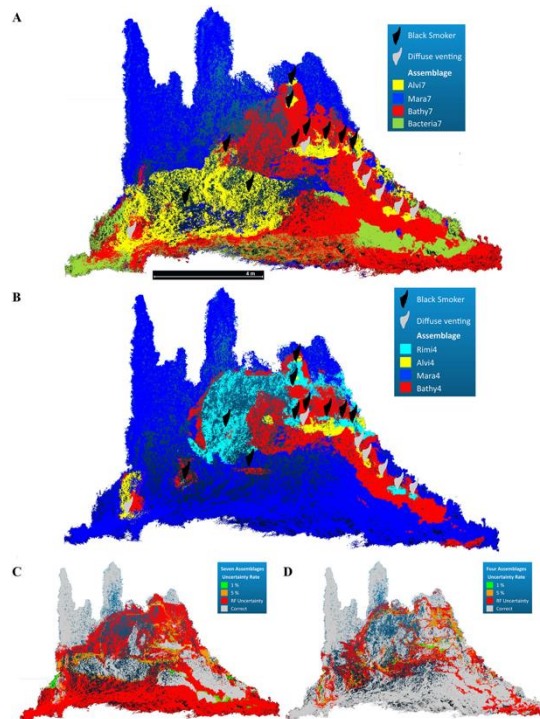


Figure 3.17-2 Figure 7 from Gerdes et al. (2019)

*Original Caption: FIGURE 7 | Predicted faunal assemblage occurrence across the reconstructed chimney complex based on random forest modeling. (A) Occurrence of the seven faunal assemblages based on the winning classes of the predicted random forest model (Accuracy = 0.4405). (B) Occurrence of the four faunal assemblages based on the winning classes of the predicted random forest model (Accuracy = 0.8497). (C,D) False positive uncertainty rate at 1%, 5% and the random forest prediction uncertainty for both assemblages.*

### 3.18 Global Patterns in Benthic Biomass

Abstract (Yool et al. 2017):

“Deep-water benthic communities in the ocean are almost wholly dependent on near-surface pelagic ecosystems for their supply of energy and material resources. Primary production in sunlit surface waters is channelled through complex food webs that extensively recycle organic material, but lose a fraction as particulate organic carbon (POC) that sinks into the ocean interior. This exported production is further rarefied by microbial breakdown in the abyssal ocean, but a residual ultimately drives diverse assemblages of seafloor heterotrophs. Advances have led to an understanding of the importance of size (body mass) in structuring these communities. Here we force a size-resolved benthic biomass model, BORIS, using seafloor POC flux from a coupled ocean-biogeochemistry model, NEMO-MEDUSA, to investigate global patterns in benthic biomass. BORIS resolves 16 size classes of metazoans, successively doubling in mass from approximately 1  $\mu\text{g}$  to 28 mg. Simulations find a wide range of seasonal responses to differing patterns of POC forcing, with both a decline in seasonal variability, and an increase in peak lag times with increasing body size. However, the dominant factor for modelled benthic communities is the integrated magnitude of POC reaching the seafloor rather than its seasonal pattern. Scenarios of POC forcing under climate change and ocean acidification are then applied to investigate how benthic communities may change under different future conditions. Against a backdrop of falling surface primary production (-6.1%), and driven by changes in pelagic remineralization with depth, results show that while benthic communities in shallow seas generally show higher biomass in a warmed world (+3.2%), deep-sea communities experience a substantial decline (-32%) under a high greenhouse gas emissions scenario. Our results underscore the importance for benthic ecology of reducing uncertainty in the magnitude and seasonality of seafloor POC fluxes, as well as the importance of studying a broader range of seafloor environments for future model development.”

Reference:

Yool, Andrew, Adrian P. Martin, Thomas R. Anderson, Brian J. Bett, Daniel OB Jones, and Henry A. Ruhl. "Big in the benthos: Future change of seafloor community biomass in a global, body size-resolved model." *Global change biology* 23, no. 9 (2017): 3554-3566.doi: 10.1111/gcb.13680

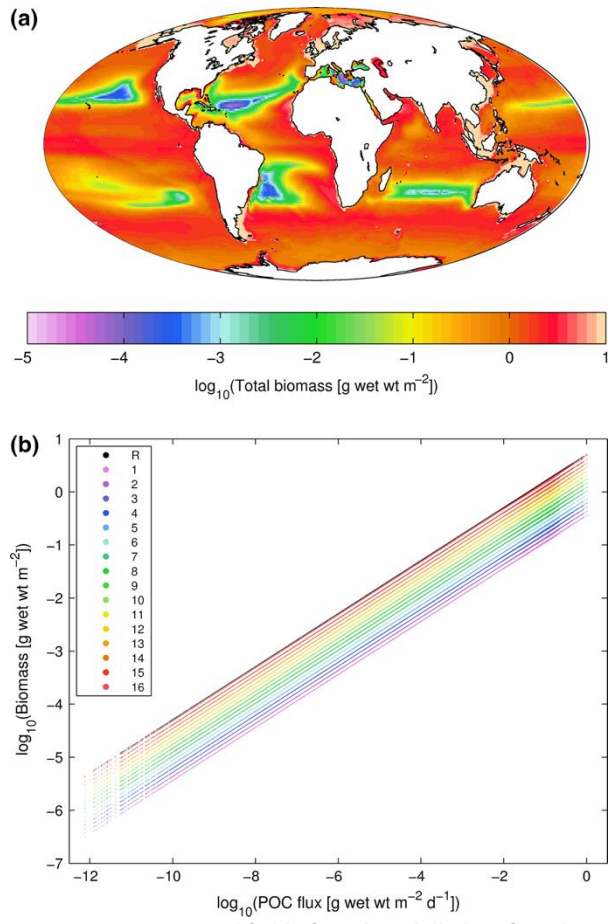


Figure 3.18-1 Mean annual field of total modelled seafloor biomass

### 3.19 OBIS-SEAMAP Data Summaries

OBIS-SEAMAP (<http://seamap.env.duke.edu/>), Ocean Biodiversity Information System Spatial Ecological Analysis of Megavertebrate Populations, is a spatially referenced online database, aggregating marine mammal, seabird and sea turtle observation data from across the globe. Data from several sea turtle and marine mammal tracking efforts were extracted from OBIS-SEAMAP data center for the study area.

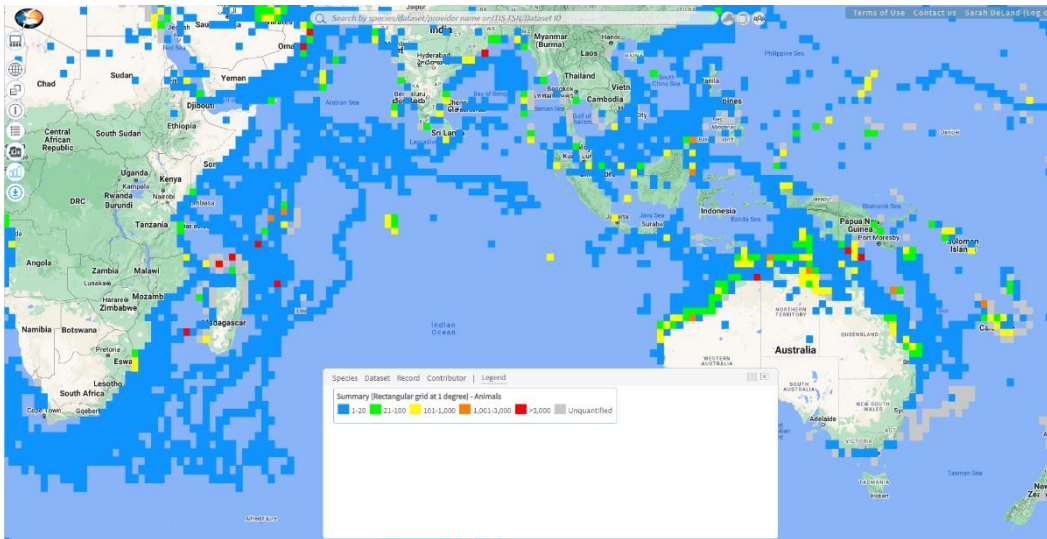


Figure 3.19-1 Turtle observations

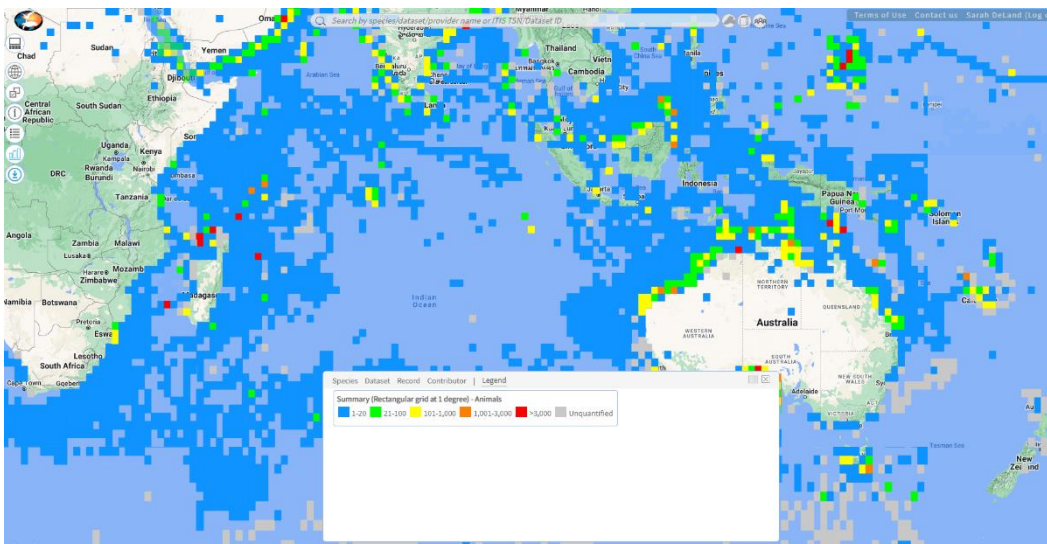


Figure 3.19-2 Marine mammal observations

### 3.20 Global patterns of marine turtle bycatch

Abstract (Wallace et al. 2010):

“Fisheries bycatch is a primary driver of population declines in several species of marine megafauna (e.g., elasmobranchs, mammals, seabirds, turtles). Characterizing the global bycatch seascape using data on bycatch rates across fisheries is essential for highlighting conservation priorities. We compiled a comprehensive database of reported data on marine turtle bycatch in gillnet, longline, and trawl fisheries worldwide from 1990 to 2008. The total reported global marine turtle bycatch was ~85,000 turtles, but due to the small percentage of fishing effort observed and reported (typically <1% of total fleets), and to a global lack of bycatch information from small-scale fisheries, this likely underestimates the true total by at least two orders of magnitude. Our synthesis also highlights an apparently universal pattern across fishing gears and regions where high bycatch rates were associated with low observed effort, which emphasizes the need for strategic bycatch data collection and reporting. This study provides the first global perspective of fisheries bycatch for marine turtles and highlights region–gear combinations that warrant urgent conservation action (e.g., gillnets, longlines, and trawls in the Mediterranean Sea and eastern Pacific Ocean) and region–gear combinations in need of enhanced observation and reporting efforts (e.g., eastern Indian Ocean gillnets, West African trawls).”

Reference:

Wallace, B.P., Lewison, R.L., McDonald, S.L., McDonald, R.K., Kot, C.Y., Kelez, S., Bjorkland, R.K., Finkbeiner, E.M., Helmbrecht, S. & Crowder, L.B. (2010) Global patterns of marine turtle bycatch. *Conservation Letters*, 3, 131–142. doi: 10.1111/j.1755-263X.2010.00105.x

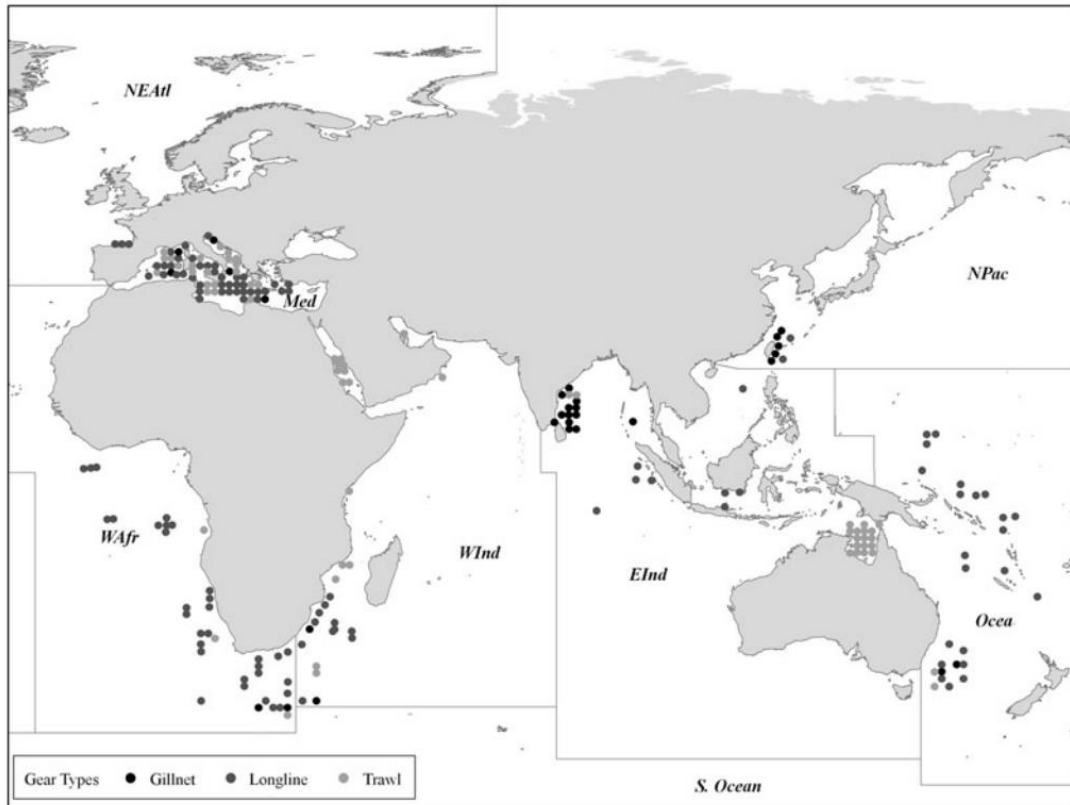


Figure 3.20-1 Overview of sea turtle bycatch data

*Original Caption: Figure 1. Geographic delineation of regions and putative distribution of marine turtle bycatch records for gillnets, longlines, and trawls. Points represent all records we compiled in our database (n= 993), including those we used in analyses (n= 700). Locations were plotted according to reported geographic coordinates, or when coordinates were not available, based on region-specific descriptions of each fishing gear.*

### 3.21 Sea turtle connectivity

Abstract (Kot et al. 2022):

“Aim: Understanding the spatial ecology of animal movements is a critical element in conserving long-lived, highly mobile marine species. Analyzing networks developed from movements of six sea turtle species reveals marine connectivity and can help prioritize conservation efforts.

Location: Global.

Methods: We collated telemetry data from 1235 individuals and reviewed the literature to determine our dataset's representativeness. We used the telemetry data to develop spatial networks at different scales to examine areas, connections, and their geographic arrangement. We used graph theory metrics to compare networks across regions and species and to identify the role of important areas and connections.

Results: Relevant literature and citations for data used in this study had very little overlap. Network analysis showed that sampling effort influenced network structure, and the arrangement of areas and connections for most networks was complex. However, important areas and connections identified by graph theory metrics can be different than areas of high data density. For the global network, marine regions in the Mediterranean had high closeness, while links with high betweenness among marine regions in the South Atlantic were critical for maintaining connectivity. Comparisons among species-specific networks showed that functional connectivity was related to movement ecology, resulting in networks composed of different areas and links.

Main conclusions: Network analysis identified the structure and functional connectivity of the sea turtles in our sample at multiple scales. These network characteristics could help guide the coordination of management strategies for wide-ranging animals throughout their geographic extent. Most networks had complex structures that can contribute to greater robustness but may be more difficult to manage changes when compared to simpler forms. Area-based conservation measures would benefit sea turtle populations when directed toward areas with high closeness dominating network function. Promoting seascape connectivity of links with high betweenness would decrease network vulnerability.”

Reference:

Kot, C. Y., Åkesson, S., Alfaro-Shigueto, J., Amorocho Llanos, D. F., Antonopoulou, M., Balazs, G. H., Baverstock, W. R., Blumenthal, J. M., Broderick, A. C., Bruno, I., Canbolat, A. F., Casale, P., Cejudo, D., Coyne, M. S., Curtice, C., DeLand, S., DiMatteo, A., Dodge, K., Dunn, D. C., ... Halpin, P. N. (2022). Network analysis of sea turtle movements and connectivity: A tool for conservation prioritization. *Diversity and Distributions*, 28, 810–829.

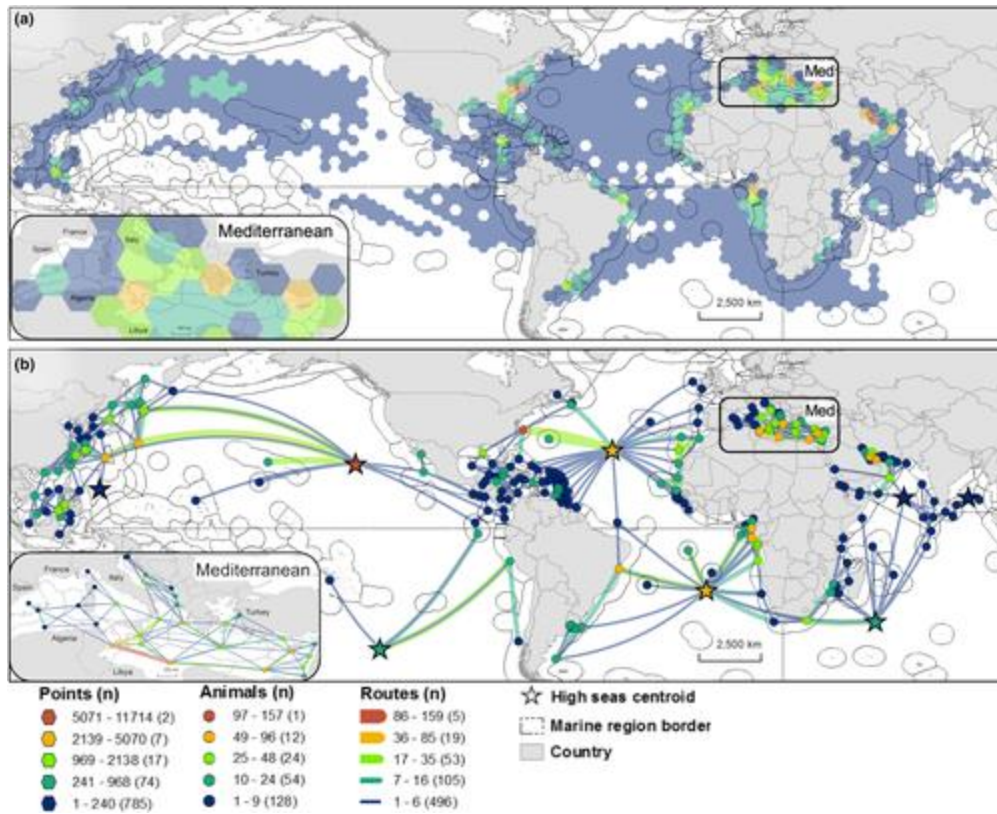


Figure 3.21-1 Sea turtle tracking data distribution

Original Caption: Figure 1. Tracking data for six sea turtle species summarized by (a) number of locations within a hexagonal grid, and (b) number of animals per marine region and number of routes taken between marine regions within a network diagram using marine region centroids as nodes. Grid cell =  $1.62 \times 105$  km hexagon; stars symbolize the centroid of individual high-sea marine regions, not animal point location; circles symbolize the centroid of individual marine regions within national jurisdictions, not animal location; links represent connections, not animal paths; two overlapping links between nodes represent connections in both directions. Data were classified using natural breaks (Jenks) within each panel; warmer colors represent higher values and cooler colors represent lower values; number of map features in parenthesis.

### 3.22 Important Bird Areas (IBAs)

BirdLife Important Bird Areas (IBAs) have been identified using several data sources: 1) terrestrial seabird breeding sites are shown with point locality and species that qualifies at the IBA (<http://www.birdlife.org/datazone/site/search>), 2) marine areas around breeding colonies have been identified based on literature review where possible to guide the distance required by each species; where literature is sparse or lacking, extensions have been applied on a precautionary basis (<http://seabird.wikispaces.com/>), and 3) sites identified by satellite tracking data via kernel density analysis, first passage time analysis and bootstrapping approaches ([www.seabirdtracking.org](http://www.seabirdtracking.org)). Together these IBAs form a network of sites of importance to coastal, pelagic, resident and or migratory species.

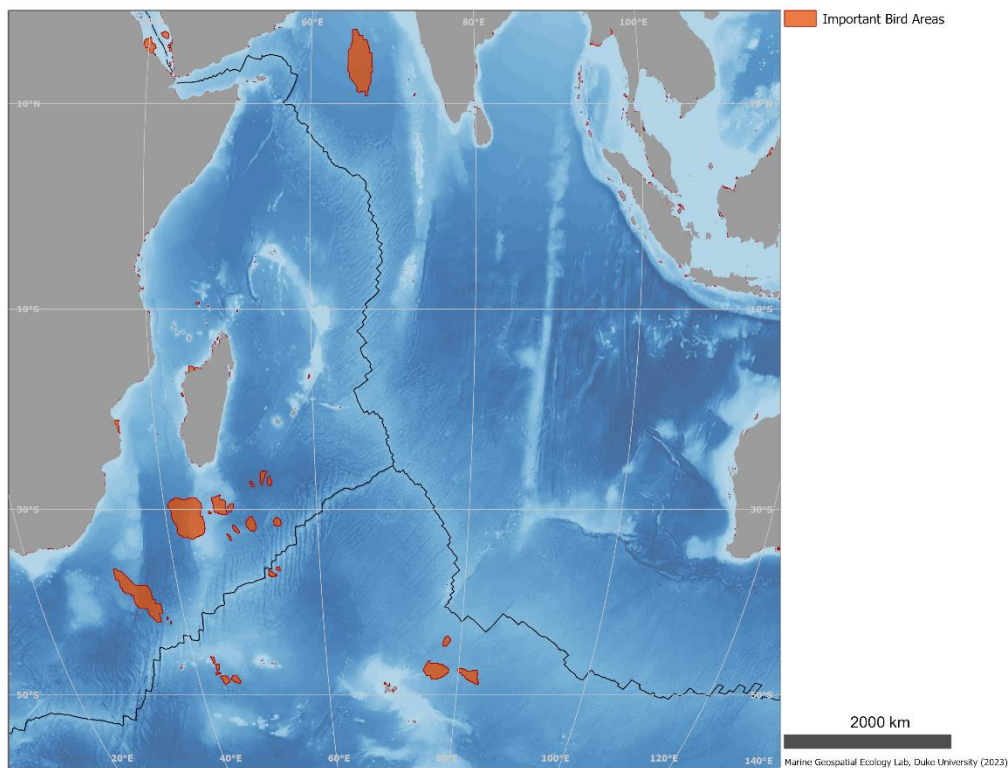


Figure 3.22-1 Important Bird Areas (BirdLife)

### 3.23 Important Marine Mammal Areas (IMMAs)

“IMMAs are identified through an expert-led process involving the collation and assessment of evidence against a set of selection criteria. This process, lasting approximately 12 months, aims to engage a wide range of representatives within the marine mammal science and conservation communities where much of the evidence necessary to assess IMMAs is held. Experts are selected based on their region-specific knowledge, experience and skills relevant to the task of weighing evidence and applying the IMMA selection criteria. Potential sources of information are actively sought in a process engaging with experts and other holders of evidence on a region-by-region basis.

A five-stage process with the help and support of the Task Force is used to identify, review, and accept or reject IMMA nominations, as follows:

Stage 1 – Nomination of preliminary ‘Areas of Interest’

Stage 2 – Development of ‘candidate IMMAs’

Stage 3 – Final review and IMMA Status Qualification

Stages 4 and 5 – Reporting, communication, final review and IMMA Status Qualification

By engaging regional experts and evidence holders, the process to identify IMMAs helps to establish common ideas, consistency and protocols for best practice across the marine mammal community. These ideas are reinforced by the independent Review Panel’s feedback on the cIMMAs assessed. This approach mirrors the regional/national scale achievements by other similar processes (e.g. seabirds in IBAs). This helps to provide an initial regional focus helping to prioritise the use of IMMAs in informing the design of effective protection networks or national management schemes, and the creation of Regional IMMA Expert Groups, trained in common methods of best practice for the future identification of IMMAs.

See IUCN Marine Mammal Protected Areas Task Force reports from previous completed regional workshops for details and real-life examples of how the IMMA selection process works.”

Source:

<https://www.marinemammalhabitat.org/immas/imma-spatial-layer-download/>

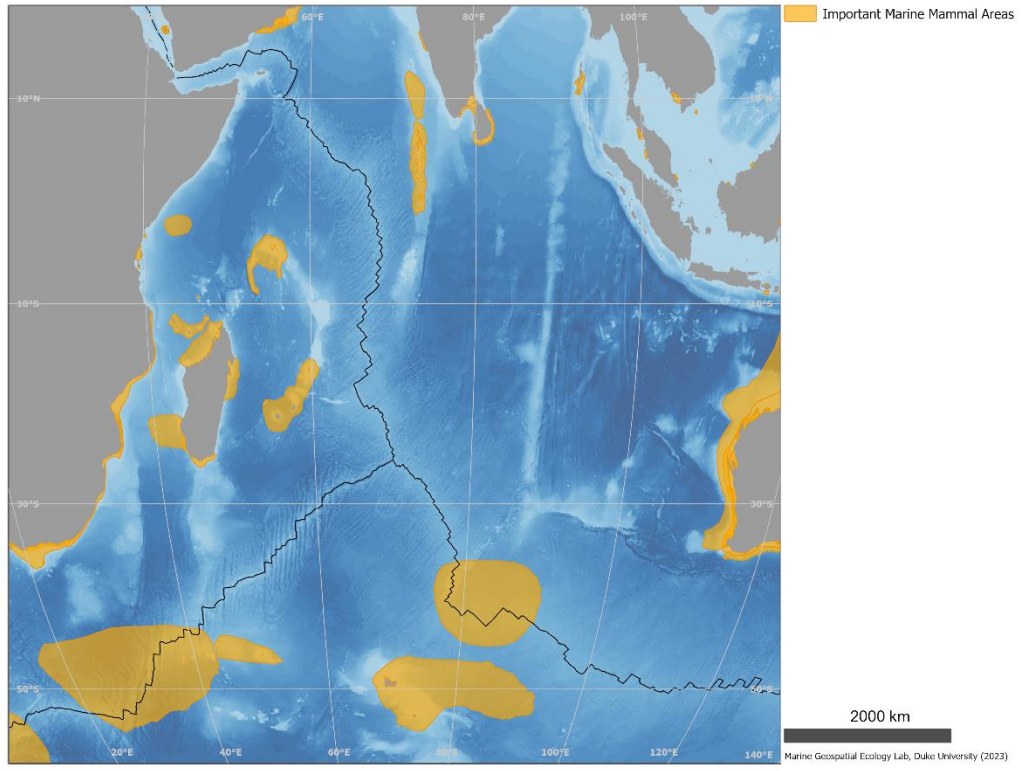


Figure 3.23-1 Important Marine Mammal Areas

### 3.24 Migratory Connectivity in the Ocean Sea Turtle Area Use

Abstract (Dunn et al 2019):

“The distributions of migratory species in the ocean span local, national and international jurisdictions. Across these ecologically interconnected regions, migratory marine species interact with anthropogenic stressors throughout their lives. Migratory connectivity, the geographical linking of individuals and populations throughout their migratory cycles, influences how spatial and temporal dynamics of stressors affect migratory animals and scale up to influence population abundance, distribution and species persistence. Population declines of many migratory marine species have led to calls for connectivity knowledge, especially insights from animal tracking studies, to be more systematically and synthetically incorporated into decision-making. Inclusion of migratory connectivity in the design of conservation and management measures is critical to ensure they are appropriate for the level of risk associated with various degrees of connectivity. Three mechanisms exist to incorporate migratory connectivity into international marine policy which guides conservation implementation: site-selection criteria, network design criteria and policy recommendations. Here, we review the concept of migratory connectivity and its use in international policy, and describe the Migratory Connectivity in the Ocean system, a migratory connectivity evidence-base for the ocean. We propose that without such collaboration focused on migratory connectivity, efforts to effectively conserve these critical species across jurisdictions will have limited effect.”

References:

Dunn, D. C., Harrison, A-L et al. 2019. The importance of migratory connectivity for global ocean policy. *Proceedings of the Royal Society B: Biological Sciences* 286:20191472.

Migratory Connectivity in the Ocean (MiCO). Highly migratory marine species nodes and corridors, developed with data contributed to MiCO. Available from the MiCO System Version 1.0. MiCO. <https://mico.eco>. Accessed 03/15/2023.

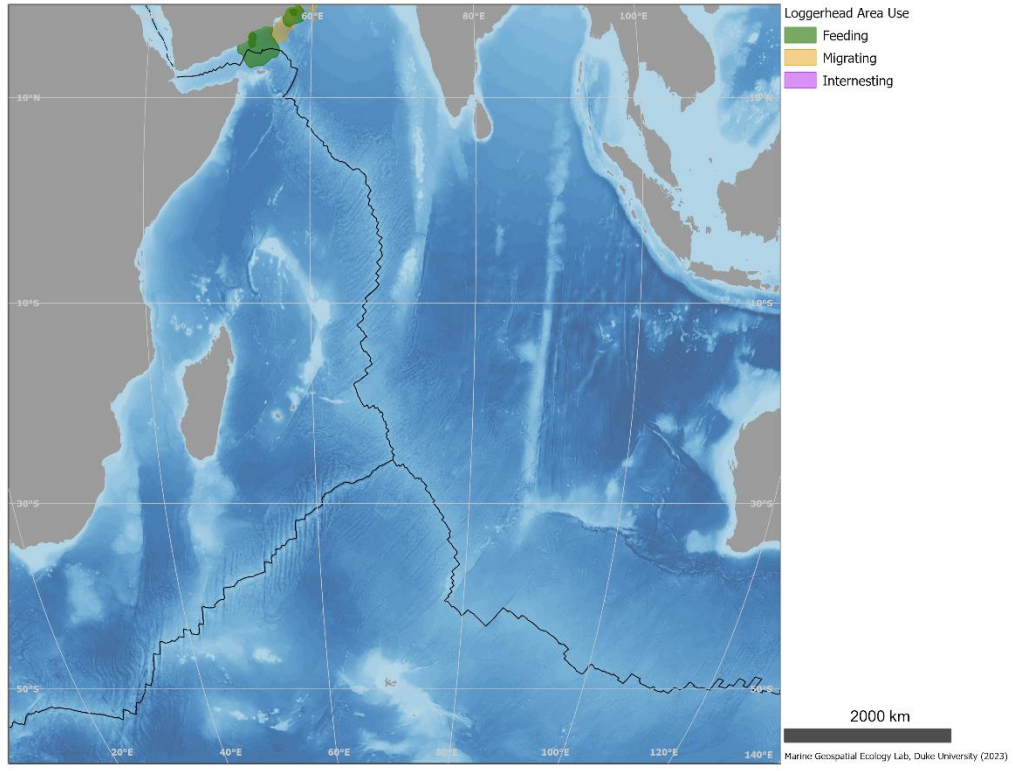


Figure 3.24-1 Loggerhead turtle area use

## 4 Biogeographic Classification

### 4.1 Global Open Ocean and Deep Seabed (GOODS) biogeographic classification

“GOODS is the first attempt at comprehensively classifying the open-ocean and deep seafloor into distinct biogeographic regions (UNESCO, 2009). The classification was produced by an international and multidisciplinary group of experts under the auspices of a number of international and intergovernmental organizations as well as governments, and under the ultimate umbrella of the United Nations Educational, Scientific and Cultural Organization (UNESCO) and its Intergovernmental Oceanographic Commission (IOC). The maps shown below include the updates made by Watling et al. (2013).

The biogeographic classification classifies specific ocean regions using environmental features and – to the extent data are available – their species composition. GOODS is hypothesis-driven and still preliminary, and will thus require further refinement and peer review in the future. However, parts of it have already been published (e.g. pelagic provinces; Spalding et al. 2012). Watling et al. (2013) tried to refine the GOODS bathyal and abyssal provinces including some new variables. Physical and chemical proxies thought to be good predictors of the distributions of organisms at the deep-sea floor, and thus used for the definition of biogeographic provinces, were: depth, temperature (T), salinity (S), dissolved oxygen (O), and particulate organic carbon flux (POC) to the seafloor.

The major open ocean pelagic and deep sea benthic zones presented by the GOODS report and by Watling et al. (2013) are considered by their authors a reasonable basis for advancing efforts towards the conservation and sustainable use of biodiversity in marine areas beyond the limits of national jurisdiction in line with a precautionary approach.”

#### References:

UNESCO. 2009. Global Open Oceans and Deep Seabed (GOODS) – Biogeographic Classification. Paris, UNESCO-IOC. (IOC Technical Series, 84.)

Watling, L., Guinotte, J., Clark, M. R., and Smith, C. R. (2013) A proposed biogeography of the deep ocean floor. *Progress in Oceanography*, 11, 91-112.

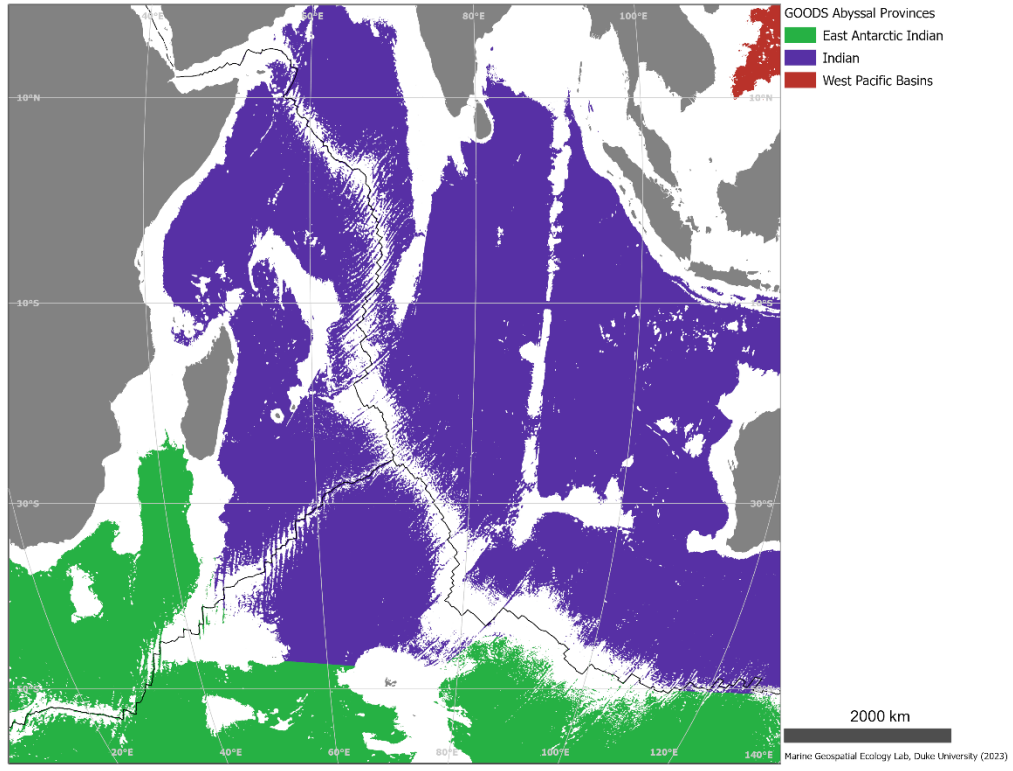


Figure 4.1-1 GOODS abyssal provinces

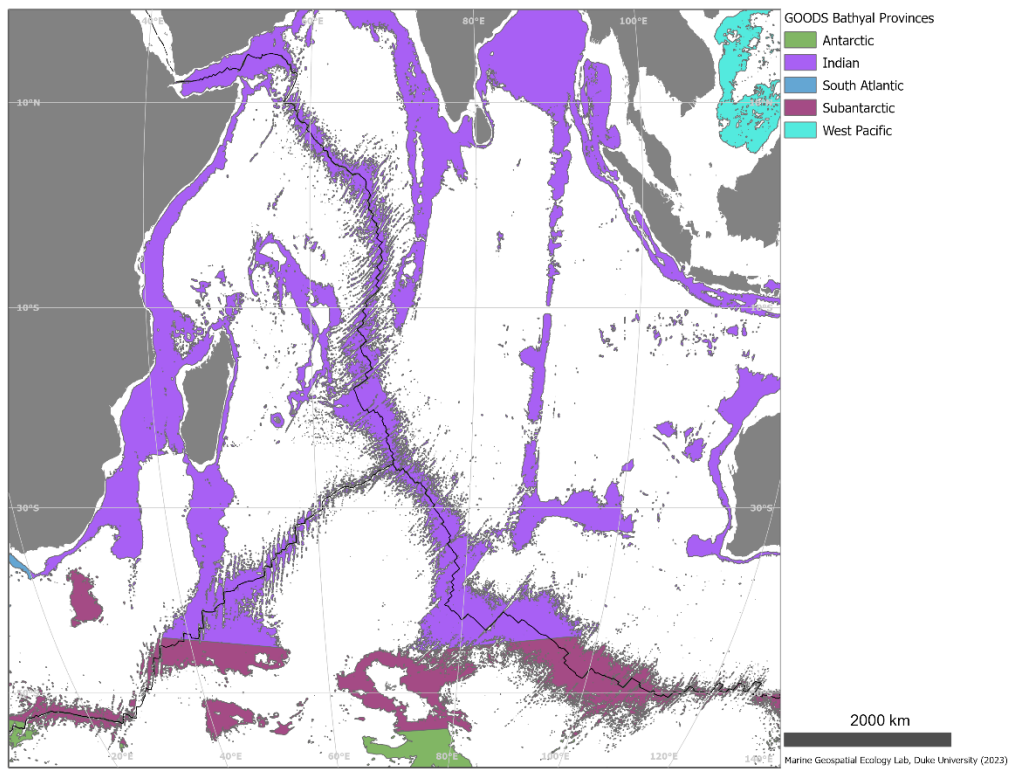


Figure 4.1-2 GOODS bathyal provinces

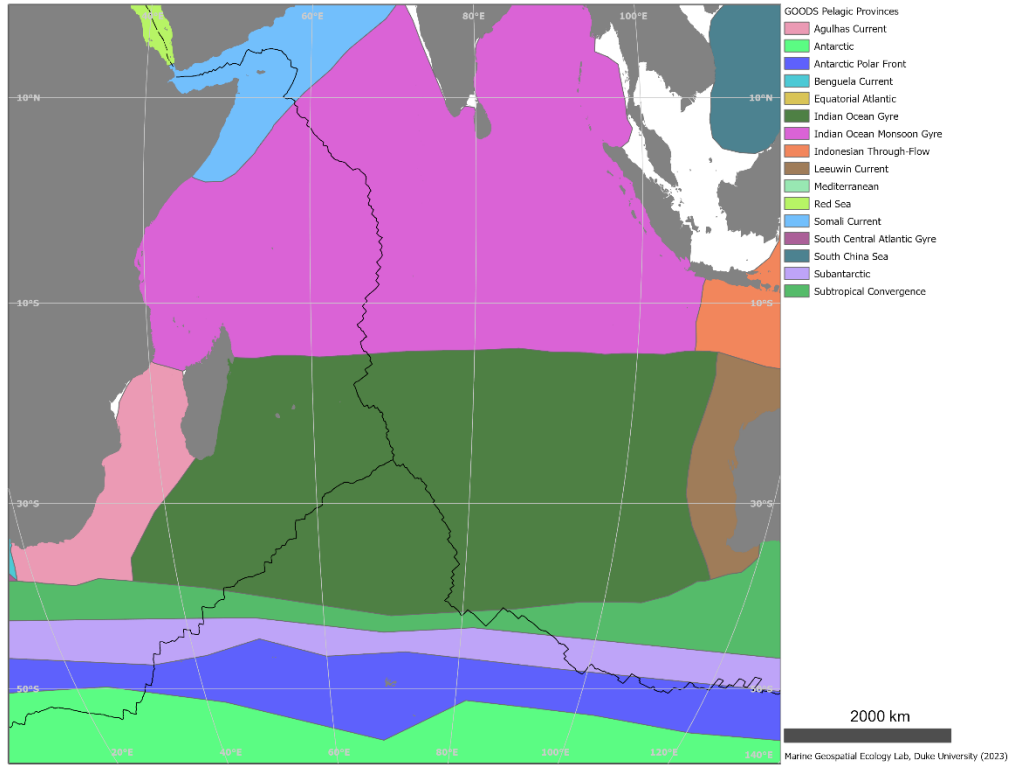


Figure 4.1-3 GOODS pelagic provinces

## 4.2 Global Mesopelagic Biogeography

Abstract (Sutton et al. 2017):

“We have developed a global biogeographic classification of the mesopelagic zone to reflect the regional scales over which the ocean interior varies in terms of biodiversity and function. An integrated approach was necessary, as global gaps in information and variable sampling methods preclude strictly statistical approaches. A panel combining expertise in oceanography, geospatial mapping, and deep-sea biology convened to collate expert opinion on the distributional patterns of pelagic fauna relative to environmental proxies (temperature, salinity, and dissolved oxygen at mesopelagic depths). An iterative Delphi Method integrating additional biological and physical data was used to classify biogeographic ecoregions and to identify the location of ecoregion boundaries or inter-regions gradients. We define 33 global mesopelagic ecoregions. Of these, 20 are oceanic while 13 are ‘distant neritic.’ While each is driven by a complex of controlling factors, the putative primary driver of each ecoregion was identified. While work remains to be done to produce a comprehensive and robust mesopelagic biogeography (i.e., reflecting temporal variation), we believe that the classification set forth in this study will prove to be a useful and timely input to policy planning and management for conservation of deep-pelagic marine resources. In particular, it gives an indication of the spatial scale at which faunal communities are expected to be broadly similar in composition, and hence can inform application of ecosystem-based management approaches, marine spatial planning and the distribution and spacing of network of representative protected areas.”

Reference:

Sutton, T.T., Clark, M.R., Dunn, D.C., Halpin, P.N., Rogers, A.D., Guinotte, J., Bograd, S.J., Angel, M.V., Perez, J.A.A., Wishner, K. and Haedrich, R.L., (2017). A global biogeographic classification of the mesopelagic zone. *Deep Sea Research Part I: Oceanographic Research Papers*, 126, pp.85-102.

Dataset downloaded from Marine Regions (August 2019)

<http://www.marineregions.org/gazetteer.php?p=details&id=50384>

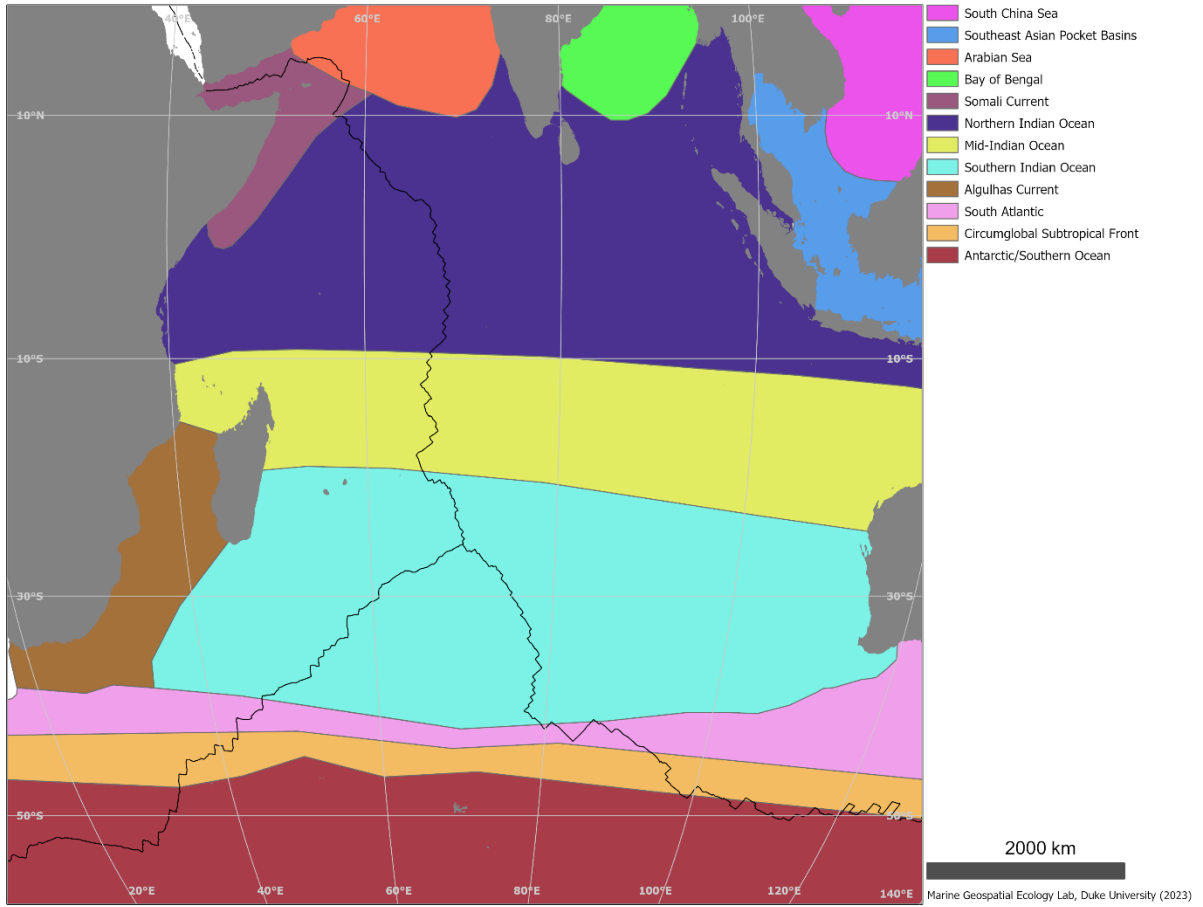


Figure 4.2-1 Mesopelagic provinces

### 4.3 Pelagic Provinces of the World

Abstract (Spalding et al. 2012):

Off-shelf waters cover 66% of the planet. Growing concerns about the state of natural resources in these waters, and of future threats have led to a growing movement to improve management and conservation of natural resources. However, efforts to assess progress and to further plan and prioritise management interventions have been held back in part by the lack of a comprehensive biogeographic classification for the high seas. In this work we review existing efforts at classifying the surface pelagic waters of the world's oceans and we present a synthesis classification which draws both on known taxonomic biogeography and on the oceanographic forces which are major drivers of ecological patterns. We describe a nested system of 37 pelagic provinces of the world, nested into a system of four broad realms. Ecologically we have also differentiated a system of 7 biomes which are spatially disjoint but united by common abiotic conditions creating physiognomically similar communities. This system builds on existing work and is further intended to align closely with the coastal biogeographic regionalisation provided by the Marine Ecoregions of the World classification. It is hoped that it will provide a valuable tool in supporting threat analysis, priority setting, policy development and active management of the world's pelagic oceans.

Reference:

Spalding MD, Agostini VN, Rice J, Grant SM (2012). Pelagic provinces of the world): a biogeographic classification of the world's surface pelagic waters. *Ocean and Coastal Management* 60: 19-30. DOI: 10.1016/j.ocecoaman.2011.12.016. Data URL: <http://data.unep-wcmc.org/datasets/38>

Dataset downloaded from:

The Nature Conservancy (2012). Marine Ecoregions and Pelagic Provinces of the World. GIS layers developed by The Nature Conservancy with multiple partners, combined from Spalding et al. (2007) and Spalding et al. (2012). Cambridge (UK): The Nature Conservancy. DOIs: 10.1641/B570707; 10.1016/j.ocecoaman.2011.12.016. Data URL: <http://data.unep-wcmc.org/datasets/38>

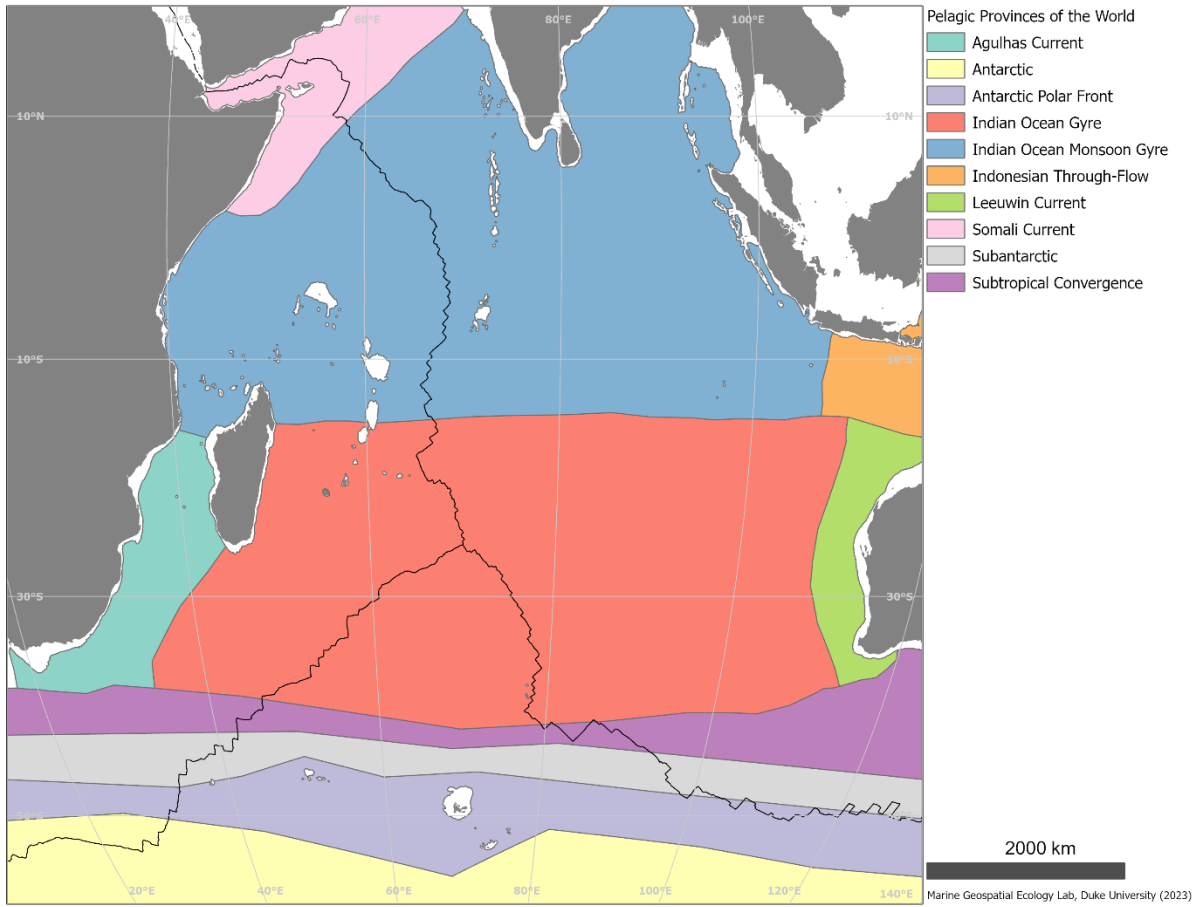


Figure 4.3-1 Pelagic provinces

## 4.4 Longhurst Marine Provinces

Abstract (Longhurst 2006):

“This dataset represents a partition of the world oceans into provinces as defined by Longhurst (1995; 1998; 2006), and are based on the prevailing role of physical forcing as a regulator of phytoplankton distribution. The dataset represents the initial static boundaries developed at the Bedford Institute of Oceanography, Canada. Note that the boundaries of these provinces are not fixed in time and space, but are dynamic and move under seasonal and interannual changes in physical forcing. At the first level of reduction, Longhurst recognized four principal biomes (also referred to as domains in earlier publications): the Polar Biome, the Westerlies Biome, the Trade-Winds Biome, and the Coastal Boundary Zone Biome. These four Biomes are recognizable in every major ocean basin. At the next level of reduction, the ocean basins are partitioned into provinces, roughly ten for each basin. These partitions provide a template for data analysis or for making parameter assignments on a global scale.”

Source: VLIZ (2009). Longhurst Biogeographical Provinces. Available online at <http://www.marineregions.org/>. Consulted on 2013-01-14.

Reference:

Longhurst, A.R. (2006). *Ecological Geography of the Sea*. 2nd Edition. Academic Press, San Diego, 560p.

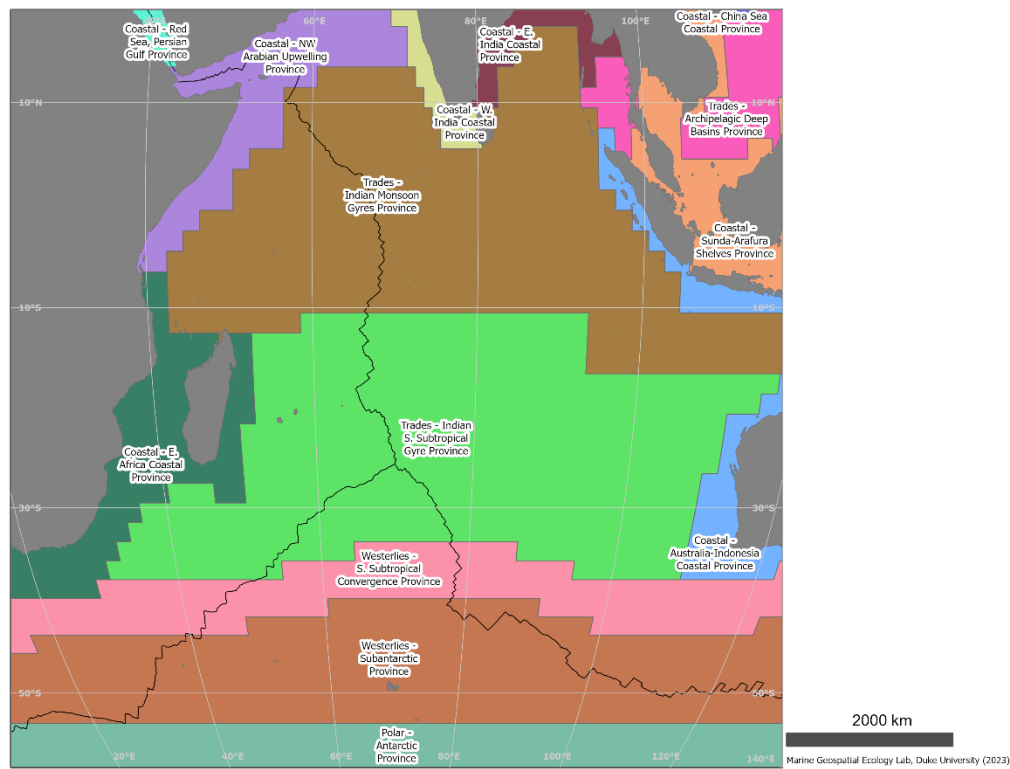


Figure 4.4-1 Longhurst marine provinces

## 4.5 Bioregions of the Indian Ocean

“This project has developed sub-regional bioregionalisations for the Indian Ocean. This combines approaches CSIRO developed in Australia, used in the Bay of Bengal (in collaboration with BOBLME) with similar approaches that have been used throughout the Indian and Pacific Oceans to derive a single combined bioregionalisation. The project has developed an expert derived bioregionalisation in the Indian and Pacific Oceans through expert workshops and novel statistical analysis of physical and biological data. The project draws on experience in CSIRO, GOBI partners, and other collaborators, using approaches currently being trialed in Australia and around the Antarctic margins, and has collaborated with regional and national stakeholders to ensure a consistent approach. This Appendix contains the descriptions of each marine region and each province with the region. Where sufficient information exists it includes a description, a qualitative ecosystem model of the system and the pressures on it and a scenario analysis that explores the way the ecosystem changes with different pressures.”

Reference:

Dunstan et al. 2020. Bioregions of the Indian Ocean. CSIRO, Australia.

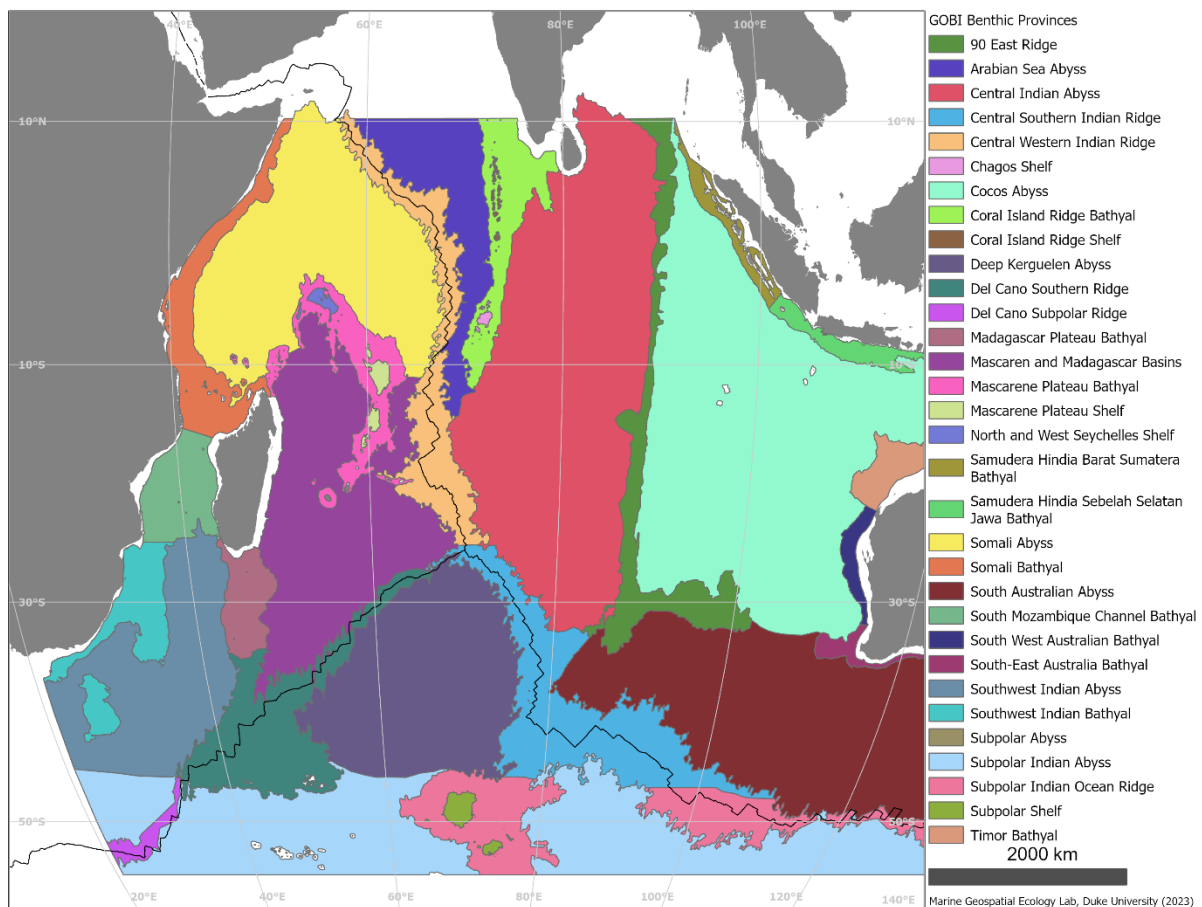


Figure 4.5-1 Benthic bioregions

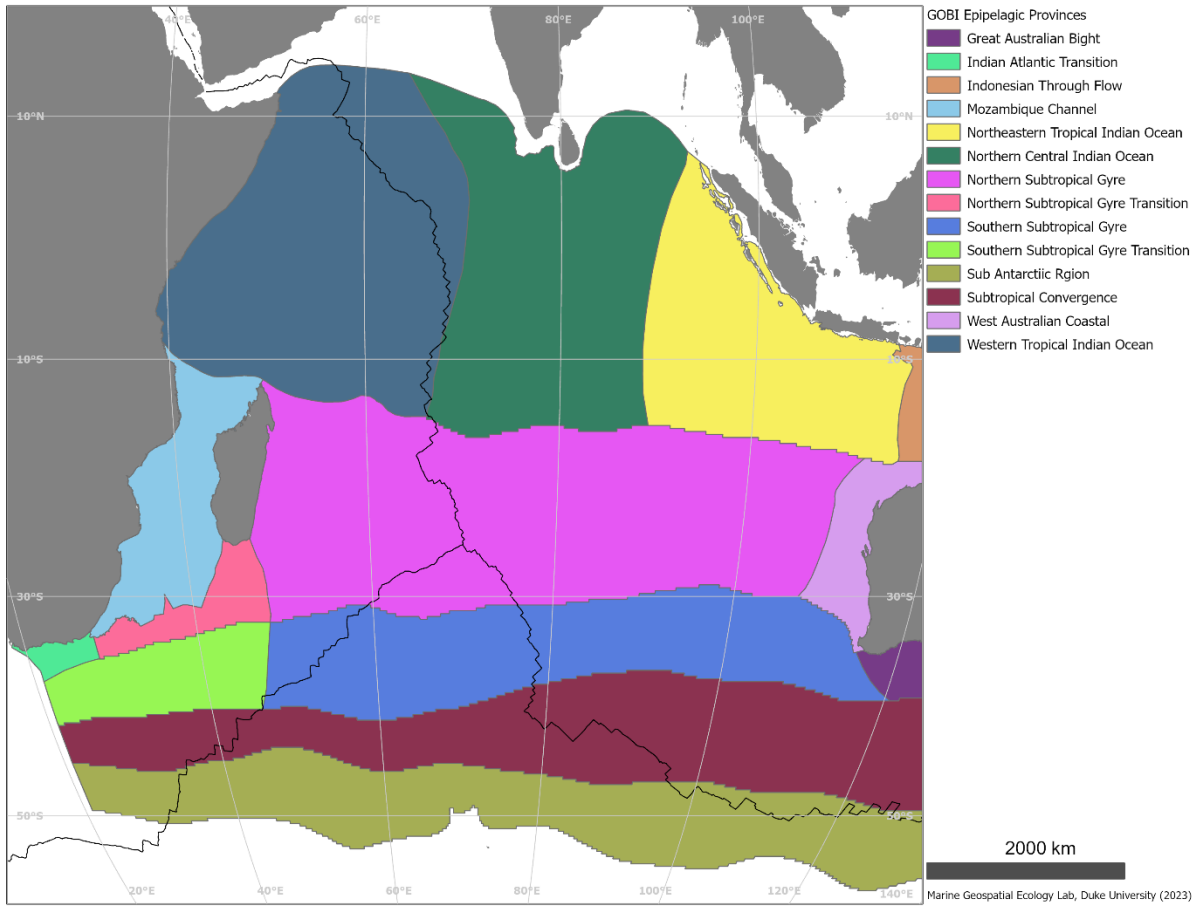


Figure 4.5-2 Epipelagic bioregions

## 4.6 Global Seascapes

Abstract (Harris & Whiteway 2009):

“Designing a representative network of high seas marine protected areas (MPAs) requires an acceptable scheme to classify the benthic (as well as the pelagic) bioregions of the oceans. Given the lack of sufficient biological information to accomplish this task, we used a multivariate statistical method with 6 biophysical variables (depth, seabed slope, sediment thickness, primary production, bottom water dissolved oxygen and bottom temperature) to objectively classify the ocean floor into 53,713 separate polygons comprising 11 different categories, that we have termed seascapes. A cross-check of the seascape classification was carried out by comparing the seascapes with existing maps of seafloor geomorphology and seabed sediment type and by GIS analysis of the number of separate polygons, polygon area and perimeter/area ratio. We conclude that seascapes, derived using a multivariate statistical approach, are biophysically meaningful subdivisions of the ocean floor and can be expected to contain different biological associations, in as much as different geomorphological units do the same. Less than 20% of some seascapes occur in the high seas while other seascapes are largely confined to the high seas, indicating specific types of environment whose protection and conservation will require international cooperation. Our study illustrates how the identification of potential sites for high seas marine protected areas can be accomplished by a simple GIS analysis of seafloor geomorphic and seascape classification maps. Using this approach, maps of seascape and geomorphic heterogeneity were generated in which heterogeneity hotspots identify themselves as MPA candidates. The use of computer aided mapping tools removes subjectivity in the MPA design process and provides greater confidence to stakeholders that an unbiased result has been achieved.”

Reference:

Harris, P.T. & Whiteway, T. (2009) High seas marine protected areas: Benthic environmental conservation priorities from a GIS analysis of global ocean biophysical data. *Ocean and Coastal Management*, **52**, 22–38.

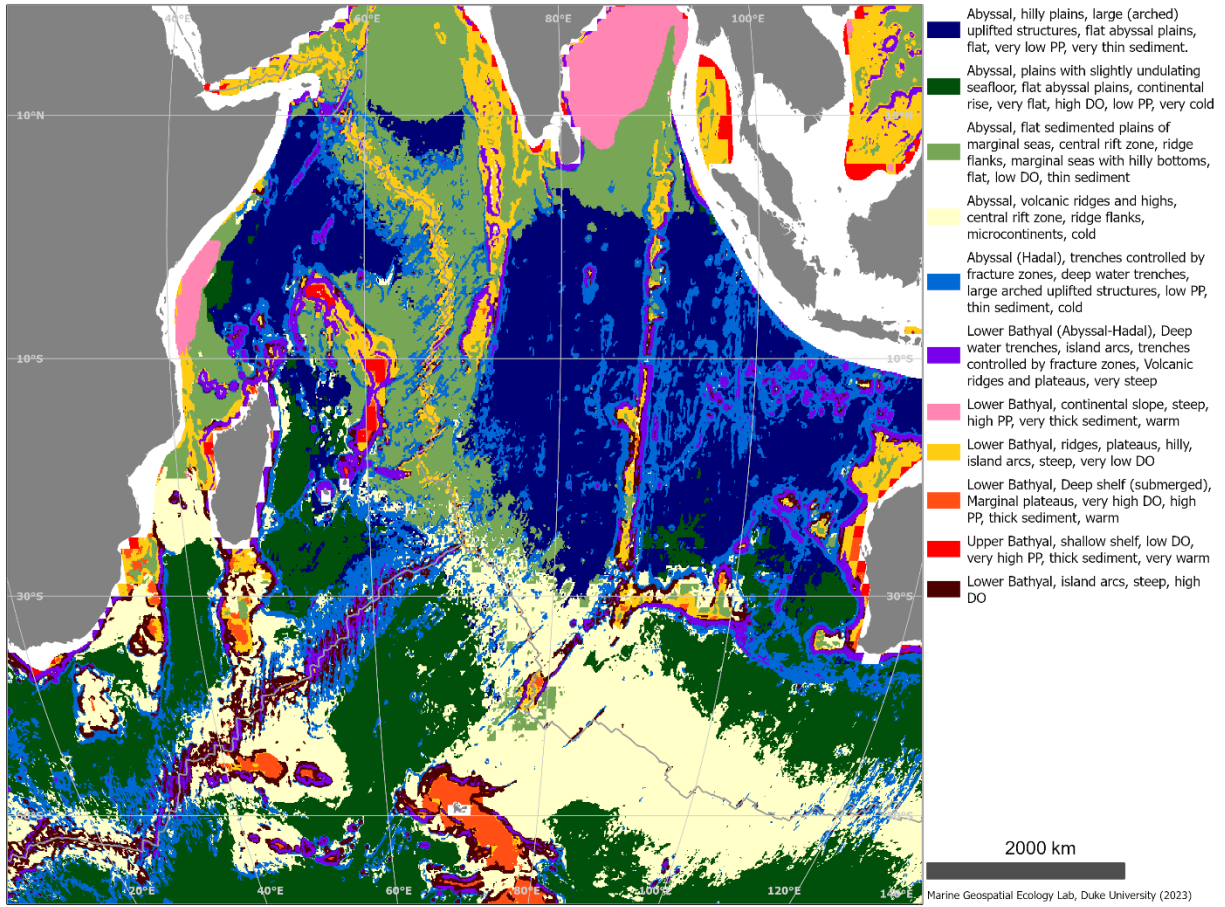


Figure 4.6-1 Global seascapes

## 4.7 Biogeography of Hydrothermal Vents in the Indian Ocean

Abstract (Zhou et al. 2022):

“The pattern of biodiversity and biogeography is crucial to informing management and conservation strategy. But a lack of study across multiple ridge systems, especially for the Carlsberg Ridge, has hampered the conception of the overall picture for the Indian Ocean vents, a top target for deep-sea exploration of massive sulphides. Here, we aim to characterize fauna from three new vent fields on the Carlsberg Ridge for the first time, and answer 1) what is the biogeographic pattern for vent fauna within the Indian Ocean and 2) how does this pattern guide the future environmental management on the Indian Ocean ridges.”

Reference:

Zhou, Y., Chen, C., Zhang, D., Wang, Y., Watanabe, H.K., Sun, J., Bissessur, D., Zhang, R., Han, Y., Sun, D. and Xu, P., 2022. Delineating biogeographic regions in Indian Ocean deep-sea vents and implications for conservation. *Diversity and Distributions*, 28(12), pp.2858-2870..  
doi:<https://doi-org.proxy.lib.duke.edu/10.1111/ddi.13535>

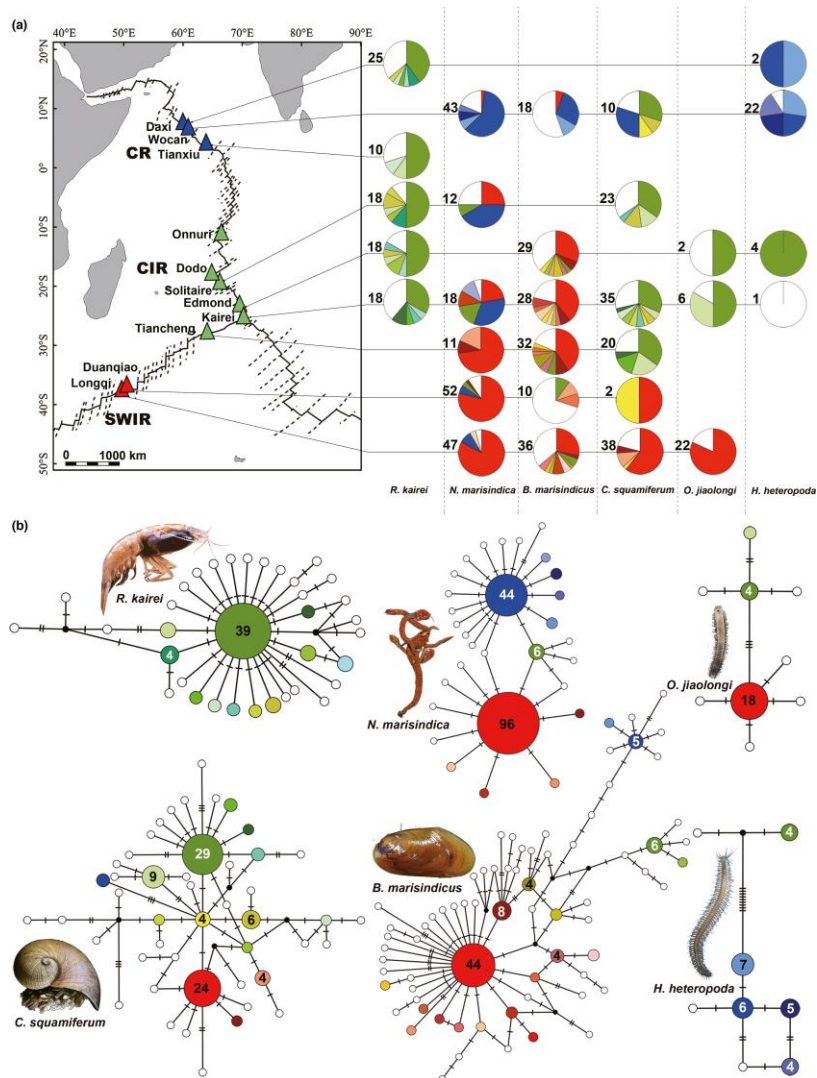


**Figure 4.7-1 Biogeographic patterns of vent fauna along Indian Ocean ridges**

*Original Caption: Figure 2. Population genetics across the three Indian Ocean ridges. (a) Haplotype distributions, sample size of each population is indicated beside the pie chart, and dotted lines in the map denote the transform faults and fractures on the ridges; (b) TCS haplotype networks, numbers in the haplotype circles indicate the size of haplotypes with occurrence >3. All haplotypes are coloured, except singletons.*

## 4.8 Biogeography and Population Divergence of Microeukaryotes

Abstract (Zhang et al. 2022):

“Deep-sea hydrothermal vents have been proposed as oases for microbes, but microeukaryotes as key components of the microbial loop have not been well studied. Based on high-throughput sequencing and network analysis of the 18S rRNA gene, distinct biogeographical distribution patterns and impacting factors were revealed from samples in the three hydrothermal fields of the southwest Indian Ocean, where higher gene abundance of microeukaryotes appeared in chimneys. The microeukaryotes in the fluids might be explained by hydrogeochemical heterogeneity, especially that of the nitrate and silicate concentrations, while the microeukaryotes in the chimneys coated with either Fe oxides or Fe-Si oxyhydroxides might be explained by potentially different associated prokaryotic groups. Population divergence of microeukaryotes, especially clades of parasitic Syndiniales, was observed among different hydrothermal fluids and chimneys and deserves further exploration to gain a deeper understanding of the trophic relationships and potential ecological function of microeukaryotes in the deep-sea extreme ecosystems, especially in the complex deep-sea chemoautotrophic habitats.

**IMPORTANCE** Deep-sea hydrothermal vents have been proposed as oases for microbes, but microeukaryotes as key components of the microbial loop have not been well studied. Based on high-throughput sequencing and network analysis of the 18S rRNA gene, population divergence of microeukaryotes, especially clades of parasitic Syndiniales, was observed among different hydrothermal fields. This might be attributed to the hydrogeochemical heterogeneity of fluids and to the potentially different associated prokaryotic groups in chimneys.”

Reference:

Zhang, Y., Huang, N. and Jing, H., 2022. Biogeography and Population Divergence of Microeukaryotes Associated with Fluids and Chimneys in the Hydrothermal Vents of the Southwest Indian Ocean. *Microbiology Spectrum*, 10(5), pp.e02632-21. DOI: <https://doi.org/10.1128/spectrum.02632-21>.

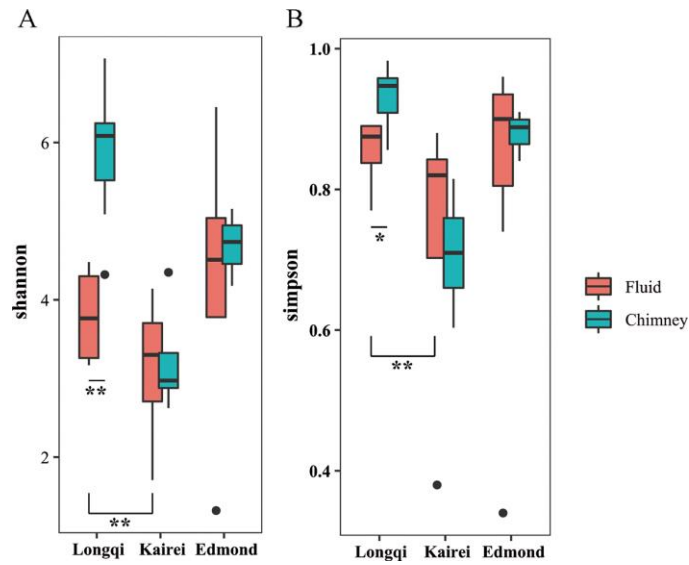


Figure 4.8-1 Microeukaryote species richness along Indian Ocean hydrothermal vents

Original Caption: Figure 1. Shannon (A) and Simpson (B) indices of microeukaryotes among the fluids and chimneys in different hydrothermal vents in the southwest Indian Ocean. \*\*,  $P < 0.01$ ; \*,  $P < 0.05$ .

## 4.9 Biogeography of Alviniconcha snail in Indian Ocean Hydrothermal Vents

Abstract (Jang et al. 2023):

“The hairy snails of the genus *Alviniconcha* are representative deep-sea hydrothermal vent animals distributed across the Western Pacific and Indian Ocean. Out of six known species in the genus *Alviniconcha*, only one nominal species of *A. marisindica* was found in the Indian Ocean from the Carlsberg Ridge (CR), Central Indian Ridge (CIR) to the northern part of Southwest Indian Ridge (SWIR) and Southeast Indian Ridge (SEIR). Recently, the *Alviniconcha* snails were found at three new vent fields, named Onnare, Onbada, and Onnuri, in the northern CIR, which promotes a more comprehensive phylogeographic study of this species. Here, we examined the phylogeography and connectivity of the *Alviniconcha* snails among seven vent fields representing the CR and CIR based on DNA sequence data of a mitochondrial COI gene and two protein-coding nuclear genes. Phylogenetic inferences revealed that the *Alviniconcha* snails of the newly found in the northern CIR and two vent fields of Wocan and Tianxiu in the CR were divergent with the previously identified *A. marisindica* in the southern CIR and mitochondrial COI data supported the divergence with at least greater than 3% sequence divergence. Population structure analyses based on the three genetic markers detected a phylogeographic boundary between Onnuri and Solitaire that divides the whole snail populations into northern and southern groups with a low migration rate. The high degree of genetic disconnection around the ‘Onnuri’ boundary suggests that the *Alviniconcha* snails in the Indian Ocean may undergo allopatric speciation. The border may similarly act as a dispersal barrier to many other vent species co-distributed in the CIR. This study would expand understanding the speciation and connectivity of vent species in the Indian Ocean.”

Reference:

Jang, S.J., Cho, S.Y., Li, C., Zhou, Y., Wang, H., Sun, J., Patra, A.K. and Won, Y.J., Geographical subdivision of *Alviniconcha* snail populations in the Indian Ocean hydrothermal vent regions. *Frontiers in Marine Science*, 10, p.550. <https://doi.org/10.3389/fmars.2023.1139190>

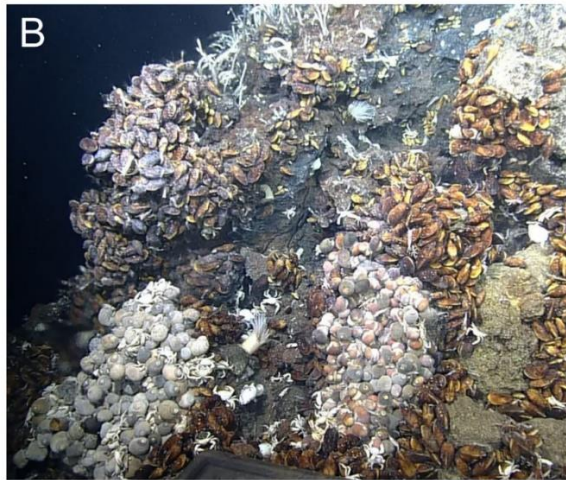
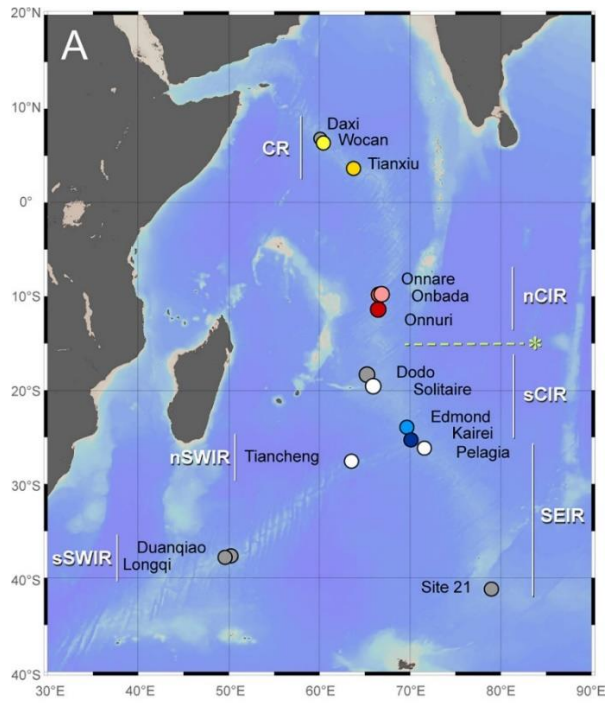


Figure 4.9-1 Biogeographic patterns of *Alviniconcha* snails along Indian Ocean ridges

*Original Caption: Figure 1. Sampling locations and hydrothermal vent fields in Indian Ocean reported to date. (A) The sampling sites of Alviniconcha snails along Carlsberg Ridge and Central Indian Ridge. The map was created using Ocean Data View v. 5.6.3 with the General Bathymetric Chart of the Oceans (GEBCO) 2014 grid. Colored circles represent sampling locations. White and gray circles represent the vent fields where Alviniconcha snails were observed but not analyzed in this study and not observed to date, respectively (Nakamura et al., 2012; Zhou et al., 2018; Gerdes et al., 2019; Sun et al., 2020). The abbreviations are described in Table 1. The dashed line with "\*" represents the phylogeographic boundary observed from Alviniconcha snails in this study. Vent community with Alviniconcha snails and Bathymodiolus mussels at the Onnare vent field (B) and Onbada vent field (C).*

## 4.10 Global Hydrothermal Vents Biogeography

Abstract (Rogers et al. 2012):

“Since the first discovery of deep-sea hydrothermal vents along the Galápagos Rift in 1977, numerous vent sites and endemic faunal assemblages have been found along mid-ocean ridges and back-arc basins at low to mid latitudes. These discoveries have suggested the existence of separate biogeographic provinces in the Atlantic and the North West Pacific, the existence of a province including the South West Pacific and Indian Ocean, and a separation of the North East Pacific, North East Pacific Rise, and South East Pacific Rise. The Southern Ocean is known to be a region of high deep-sea species diversity and centre of origin for the global deep-sea fauna. It has also been proposed as a gateway connecting hydrothermal vents in different oceans but is little explored because of extreme conditions. Since 2009 we have explored two segments of the East Scotia Ridge (ESR) in the Southern Ocean using a remotely operated vehicle. In each segment we located deep-sea hydrothermal vents hosting high-temperature black smokers up to 382.8uC and diffuse venting. The chemosynthetic ecosystems hosted by these vents are dominated by a new yeti crab (*Kiwa* n. sp.), stalked barnacles, limpets, peltospiroid gastropods, anemones, and a predatory sea star. Taxa abundant in vent ecosystems in other oceans, including polychaete worms (*Siboglinidae*), bathymodiolid mussels, and alvinocaridid shrimps, are absent from the ESR vents. These groups, except the *Siboglinidae*, possess planktotrophic larvae, rare in Antarctic marine invertebrates, suggesting that the environmental conditions of the Southern Ocean may act as a dispersal filter for vent taxa. Evidence from the distinctive fauna, the unique community structure, and multivariate analyses suggest that the Antarctic vent ecosystems represent a new vent biogeographic province. However, multivariate analyses of species present at the ESR and at other deep-sea hydrothermal vents globally indicate that vent biogeography is more complex than previously recognised.”

Reference:

Rogers, A.D., Tyler, P.A., Connelly, D.P., Copley, J.T., James, R., Larter, R.D., Linse, K., Mills, R.A., Garabato, A.N., Pancost, R.D. and Pearce, D.A., (2012). The discovery of new deep-sea hydrothermal vent communities in the Southern Ocean and implications for biogeography. *PLoS Biology*, 10(1), p.e1001234. Doi: 10.1371/journal.pbio.1001234

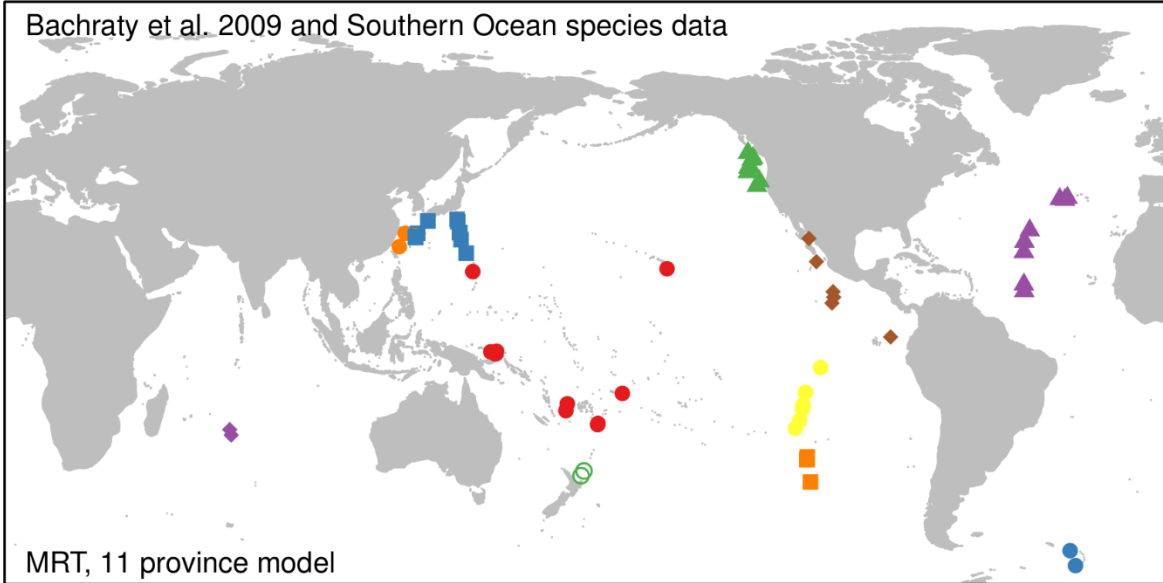


Figure 4.10-1 Results of geographically constrained clustering using multivariate regression trees. Figure 6 from Rogers et al. (2012)

## 5 Human Uses

### 5.1 Demersal Destructive Fishing

Here we include a map of demersal destructive fishing from Halpern et al. (2015). These data were created as an input for an analysis of the global impact of human uses on the marine ecosystem.

Reference:

Halpern, B. S. et al. 2015. Spatial and temporal changes in cumulative human impacts on the world's ocean. - Nat Commun 6: 1–7.

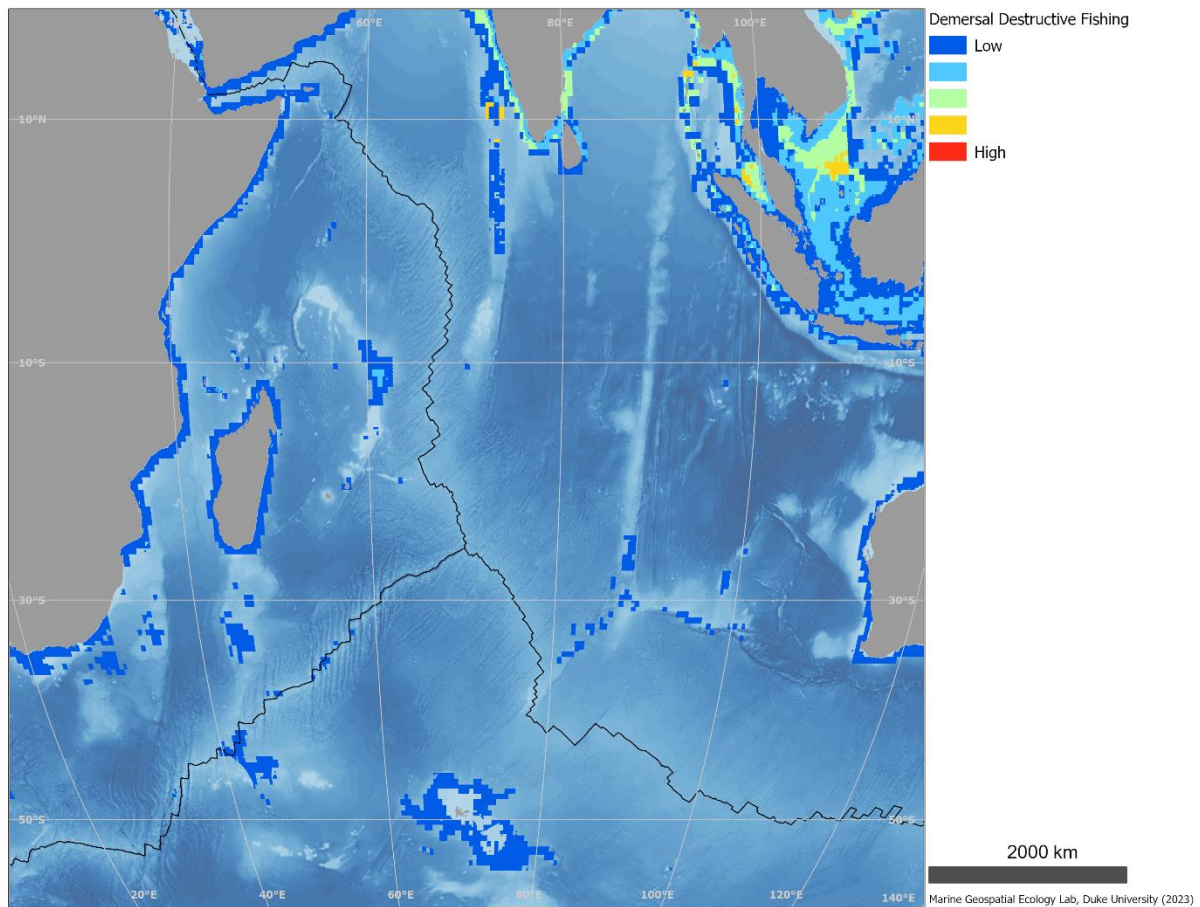


Figure 5.1-1 Demersal destructive bottom fishing

## 5.2 Fishing Effort by Gear Type, Global Fishing Watch

### Abstract

“Although fishing is one of the most widespread activities by which humans harvest natural resources, its global footprint is poorly understood and has never been directly quantified. We processed 22 billion automatic identification system messages and tracked >70,000 industrial fishing vessels from 2012 to 2016, creating a global dynamic footprint of fishing effort with spatial and temporal resolution two to three orders of magnitude higher than for previous data sets. Our data show that industrial fishing occurs in >55% of ocean area and has a spatial extent more than four times that of agriculture. We find that global patterns of fishing have surprisingly low sensitivity to short-term economic and environmental variation and a strong response to cultural and political events such as holidays and closures.”

### Reference:

Kroodsma, David A., Juan Mayorga, Timothy Hochberg, Nathan A. Miller, Kristina Boerder, Francesco Ferretti, Alex Wilson, et al. 2018. “Tracking the Global Footprint of Fisheries.” *Science* 359 (6378): 904–8. <https://doi.org/10.1126/science.aao5646>.

“Daily fishing effort, gridded at 0.01 degrees, by geartype and flag state, is available to download. Fishing effort is available for the time period 2012 to 2020.”

Source: <https://globalfishingwatch.org/datasets-and-code/fishing-effort/>

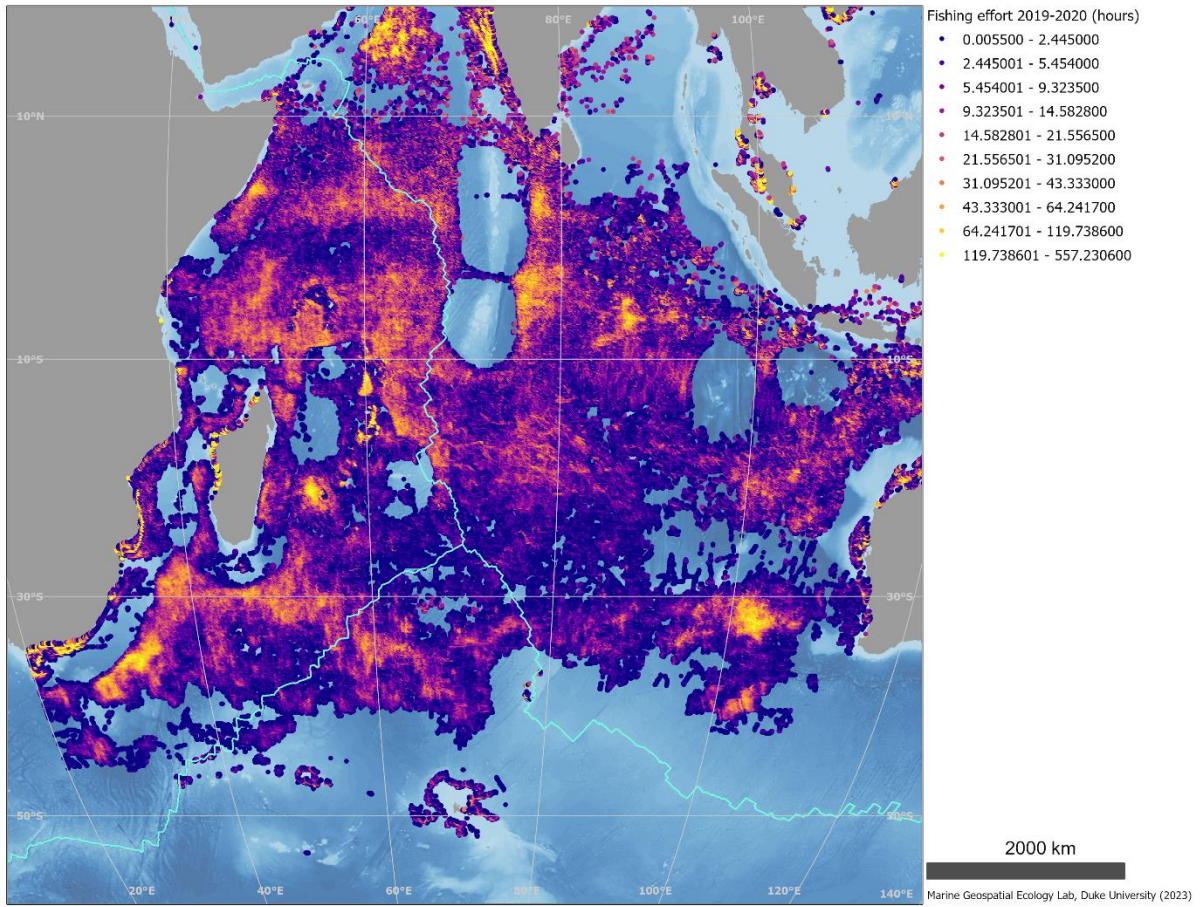


Figure 5.2-1 Total fishing effort for all gears from 2019-2020

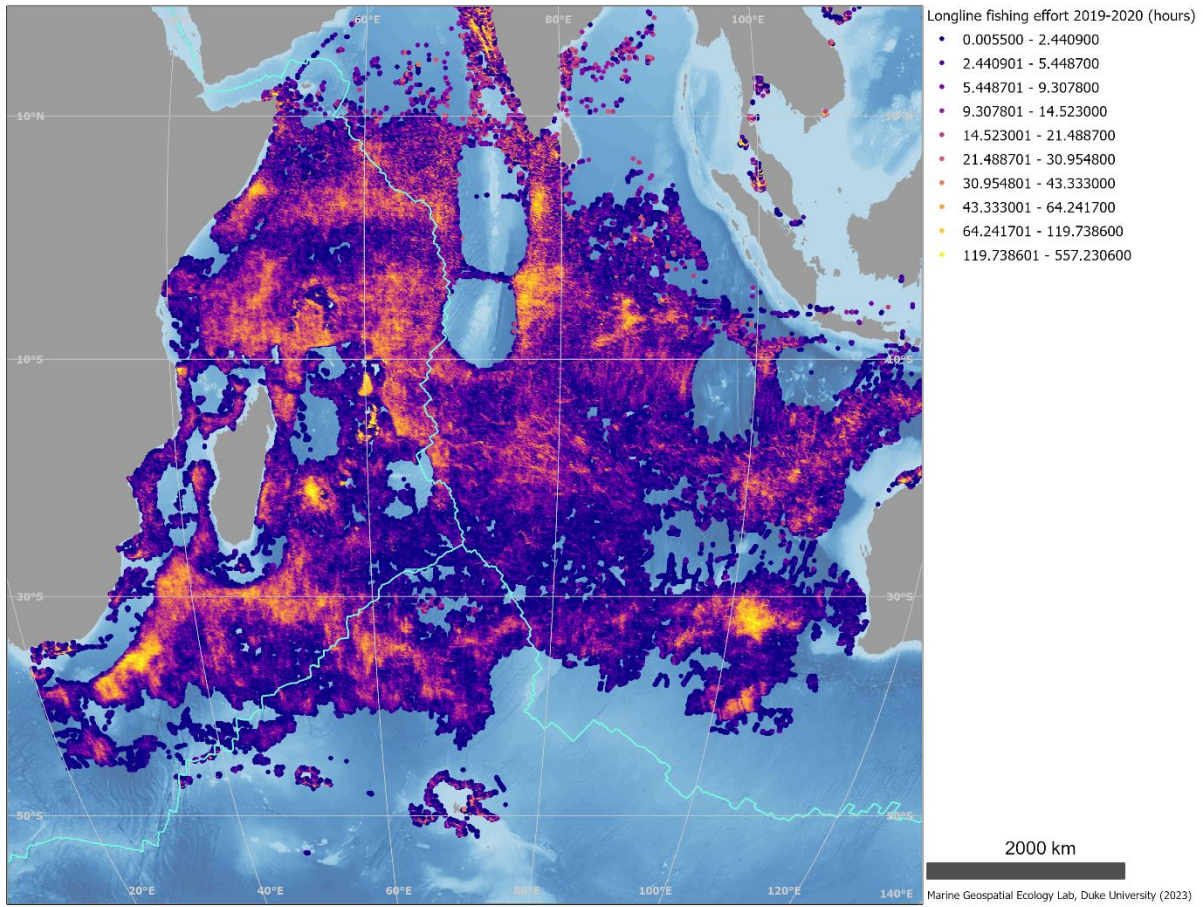


Figure 5.2-2 Longline fishing effort from 2019-2020

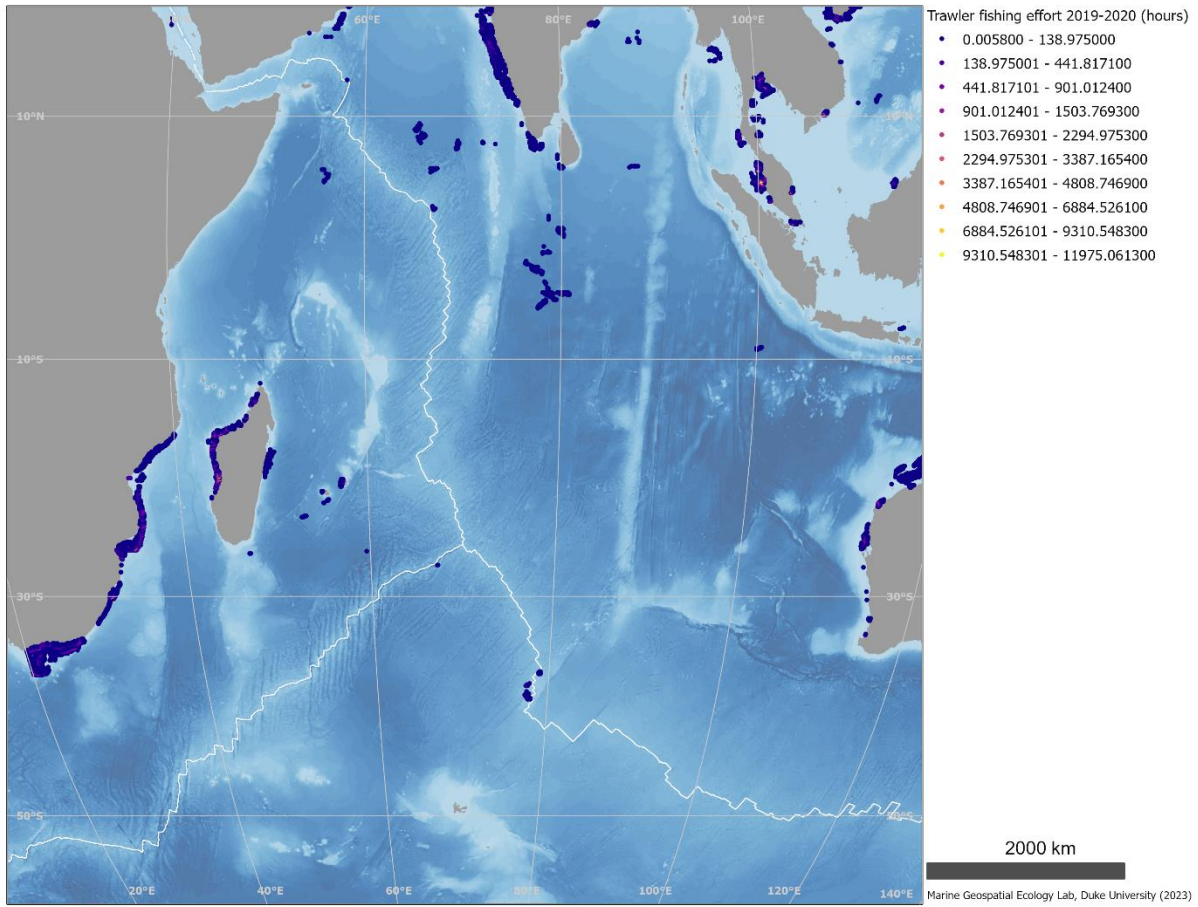


Figure 5.2-3 Trawler fishing effort from 2019-2020

### 5.3 Commercial Shipping

“This data was obtained through a partnership with IMF, as part of IMF's World Seaborne Trade Monitoring System (Cerdeiro, Komaromi, Liu and Saeed, 2020). The data analysis was supported by the World Bank's ESMAP and PROBLUE programs.

The dataset contains 6 density layers, with vessel types aggregated to suit the needs of the WBG Offshore Wind Development Program:

- 1) Commercial ships
- 2) Fishing ships
- 3) Oil & Gas [note: this is just platforms, rigs, and FPSOs]
- 4) Passenger ships
- 5) Leisure vessels
- 6) GLOBAL ship density layers of all ship categories combined

The raster layers were created using IMF's analysis of hourly AIS positions received between Jan-2015 and Feb-2021 and represent the total number of AIS positions that have been reported by ships in each grid cell with dimensions of 0.005 degree by 0.005 degree (approximately a 500m x 500m grid at the Equator).

The AIS positions may have been transmitted by both moving and stationary ships within each grid cell, therefore the density is analogous to the general intensity of shipping activity.”

Reference:

IMF's World Seaborne Trade monitoring system (Cerdeiro, Komaromi, Liu and Saeed, 2020)

Source:

<https://datacatalog.worldbank.org/search/dataset/0037580>

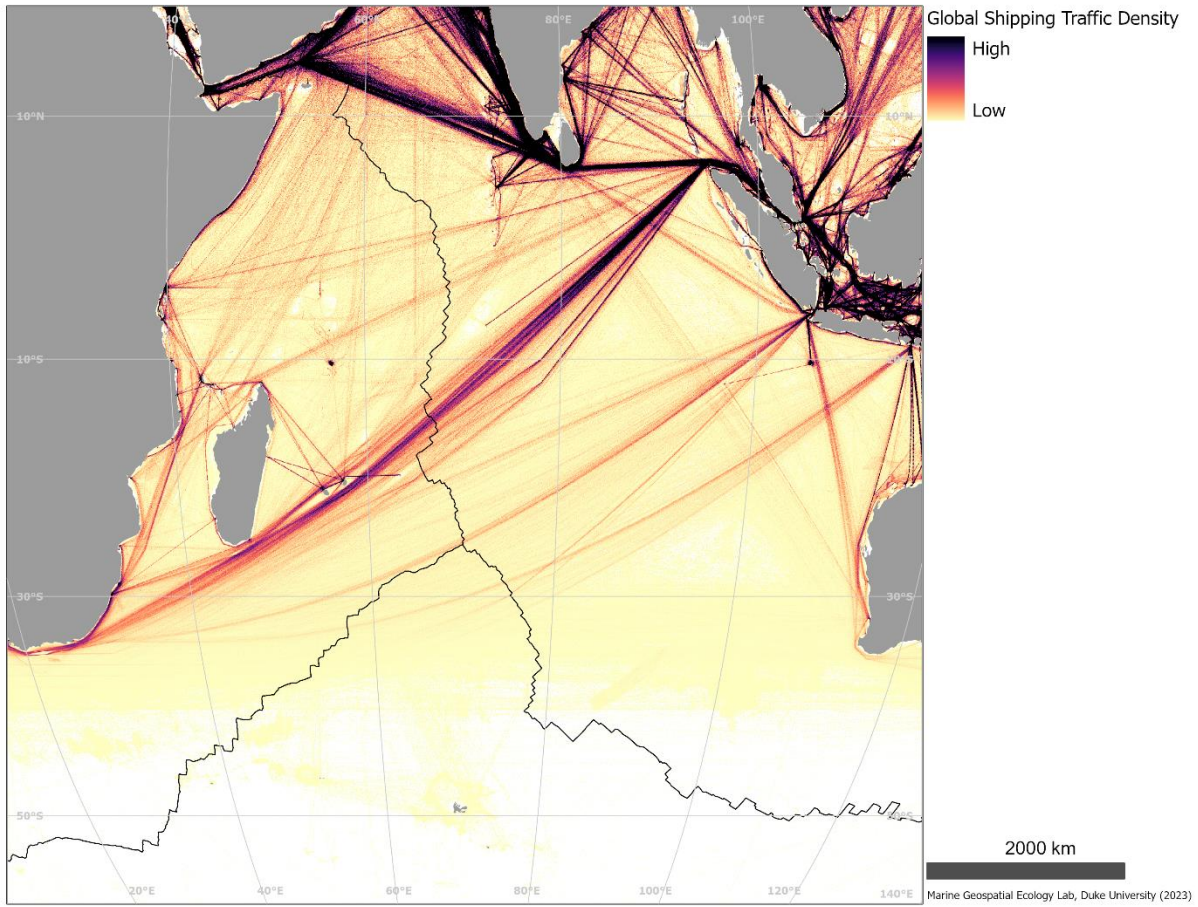


Figure 5.3-1 Commercial shipping

## 5.4 ISA Contract Areas for the Exploration of Mineral Resources

The International Seabed Authority (ISA; <https://www.isa.org.jm/>) provides the localization of all potential mineral resources (polymetallic nodules, polymetallic sulphides and cobalt-rich ferromanganese crusts) across the world's oceans.

The International Seabed Authority has entered into 15-year contracts for exploration for polymetallic nodules (18 contracts), polymetallic sulphides (7 contracts) and cobalt-rich ferromanganese crusts (5 contracts) in the deep seabed.

Eighteen of these contracts are for exploration for polymetallic nodules in the Clarion-Clipperton Fracture Zone (16), Central Indian Ocean Basin (1) and North-west Pacific (1). There are seven contracts for exploration for polymetallic sulphides in the South West Indian Ridge, Central Indian Ridge and the Mid-Atlantic Ridge and five contracts for exploration for cobalt-rich crusts in the North-west Pacific.

The current areas of exploration are as per the following maps and data produced by the Authority: <https://www.isa.org.jm/maps>

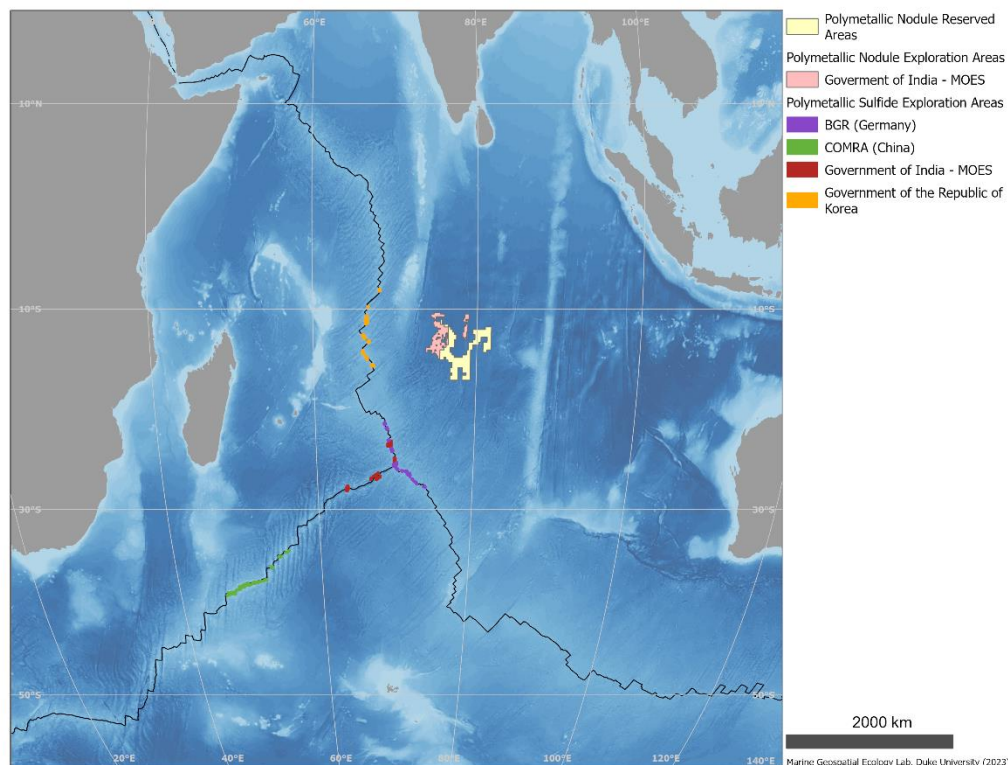


Figure 5.4-1 ISA exploration areas for polymetallic sulphides and polymetallic nodules in the Indian Ocean

## 5.5 Undersea Telecommunications Cables

“This dataset is an attempt to consolidate all the available information about the undersea communications infrastructure. The initial data was harvested from Wikipedia, and further information was gathered by simply googling and transcribing as much data as possible into a useful format, namely a rich geocoded format.”

Source:

<https://koordinates.com/layer/3722-undersea-telecommunication-cables/>

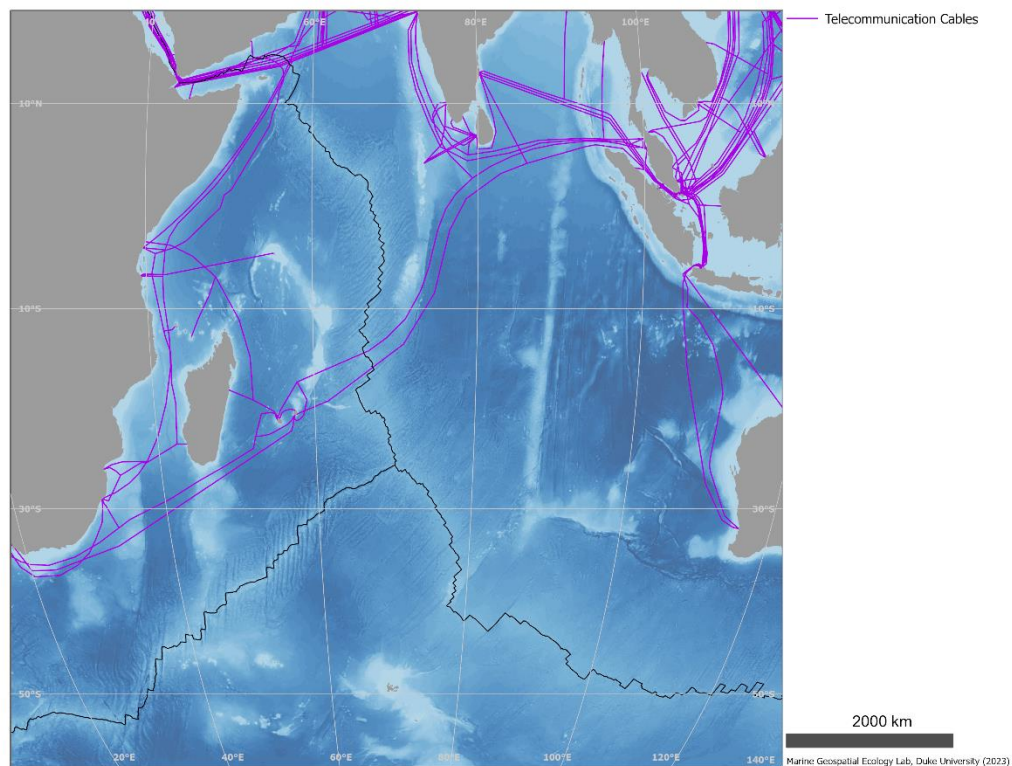


Figure 5.5-1 Undersea telecommunications cables

## 5.6 Cumulative Human Impacts on the World's Ocean

Abstract (Halpern 2015):

“Human pressures on the ocean are thought to be increasing globally, yet we know little about their patterns of cumulative change, which pressures are most responsible for change, and which places are experiencing the greatest increases. Managers and policymakers require such information to make strategic decisions and monitor progress towards management objectives. Here we calculate and map recent change over 5 years in cumulative impacts to marine ecosystems globally from fishing, climate change, and ocean- and land-based stressors. Nearly 66% of the ocean and 77% of national jurisdictions show increased human impact, driven mostly by climate change pressures. Five percent of the ocean is heavily impacted with increasing pressures, requiring management attention. Ten percent has very low impact with decreasing pressures. Our results provide large-scale guidance about where to prioritize management efforts and affirm the importance of addressing climate change to maintain and improve the condition of marine ecosystems.”

Reference:

Halpern, B. S. et al. 2015. Spatial and temporal changes in cumulative human impacts on the world's ocean. - Nat Commun 6: 1–7. doi:10.1038/ncomms8615

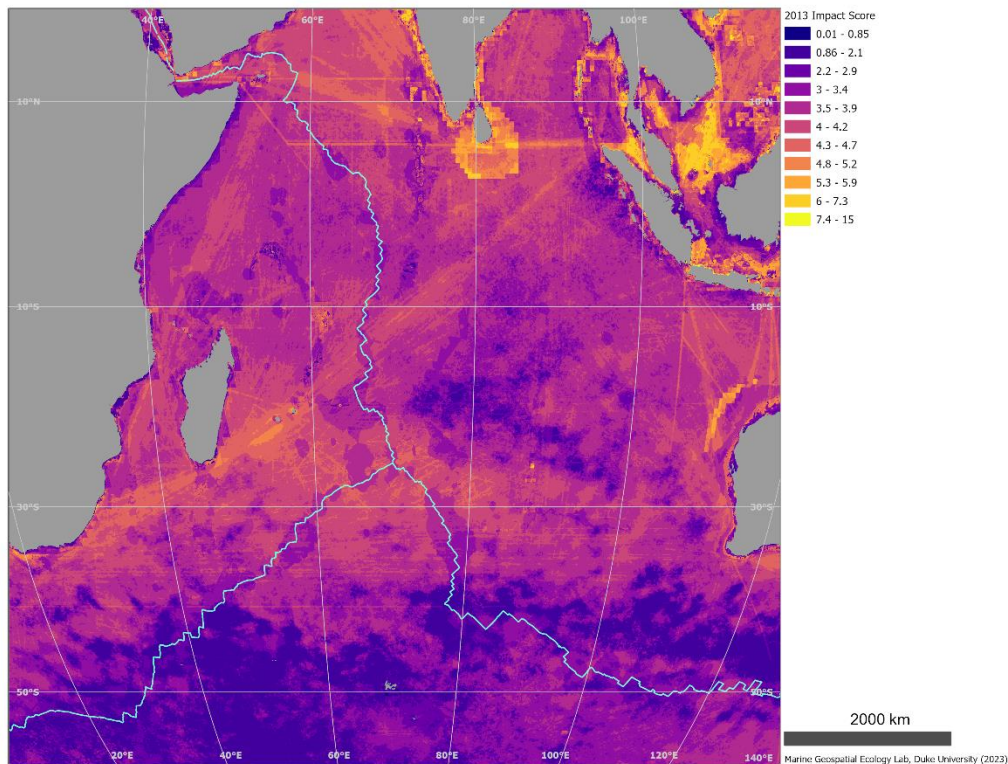


Figure 5.6-1 Cumulative human impact, 2013

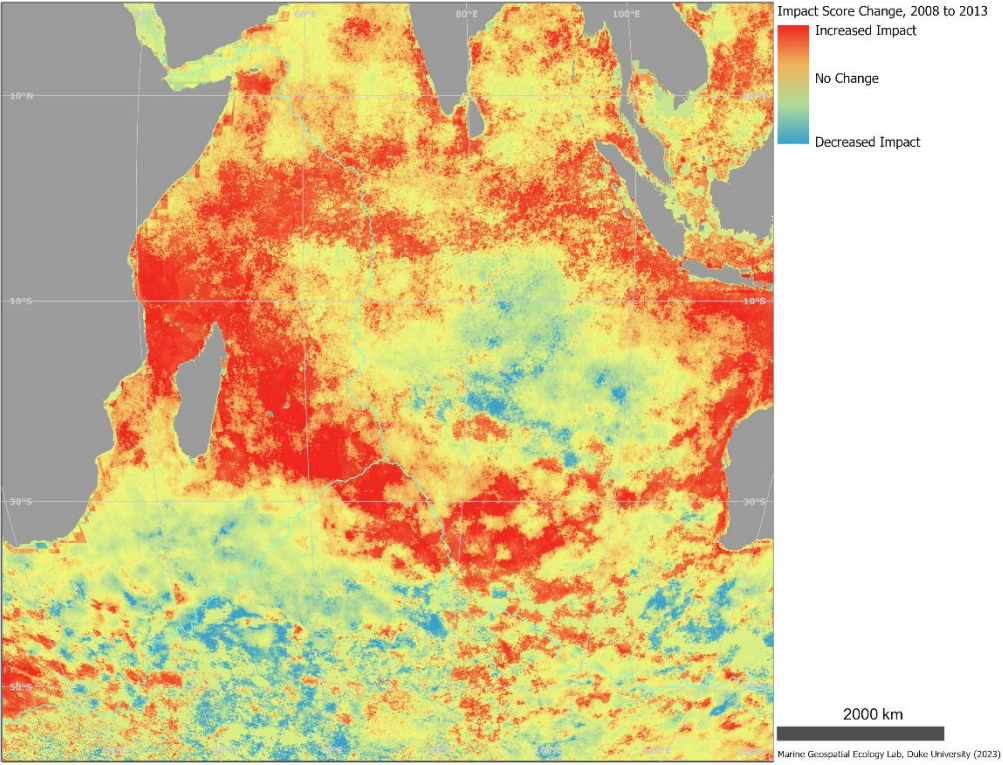


Figure 5.6-2 Change in cumulative human impact, 2008 to 2013

## 6 Areas Defined for Management and/or Conservation Objectives

### 6.1 Regional Fisheries Management Organizations (RFMO)

Regional Fishery Bodies (RFBs) are a mechanism through which States or organizations that are parties to an international fishery agreement or arrangement work together towards the conservation, management and/or development of fisheries (<http://www.fao.org/fishery/topic/16800/en>). The mandates of RFBs vary. Some RFBs have an advisory mandate, and provide advice, decisions or coordinating mechanisms that are not binding on their members. Some RFBs have a management mandate – these are called Regional Fisheries Management Organizations (RFMOs). They adopt fisheries conservation and management measures that are binding on their members. The RFMO in this area is the South Indian Ocean Fisheries Agreement.

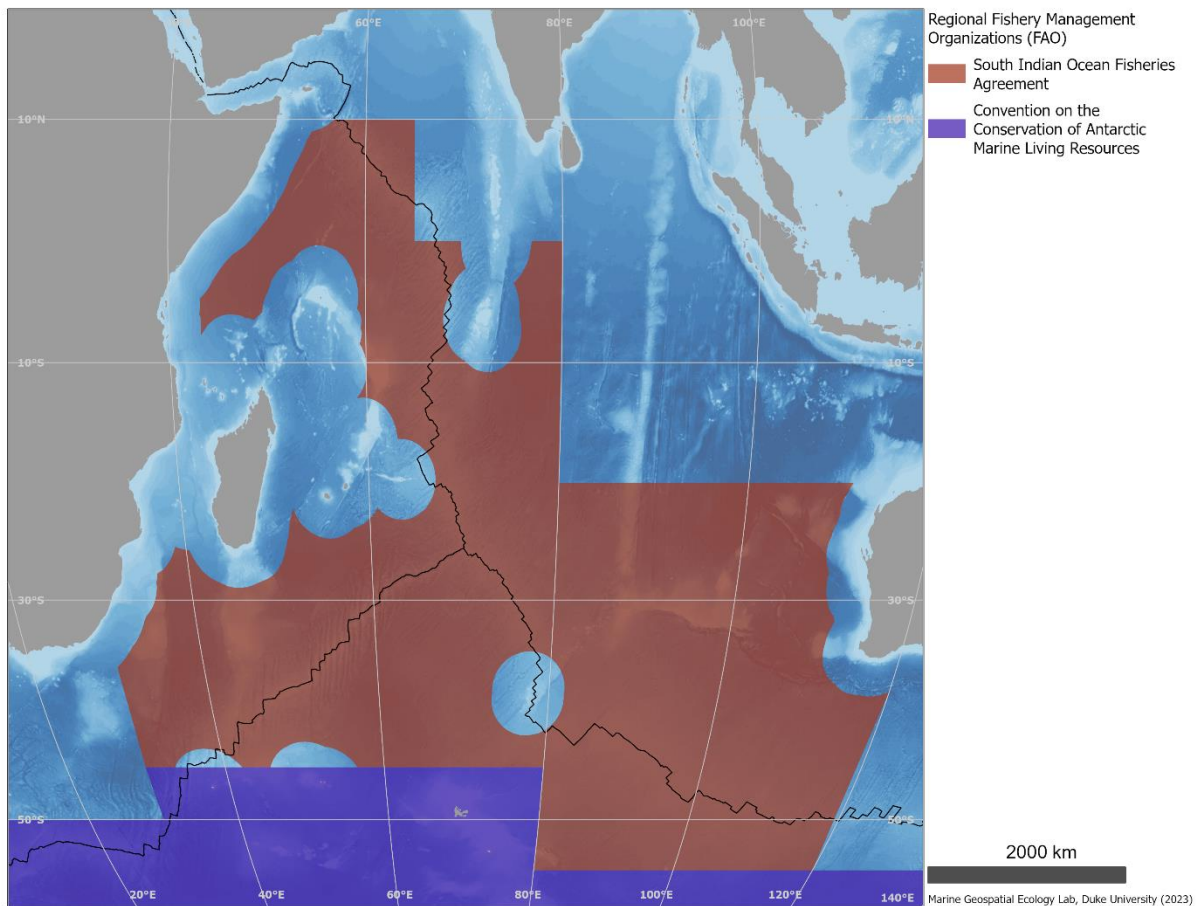


Figure 6.1-1 RFMOs in the North Atlantic Ocean

## 6.2 VME Closed Areas to Bottom Fishing Activities

SIOFA has closed areas to bottom fishing activities (SIOFA, 2021). Although the exact definition for such protection zones varies between RFMOs, they have been implemented to ensure the protection of VMEs.

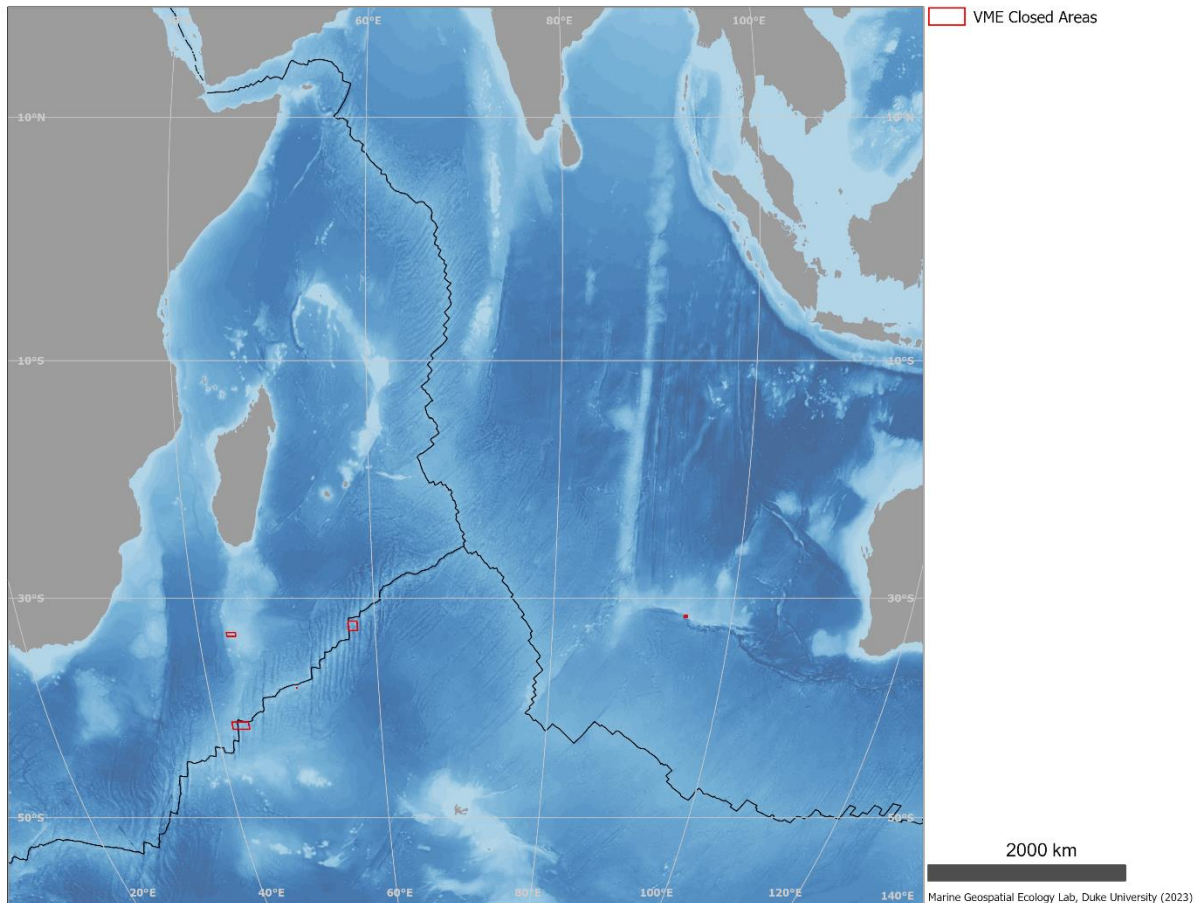


Figure 6.2-1 VME closed areas

## 6.3 Marine Protected Areas

“Protected Planet is the most up to date and complete source of information on protected areas, updated monthly with submissions from governments, non-governmental organizations, landowners and communities. It is managed by the United Nations Environment Programme's World Conservation Monitoring Centre (UNEP-WCMC) with support from IUCN and its World Commission on Protected Areas (WCPA). It is a publicly available online platform where users can discover terrestrial and marine protected areas, access related statistics and download data from the World Database on Protected Areas (WDPA).”

Source: <https://www.protectedplanet.net/c/world-database-on-protected-areas>

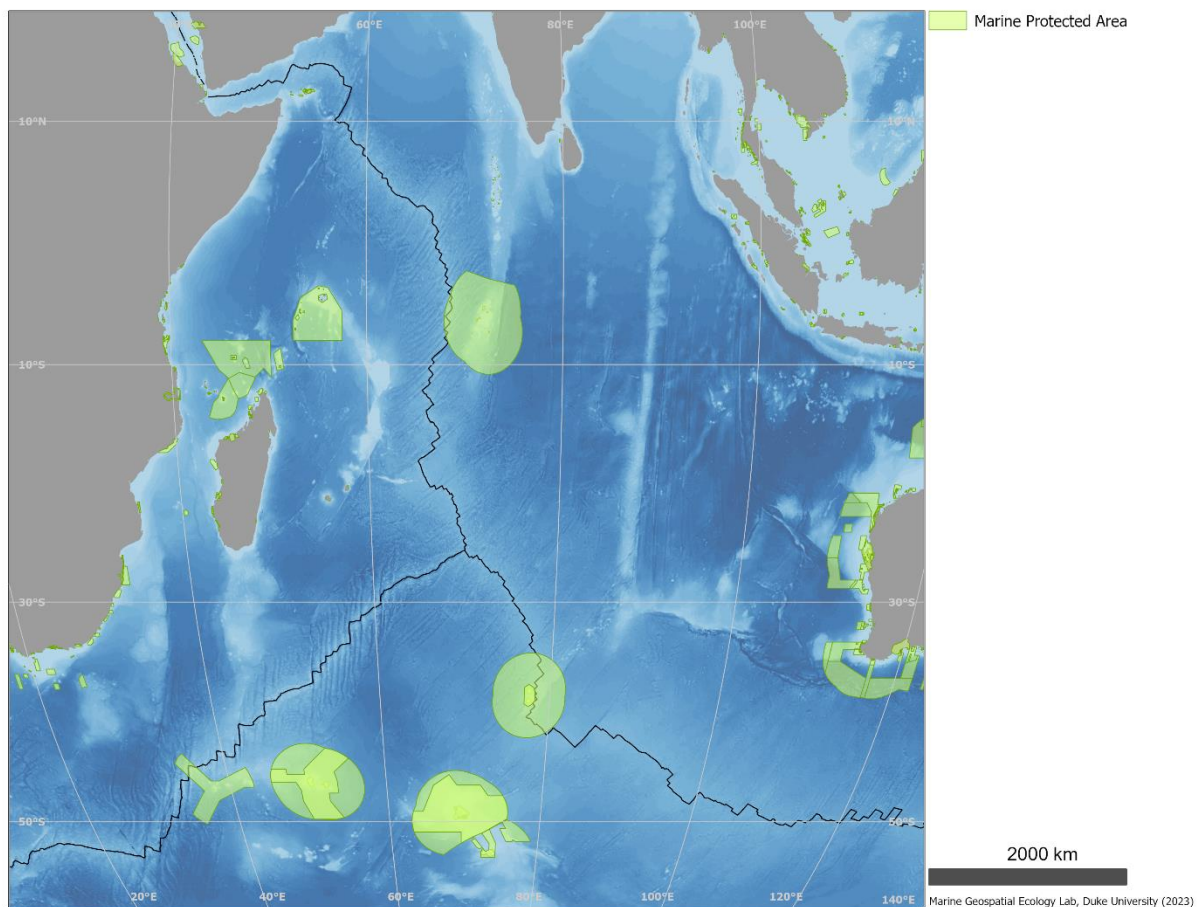


Figure 6.3-1 Marine protected areas

## 6.4 Convention on Biological Diversity Ecologically or Biologically Significant Areas (EBSAs)

In 2008, the ninth meeting of the Conference of the Parties to the Convention on Biological Diversity (COP 9) adopted the following scientific criteria for identifying ecologically or biologically significant marine areas (EBSAs) in need of protection in open-ocean waters and deep-sea habitats. For more details on the EBSA criteria, please see:

[www.cbd.int/doc/meetings/mar/ebsaws-2014-01/other/ebsaws-2014-01-azores-brochure-en.pdf](http://www.cbd.int/doc/meetings/mar/ebsaws-2014-01/other/ebsaws-2014-01-azores-brochure-en.pdf). CBD scientific criteria for ecologically or biologically significant areas (EBSAs) (annex I, decision IX/20) includes: Uniqueness or Rarity, Special importance for life history stages of species, Importance for threatened, endangered or declining species and/or habitats,

Vulnerability, Fragility, Sensitivity, or Slow recovery, Biological Productivity, Biological Diversity, Naturalness. From 2011 to 2019, the CBD convened regional workshops that identified over 300 areas meeting the internationally agreed criteria for Ecologically and Biologically Significant Areas (EBSAs).

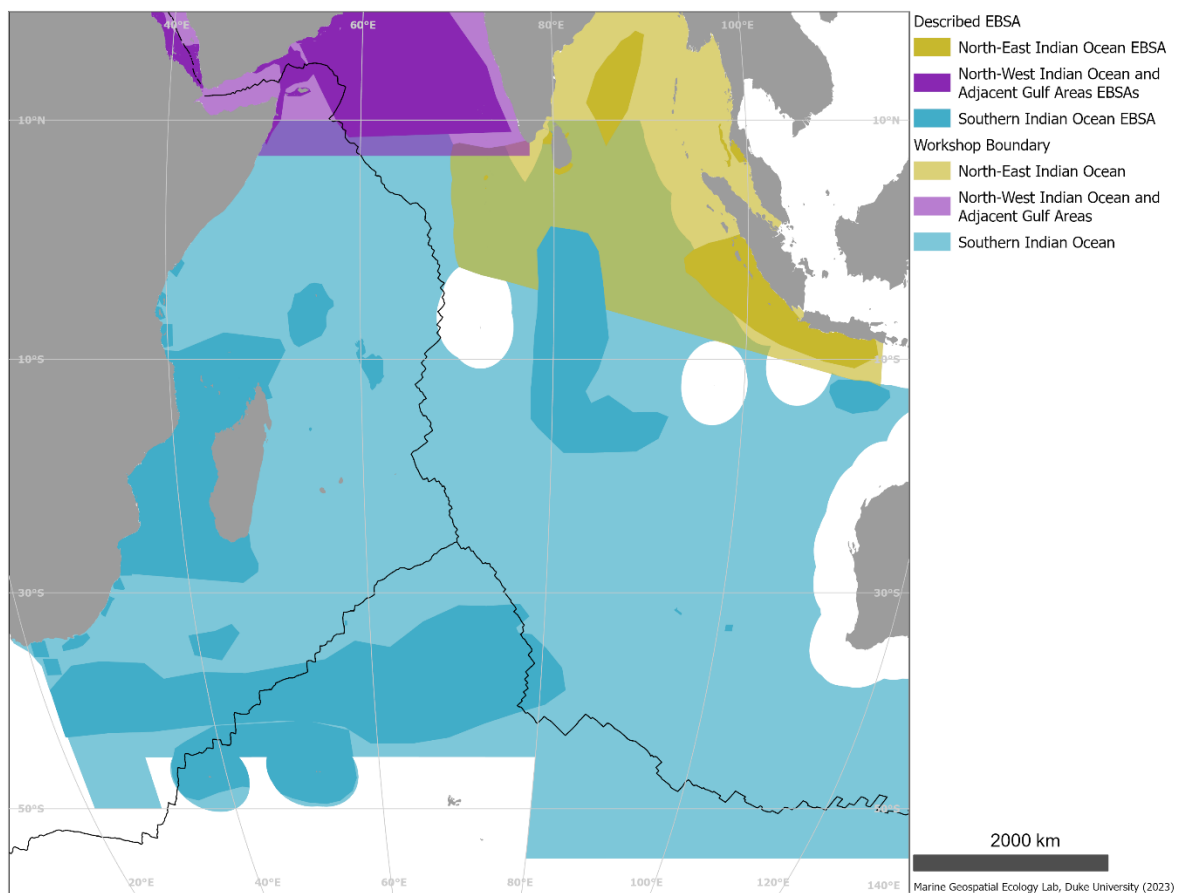


Figure 6.4-1 Convention on Biological Diversity's Ecologically or Biologically Significant Areas (EBSAs)

## 6.5 Assessment for Sites in Need of Protection in the Indian Ocean

Abstract (Van der Mose et al. 2023):

“Deep-sea hydrothermal vent fields are among the most pristine and remarkable ecosystems on Earth. They are fueled by microbial chemosynthesis, harbor unique life and can be sources of precipitated mineral deposits. As the global demand for mineral resources rises, vent fields have been investigated for polymetallic sulfides (PMS) and biological resources. The International Seabed Authority (ISA) has issued 7 contracts for PMS exploration, including 4 licenses for vent fields in the Indian Ocean. Here, we provide a summary of the available ecological knowledge of Indian vent communities and we assess their vulnerability, sensitivity, ecological and biological significance. We combine and apply scientific criteria for Vulnerable Marine Ecosystems (VMEs) by FAO, Particular Sensitive Sea Areas (PSSAs) by IMO, and Ecologically or Biologically Significant Areas (EBSAs) by CBD. Our scientific assessment shows that all active vent fields in the Indian Ocean appear to meet all scientific criteria for protection, and both the high degree of uniqueness and fragility of these ecosystems stand out.”

Reference:

van der Most, N., Qian, P.Y., Gao, Y. and Gollner, S., 2023. Active hydrothermal vent ecosystems in the Indian Ocean are in need of protection. *Frontiers in Marine Science*.  
<https://doi.org/10.3389/fmars.2022.1067912>

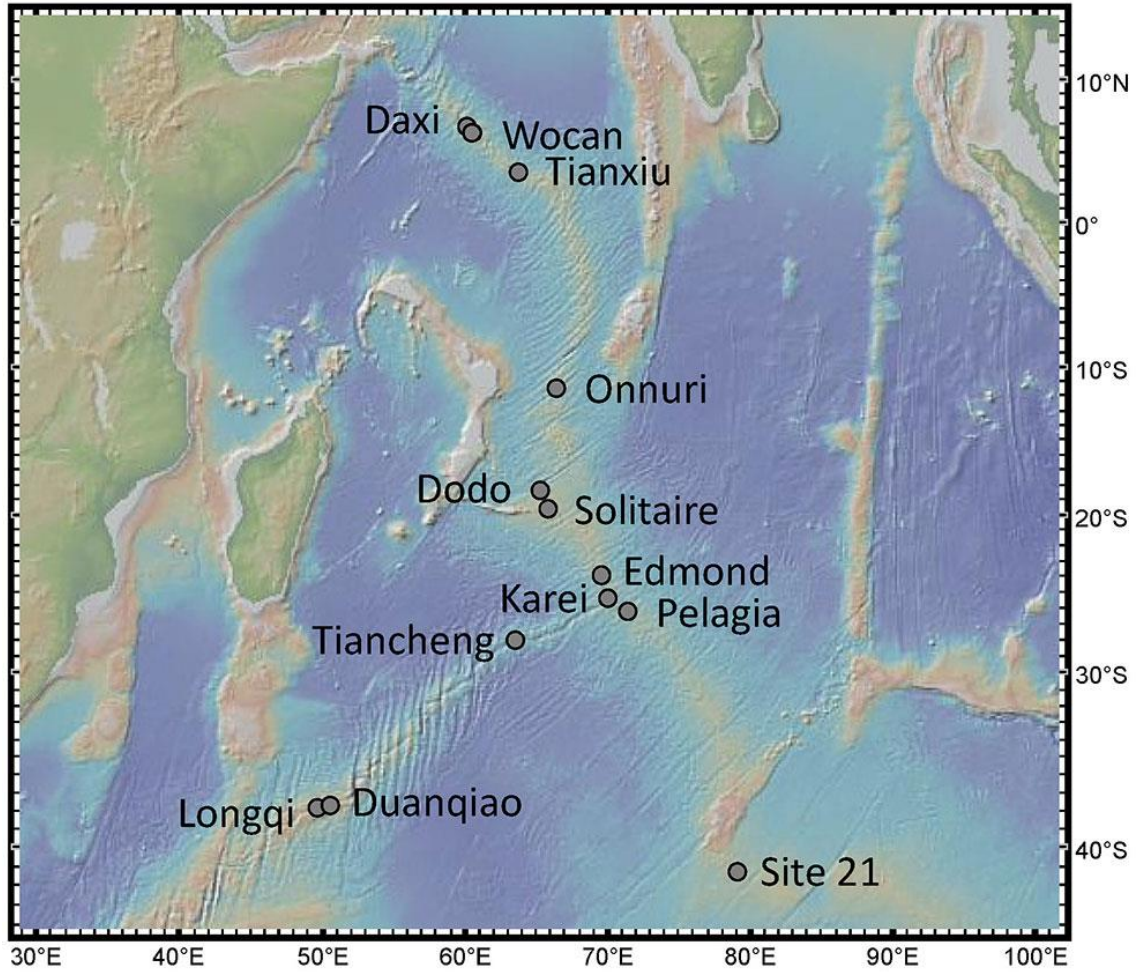


Figure 6.5-1 Confirmed active hydrothermal vents along the Indian Ocean ridges

Original Caption: Figure 1. Location of the 13 active confirmed hydrothermal vent fields in the Indian ocean. Map created with GeoMapApp.

## 6.6 Western Indian Ocean Symphony Tool

“The WIO Symphony web tool supports your marine spatial planning by assessing environmental impact from human activities. WIO Symphony lets you visualize data, test scenarios, and compare different ways of using the ocean:

- Show data
- Create maps
- Calculate cumulative impact on environment
- Compare options

WIO Symphony provides a useful tool for management and marine spatial planning that supports an ecosystem-based approach. A similar tool called Symphony Sweden was developed and used for the Baltic Sea. The WIO Symphony project is a sister-project to that, a collaboration between the Nairobi Convention, its ten member states in East Africa and a team of Swedish institutions lead by the Swedish Agency for Marine and Water Management.

The aim of the WIO Symphony collaboration is to co-develop and implement a practical assessment tool for marine spatial planning in the Western Indian Ocean region. By incorporating information and knowledge from national, regional and international experts, the WIO Symphony tool enables estimations of how pressures from human activities in the ocean affect nature values in each location in the Western Indian Ocean.”

Source: <http://www.nairobiconvention.org/wio-symphony/>

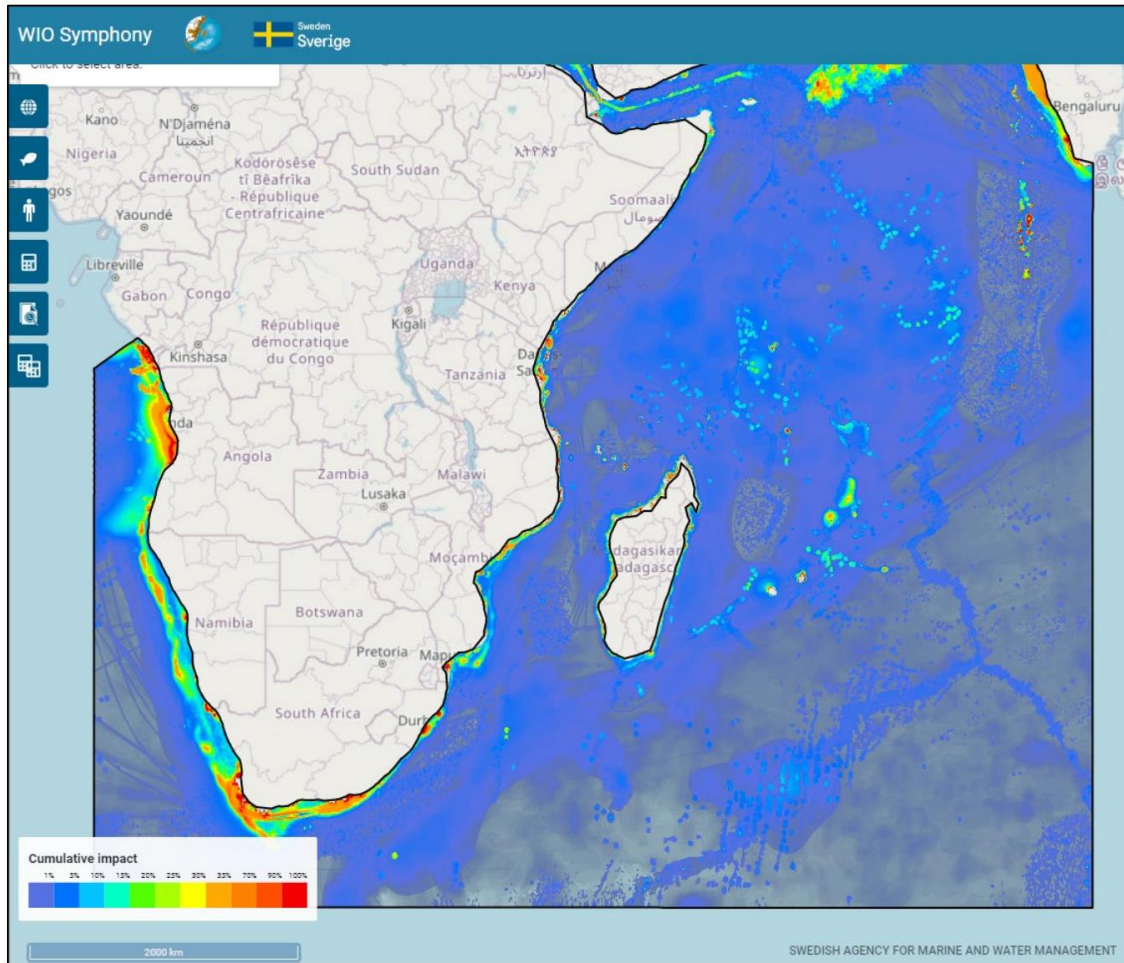


Figure 6.6-1 An example of the WIO Symphony tool

## 7 Acknowledgments

The data collection team gratefully acknowledge contributions from:

Wanfei Qui, Luciana De Melo Santos Genio – ISA Secretariat

Piers Dunstan, Skip Woolley - CSIRO Australia

Linus Hammar, Swedish Agency for Marine and Water Management

Cindy Van Dover - Duke University

Daniel C. Dunn - University of Queensland, Duke University